DISSERTATION

Nuclear and chemokine receptors are involved in lymphomagenesis

submitted by
Ing. Katrin Pansy BSc MSc

for the Academic Degree of
Doctor of Philosophy (PhD)

at the
Medical University of Graz
Division of Hematology

under the Supervision of
Sen.Scientist Priv.-Doz. Mag.rer.nat. Dr.scient.med.
Alexander DEUTSCH

2024

STATUTORY DECLARATION

I hereby declare that this thesis is my own original work and that I have fully acknowledged by name all of those individuals and organizations that have contributed to the research for this thesis. Due acknowledgement has been made in the text to all other material used. Throughout this thesis and in all related publications I followed the "Guidelines of the Medical University of Graz on Good Scientific Practice".

Graz, 9th of April 2024

DISCLOSURES

Part I of this thesis has been published in

Katrin Pansy[1], Julia Feichtinger[2], Barbara Ehall[1], Barbara Uhl[1], Miriam Sedej[3], David Roula[3], Beata Pursche[1], Axel Wolf[4], Manuel Zoidl[5], Elisabeth Steinbauer[6], Verena Gruber[6], Hildegard T. Greinix[1], Katharina T. Prochazka[1], Gerhard G. Thallinger[7,8], Akos Heinemann[3], Christine Beham-Schmid[6], Peter Neumeister[1], Tanja M. Wrodnigg[5], Karoline Fechter[1], Alexander J. Deutsch[1]. **The *CXCR4-CXCL12*-Axis Is of Prognostic Relevance in DLBCL and Its Antagonists Exert Pro-Apoptotic Effects In Vitro**. Int J Mol Sci. 2019 Sep 24;20(19):4740. doi: 10.3390/ijms20194740. PMID: 31554271; PMCID: PMC6801866.

1 Division of Hematology, Medical University Graz; Auenbruggerplatz 38, 8036 Graz, Austria
2 Division of Cell Biology, Histology and Embryology, Gottfried Schatz Research Center for Cell Signaling, Metabolism and Aging, Medical University of Graz, Neue Stiftingtalstraße 6/II, 8010 Graz, Austria
3 Otto Loewi Research Center for Vascular Biology, Immunology and Inflammation, Division of Pharmacology, Medical University of Graz, Universitätsplatz 4/I, 8010 Graz, Austria
4 Division of General Otorhinolaryngology, Medical University of Graz, Auenbruggerplatz 26, 8036 Graz, Austria
5 Institute of Organic Chemistry, Graz University of Technology, Stremayrgasse 9/4, 8010 Graz, Austria
6 Diagnostic & Research Institute of Pathology, Medical University Graz, Neue Stiftingtalstraße 6, 8010 Graz, Austria
7 Institute of Computational Biotechnology, Graz University of Technology, Petersgasse 14/V, 8010 Graz, Austria
8 OMICS Center Graz, BioTechMed Graz, Stiftingtalstraße 24, 8010 Graz, Austria

In this sense, all co-authors have agreed to the inclusion of their published data in the dissertation and permission to reproduce illustrations and figures from their own publications has been granted.

Co-Author contributions:
Julia Feichtinger was implicated in data analysis, including statistical analysis as well as the examination of publicly accessible gene expression data.

Barbara Ehall contributed to carrying out experiments and data interpretation.

Barbara Uhl contributed to data analysis.

Miriam Sedej performed migration assays.

David Roula performed migration assays.

Beata Pursche contributed to carrying out experiments and data interpretation.

Axel Wolf gathered clinical data and played a significant role in interpreting the data and contributing to the study's design.

Manuel Zoidl synthesized WK1.

Elisabeth Steinbauer performed IHC stainings.

Verena Gruber performed IHC stainings.

Hildegard Greinix provided lab space and helped with study design.

Katharina Prochazka contributed to data analysis.

Gerhard Thallinger contributed to data analysis.

Akos Heinemann performed migration assays

Christine Beham-Schmid helped with IHC analysis.

Peter Neumeister collected clinical data, helped with data interpretation and study design.

Tanja Wrodnigg synthesized WK1.

Karoline Fechter contributed to carrying out experiments, data interpretation and manuscript writing.
Alexander Deutsch led, organized, and managed the project, contributing to the writing of the manuscript as well.

All co-authors have provided consent for the incorporation of their published data into the dissertation, and necessary permissions from both the publisher and copyright holders for reproduction have been secured.

During my PhD studies, I additionally contributed to the following publications:

- Uhl B, Prochazka KT, **Pansy K**, Wenzl K, Strobl J, Baumgartner C, Szmyra MM, Waha JE, Wolf A, Tomazic PV, Steinbauer E, Steinwender M, Friedl S, Weniger M, Küppers R, Pichler M, Greinix HT, Stary G, Ramsay AG, Apollonio B, Feichtinger J, Beham-Schmid C, Neumeister P, Deutsch AJ. Distinct Chemokine Receptor Expression Profiles in De Novo DLBCL, Transformed Follicular Lymphoma, Richter's Trans-Formed DLBCL and Germinal Center B-Cells. Int J Mol Sci. 2022 Jul 17;23(14):7874. doi: 10.3390/ijms23147874.
- Neumeister P, Schulz E, **Pansy K**, Szmyra M, Deutsch AJ. Targeting the Microenvironment for Treating Multiple Myeloma. Int J Mol Sci. 2022 Jul 10;23(14):7627. doi: 10.3390/ijms23147627.
- Krstic J, Deutsch A, Fuchs J, Gauster M, Gorsek Sparovec T, Hiden U, Krappinger JC, Moser G, **Pansy K**, Szmyra M, Gold D, Feichtinger J, Huppertz B. (Dis)similarities between the Decidual and Tumor Microenvironment. Biomedicines. 2022 May 4;10(5):1065. doi: 10.3390/biomedicines10051065.
- Uhl B, Prochazka KT, Fechter K, **Pansy K**, Greinix HT, Neumeister P, Deutsch AJ. Impact of the microenvironment on the pathogenesis of mucosa-associated lymphoid tissue lymphomas. World J Gastrointest Oncol. 2022 Jan 15;14(1):153-162. doi: 10.4251/wjgo.v14.i1.153.
- **Pansy K**, Uhl B, Krstic J, Szmyra M, Fechter K, Santiso A, Thüminger L, Greinix H, Kargl J, Prochazka K, Feichtinger J, Deutsch AJ. Immune Regulatory Processes of the Tumor Microenvironment under Malignant Conditions. Int J Mol Sci. 2021 Dec 10;22(24):13311. doi: 10.3390/ijms222413311.
- Krappinger JC, Bonstingl L, **Pansy K**, Sallinger K, Wreglesworth NI, Grinninger L, Deutsch A, El-Heliebi A, Kroneis T, Mcfarlane RJ, Sensen CW, Feichtinger J. Non-coding Natural Antisense Transcripts: Analysis and Application. J Biotechnol. 2021 Nov 10;340:75-101. doi: 10.1016/j.jbiotec.2021.08.005.
- Fechter, K; Feichtinger, J; Prochazka, K; Unterluggauer, JJ; **Pansy, K**; Steinbauer, E; Pichler, M; Haybaeck, J; Prokesch, A; Greinix, HT; Beham-Schmid, C; Neumeister, P; Thallinger, GG; Deutsch, AJA; Cytoplasmic location of NR4A1 in aggressive lymphomas is associated with a favourable cancer specific survival. Scientific Reports 2018; 8(1):14528-14528. doi: 10.1038/s41598-018-32972-4.

ACKNOWLEDGEMENTS

First, I express my deepest gratitude to my supervisor, **Dr. Alexander Deutsch**, for his support, mentorship and guidance during many years in his lab. He has been an outstanding mentor, providing valuable insights, encouragement and constructive feedback that have contributed to my personal and professional development. I want to thank him for guidance and support, even during challenging times. His mentorship has enriched my academic experience and positively impacted my career progression.

I would like to express my gratitude to the entire Deutsch Lab, especially to **Sandra Haingartner** and **Marta Szmyra-Połomka**, for their collaboration, collegiality, and collective efforts, which have made my research endeavors both rewarding and enjoyable. I am grateful to work with a talented and dedicated group. Your passion for science, commitment to excellence and genuine friendship create an inspiring environment.

I would also like to thank **Karoline Fechter**, **Julia Unterluggauer-Herzog**, **Timna Bergmann**, and **Sonja Jantscher**, and the others I forgot to mention, for their friendship and support during our time together in the lab. Your positive energy and willingness to lend a helping hand made the lab environment more welcoming and enjoyable. Although you have moved on to new opportunities, your presence in the lab is still felt and your contributions are greatly appreciated. Thank you for being an integral part of my academic journey and for leaving a legacy of excellence and collegiality.

I am also grateful to all of my friends, especially **Bianca Kerschbaumer** and **Natascha Scheikl**, who have cheered me on from afar, sent words of encouragement, and celebrated my milestones, no matter how big or small. Your friendship has made this journey more fulfilling and meaningful.

This thesis is dedicated to my **parents** with love and appreciation for their unwavering support and constant encouragement throughout my academic journey. I am grateful for their belief in me, which has been my greatest motivation.

I am grateful to my boyfriend **Philipp Mauerhofer** for his love, support and understanding during this journey.

Finally, I would like to acknowledge the financial support of the DOC Fellowship Program of the **Austrian Academy of Sciences ÖAW** (award 25690) and a research grant from the **Austrian Society for Hematology & Medical Oncology (OeGHO)**, which made this thesis possible. I am grateful for this opportunity. Thanks to the **Medical University of Graz** for being a part of the PhD program in **Molecular Medicine** (MolMed).

TABLE OF CONTENT

ABBREVIATIONS

Ab	antibody
ABC	activated B cell-like
ADARB	adenosine deaminase RNA specific B1
ADCC	antibody-dependent cellular cytotoxicity
AF	activation function
AID	activation-induced cytidine deaminase
AML	acute myeloid leukemia
APC	antigen-presenting cell
B2M	β2-microglobulin
BAD	BCL2 Associated Agonist Of Cell Death
BAK	BCL2 Antagonist/Killer
BAX	BCL2-associated X protein
BCL-2	BCL2 Apoptosis Regulator
BCL-6	Bcell lymphoma 6
BCL-XL	B cell lymphoma extra large
BCR	B cell receptor
BIK	BCL2 Interacting Killer
BIM	BCL2 Like 11
BL	Burkitt's lymphoma
BLIMP1	B lymphocyte-induced maturation protein-1
BM	bone marrow
BMF	BCL2 Modifying Factor
Breg	regulatory B cell
BSA	body surface area
BTLA	B- and T-lymphocyte attenuator
BTN	butyrophilin
BTNL	butyrophilin-like
BUB1	BUB1 mitotic checkpoint serine/threonine kinase
CAF	cancer-associated fibroblast
CARD11	caspase recruitment domain-containing protein 11
cDCs1	conventional DC type 1 cells
CFLAR	CASP8 and FADD Like Apoptosis Regulator
cHL	classical Hodgkin lymphoma
CLL	chronic lymphocytic leukemia
CLP	common lymphoid precursor cells
CNS	central nervous system
COL1A	collagen Type I Alpha 1 Chain
CREB	cAMP response component-binding protein
CREBBP	cAMP response component-binding protein
Csn-B	cytosporin B
CSR	class switch recombination

CTLA-4	cytotoxic T-lymphocyte-associated protein 4
CXCL12	C-X-C motif chemokine ligand 12
CXCR4	CXC chemokine receptor 4
CXCR7	C-X-C chemokine receptor 7
DBD	DNA binding domain
DC	dendritic cell
DHL	double-hit lymphoma
DLCBL	diffuse large B cell lymphoma
DMEM	Dulbecco's Modification of Eagle's Medium
DR5	direct repeat with 5-bp length
DUSP1	dual specificity phosphatase 1
DZ	dark zone
EBV	Epstein-Barr virus
ECM	extracellular matrix
EGFR	epidermal growth factor receptor
EP300	E1A-binding protein p300
ERK1/2	extracellular signal-regulated kinases
ETV5	ETS variant transcription factor 5
EZH2	enhancer of zeste homolog 2
FBS	fetal bovine serum
FBXO11	F-box protein 11
FDC	follicular dendritic cell
FL	follicular lymphoma
FMO	fluorescence minus-one
FN1	fibronectin 1
FoxP3	forkhead box P3
GAPDH	glyceraldehyde-3-phosphate dehydrogenase
GATA3	GATA binding protein 3
GC	germinal center
GCB	germinal center B cell-like
GDP	guanosine diphosphate
GEP	gene expression profiling
GNA13	guanine nucleotide-binding protein subunit alpha-13
GPCR	G protein-coupled receptor
GTP	guanosine triphosphate
HIV	human immunodeficiency virus
HL	Hodgkin's lymphoma
HPRT	hypoxanthine-guanine phosphoribosyltransferase
HSC	hematopoietic stem cells
HSV8	human herpesvirus 8
HTLV	human T-cell leukemia virus
HVEM	herpesvirus entry mediator
i.v.	intravenous

ICB	immune checkpoint blockade
Icos	inducible T cell costimulator
IMDM	Iscove's Modified Dulbecco's Medium
JAK/STAT	janus kinases-signal transducer and activator of transcription
KLF10	kruppel like factor 10
LAG-3	lymphocyte-activation gene 3
LBD	ligand binding domain
LPS	lipopolysaccharide
LZ	light zone
mAb	monoclonal antibody
MALT	marginal zone B cell
MAPK	protein kinase B mitogen-activated protein kinase
MCL	mantle cell lymphoma
Mcl-1	myeloid cell leukemia 1
mDC	monocyte-derived DC
Mdm2	murine double minute 2
MDS	myelodysplastic syndrome
MDSC	myeloid-derived suppressor cell
MEF2B	myocyte enhancer binding factor 2B
MHC	major histocompatibility complex
MLL2	histone methyltransferase
MMP2	matrix metalloproteinase-2
MPN	myeloproliferative neoplasm
MXD1	MAX dimerization protein 1
MYD88	myeloid differentiation primary response 88
MZL	nodal marginal zone lymphoma
NBRE	NGFI-B response element
NHL	non-Hodgkin's lymphoma
NK	natural killer
NOS	not otherwise specified
NOXA	phorbol-12-myristate-13-acetate-induced protein 1
NurRE	Nur response element
OAS3	2'-5'-oligoadenylate synthetase 3
OVA	ovalbumin
P19Arf	p19 ADP ribosylation factor
PAX5	paired box protein Pax-5
PBS	phosphate buffered saline
PC	plasma cell
PCR	polymerase chain reaction
PD-1	programmed cell death protein 1
PD-L1	programmed cell death 1 ligands 1
PD-L2	programmed cell death 1 ligands 2
pDC	plasmacytoid DC

PI3K	phosphoinositide 3-kinase
PMBCL	primary mediastinal (thymic) large B cell lymphoma
PPIA	peptidylprolyl isomerase A
PRDM1	PR domain zinc finger protein 1
PTEN	phosphatase and tensin homolog
PUMA	p53 up-regulated modulator of apoptosis
RGS1	regulator of G protein signaling 1
RPMI	Roswell Park Memorial Institute
RXR	retinoid X receptor
sBL	sporadic BL
SDF-1	stromal cell-derived factor 1
SHM	somatic hypermutation
SLL	small cell lymphocytic lymphoma
SPF	specific pathogen-free
STAT	signal transducer and activator of transcription
TAM	tumor-associated macrophages
TAMC	tumor-associated mast cell
TAN	tumor-associated neutrophils
TCR	T cell receptor
TfH	follicular helper T
Th	T helper
Thf	follicular helper T cell
THL	triple-hit lymphoma
TIGIT	T cell immunoreceptor with immunoglobulin and ITIM domain
TIM-3	T-cell immunoglobulin and mucin domain-3
TLR	toll-like receptors
TME	tumor microenvironment
TNF	tumor necrosis factor
TNFRSF14	tumor necrosis factor receptor superfamily member 14
Treg	regulatory T cell
VISTA	V-domain immunoglobulin suppressor of T cell activation
VNTR	variable number tandem repeat
WHO	World Health Organization
IFN	interferon

LIST OF FIGURES

LIST OF TABLES

ABSTRACT GERMAN

In diesem ersten Teil der Dissertation wird die Bedeutung der Untersuchung der *CXCR4-CXCL12*-Achse beim diffusen großzelligen B-Zell-Lymphom (DLBCL) hervorgehoben. Bei mehr als 20 verschiedenen Krebsarten spielt die *CXCR4-CXCL12*-Achse eine entscheidende Rolle bei mehreren kritischen Prozessen wie der Proliferation, dem Überleben, der Migration, der Invasion und der Metastasierung von Tumorzellen. Die Forschung zu dieser Achse beim DLBCL ist jedoch begrenzt und uneinheitlich. Um diese Lücke zu schließen, haben wir eine umfassende Studie zur *CXCR4-CXCL12*-Achse in unserer DLBCL-Kohorte durchgeführt und die Wirkung von CXCR4-Antagonisten auf Lymphomzelllinien *in vitro* untersucht. Unsere Ergebnisse beim DLBCL zeigten eine signifikante 140-fache Erhöhung der *CXCR4*-Expression im Vergleich zu nicht-neoplastischen Kontrollen. Darüber hinaus war eine hohe *CXCR4*-Expression mit einem schlechten klinischen Outcome assoziiert. Die Analyse der korrespondierenden Knochenmarkbiopsien zeigte eine Korrelation zwischen der *CXCL12*-Expression und der Infiltrationsrate des Lymphoms sowie eine Reduktion der *CXCR4*-Expression nach therapieinduzierter Remission des Knochenmarkbefalls. Darüber hinaus haben wir die Wirkung von drei CXCR4-Antagonisten *in vitro* untersucht: AMD3100 (Plerixafor), AMD070 (Mavorixafor) und WK1 - ein Niacin-Derivat von AMD070, das in unserer Studie synthetisiert wurde. WK1 zeigte eine stärkere pro-apoptotische Wirkung als AMD070 und induzierte die Expression von pro-apoptotischen Genen in *CXCR4*-positiven Lymphomzellen. Interessanterweise führte die Behandlung mit WK1 zu einer verminderten Expression von Genen, die mit den JNK-, ERK1/2- und NF-κB/BCR-Signalwegen assoziiert sind. Zusammenfassend deuten unsere Daten darauf hin, dass die *CXCR4-CXCL12*-Achse einen entscheidenden Einfluss auf die Pathogenese des DLBCL hat und ein vielversprechendes therapeutisches Ziel bei aggressiven Lymphomen darstellt.

Im zweiten Teil der Arbeit wurden die Auswirkungen von *Nr4a1*-Defizienz auf das Tumormikromilieu (TME) und die Immunantwort in einem Lymphommausmodell untersucht. Die Transplantation von *Nr4a1*-defizienten Lymphomzellen in C57BL/6-Wildtyp-Mäuse führte zu einer erhöhten Infiltration der Milz mit malignen B-Zellen, einer verminderten Infiltration mit CD3+ T-Zellen, einschließlich CD4+ und CD8+ T-Zell-Subtypen, und einem erhöhten Gehalt an M2-Makrophagen und Tregs, was auf eine Immunsuppression und ein an Immunzellen verarmtes TME hinweist. Darüber hinaus deutete ein erhöhter Anteil von CD3+ T-Zellen, die mehrere Immun-Checkpointproteine mitexprimieren, in Mäusen, denen *Nr4a1*-defiziente Lymphomzellen transplantiert worden waren, auf ein immunodepletiertes, erschöpftes TME hin. Co-Kultivierungsversuche zeigten eine Abnahme der T-Zell-vermittelten Lyse von Lymphomzellen in Abwesenheit von *Nr4a1*, ein Phänomen, das teilweise durch *Ctla4-/- OT-I*

CD8+ T-Zellen abgeschwächt wurde. Diese Ergebnisse deuten darauf hin, dass *Nr4a1* an der Modulation der T-Zell-Funktionalität beteiligt ist. Der Verlust von *Nr4a1* führte zu einer erhöhten Phosphorylierung verschiedener Kinasen, die mit Signalwegen assoziiert sind, die am Zellwachstum, der Apoptose und der Immunregulation beteiligt sind. Insgesamt unterstreichen unsere Ergebnisse die immunregulatorische Rolle von *Nr4a1* bei der Zusammensetzung des TME und der Regulation von Immun-Checkpoints in murinen Lymphomen.

ABSTRACT ENGLISH

In this first part of the thesis, the importance of studying the *CXCR4/CXCL12* axis in diffuse large B cell lymphoma (DLBCL) is highlighted. In over 20 different cancers, the CXCR4-CXCL12 axis plays a crucial role in several key processes, including survival, tumor cell proliferation, migration metastasis, and invasion. However, research on the interplay of CXCR4 and CXCL12 in DLBCL is limited and inconsistent. To close this gap, we conducted a comprehensive study of the *CXCR4-CXCL12* axis in our cohort of DLBCL patients. Additionally, we examined the impact of CXCR4 antagonists on lymphoma cell lines *in vitro*. In our study of DLBCL, we discovered a remarkable 140-fold upregulation in CXCR4 expression when compared to non-neoplastic controls. Moreover, elevated CXCR4 expression correlated with unfavorable clinical outcomes. Analysis of corresponding bone marrow biopsies revealed a correlation between *CXCL12* expression and lymphoma infiltration rate. Further, we found a decrease in *CXCR4* expression following treatment-induced remission of bone marrow involvement. In addition, we evaluated the effects of three CXCR4 antagonists in vitro: AMD3100 (Plerixafor), AMD070 (Mavorixafor), and WKI-a niacin derivative of AMD070 synthesized in our study. Notably, WK1 exhibited more potent pro-apoptotic effects compared to AMD070, inducing the expression of pro-apoptotic genes in CXCR4+ lymphoma cells. Interestingly, WK1 treatment led to decreased expression of genes associated with the ERK1/2, JNK, and NF-κB/BCR pathways. In summary, our findings indicate that the CXCR4-CXCL12 axis plays a substantial role in the development of DLBCL and presents a hopeful avenue for therapeutic intervention in aggressive lymphomas.

The second part of the thesis investigated the effect of *Nr4a1* loss/deficiency on the tumor microenvironment (TME) and the immune response in a lymphoma mouse model. Transplantation of lymphoma cells with *Nr4a1* loss into immunocompetent C57BL/6 wild-type mice resulted in increased splenic malignant B cell infiltration, decreased CD3+ T cell infiltration including subtypes of CD4+ T cells and CD8+ T cells, and an increased M2 macrophages- and Tregs-content, indicating immunosuppression and an immune cell depleted TME. Furthermore, a higher content of CD3+ T cells co-expressed of several immune checkpoint proteins in mice transplanted with lymphoma cells with *Nr4a1* loss indicated an immunodepleted, exhausted TME. Co-culture assays revealed a decrease in T cell-mediated lymphoma cell lysis in the absence of *Nr4a1*, a phenomenon partially alleviated by *Ctla4-/- OT-1* CD8+ T cells. These findings suggest Nr4a1's involvement in modulating T cell functionality. *Nr4a1*-deficiency resulted in increased phosphorylation of several kinases related with signaling pathways implicated in cell growth, apoptosis, and immune regulation. Collectively,

our findings emphasize the immunoregulatory role of *Nr4a1* in shaping the TME and immune checkpoint regulation in murine lymphomas.

1. Introduction

1.1. B cells or B lymphocytes

1.1.1. The function of B cells, their development, activation and differentiation

B cells or B lymphocytes are white blood cells and a key component of adaptive immunity and are derived from bone marrow hematopoietic stem cells. They express unique receptors (BCRs) on the surface. Each BCR is individual to a single B cell. B cells produce immune globulin (Ig), called antibodies against foreign antigens and pathogens. Additionally, B cells have various subsets that perform specific functions in innate and adaptive humoral immune responses [1,2]. Disorders in B cell development, selection, and function lead to autoimmunity, allergy, immunodeficiency, and malignancy [3].

The development of B cells is complex due to their many functions, and they undergo a series of differentiation steps. During this process, there are many changes in cell surface markers and functional properties. Immature B cells are produced prenatally in the fetal liver. Subsequently they are produced all along life in primary lymphoid tissue, the bone marrow (BM), from hematopoietic stem cells (HSCs), where early B cell development takes place. Meanwhile, HSCs differentiate into common lymphoid precursor cells (CLPs), which in turn give rise to a variety of intermediary B precursor cells from pre-pro-B cells to pro-B cells and pre-B cells. B cell precursors then undergo a series of differentiation steps leading to the expression of mature BCR capable of binding antigens. This step is completed by forming a functional and non-auto-reactive surface antigen receptor by rearranging the DNA segments encoding the heavy and light chains of immunoglobulin loci, termed VDJ recombination: V (variable), D (diversity) and J (combined), and generating a repertoire of B cell receptor genes. To prevent autoimmunity, immature naive B cells lacking a functional BCR or those that are self-reactive undergo apoptosis or programmed cell death. Immature B cells that survive the selection process become mature naïve B cells, exit the BM, and migrate to peripheral lymphoid tissues, for example spleen and lymph nodes [2,4–6]. Most naive B cells discriminate into follicular B cells and circulate between secondary lymphoid organs in search of an antigen. However, small amount of naive B lymphocytes becomes marginal zone (MZ) B cells. In the germinal centers (GCs) of secondary lymphoid organs, B lymphocytes experience further changes to their BCR. During T cell-dependent immune responses, antigen-activated B lymphocytes experience clonal expansion and selection. Somatic hypermutation (SHM) and class switch recombination (CSR) are the processes responsible for genetic modification of Ig genes. SHM randomly mutates rearranged VDJ genes to generate a diverse B cell population. CSR alters the expressed Ig isotype from IgM to IgE, IgG or IgA [7–10]. These steps allow the generation of high-affinity antibodies and effector functions that are best matched to a specific

pathogen or environment. B cells with somatic mutations and high antigen affinity undergo positive selection. Subsequently, these GC B cells discriminate into either memory B cells or plasma cells to express these modified Ig genes [2].

1.1.2. B cell dynamics in germinal centers (GC)

The gradual increase in antibody affinity over time is a hallmark of the humoral immune response. Functional B lymphocytes expressing BCR migrate from the bone marrow to secondary lymphoid tissue. When they encounter an antigen, precursor B lymphocytes in the GC are activated by interacting with CD4+ T cells in the T cell-rich area of the lymphoid organs. This leads to the differentiation of blasts, rapid clonal expansion, and the formation of a mature GC. GCs are specialized structures that emerge within secondary lymphoid organs following exposure to foreign antigens. They serve as the main site for both clonal expansion and the maturation of antibody affinity and are distinguished the presence of a light zone (LZ) and a dark zone (DZ). Each zone has different functions and cellular compositions [11,12]. The DZ is characterized by highly proliferative B cells, whereas the LZ comprises of B lymphocytes, follicular dendritic cells (FDCs), follicular helper T cells (Thf) and macrophages [13]. Inside the GC, B cells experience somatic mutations through CSR and SHM, facilitated by activation-induced cytidine deaminase (AID) acting on genes encoding their BCR. This process is followed by selection, leading to the generation of clones of B cells that have a high affinity for the antigen [9,14]. In short, the SHM process during proliferation leads to point mutations and thus variants in the variable region of the Ig gene of the immunoglobulin heavy (IgH) and immunoglobulin light (IgL) chain. This enables the selection of B cells that generate a diverse range of antibodies with enhanced affinity [15]. B cells transition from the DZ to the LZ within the germinal center, where they undergo a process of selection aimed at improving their ability to bind antigens effectively. This selection process is guided by FCDs and Thf. B cells in the LZ with unfavorable antibodies are then negatively selected, while those with more favorable BCRs are positively selected, and a small fraction are returned to the DZ and undergo CSR before re-entering the DZ. CSR alters the constant region of the IgH locus through a double-strand break (DSB)-dependent process. This mechanism is responsible for generating B cells that produce antibodies with multiple IgH effector functions, optimizing their ability to eradicate pathogens [16,17]. During affinity maturation, B cells in the DZ undergo further proliferation and SHM, resulting in B cell populations with a BCR that has an even higher affinity for the antigen. Finally, these B cells undergo maturation into long-lasting memory B lymphocytes and plasma cells [17].

1.2. Lymphoma

1.2.1. Definition of lymphomas

There are different subtypes of lymphoma known which originate from lymphoid cells and affect both lymphoid and hematopoietic tissues such as lymph nodes. However, they can also migrate to extranodal sites such as the liver and lungs [18,19]. To date, the World Health Organization (WHO) has formally categorized approximately 100 different types of lymphoid malignancies. Classification of lymphoid malignancies involves several factors. These include immunophenotype, morphology, clinical and genomic characteristics of the affected cells according to differences in cell origin and maturation state. Currently, the WHO distinguishes over 30 types of B cell lymphomas, comprising more than 50 subtypes, as of the 2023 update [20]. In the Western world, the two major subgroups of lymphoma are Hodgkin's lymphoma (HL) and non-Hodgkin's lymphoma (NHL). NHL is categorized into B cell lymphomas, which account for approximately 90% of cases, T cell lymphomas, which account for approximately 10% of cases, and natural killer (NK) cell lymphomas, which account for less than 1% of cases. Based on the growth rate of the cancer cells, NHL can also be divided into two subgroups, namely indolent (slow-growing) and aggressive (fast-growing). Indolent lymphomas are low-grade lymphomas with less aggressive features and are slow-growing NHLs that develop and spread slowly. They may not immediately require treatment but they are generally considered incurable and have a longer clinical course. In many cases, when indolent lymphoma is diagnosed early and treated appropriately, young people in early stages can show good overall survival. Nevertheless, survival outcomes may be compromised in patients who transition to a more aggressive form of lymphoma or those who respond poorly to the initial treatment [21–23]. 40% of all NHL lymphomas are indolent lymphoma. This category encompasses several types of lymphoma, including nodal marginal zone lymphoma (MZL), follicular lymphoma (grade 1-3a), small cell lymphocytic lymphoma (SLL)/chronic lymphocytic leukemia (CLL), extranodal marginal zone B cell lymphoma (MALT lymphoma), lymphoplasmacytic lymphoma, splenic marginal zone lymphoma, and Waldenström's macroglobulinemia [24].

Aggressive lymphomas, with a survival rate of 60-70%, stand as the most prevalent form of lymphoid malignancy. They include different subtypes of diffuse large B cell lymphoma (DLBCL), Burkitt's lymphoma (BL), follicular lymphoma (FL III) grade 3b, primary mediastinal (thymic) large B cell lymphoma (PMBCL), mantle cell lymphoma (MCL) and AIDS-associated lymphoma [19,20,25,26]. However, DLBCL stands out as the most common type of NHL, accounting for approximately 30% of all cases [27].

Based on data from the Austrian cancer registry, approximately 16 new cases per 100,000 individuals are diagnosed annually, leading to seven deaths per 100,000 persons. The five-year survival rate is approximately 65%. B cell lymphomas account for around 75% of all newly diagnosed cases, while T cell or NK lymphomas make up approximately 8% [28].

1.2.2. Origin and pathogenesis of B cell lymphomas

Different stages of B cell maturation, including mature B cells and memory B cells, have the potential to develop into different types of B cell lymphoma. B cell lymphomas are classified according to their proposed normal B cell pendant, which denotes the stage or subset of normal B cells from which the B cell lymphoma is believed to have emerged (shown in Figure 1). A critical feature of malignant B cells is their cell of origin, which is determined by similarities in phenotypic and gene expression profiles between malignant and normal B cells. Many B cell lymphomas have defects in the VDJ recombination process, CSR, and SHM. These processes are critical for lymphomagenesis and significantly contribute to the in the generation of diverse BCRs as well as the maturation of B cells. Subgroups of B cell NHL, such as DLBCL, exhibit highly mutated IgG genes, suggesting their origin from GC or post-GC B cells. [29,30]. The gene expression patterns seen in FL, BL, and GCB-DLBCL mirror those found in normal germinal center B cells, underscoring their lineage from B cells that have experienced germinal center reactions [31–33]. In contrast, the activated B cell-like (ABC)-DLBCL subtype appears to resemble GC cells that have undergone an arrested or aborted differentiation in the early stages of post-GC plasma cell differentiation. Moreover, many different subtypes of B cell lymphoma are characterized by chromosomal translocations involving an IgG locus and a proto-oncogene during IgG transformation [32,34].

Other transforming events implicated in the lymphomagenesis include mutations of tumor suppressor genes (such as p53), genomic amplifications, and non-Ig [35]. Apart from proto-oncogene translocations, viral infections by pathogens such as human immunodeficiency virus (HIV), human herpesvirus 8 (HSV8), human T-cell leukemia virus (HTLV) and Epstein-Barr virus (EBV) are also recognized contributors to the onset of B cell lymphoma [36]. Some types of lymphomas are dependent on BCR expression and/or signaling and utilize the survival signals from BCR expression. This event promotes malignant B cell survival, while others do not express functional BCR or express low levels [37,38]. The recognition of lymphoma cells by antigens is crucial for their survival and proliferation in different subtypes [37].

Finally, the tumor microenvironment (TME) significantly influences lymphomagenesis by supporting the proliferation and/or survial of malignant B cells. Additionally, it contributes to immune evasion and resistance to therapy [39].

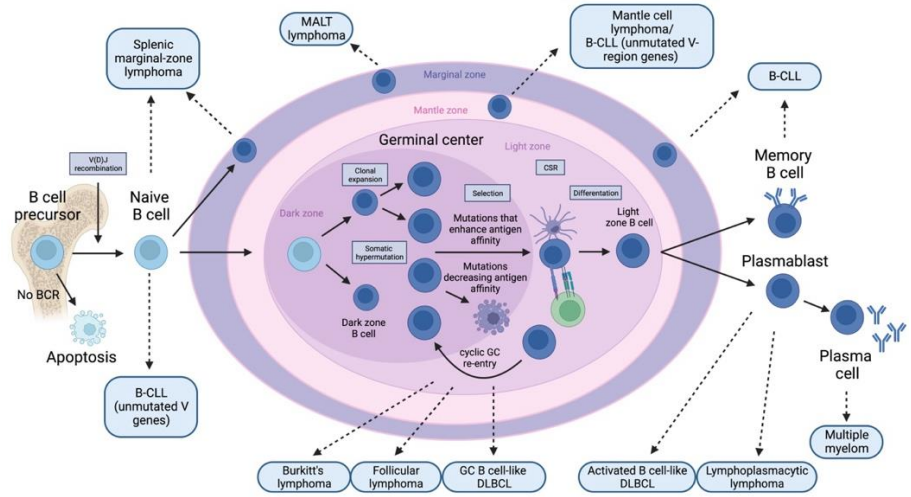

Figure 1: B cell differentiation in the germinal center (GC) and the cellular origin of B cell lymphomas. Human B cell lymphomas are assigned to the normal B-cell counterpart that is proposed for them. Most lymphomas originate from GC B cells or from B cells that have passed through the GC – adapted from Küppers et al., 2005 [25]. Created with BioRender.com

1.2.3. Diffuse large B cell lymphoma (DLBCL)

DLBCL is the most common type of B cell NHL. It accounts for 30-40% of newly diagnosed cases. DLBCL can affect patients of all ages, but it is more commonly diagnosed in older individuals, with a median age of around 70 years at presentation. The occurrence of DLBCL rises with age, being uncommon among children and young adults [40]. DLBCL can arise either *de novo* or through the transformation of indolent lymphomas, such as FL or CLL [41,42]. In recent decades, substantial advancements have been made in comprehending the biology of DLBCL, notably through the identification of genetic and molecular abnormalities that play a role in its initiation and progression. However, it remains a challenging clinical problem as up to one-third of patients fail to respond to the first-line treatment with rituximab, cyclophosphamide, doxorubicin, vincristine, and prednisone (R-CHOP), or encounter a relapse after the initial treatment. This suggests that additional research is required on this type of cancer [43].

According to gene expression profiling (GEP), DLBCL is categorized into three distinct subtypes: GCB, ABC, and primary mediastinal B cell lymphoma (PMBL) [44,45]. GCB-DLBCL generally has a more favorable clinical prognosis compared to the more aggressive ABC-DLBCL subtype [46]. GCB-DLBCL shows an expression profile with an enrichment of genes transcribed in proliferating GC B cells, including B cell lymphoma 6 (BCL-6) and CD10, and a lack of markers for post-GC differentiation. Malignant B cell clones undergo SHM and frequently exhibit CSR [32]. In contrast, the transcriptional profile of ABC-DLCBL is related to a BCR-activated B cell derived from plasma cell differentiation. GC-specific markers are downregulated, but genes involved in the plasma cell expression program are upregulated, such as XBP1, the master regulator of Ig secretion [47]. The NF-κB pathway exhibits consistent

activation and drives the transcription factor IRF4, which in turn drives plasma cell differentiation [48–50].

1.2.4. DLBCL-associated genetic lesions

While some genetic alternations such as chromosomal changes, abnormal transcriptional regulation and different intracellular signaling pathways are common to all subgroups of DLBCL associated with a particular subtype of DLBCL, others are preferentially or even exclusively present. Alterations in chromatin modifiers are found in 30% of DLBCL cases. Common structural alterations are responsible for the inactivation of two closely related histone and non-histone acetyltransferases, E1A-binding protein p300 (EP300) and CREB-binding protein (CREBBP). Altered CREBBP/EP300 proteins are responsible for the constitutive expression of BCL-6 and reduced levels of the tumor suppressor p53 due to inadequate acetylation of both proteins [51,52]. Nevertheless, a prevalent genetic anomaly associated with BNHL is another chromatin remodeling protein, histone methyltransferase (MLL2), also referred to as KMT2D. It is present in approximately one-third of DLBCL patients and in over 80% of FL patients [53]. BCL-6 is a proto-oncogene primarily found in GC B cells. It exerts negative regulation over various biological processes and serves as a central regulator in the formation of GCs. However, overexpression of this gene is a primary mechanism for malignant transformation of B cells [54]. However, the activity of BCL-6 is directly or indirectly deregulated by various genetic alterations in both molecular subtypes of DLBCL in approximately 30% of all cases. Overexpression of BCL-6 can be caused by chromosomal translocations, point mutations and epigenetic mutations that negatively impact the DNA damage response, cell cycle progression and arrest and therefore the activation of B cells that contribute to lymphomagenesis. BCL-6 overexpression can also be caused by several indirect mechanisms, including gain-of-function mutations in myocyte enhancer binding factor 2B (MEF2B), a positive regulator, and/or by inactivating of F-box protein 11 (FBXO11), which is involved for the ubiquitination and degradation of BCL-6 [52].

DLBCL frequently downregulates the cell surface receptors major histocompatibility complex class I and II (MHC I/II) to evade immune surveillance. In 40-60% of DLBCL cases there is a loss of MHC I, in 40-50% of cases there is a loss of MHC II, and in approximately 20% of cases there is a simultaneous loss of both molecules. Recurrent mutations in the HLA genes β_2-microglobulin (B2M), guanine nucleotide-binding protein subunit alpha-13 **(**GNA13), enhancer of zeste homolog 2 (EZH2), MEF2B, and phosphatase and tensin homolog (PTEN) loss are associated with MHC loss and support the molecular definition of immune evasion in DLBCL [55–59].

Finally, cytogenetic alterations affecting genes responsible for programmed death ligands (PD-Ls) have been reported in several types of BNHL, such as PMBCL (12%) and HL

(3%), and have also been found in DLBCL-NOS (not otherwise specified) subtypes (4%) [60,61]. Approximately 20% of DLBCL patients display elevated levels of PD-L1, while PD-L2 remains unaffected, primarily due to genetic aberrations affecting 9p24.1 gene locus. This contributes to the pathogenesis of DLBCL [60,62–65].

1.2.5. GCB-DLBCL-associated genetic lesions

The t(14;18) translocation affecting the *BCL-2* gene is identified in 30% of GCB-DLBCL patients. This translocation leads to the abnormal expression of BCL-2 as the coding exon of *BCL-2* becomes regulated by the IG locus. BCL-2 serves as a crucial anti-apoptotic protein expressed in numerous tissues, except for the GC [66]. BCL-2 overexpression in combination with MYC overexpression has been linked with a poorer clinical outcome to the presence of either one alone. This is likely due to the interplay between the two proteins MYC and BCL-2 in promoting tumor growth and survival. MYC functions as a transcription factor involved in diverse biological processes, including proliferation, differentiation, and apoptosis. Under normal conditions, MYC transcription in GC B cells is repressed by BCL-6. In 10-14% of GCB-DLCBL cases, MYC exhibits ectopic and constitutive expression as a result of a chromosomal translocation that connects its coding domain to the Ig-chain loci. This translocation is also correlated with poorer clinical outcomes in these patients [67]. The combination of chromosomal translocations of MYC and BCL-2 or, less commonly, BCL-6 is called double-hit lymphoma (DHL) or, with three concurrent translocations, triple-hit lymphoma (THL) and is found in 5-10% of DLBCL cases [68].

In 22% of GCB-DLBCL cases, mutations are detected in the *EZH2* gene, which plays a role in histone modification. Activation of EZH2 by BCL-6 promotes gain-of-function epigenetic alterations. EZH2 functions as a histone methyltransferase and is prominently expressed in GC B cells. It regulates the repression of genes involved in proliferation checkpoints and transiently suppresses the differentiation of GC B cells [69]. In addition, 15-33% of GCB-DLBCL cases have a mutation in GNA13, the gene encoding Gα13 (an alpha subunit of G protein). Gα13 signaling serves distinct functions and is crucial for the localization of GC B cells. Disruption of Gα13 signaling, caused by mutations in GNA13 and other associated genes within this pathway, appears to play a role in the development of lymphomas. [70–72]. Tumor necrosis factor receptor superfamily member 14 (TNFRSF14), also known as herpesvirus entry mediator (HVEM), acts as a tumor suppressor in DLBCL. Deletions and mutations in TNFRSF14 are detected in 30% of patients diagnosed with GCB-DLBCL. These alterations result in the loss of TNFRSF14 expression on the surface of lymphoma cells, promoting the activation of B cell proliferation and fostering the lymphomagenesis of GCB-DLBCL [73,74].

1.2.6. ABC-DLBCL-associated genetic lesions

In ABC-DLBCL, the NF-κB pathway is consistently activated downstream of BCR and TLR, frequently attributed to genetic activation of the BCR pathway. Mutations in caspase recruitment domain-containing protein 11 (CARD11), CD79B and myeloid differentiation primary response 88 (MYD88) lead to the activation of distinct components within the BCR pathway. Gain-of-function mutations in CD79B and, rarely, CD79A are found in 21% of cases and affect the downstream BCR signaling pathway. These mutations increase BCR surface expression and attenuate the inhibition of BCR signaling. In 10-15% of cases, missense mutations affect the gene encoding CARD11, serving as another intermediary between antigen stimulation and the NF-κB pathway. This results in the persistent activation of NF-κB and increased NF-κB activity upon stimulation of the antigen receptor [75]. The gain-of-function driver mutation, MYD88 L265P substitution, is present in nearly 30% of ABC-DLBCL cases. It enhances cell survival by activating NF-κB [76]. An additional mutation affecting the NF-κB pathway involves the A20 gene, which acts as a negative regulator of NF-κB signaling triggered by toll-like receptor (TLR) and BCR activation. Biallelic truncating mutations and/or deletions in the A20 gene result in its inactivation and are observed in approximately 30% of ABC-DLBCL cases [77,78].

Genetic mutations also hinder the terminal differentiation of B cells. Approximately 25% of cases exhibit biallelic loss-of-function mutations or deletions in PR domain zinc finger protein 1 (PRDM1)/B lymphocyte-induced maturation protein-1 (BLIMP1), leading to BLIMP1 inactivation. BLIMP1 plays a critical role in the terminal differentiation of GC B cells into plasma cells by repressing the expression of key GC master genes like Paired box protein Pax-5 (PAX5) and BCL-6 [79].

1.2.7. Follicular lymphoma (FL)

FL is considered an incurable malignancy and ranks as the third most prevalent form of lymphoma, constituting 20-35% of all NHL cases. The clinical behavior of FL is characterized by high unpredictability. It can range from an indolent, slowly progressing disease to an aggressive form with rapid progression. Transformation of an indolent FL into a more aggressive lymphoma, such as DLBCL (transformed FL), occurs in 30-50% of patients and is associated with poorer clinical outcomes and reduced survival rates. FL can be categorized into three grades based on the proportion of centroblasts (0.5-5 = grade 1, 6-15 = grade 2, >15 = grade 3). Grade 3 can be subdivided into a (centroblasts still present - similar to FL grade 1-2) and b (sheets of centroblasts - clinical course more similar to DLBCL). A higher number of centroblasts is considered to be more aggressive and the likelihood of transformation to DLBCL is higher [80,81].

FLs arise from clonal proliferation of neoplastic follicle center cells of intact GCs exhibiting active somatic hypermutation. During the early stages of B cell development, a VDJ recombination error can cause a BCL-2 t(14;18) (q32:q21) translocation, leading to the *BCL-2* gene being overexpressed constitutively. B cells harboring this t(14;18) mutation and displaying ectopic expression of BCL-2 trigger an anti-apoptotic program, thereby promoting the survival of malignant B cells. They can enter GCs and proliferate. After leaving the GC, FL-like B cells traffic and acquire further genetic changes to progress to the full malignant phenotype [82]. BCL-2 translocation is found in 85% of cases, but this overexpression is not sufficient to promote lymphomagenesis and further genetic events are required. However, genetic and epigenetic as well as microenvironmental factors appear to play important roles in developing FL [33,83–86].

1.2.8. Burkitt lymphoma (BL)

Burkitt's lymphoma is an extremely aggressive B cell malignancy originating from GC or post-GC B cells and is characterized by the continuous expression of MYC due to chromosomal translocation. The incidence of this occurrence can peak at any age, yet it is predominantly prevalent during the initial decade of one's lifespan. Three BL subtypes are described according to distinct epidemiology, risk factors and clinical presentations. Sporadic BL (sBL) occurs in 20-30% of pediatric lymphoma patients and is observed in the United States and Western Europe. In adults, sporadic Burkitt's lymphoma (sBL) accounts for around 1% of NHL cases in the United States. Endemic Burkitt's lymphoma is notably prevalent among pediatric patients in equatorial regions of Africa and South America and is linked to endemic malaria. Additionally, it exhibits a strong association with Epstein-Barr virus (EBV), implying a direct involvement of the virus in lymphomagenesis [87,88]. The third subtype of Burkitt's lymphoma, termed immunodeficiency-associated BL, is frequently detected in individuals living with HIV. It is also present in recipients of allografts and in patients with congenital immunodeficiency [89]. Lymphomagenesis in BL is driven by chromosomal rearrangements involving the *c-MYC* oncogene on chromosome 8q24 and one of the IG genes, leading to elevated levels of the MYC transcription factor. The most prevalent translocation observed is t(8;14)(q24;q32). The translocation results in the fusion of c-MYC on chromosome 8 with the IgH locus on chromosome 14, leading to the formation of IgH/MYC [90]. Less common are translocations of MYC involving the light chain chromosomes 8 (t(2;8)(p11;q24)) or 22 ((8;22)(q24;q11)). The molecular consequence is the constitutive activation and overexpression of the MYC oncogene [91]. Apart from MYC rearrangements, somatic single nucleotide variants, deletions and insertions of the ID3-TCF3-CCDND3 pathway re prevalent genetic occurrences in BL. These alterations account for about 90% of cases in children but are notably less frequent in adult BL [92].

1.3. Chemokines and chemokine receptors

Chemokines, which are small soluble signaling proteins secreted by cells, serve as guides for immune cells as they navigate through tissues. Weighing approximately 8-10 kDa, these cytokines are pivotal in triggering and advancing numerous pathological conditions, including cancer, infections, inflammation, autoimmune diseases, and degenerative disorders of the nervous system. Various cell types, such as immune cells, epithelial cells, and stroma cells, release chemokines. The structure of a chemokine typically consists of a short N-terminal region, three-stranded β-chains, and an α-helix [93].

Chemokines are categorized into four subfamilies: C, CC, CXCR, and CX3C. This categorization is based on the arrangement of conserved cysteine near the N-terminus. In this classification system, 'C' represents cysteine and 'X' represents any other amino acid, while 'X3' signifies three consecutive amino acids between two cysteines. Normally, chemokines bind on specific cell surface chemokine receptors of target cells to initiate an intracellular signaling cascade that triggers many cellular responses like chemotaxis, adhesion, activation and even cell proliferation [94].

Chemokine receptors are members of the G protein-coupled receptor (GPCR) superfamily composed of seven α-helices spanning the membrane with an intracellular C-terminus and extracellular N-terminus. The seven transmembrane helices are linked by three extracellular and three intracellular loops [94]. Each chemokine can typically bind to one or more specific chemokine receptors, and conversely, each chemokine receptor can bind to multiple chemokines. These chemokine-chemokine receptor interactions enables the control of complex cellular responses. When chemokines attach to their receptors, it triggers the release of free heterotrimeric G proteins (Gα, Gβ, and Gγ subunits) into the cytoplasm. These G proteins then undergo a transformation, where guanosine diphosphate (GDP) is replaced by guanosine triphosphate (GTP), resulting in an α monomer and a βγ dimer. These, in turn, activate several intracellular signaling pathways and downstream effectors that promote a number of biological events involved in proliferation, apoptosis, cell survival and migration [95].

1.3.1. The role of CXCR4/CXCL12 axis in B cell lymphomas

CXCL12 (or SDF-1), is secreted by stromal cells in BM and secondary lymphoid tissues, serving as survival and growth factor. CXCL12 binds to C-X-C chemokine receptor 4 (CXCR4) and C-X-C chemokine receptor 7 (CXCR7). Notably, CXCL12 and CXCL14 are the exclusive chemokines that attach to CXCR4. CXCR4 is found on the surface of many hematopoietic cells, including B cell precursors, B lymphocytes, monocytes/macrophages, neutrophils, blood-derived dendritic cells, CD34+ progenitors from BM and blood, Langerhans cells, macrophages, and immature and mature T cells in the thymus [96].

The CXCR4/CXCL12 axis promotes the retention of B cell precursors in the bone marrow microenvironment, where they mature and undergo selection. Regulation of B cell retention in the bone marrow involves dynamic interactions between the chemokine receptor CXCR4 and its ligand CXCL12. Pro-B cells expressing high levels of CXCR4 migrate to the bone marrow, where stromal cells produce CXCL12. During B cell maturation, CXCR4 expression is downregulated, allowing mature B cells to migrate away from CXCL12-rich niches [97,98].

The CXCL12/CXCR4 axis exerts a considerable influence on cancer cells through two distinct pathways. First, autocrine effects stimulate processes that contribute to tumor growth, metastasis and angiogenesis. Second, indirect effects emerge, including the migration of malignant cells expressing CXCR4 towards non-malignant stromal cells producing CXCL12, or the mobilization of CXCR4-positive stromal cells towards the tumor microenvironment. [96,99,100].

Upon engagement of CXCL12 and CXCR4, numerous signaling pathways are activated, including protein kinase B mitogen-activated protein kinase (MAPK), phosphoinositide 3-kinase (PI3K)/Akt/mTOR, Wnt and epidermal growth factor receptor (EGFR) pathways and NF-κB. These activations contribute to tumor cell growth, migration, and invasion. Briefly, the activation of CXCL12/CXCR4 leads to phosphorylation of EGFR. CXCL12/CXCR4 activation stimulates the extracellular signal-regulated kinases (ERK1/2) and Akt, which are linked to cell proliferation signals in malignant cells. Via a positive feedback loop, CXCL12/CXCR4 can activate the Ras and MAPK pathways, resulting in the upregulation of several transcription factors like c-MYC. These factors promote CXCR4 expression and drive tumor cell proliferation The PI3K/Akt and Wnt pathways are also modulated by the CXCL12/CXCR4 axis. Additionally, CXCL12/CXCR4 inhibits tumor cell apoptosis by activating the NF-κB pathway and augmenting the expression of the anti-apoptotic gene *BCL-2*. BCL-2 is directly targeted by the pro-apoptotic protein BAD or indirectly through the activation of the transcription factor cAMP response element-binding protein (CREB) [96].

Despite their significance, the prognostic implications and functional mechanisms of CXCR4 expression in malignant lymphomas remain incompletely understood. In leukemia, CXCR4 expression correlates with shorter disease-free survival, and leukemic blasts expressing CXCR4 are prone to localize in normally restricted bone marrow niches, conferring protection against chemotherapy-induced apoptosis [101,102]. CXCR4 expression has been identified in both the nucleus and cytoplasm of lymphoma cells among patients diagnosed with primary central nervous system (CNS) lymphoma. Notably, strong nuclear CXCR4 expression is primarily observed in nodal DLBCL cases, which is linked with bone marrow infiltration of the lymphoma and signifies a poorer prognosis in terms of survival [103–105]. In addition, the elevated expression of CXCR4 has been identified as a predictive factor for DLBCL [106,107].

1.3.2. The CXCR4/CXCL12 axis as therapeutic target

Therapeutic reagents for blocking of CXCR4 receptors, AMD3100 (AMD acronym for AnorMeD), also known as plerixafor, and AMD070, also known as Mavorixafor, have been demonstrated to be potent and selective inhibitors of CXCR4. So far, AMD3100 represents a novel and promising therapeutic strategy for addressing a range of refractory diseases. Bone marrow stromal cells produce CXCL12, a key factor facilitating the homing of HSCs to the bone marrow. Inhibiting its receptor CXCR4 with AMD3100 leads to the mobilization of HSCs from the bone marrow into the peripheral blood [108–110]. However, AMD070 affects the migration, proliferation, and cancer cell survival mediated by CXCL12 and the modulation of the MAPK signaling pathway [111,112]. Currently, both antagonists, AMD3100 and AMD070, are under investigation in numerous clinical trials for cancer treatment. AMD3100 has demonstrated efficacy in mobilizing bone marrow stem cells for autologous transplant in individuals with leukemias and lymphomas, offering a favorable side effect profile compared to alternative compounds [113].

1.4. NR4As family

The NR4A family consists of three members: NR4A1 (Nur77/NGFI-B), NR4A2 (Nurr1), and NR4A3 (Nor-1) (114). These receptors function as transcription factors without an endogenous ligand and are members of the steroid hormone receptor superfamily. All three family members share a similar structural organization (Figure 2).

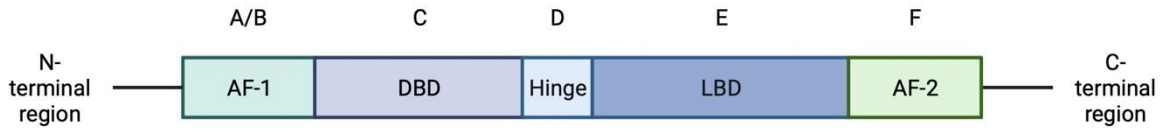

Figure 2: Arragement of the NR4A nuclear orphan receptor domain. The NR4A nuclear orphan receptor domain is characterized by several components. At the beginning, the N-terminal region (A/B) includes AF-1 (amino-terminal region 1), responsible for activation function 1. This is followed by the DNA binding domain (DBD), a hinge region (D), and the ligand binding domain (LBD). Finally, in the C-terminal region, there is AF-2 (amino-terminal region 2), which encodes a dispensable activation function 2 domain. – adapted from Safe et al., 2021 [114]. Created with BioRender.com

The activation function 1 (AF-1) domain, essential for recruiting additional transcription factors and initiating transcriptional activity, resides in the N-terminal region. Within the NR4A superfamily, both the DNA binding domain (DBD) and the ligand binding domain (LBD) exhibit considerable similarity in amino acid sequence, with around 91-95% likeness in the DBD and approximately 60% in the LBD. Conversely, AF-1 displays notable divergence, serving a pivotal role in NR4A transactivation. Despite this divergence, the three members share overlapping and complementary biological functions owing to their sequence and structural

homology [115]. NR4A receptors have a nuclear localization signal on their DBD and are therefore located in the nucleus. The DBD, which consists of two zinc fingers, guides the receptor to a specific DNA sequence. Upon reaching this sequence, the receptor can bind either as a monomer to the consensus sequence known as the NGFI-B response element (NBRE; AAAGGTCA) or as a homo- or heterodimer to Nur response elements (NurREs; TGATATTTn6AAATGCCA) found in the promoter sequences of its downstream target genes. NR4A1 and NR4A2 receptors have the capability to form heterodimers with the retinoid X receptor (RXR) and subsequently bind to a direct repeat with a 5-bp length spacer (DR5) motif. This process serves as a mechanism by which NR4A receptors can effectively regulate multiple target genes *in vivo* [116,117].

NR4A1 is classified as an immediate early gene and its expression is swiftly triggered in response to a range of stimuli such as peptide hormones, growth factors, inflammatory and physiological stimuli, cytokines, and cellular stress in a variety of tissues and cultured cells. The functioning of NR4A receptors is chiefly governed by receptor expression, aligning with their designation as immediate-early genes, alongside post-translational modifications and proteasome-mediated degradation [116].

Though no naturally occurring ligand has been discovered, various exogenous compounds have been recognized for their ability to interact with NR4A1, acting either as agonists or antagonists. Among these are cytosporin B (Csn-B) and celastrol [118–120]. Furthermore, their expression can be promptly induced by diverse cellular signaling pathways, including T cell receptor (TCR) signaling in T cells, G protein-coupled receptors (GPCRs), mechanical stress, protein kinase receptors, and cyclic AMP activation [121,122].

NR4As oversee a broad spectrum of physiological processes, encompassing metabolism, vascular homeostasis, cardiovascular and neurological functions. They also hold a pivotal role in orchestrating immune cell homeostasis during inflammatory and cancer-related responses. Their influence extends through the direct activation or repression of transcriptional targets [123]. NR4A1 can also translocate from the nucleus to the mitochondria or endoplasmic reticulum (ER) to induce autophagy and/or apoptosis, thereby exerting non-genomic functions that influence cell biological processes [124,125].

1.4.1. NR4As in malignancies

NR4As have been shown to perform various functions in different cell types, such as DNA repair, apoptosis, proliferation, cellular stress response, autophagy, neuronal signaling, endocrinology as well as hematopoietic, immune and metabolic processes. Hence, dysregulation of these receptors is associated with the initiation and advancement of diverse diseases, spanning from obesity, allergies, and atherosclerosis to inflammation and cancer. Among the Nur77-family genes, *NR4A1*, extensively studied, plays multifaceted roles in

tumorigenesis [126]. Blood-related malignancies, such as leukemias and lymphomas, show diminished levels of NR4A gene expression level. Specifically, NR4A1 and NR4A3 are known as dominant tumor suppressors in acute myeloid leukemia (AML). Simultaneous knockout of the *Nr4a1* and *Nr4a3* genes, AML develops quickly, resulting in a lifespan of only 3-4 weeks. These findings strongly indicate that the NR4A1 and NR4A3 receptors possess significant tumor suppressor capabilities in AML. Leukemic blasts from patients with AML showing decreased or undetectable levels of NR4A1 and NR4A3. Similar observations have been made in cell lines derived from different leukemia types [127]. Hypoallelic mice with reduced expression of *Nr4a1* and *Nr4a3* (*Nr4a1*+/- and *Nr4a3*-/-; *Nr4a1*-/- and *Nr4a3*+/-) develop a chronic myeloid malignancy. This condition can lead to the development of myelodysplastic/myeloproliferative neoplasms (MDS/MPN) and more rarely to AML [128].

In aggressive lymphoma patients, reduced levels of NR4A1 and NR4A3 were linked to poorer overall survival in FL and DLBCL. DLBCL patients with elevated NR4A3 expression tend to respond positively to R-CHOP treatment, leading to better outcomes compared to those with poor responses or anticipated resistance to therapy. Its ectopic overexpression triggers apoptosis in lymphoma cell lines and inhibits lymphoma formation by upregulation of pro-apoptotic genes such as *Puma*, *Trail*, *Bim* and *Bak* [129,130]. Furthermore, an increase in cytoplasmic NR4A1 levels correlate with enhanced survival rates in GCB-DLBCL [131].

NR4A1 has been extensively studied in malignancies compared to NR4A2 or NR4A3. While NR4A1 has demonstrated pro-oncogenic properties in solid tumors, its role in blood cancers exhibits significant differences, showing tumor suppressor-like behavior. This is in contrast to its oncogenic-like activity when combined with NR4A2 in solid malignancies [114].

1.5. The *EμMyc* lymphoma mouse model

The *EμMyc* transgenic mice were developed to mimic lymphoid tumors by incorporating the *Myc* translocation. In these transgenic mice, a normal *Myc* gene was isolated and linked to the *Eμ* promotor, a promotor in the IgH. Consequently, the genetically modified mice express the transgene exclusively in B lymphocytes, resulting in B cell proliferation compared to normal non-transgenic B cells. During the prenatal stage, mice experience a proliferation of polyclonal pre-B cells. As they grow, they develop malignant monoclonal B cell lymphomas, typically emerging after a delay of 12 to 16 weeks. In addition, 90% of these mice develop leukemia/lymphoma originating from B cells within the initial six months of their lifespan [132–134]. Indeed, consistent observations indicate the occurrence of immature (pre-B) and occasionally mature B cell lymphomas in *EμMyc* mice. Notably, Significantly, the majority of lymphomas detected in *EμMyc* mice are located in the pre-B and immature B cell phases. Pathologically, these mice exhibit disseminated lymphomas, as evidenced by enlarged spleens and lymph nodes, which can be detected prior to disease onset [133].

Despite its role as a proto-oncogene, the transformation-inducing effects of c-Myc are typically counteracted by two mechanisms that serve as a safety guard against *EμMyc*–induced lymphomagenesis. One mechanism involves the p53 accumulation facilitated by the p19 ADP ribosylation factor ($p19^{ARF}$)-murine double minute 2 (Mdm2)-p53 pathway to activate apoptosis and senescence. The other mechanism implicates the suppression of anti-apoptotic genes like *Bcl-2* and *B cell lymphoma extra large* (*Bcl-XL*), also resulting in stimulation of apoptosis. Hence, *EμMyc* mice require further genetic alterations to undergo malignant transformation, known as "2^{nd} hit", by interfering with or disrupting these pathways. Mutations that inactivate the *$p19^{ARF}$-Mdm2-p53* signaling pathway [135] or overexpression of *Bcl-2*, *Bcl-XL*, and *myeloid cell leukemia 1 (Mcl-1)* are involved in lymphomagenesis [136–138].

1.6. Tumor microenvironment in lymphoma

The biology and clinical behavior of aggressive lymphomas are influenced not only by intrinsic lymphoma cell characteristics, but also by interactions with the lymphoma tumor microenvironment (TME).

The TME can be categorized into two components: the immune microenvironment and the non-immune microenvironment (Figure 3). Within the innate immune system, various types of cells are present, for example mast cells, neutrophils, eosinophils, macrophages, dendritic cells (DCs), and natural killer (NK) cells (as described in Figure 4). T and B cells are part of the adaptive immune system (as described in Figure 5 and Figure 6). The non-immune microenvironment is predominantly constituted by stromal cells like mesenchymal stromal cells, extracellular matrix (ECM), pericytes, cancer-associated fibroblasts (CAFs), and additional secreted molecules such as extracellular vesicles, cytokines, growth factors, and chemokines. Pansy *et al*. reviewed the composition and function of the TME in detail [139].

Collectively, these cells work together to create an immunosuppressive environment within tumors which helps the tumor evade the immune system, aiding the tumor in evading immune detection while also exerting significant influence over the anti-tumor immune response. Extrinsic stimuli from the TME and ECM are critical for tumorigenesis, progression and therapeutic response within the lymphoma niche. Critically, the critical interplay between stromal cells and immune cells within the TME enables malignant B cells to evade the host's anti-tumor immune response by activating poorly elucidated mechanisms of immune evasion. [39,139].

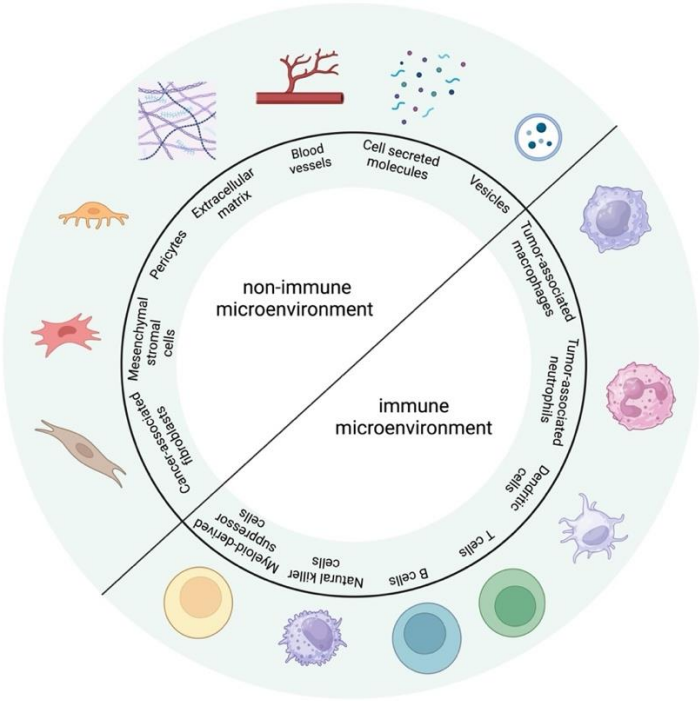

Figure 3: Composition of the tumor microenvironment (TME) in lymphomas. The TME is divided into two components: the immune and non-immune microenvironments. The immune microenvironment is composed of cells of both the innate and adaptive immune systems. Innate immune cells include neutrophils, eosinophils, macrophages, dendritic cells (DCs), mast cells, and natural killer (NK) cells. The adaptive immune system includes T and B cells. The non-immune microenvironment is mainly made up of elements like the mesenchymal stromal cells, pericytes, ECM, CAFs, and various secreted molecules like extracellular vesicles, cytokines, growth factors, chemokines. Created with BioRender.com

The composition of the TME in DLBCL is defined by the complex interplay between lymphoma cells, which typically represent 60-80% of the cellular content, and the various host immune cell populations. Among these are around 20% of NK cells, roughly 15% of DCs, about 15% of M2-type macrophages, approximately 10% of CD4+ T cells, and fewer than 5% of CD8+ T cells [140]. Significant disparities exist in the composition and reliance of immune cells on the TME across different B cell lymphoma types. Although the TME exhibits a modified composition, it still plays a pivotal role in impacting the survival outcomes of patients with DLBCL, along with influencing their response to treatment and the progression or recurrence of the disease [141].

Cell Type	Marker	Production	Function
 Macrophages	CD14+ CD16+ CD64+ CD68+ CD80+ (M1) CD206+ (M2)	M1: IL-12 IL-23 TNF-α M2: IL-10 TGF-β	Macrophages, derived from monocytes, are essential components of host defense against pathogens. They play a pivotal role in stimulating the adaptive immune system by acting as antigen-presenting cells (APCs) and contributing to tissue remodeling. When exposed to Th1 cytokines such as IFN-γ and/or lipopolysaccharide (LPS), macrophages adopt the M1 phenotype, leading to the secretion of pro-inflammatory cytokines. Conversely, activation by Th2 cytokines like IL-4, IL-10, and IL-2 prompts macrophages to assume the M2 phenotype, resulting in the production of anti-inflammatory factors. Malignant conditions: Tumor-associated macrophages (TAMs) have various roles in tumor progression, including metastasis, tumor cell proliferation, invasion, angiogenesis, and the supression of T cell-mediated anti-tumor immune responses. TAMs exhibit characteristics of both M1 and M2 phenotypes, demonstrating a spectrum of differentiation states. This contributes to the complex dynamics within the tumor microenvironment.
 Neutrophils	CD11b+ CD15+ CD16+ CD62L+ CD66b+	N1: ICAM1 TNF-α N2: VEGF MMP9	Neutrophils are essential cells in the innate immune system, serving as the first line of defense against infections, injuries, and pathogenic challenges. Malignant conditions: Tumor-associated neutrophils (TANs) can exhibit either anti-tumor properties as N1 TANs, by mediating cytotoxicity, or pro-tumor effects as N2 TANs, by secreting angiogenesis and invasion-promoting factors.
 Eosinophils	Siglec8+ CD193+ CD11b+ CD14- CD62L+	TNF-α granzyme IL-18	Eosinophils play a central role in managing parasitic infections, as well as combating bacterial and viral pathogens. Additionally, they are integral in inflammatory responses and allergic processes. Malignant conditions: Eosinophils can exert anti-tumorigenic or pro-tumorigenic functions in various types of tumors. These functions are mediated by the secretion of either anti-tumorigenic or pro-tumorigenic molecules, depending on the specific milieu.
 Mast cells	CD117+ CD203+	VEGF FGF-2	Mast cells are a crucial myeloid part of the immune system and play an important role in the innate immune response as well as in the acquired immune response. Malignant conditions: Tumor-associated mast cells (TAMCs) have the potential to promote tumor growth by releasing factors that facilitate growth and angiogenesis. However, in specific cancer contexts, TAMCs can induce tumor cell apoptosis through the release of interleukin-4 (IL-4) and tumor necrosis factor-alpha (TNF-α).
 Myeloid-derived suppressor cells (MDSCs)	CD11b+ CD33+ CD14+ CD15+ CD16+ HLA- DR-	NO ROS iNOS Arginase1 PD-L1 MMP9	MDSCs are a heterogeneous population of immature immune cells derived from the myeloid compartment. They play an essential role in negatively regulating immune responses. Malignant conditions: MDSCs are induced by GM-CSF, VEGF, and IL-6, which are primarily produced by tumor cells. They can manipulate the inflammatory microenvironment via amino acid depletion and/or expression of immunoinhibitory ligands to suppress T cell effector function.
 Dendritic cells (DCs)	HLA- DR^{+} $lineage^{-}$	IFNs	DCs are crucial for coordinating the immune response and play a central role in immunity. Their primary functions include endocytosis, antigen presentation, and production of interferon (IFN). Malignant conditions: DCs are crucial in promoting and sustaining anti-tumor immunity. However, their antigen-presenting function may be inefficient in the TME. DCs possess the capability to differentiate into regulatory DCs that exhibit immunosuppressive properties, thereby restricting T cell activity.
 NK cells	CD3- CD56+	GM-CSF IL-5 IL-8 IL-10 IL-13 CCL2 CCL3 CCL4 CCL5 CXCL10	NK cells are a type of innate lymphoid cell that have both cytotoxic and cytokine-producing effector functions. They are able to distinguish between target cells, such as virus-infected or malignant cells, and healthy cells based on their various cell surface receptors, which include both activating and inhibitory receptors. NK cell receptors recognize a range of ligands, including stress-induced self-ligands, infectious non-self-ligands, and TLR ligands, leading to the production of interferon-gamma (IFN-γ) and exertion of cytotoxicity. Tolerance to self-ligands is maintained through the interaction between inhibitory receptors and MHC class I molecules. Additionally, NK cells express the low-affinity Fc receptor CD16, enabling them to engage in antibody-dependent cellular cytotoxicity (ADCC). NK cells also play a crucial role in coordinating adaptive immune responses by secreting interleukin (IL).Human NK cells can be categorized into two main subgroups based on their functions and surface markers. Cytotoxic NK cells are identified as $CD^{56dim}CD^{16hi}$, while immunomodulatory and cytokine-producing NK cells are identified as $CD^{56bright}CD^{16lo}$. Malignant condition: NK cells are able to directly mediate the lysis of tumor cells. They also control T cell-mediated anti-tumor immune responses by the secretion of IL and are involved in ADCC.

Figure 4: Cells of the innate immune system present in TME. – adapted from Pansy *et al*., 2021 [139]. Created with BioRender.com

Cell Type	Marker	Production	Function
 B cells	CD19+ CD20+	various cytokines	B cells serve as pivotal contributors to humoral immunity by generating antibodies (Abs). They detect antigens via the BCR, comprised of membrane-bound antibodies. B cells are categorized into distinct subsets: (1) B1 B cells, primarily residing in the peritoneal and pleural cavities; (2) B2 or follicular (FO) B cells, situated in lymph nodes; and (3) marginal zone B cells, found within the marginal sinus of the spleen. These diverse subsets undergo activation via T cell-dependent or -independent mechanisms. Reactive conditions: The process of B cell activation commences upon binding of the B cell to an antigen via its BCR. This activation triggers proliferation and differentiation, leading to the formation of plasma B cells. They are tasked with generating and secreting antibodies, thus playing a central role in the immune response. Malignant conditions: B cells play multifaceted roles in the immune response against tumors. They can participate in presenting tumor-specific antigens to T cells, producing tumor-specific antibodies, and modulating the immune system's activity through regulatory functions as regulatory B cells (Bregs).
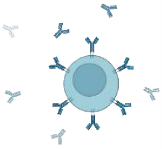 Ab-producing B cells	CD19+ CD20+	tumor-specific IgG and IgA	Reactive conditions: During viral and/or bacterial infections, as well as autoimmune diseases, B cells play a crucial role by secreting antibodies (Abs), thus initiating a targeted and specific immune response. Malignant conditions: By triggering the complement cascade, facilitating phagocytosis by macrophages, and enhancing the tumor-killing activity of NK cells, the antibody production mediated by B cells can effectively lead to the elimination of tumor cells.
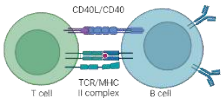 B cells as APCs	CD19+ CD20+ CD21+ CD23+ CD27− IgG1+ CD40+ CD80+ CD86+ MHC class II+	IL-2 IL-6 CCL3 CCL4 ICAM1 GM-CSF	Reactive conditions: B cells possess the capability to detect antigens during inflammatory processes in a T cell-independent manner. Additionally, they serve the function of presenting these antigens via their MHC class II surface molecules, thereby eliciting T cell responses. Malignant conditions: In several types of cancer, B cells are often found in proximity to T cells, even in the absence of DCs. These B cells function as APCs for CD4+ T cells. There exist two distinct forms of these B cells, each contributing to either anti-tumor immune responses or the establishment of an immunosuppressive intratumoral environment: (1) activated B cells (identified by markers CD69+, HLA-DR+, CD27+, CD21+), which possess Th1 T-cell activating capabilities, promoting anti-tumor immune responses; and (2) exhausted B cells (identified by markers CD69+, HLA-DR+, CD27-, CD21-), which contribute to the generation of regulatory T cells (Tregs), thus fostering an immunosuppressive condition.
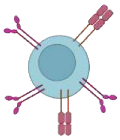 Bregs	IL-10 IL-35 TGF-β	IL-2 IL-12 IFN-γ TNF-α	Reactive conditions: In autoimmune diseases, such as systemic lupus erythematosus (SLE) and multiple sclerosis, Bregs are primarily involved in mediating immune tolerance. Malignant conditions: Bregs exhibit a tumor-promoting function by orchestrating various immunosuppressive mechanisms. They suppress the proliferation of CD4+ T cells and promote the expression of the immunosuppressive marker forkhead box P3 (FOXP3) in Tregs through the secretion of IL-10 and TGF-β. Moreover, Bregs can dampen the effector function of CD8+ T cells via IL-10. Additionally, through the secretion of IL-10, IL-35, and TGF-β, Bregs induce the expression of the immunoinhibitory receptor programmed cell death ligand 1 (PD-L1) on cancer cells, further contributing to immune evasion within the tumor microenvironment.

Figure 5: Subsets of B cells from the adaptive immune system found within the TME. – adapted from Pansy *et al*., 2021 [139]. Created with BioRender.com

	Cell Type	Marker	Production	Function
	T cells	CD3+	various cytokines	The T cell receptor (TCR) complex is expressed by most human T cells and is composed of two variable regions: the α chain and the β chain (αβ TCR). A smaller subset of T cells, referred to as γδ-T cells, express only γ- and δ-chains. Reactive conditions: T cells recognize foreign or "non-self" material presented as MHC class I or II-bound peptides on the cell surface. They play a critical role in the immune response, including bacterial and viral infections via MHC-mediated antigen presentation, and in the rejection of tissues and cells due to MHC mismatches. Malignant conditions: T cells are essential for anti-tumor immunity as they identify tumor-specific antigens that are present on MHC molecules.
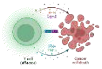	CD8+ T cells	CD3+ CD8+	IL-2 IL-12 Type I IFN granzymes perforin	Reactive conditions: CD8+ T cells are responsible for mediating immune responses against foreign pathogens like viruses and bacteria, resulting in the lysis of infected cells. Malignant conditions: CD8+ T cells can mediate the anti-tumor immune response by recognizing tumor-specific antigens expressed on MHC class I molecules, resulting in tumor cell killing.
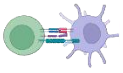	CD4+ T cells	CD3+ CD4+	Various cytokines	Reactive conditions: Antigens activate CD4+ T cells through APCs, which can differentiate into various types of T helper (Th) cells, including Th1, Th2, Th9, Th17, follicular helper T cells (Tfh), and regulatory T cells (Tregs). Malignant conditions: Compared to CD8+ T cells, CD4+ T cells have been less studied in the context of cancer immunity. However, this T cell subtype has been reported to have both tumor-promoting and anti-tumor immune responses.
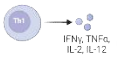	Th1	CD3+ CD4+ STAT4+ T-bet+	IL-2 IL-12 IFN-γ TNF-α	Reactive conditions: Th1 cells secrete IFN-γ, which activates macrophages and CD8+ T cells. This is essential to help protect against intracellular pathogens. Malignant conditions: Th1 cells can activate cytotoxic CD8+ T cells, macrophages, and other APCs to promote anti-tumor immunity.
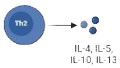	Th2	CD3+ CD4+ Gata3+	IL-4 IL-5 IL-10 IL-13	Reactive conditions: Th2 cells orchestrate humoral immune responses, primarily targeting extracellular antigens. These responses activate effector immune cells, including B cells, eosinophils, basophils, and mast cells, as well as CD8+ T cells. Malignant conditions: Th2 cells have the capacity to secrete cytokines that downregulate anti-tumor CD8+ T cell-mediated immunity, consequently fostering tumor growth. This immunosuppressive function is often mediated by IL-10, which inhibits DC-mediated antigen presentation and promotes the activation of immunosuppressive Tregs. However, Th2-driven immune responses, characterized by IL-4 production and eosinophil activation, can paradoxically suppress tumor growth.
	Th9	CD3+ CD4+ IRF-4+	IL-9 IL-21 IL-10	Reactive conditions: Th9 cells play a role in several immune response pathophysiological conditions, including allergic reactions, inflammation, and extracellular pathogen elimination. Malignant conditions: Th9 cells may have a crucial role in eliciting CD8+ T cell-mediated anti-tumor immune responses. Additionally, they can activate innate immune cells, such as DCs, mast cells, and NK cells, thereby enhancing a robust anti-tumor immune response.
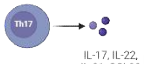	Th17	CD3+ CD4+ RORγt+	IL-17A IL-17F IL-21 IL-22 CCL20	Reactive conditions: Th17 cells are involved in immune responses against bacteria and fungi by recruiting neutrophils and macrophages. Malignant conditions: Th17 cells and their associated cytokines, including IL-17, have been shown to have both anti-tumor and tumor-promoting effects by influencing the TME.
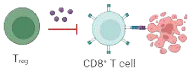	Tregs	CD3+ CD4+ CD25+ FOXP3+	TGF-β IL-2 GITR9 PD-L1 CTLA-4 TIGIT GARP	Reactive conditions: In order to maintain immune homeostasis, Tregs specialize in suppressing abnormal immune responses to both self and foreign antigens. They inhibit the proliferation of T cells as well as the expression of anti-inflammatory cytokines. Malignant conditions: Tregs have the ability to suppress the anti-tumor immunity, which can lead to the development and progression of tumors.
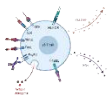	γδ- T cells	CD3+ TCRγδ+	IFN-γ	Reactive conditions: γδ T cells possess the unique ability to recognize a diverse array of antigens independent of major histocompatibility complex (MHC) presentation. They can directly target and eliminate infected or abnormal cells through their cytotoxic activity, or indirectly activate other immune cells. These cells contribute to various physiological processes including pathogen clearance, inflammation, and maintenance of tissue homeostasis. Malignant conditions: γδ T cells exhibit tumor suppressor functions by virtue of their cytolytic properties and their ability to activate other immune cells. However, they can also exert a tumor-promoting effect, primarily mediated by other effector cells. This dual role has been observed in various types of cancer.
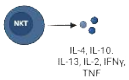	NKT cells	CD3 CD56 CD4+/− CD8+/−	IFN-γ TNF IL-4 IL-10 IL-13 IL-2	Reactive conditions: Upon activation, NKT cells release a significant number of immunomodulatory cytokines that significantly affect immune responses to infectious agents, autoantigens, tissue grafts, and allergens. Malignant conditions: During early tumor development, NKT cells can stimulate T and NK cells to eliminate tumor cells. However, if these cells become overstimulated, they can differentiate into immunosuppressive NKT cell subsets, which can facilitate tumor progression and immune escape.

Figure 6: Subsets of T cells from the adaptive immune system found within the TME. – adapted from Pansy *et al*., 2021 [139]. Created with BioRender.com

1.7. Immune escape in lymphomas

In order to activate T cells with specificity to antigens, it's crucial that antigen-presenting cells (APCs) display antigenic peptides that are not directly attached to an MHC class I or II molecule. When the T cell receptor (TCR) recognizes matching peptide-MHC complexes on APCs, co-signaling receptors gather alongside TCR molecules at the immunological synapse, adhering to the conventional two-signal framework. These co-signaling receptors collaborate

with the TCR signal, either enhancing (co-stimulatory receptors) or dampening (co-inhibitory receptors) T cell activation and function synergistically. The activation of T cells is additionally well-regulated by co-inhibitory receptors known as immune checkpoint molecules [142]

The immune checkpoints and their associated ligands can be classified into several families. Among them are the B7-CD28 families, which encompass cytotoxic T-lymphocyte-associated protein 4 (CTLA-4), programmed cell death protein 1 (PD-1), CD80, CD86, V-domain immunoglobulin suppressor of T-cell activation (VISTA), B- and T lymphocyte suppressor (BTLA), HVEM, and CD160. Additionally, there is the TIM family, which includes T cell immunoglobulin and mucin domain-3 (TIM-3), CD66a, and galectin-9, along with the immunoglobulin (Ig) superfamily containing lymphocyte activation gene 3 (LAG-3). Another family of immune checkpoints consists of nectin and nectin-like binding receptors, such as T cell immunoreceptor with immunoglobulin and ITIM domain (TIGIT), CD155, CD113, and the butyrophilin family (butyrophilins (BTN) and butyrophilin-like (BTNL) molecules). Additionally, there are intracellular checkpoints known (shown in Figure 7). Typically, immune checkpoints and their ligands are positioned to regulate the activity of activated T cells at the immune synapse, effectively orchestrating feedback inhibition to modulate immune responses. This mechanism sets boundaries for self-tolerance and reduces the potential harm to neighboring tissues during immune responses that induce inflammation [139]. Immune checkpoints can cause an immunosuppressive state in the TME. Under malignant conditions, immune checkpoints and Tregs in TME may prevent immune-mediated cancer cell elimination, contributing to cancer development, as reviewed in detail by Pansy *et al*. [139,143,144].

Blockade of these inhibitory receptors and/or their corresponding ligands, particulary CTLA-4, PD-1/PD-L1, and LAG-3, by humanized monoclonal antibodies (mAbs), a strategy known as immune checkpoint blockade (ICB), has demonstrated efficacy in numerous cancers by stimulating the immune system's attack on tumor cells [166,167]. Numerous immune checkpoint inhibitors (ICIs) like TIGIT, LAG-3, TIM-3, and TIM-3 inhibitors are undergoing clinical trials to evaluate their potential in treating diverse solid tumors and leukemias [145,146]. The efficacy of ICBs varies greatly due to the variable expression and co-expression levels of these checkpoints in different tumors. In short, the reasons for resistance to ICB remain unclear. Contributing factors may involve the absence of immune checkpoint expression, TME diversity including diminished immune cell variety, insufficiently active immune cells, the existence of particular TCR clones, and the simultaneous expression of other immune checkpoints, for example TIGIT, LAG-3 and TIM-3 [147–151].

In hematologic neoplasms, adoptive immunotherapy using allogenic stem cell transplantation holds promise as a potentially curative approach Additionally, clinical trials investigating ICB, particularly in of B cell lymphoma, are currently underway [152,153]. A

significant discovery regarding immune checkpoint blockade (ICB) is that in relapsed or refractory classical Hodgkin lymphoma (cHL), blocking PD-1 is linked to impressive response rates ranging from 65% to 84%. This is attributed to frequent amplification of the PD-1 ligand gene locus (9p24.1), which encodes programmed cell death 1 ligands 1 and 2 (PD-L1/L2), resulting in elevated levels of PD-L1 (B7-H1, CD274) and/or PD-L2 (B7-DC, CD273) [154]. Furthermore, in cHL, overexpression of PD-L1 and PD-L2 can occur due to Janus kinases-signal transducer and activator of transcription (JAK/STAT) amplification or because of EBV infection [154,155]. Unlike cHL, the majority of B cell NHLs, multiple myelomas, and leukemias demonstrate markedly inadequate response rates to ICB. Interestingly, approximately 20% of diffuse large DLBCL patients exhibit enhanced PD-L1 expression, attributed to genetic modifications at the 9p24 locus, which do not affect PD-L2, and this phenomenon plays a role in pathogenesis [60,65,156]. Approximately one-third of DLBCL patients relapse or develop resistance to initial chemoimmunotherapy with R-CHOP. Among them, approximately 30% to 50% can achieve remission and potential cure through autologous stem cell transplantation, provided the malignancy remains sensitive to chemotherapy. However, the prognosis for patients with chemotherapy-resistant malignancy is poor [157].

For these patients, ICB has great potential to improve outcomes. Alternatively, there may still be a role for checkpoint inhibition in the treatment of newly diagnosed DLBCL. The presence of alternative immune checkpoint molecules being co-expressed might offer an explanation for the diminished response rates to CTLA-4 and PD-1/PD-L1 checkpoint blockade, along with considerations regarding the composition of the TME. It has been shown to contribute to lymphomagenesis in DLBCL and has been poorly studied in lymphoma entities [147,153].

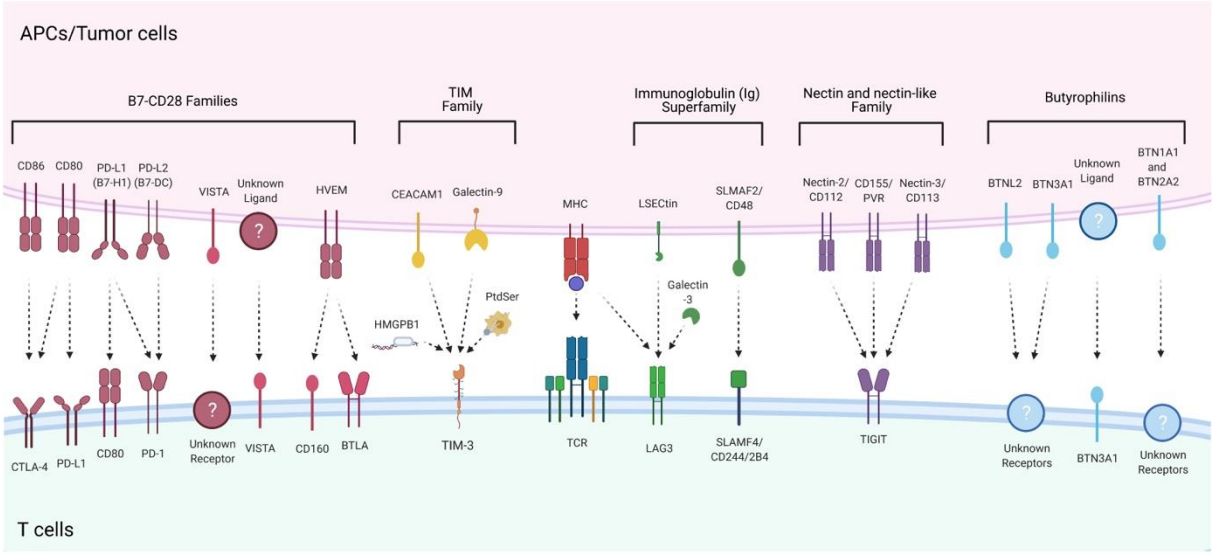

Figure 7: Overview of immune checkpoint molecules/co-inhibitory receptors and their ligands that cause immunosuppressive conditions in the TME. Immune checkpoints and their ligands can be classified into the B7-CD28 families (CTLA-4, PD-1, CD80, CD86, VISTA, BTLA and HVEM, CD160), the TIM family (TIM-3, CEACAM1, galactin-9), the immunoglobulin (Ig) superfamily (LAG-3), nectin and nectin-like binding receptors (TIGIT, CD155, CD113), and butyrophilins (BTNs, BTNLs), as well as intracellular checkpoints. These molecules are typically found on T cells, whereas their ligands are expressed on APCs, tumor cells, and/or T cells themselves. This interaction triggers a co-inhibitory signal designed to dampen effector T cell responses. – adapted from Pansy *et al*., 2021 [139]. Created with BioRender.com

Moreover, downregulation of MHC cell surface molecules is a clinically relevant mechanism of immune evasion in lymphomas. In DLBCL, approximately 40-60% of cases exhibit loss of MHCI, while MHC II is absent in around 20-40% of cases. The loss of MHC is associated with a recurrent mutation in the HLA genes *B2M* and *EZH2*, *GNA13*, and *MEF2B*, and the loss of *PTEN*, which supports the molecular definition of this immune evasion in DLBCL [55–59]. However, the immunobiology of additional mechanisms of immunosuppression and tumor evasion remains poorly understood, including aberrant expression and activity of multiple co-inhibitory ligand-receptor axes in lymphomas. In general, these immune checkpoint pathways are exploited by cancer cells to evade immune attack.

1.8. Preliminary data

1.8.1. Acceleration of *Myc*-induced lymphomagenesis and increased expression of immunoregulatory genes caused by *Nr4a1* loss

To assess the role for *Nr4a1* in tumorigenesis in *Myc*-induced lymphoma mouse models, we crossed mice lacking *Nr4a1* with transgenic *EμMyc* mice. These transgenic mice are known to develop malignant monoclonal lymphomas with an average latency period of 12–16 weeks [132–134]. A cohort of *EμMyc Nr4a1+/+* (n=134), *EμMyc Nr4a1+/-* (n=59) and *EμMyc Nr4a1-/-* (n=84) mice was generated for analysis up to the exhibition of visible disease. In contrast to *EμMyc Nr4a1+/+* mice, the *EμMyc Nr4a1-/-* mice displayed significantly a reduced survival and accelerated development of lymphomas, with a median survival of 92

days compared to 123 days for *EμMyc Nr4a1+/+* and 101 days for *EμMyc Nr4a1+/-* ($p<0.001$, Figure 5a). Taken together, these findings suggest that the abscence of *Nr4a1* accelerates lymphomagenesis in a *Myc*-driven lymphoma mouse model.

To determine the genes affected by *Nr4a1* in *Myc*-induced lymphomagenesis, we conducted RNA-Seq analysis on lymphomas in *EμMyc Nr4a1-/-* mice versus *EμMyc Nr4a1+/+ mice* (n=5 each). In total, we found 75 genes (57 up-regulated and 18 down-regulated genes, Figure 8b) that showed a significant differential expression ($p<0.05$).

Genes with immunoregulatory roles, such as *Tim-3*, *Pdl2*, and *inducible T cell costimulator (Icos)* [61,158,159], were up-regulated in tumors from EμMyc Nr4a1-/- mice. In addition, the transcription factor GATA binding protein 3 (Gata3), which directs T cell differentiation toward Th2 cells [160], was also significantly upregulated.

Further bioinformatic analysis revealed that the majority of differentially expressed genes were closely associated with immune function, immune cells and processes related to differentiation (Figure 8b). These findings provide strong evidence suggesting that Nr4a1 plays a significant role in immune regulation and pathways implicated in aggressive lymphomas.

Therefore, we examined the expression levels of genes linked to immune regulation and tumor cell evasion as described by Cogdill *et al.* [161] using qPCR. Therefore we compared lymphomas of *EμMyc Nr4a1-/-* and *EμMyc Nr4a1+/+* mice. Interestingly, *Ifng,* an effector cytokine [162,163], was notably diminished in lymphomas originating from *EμMyc Nr4a1-/-* mice (Figure 8c). In addition, elevated expression levels were found for inhibitory ligands such as *Pdl1*, *Pdl2*, *Cd80*, *Cd86*, *Galectin 9* (*Gal9*), *Cd112*, *Cd155* and *Hvem* (as shown in Figure 8c), together with their corresponding receptors *Pd1*, *Ctla-4*, *Tim3*, *Cd226*, *Cd96*, *Cd160*, *Btla* and *Lag3* (as shown in Figure 8c). These findings suggest that the absence of *Nr4a1* significantly affects the regulation of immune evasion in *Myc*-driven lymphomagenesis.

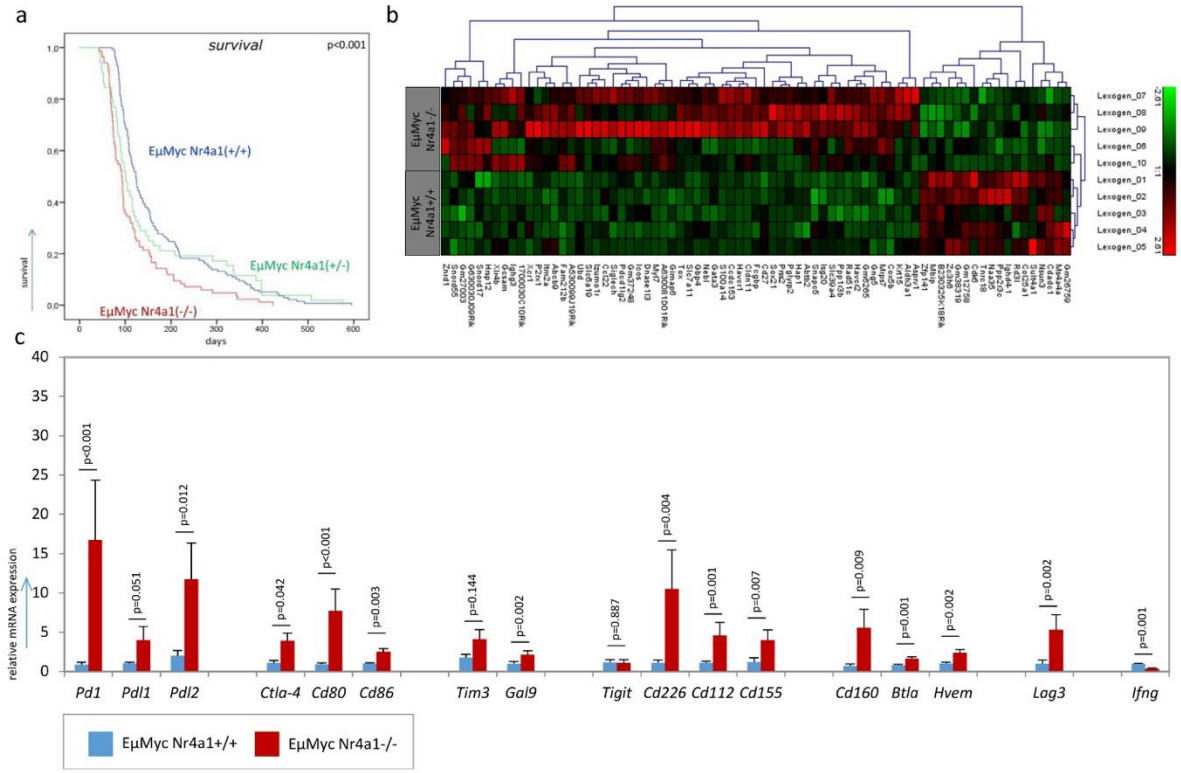

Figure 8: Comprehensive analysis of survival and gene expression in EμMyc mice with or without *Nr4a1*. (a) Survival comparison between *EμMyc* mice with different *Nr4a1* genotypes. (b) Analysis of gene expression in lymphomas of *EμMyc Nr4a1-/-* and *EμMyc Nr4a1+/+* mice. Heatmap showing differentially expressed genes. (c) Relative expression of cytokines, inhibitory receptors and ligands associated with immune regulation in lymphomas from *EμMyc Nr4a1-/-* and *EμMyc Nr4a1+/+* mice (n=20 per genotype).

We found a reduced survival and a consistent expression profile of these genes (Figure 9a I & II) in tumors from immunocompetent C57BL/6 mice transplanted with *EμMyc Nr4a1-/-* lymphoma cells versus EμMyc *Nr4a1+/+* lymphoma cells. This suggests that alterations in immune regulators are persistent features in *Nr4a1*-deficient lymphomas and are mediated by the lymphoma cells themselves. Conversely, transplantation of *EμMyc Nr4a1-/-* lymphoma cells into immunodeficient Fox Chase SCID Beige mice – lacking B-, T- and NK cells - showed no change in survival (Figure 9b I) compared to transplanted *EμMyc Nr4a1+/+* lymphoma cells. Notably, a distinct expression pattern was observed for the *Pd1-Pdl1-Pdl2*, *Ctla4-Cd80-Cd86*, *Btla-Hvem* and *Lag3* axes in the immunodeficient environment. Higher expression of *Pdl1*, *Pdl2*, Cd80 and *Cd86* was observed in transplanted *Nr4a1*-deficient lymphomas (Figure 3b II), whereas no expression of *Pd1* and *Ctla-4* was observed. However, other inhibitory ligands and receptors such as *Tim-3*, *Cd226*, *Cd96*, *Cd160*, *Btla* and *Lag3* (Figure 9b II) showed a similar expression pattern in both *EμMyc Nr4a1-/-* and *EμMyc Nr4a1+/+* lymphomas. The gene expression analysis in immunodeficient mice suggests that *Pd1* and *Ctla-4* might be specifically expressed on T cells, whereas the other inhibitory receptors – *Tim-3*, *Cd226*, *Cd96*, *Cd160*, *Btla* and *Lag3* - might be aberrantly expressed on lymphoma cells. General, it was observed that the development and engraftment of *Nr4a1*-deficient lymphomas were

accelerated in immunocompetent mice, but remained unaffected in an immunodeficient environment, similar to the pattern seen in mice transplanted with Nr4a1-competent cells. These findings imply that *Nr4a1* plays a role in modulating immune evasion through its regulation of the expression of inhibitory receptors and their corresponding ligands.

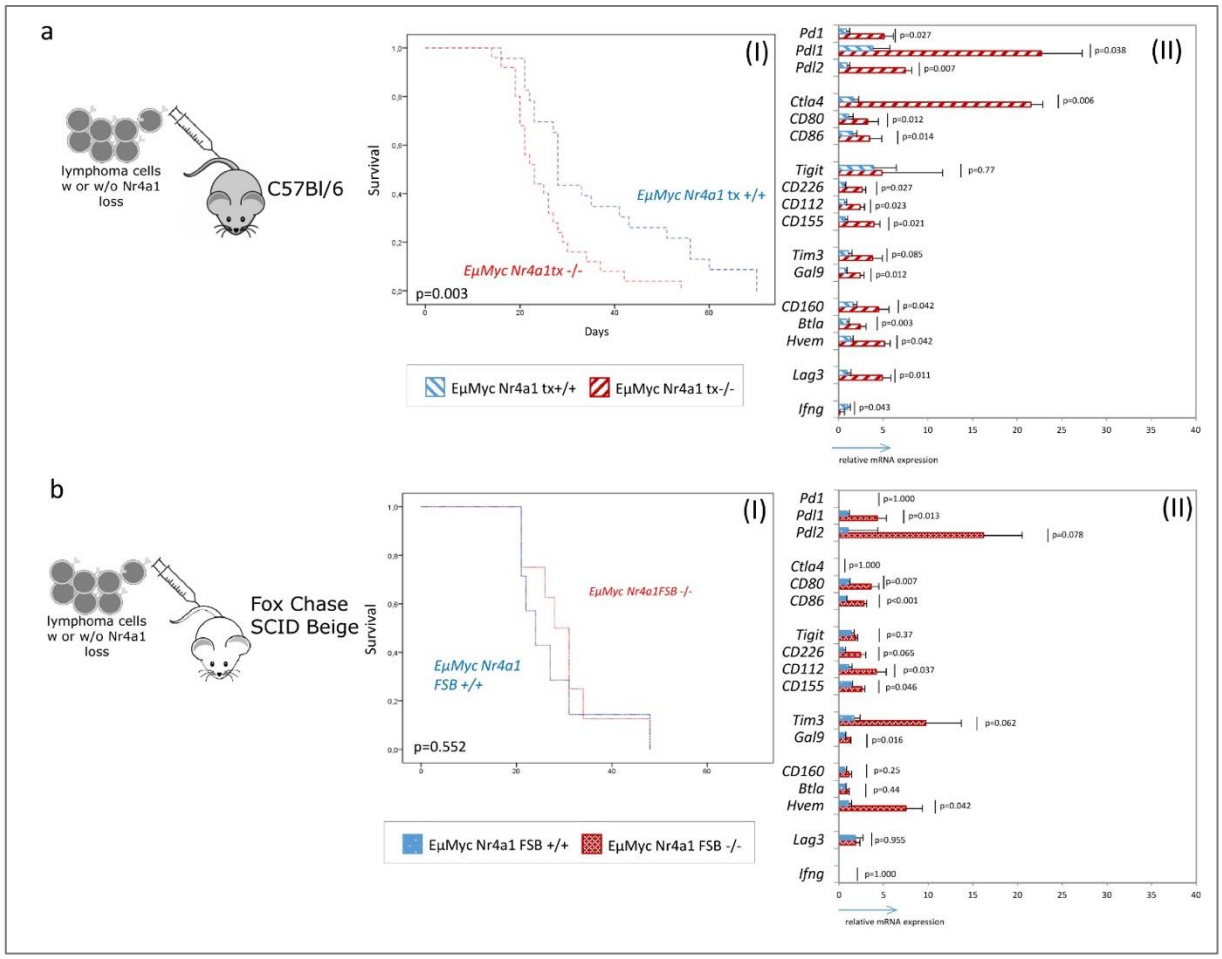

Figure 9: Comprehensive analysis of survival and gene expression in immunocompetent and immunodeficient mice transplanted with murine lymphoma cells with or without *Nr4a1* loss. Survival (I) and relative expression of immunoregulatory cytokines, inhibitory receptors and ligands (II) in (a) wild-type C57Bl/6 mice (n=15 per group) and (b) Fox Chase SCID Beige mice (n=10 per group) after transplantation with lymphoma cells originating from *EμMyc* mice of *Nr4a1 +/+* and *Nr4a1 -/-*.

To characterize the immune cell landscape within the lymphoma TME, we performed flow cytometric analysis of tumors derived from immunocompetent C57BL/6 mice transplanted with either *EμMyc Nr4a1+/+* or *EμMyc Nr4a1-/-* lymphoma cells. In particular, increased levels of neutrophils (0.57% vs 0.12%, Figure 10a), macrophages (0.41% vs 0.22%, Figure 10a), CD3+ T cells (6.8% vs 2.7%, Figure 10b), CD4+ T cells (3.5% vs 0.95%, Figure 10b) and CD8+ T cells (1.75% vs 0.68%, Figure 10b) were observed in mice transplanted with *EμMyc Nr4a1-/-* lymphoma cells. These findings strongly suggest that *Nr4a1* likely holds a crucial role in molding the composition of immune cells in the TME in aggressive lymphomas.

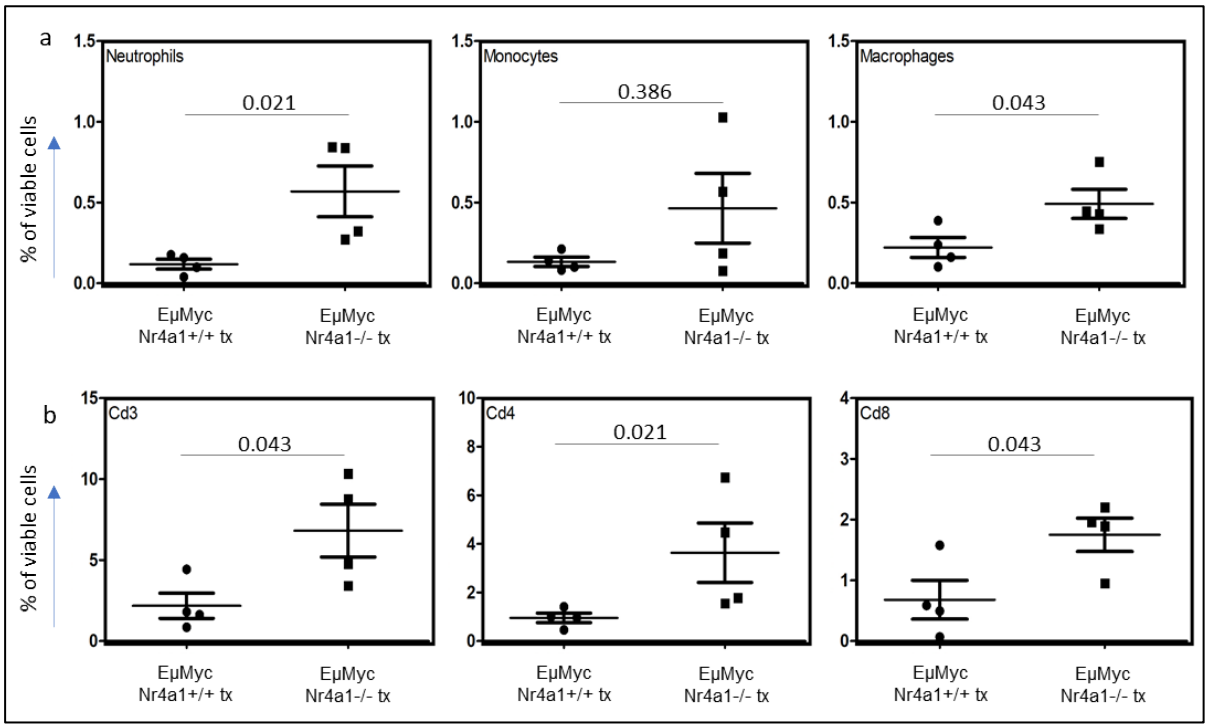

Figure 10: Profiling of immune cells by flow cytometric analysis in tumors from immunocompetent wild-type mice transplanted with *EμMyc Nr4a1+/+* or *EμMyc Nr4a1-/-* lymphoma cells. (a) Proportion of innate immune cells observed in transplanted lymphomas. (b) Proportion of adaptive immune cells observed in transplanted lymphomas. Marker panel: Neutrophils: CD45+, Ly6G+, CD19-; Monocytes: CD115+, Ly6G-, Siglec F-; Macrophages: CD11b+, F4/80, Lin-, B220-; CD3+ T cells: CD3+, B220-; CD4+ T cells: CD3+, CD4+, B220-; CD8+ T cells: CD3+, CD8+, B220-. Each genotype was performed with 4 biological replicates.

Further analysis using flow cytometry to investigate PD1, PDL1 and TIM-3, for which antibody panels were established in our laboratory at the time, revealed higher expression of PD1 on CD3+ T cells in mice transplanted with *EμMyc Nr4a1-/-* lymphoma cells (Figure 11a), indicating an exhausted phenotype in these T cells. Furthermore, an increased expression of PDL1 was observed on lymphoma cells (Figure 11c) within the same tumors. However, no significant difference was observed for TIM-3. These findings corroborate the mRNA expression analysis of the transplanted tumors (showing increased expression of immune checkpoints in the *EμMyc Nr4a1-/-* setting as shown in Figure 9a (II)) and highlight the regulatory role of the *Nr4a1* on immune checkpoint axes. In addition, these observations suggest that immune checkpoint components are also present on cells within the TME and that their expression is controlled by *Nr4a1*, suggesting the activation of processes aimed at immune evasion.

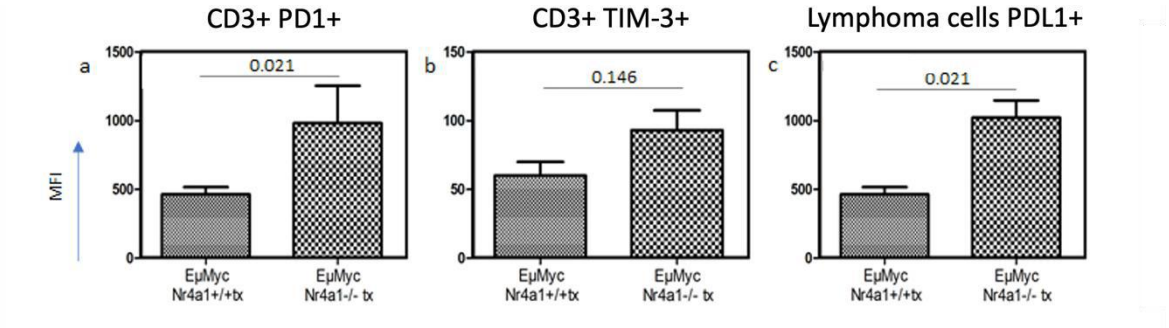

Figure 11: Analysis of PD1 (a) and TIM-3 (b) expression on CD3+ T cells, alongside PDL1 expression on lymphoma cells (c). Flow cytometric analysis was used to assess mean fluorescence intensity (MFI) within different subpopulations defined by the marker profiles described in Figure 10. Each bar represents the mean MFI values of biological replicates (n=4 / genotype) ± standard deviation.

Furthermore, our analysis of cytokines and checkpoint components through qPCR revealed parallels with our mouse model findings when comparing individuals with high and low NR4A1 levels in our human DLBCL cohort (shown in Figure 12a). In addition, by immunohistochemical analysis of PD1, PDL1 and PDL2, we identified a significantly higher proportion of PD1+ reactive immune cells (23.3% vs. 6.75%, p=0.002, Figure 12b), together with significantly increased PDL1 expression (immunoreactivity score: 6. 5 vs. 2.3, p=0.020, Figure 12b) and a noticeable increased PDL2 expression (immunoreactivity score: 26.2 vs. 18.5, p=0.064, Figure 12b) in human lymphoma cells within the NR4A1 low expressing DLBCLs. These findings validate the results observed in our preclinical models and reinforce their relevance in the human context.

In conclusion, our recent findings strongly indicate that the absence of NR4A1/Nr4a1 correlates with elevated expression of several immune checkpoints, ultimately resulting in accelerated lymphoma development within an immunocompetent setting.

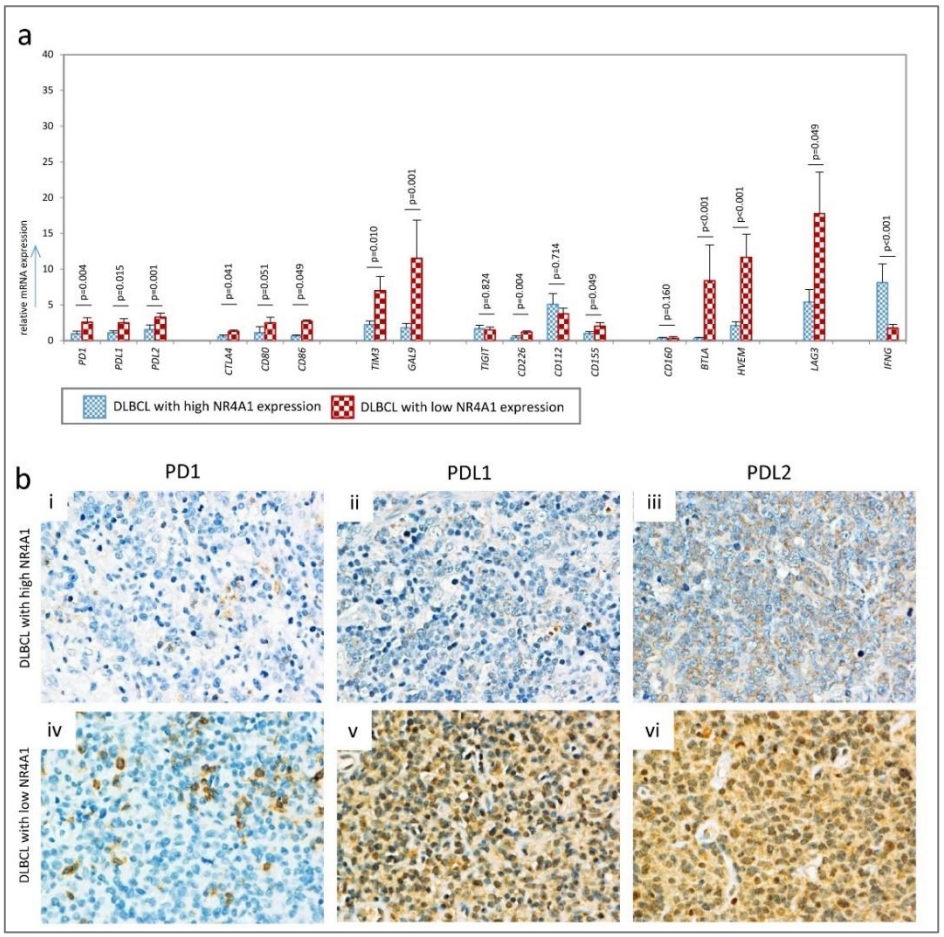

Figure 12: Relative expression analysis and immunohistochemical staining of PD-1, PDL1 and PDL2 in NR4A1 high and low DLBCL. (a) Relative expression of inhibitory receptors, ligands and cytokines involved in immune regulation. (b) Representative immunohistochemical stains of PD-1 (i and iv for NR4A1 high and low DLBCL), PDL1 (ii and v for NR4A1 high and low DLBCL) and PDL2 (iii and vi for NR4A1 high and low DLBCL).

2. Aim of the thesis

2.1. Aim Part 1 – Investigation of the interplay between CXCR4 and CXCL12 in DLBCL

The purpose of this study was to comprehensively investigate the interplay of the CXCR4 receptor and their ligand CXCL12 in DLBCL. Previous data on this axis in DLBCL are limited and inconsistent. To address this, we analyzed the interplay of CXCR4 and CXCL12 in our cohort of DLBCL patients. Moreover, we evaluated the effect of CXCR4 antagonists - including AMD3100 (plerixafor), AMD070 (mavorixafor) and WK1 (a niacin derivative of mavorixafor) - in *in vitro* experiments using lymphoma cell lines.

2.2. Aim Part 2 – Understanding the role of *Nr4a1* in aggressive lymphomas and the tumor microenvironment

Initial findings from murine lymphoma models and samples obtained from patients with DLBCL indicate a crucial function for NR4A1 in regulating immune evasion mechanisms in

aggressive lymphomas. This involves the modulation of the expression of co-inhibitory and co-stimulatory molecules, along with their corresponding ligands and receptors. The goal of the second part was to comprehensively dissect the function of *Nr4a1* in the TME and tumor-immune cell interactions during the process of lymphomagenesis. Our hypothesis is that loss of *Nr4a1* hinders effective T cell function via the receptors within the B7-CD28 (immune checkpoint) family networks, potentially contributing to the inhibition of immune surveillance.

3. Methods

3.1. Investigation of the interplay between CXCR4 and CXCL12 in DLBCL

3.1.1. Patient samples

This study included 71 histologically confirmed DLBCL (50 *de novo* and 21 transformed lymphoma samples) diagnosed between 2000 and 2010 (with last follow-up until May 2019). These patients had received rituximab-containing therapy at the Department of Hematology, Medical University of Graz (shown in Table 1). Analysis of transformed DLBCL samples initially diagnosed as FL showed only the presence of the high-grade component. The clonal relationship between the initial FL sample and the transformed DLBCL sample was evaluated by immunoglobulin heavy chain PCR analysis of their respective matched samples. All samples were classified as DLBCL according to the WHO classification [164]. According to the IHC profiles determined using the Hans algorithms [165], all cases were categorized as follows: 46 cases were classified as GCB-DLBCL and 25 as nGCB-DLBCL. Considering that the expression pattern of the transformed DLBCL samples derived from FLs closely resembled that of GCB-DLBCL samples, they were incorporated into this subtype for analysis [166]. In this retrospective study, we utilized patient specimens collected during standard diagnostic processes. Therefore, written informed consent was not obtained from the patients. The protocol received approval from the Ethics Committee of the Medical University of Graz in October 3, 2016 (No. 28-516/ex 15/16) and was conducted in accordance with the Declaration of Helsinki. Furthermore, germinal center B cells were incorporated into this study as a non-neoplastic control. These cells were isolated from the tonsils of young patients undergoing routine tonsillectomy, following the detailed methodology previously outlined by our research team [129,130].

Table 1: Clinical and pathological characteristics of the lymphoma group

Clinico-Pathologic Parameters		DLBCL patients (*n*= 71)	Proportion
Subtype	nGCB	25	35.2%
	GCB	46	64.8%
Sex	female	37	52.11%
	male	34	47.9%
Age	≤60a	19	26.8%
	>60a	52	73.2%
Stage	1	16	20.5%
	2	18	23.5%
	3	26	34%
	4	17	22%

3.1.2. Sequencing of CXCR4

The sequencing of CXCR4 and CXCR7 as outlined in previous methodologies established by our research team, employing direct DNA sequencing techniques [167]. Fifteen to twenty tissue sections, each ten micrometers thick, were extracted from the fresh frozen specimens listed Table 1. These sections were then microdissected and processed to isolate DNA. To prevent any potential mixing of samples, a fresh microtome blade was utilized for each tissue section. Subsequently, the dissected pieces were placed into individual 2 ml sterile tubes. DNA extraction from both human samples and cell lines was performed using the QIAamp® DNA Mini Kit (#51304, Qiagen, Hilden, Germany), following the manufacturer's instructions. Polymerase chain reaction (PCR) was conducted using peqGOLD PCR Master-Mix and Hot Start-Mix S (#01-1320 and #01-1630, Peqlab, Erlangen, Germany). Each well had a total reaction volume of 25µl, consisting of 1x Hot Start-Mix S, forward and reverse primers (refer to Table 2; Eurofins MWG Synthesis GmbH, Ebersberg, Germany) at a final concentration of 10 pmol/µl, and 2µl of the extracted DNA. The PCR process followed this cycling protocol: an initial step at 95°C for 5 minutes, succeeded by 40 cycles. Each cycle included DNA denaturation at 95°C for 30 seconds, followed by primer annealing: CXCR7 exon1 at 54°C, CXCR4 exon2 at 55°C, and CXCR4 exon1 at 59°C, all for 30 seconds. Subsequently, extension occurred at 72°C for 60 seconds, with a final step at 72°C for 7 minutes.

The rearranged IgHV genes were amplified by seminested PCR. Primers were used as previously described [168] IgHV mutation status was calculated using the IMGT database as described. PCR products underwent purification and sequencing from both ends utilizing the BigDye terminator chemistry 3.1 (#4337455, Applied Biosystems, Foster City, CA, USA). The reaction mixture comprised Big Dye™ Terminator v1.1 Cycle Sequencing RR-100, Big Dye™ Terminator v1.1 Cycle 5x Sequencing Buffer, 1 µl of either forward or reverse primer (refer to Table 2), and 2 µl of the purified PCR product, reaching a final volume of 20 µl per well. The

samples underwent cycling with the following protocol, ramping at a rate of 1°C per second: an initial incubation at 96°C for 1 minute, followed by 25 cycles. Each cycle included denaturation at 96°C for 10 seconds, annealing at 50°C for 5 seconds, and extension at 60°C for 4 minutes, concluding with a hold step at 4°C before purification. Sequencing was conducted on an ABI3130-xl automated sequencer (Applied Biosystems, Foster City, CA, USA) at VBC Biotech in Vienna. The resulting sequences were analyzed using GeneMapper® and SeqScape® software (Applied Biosystems, Carlsbad, CA, USA), employing the GenBank file for CXCR4 (NG_011587.1). Each sample underwent sequencing at least three times.

Table 2: Oligonucleotide sequences of used primers for mutational profiling of CXCR4.

Gene-ID	Sequence
CXCR4-ex1 seq fw	CAGCAGGTAGCAAAGTGAC
CXCR4-ex1 seq rev	TCAAGAAAACTCCTTTCGGTG
CXCR4-ex2 seq fw	ATGGGAAAAGATGGGGAGG
CXCR4-ex2 seq rev	AGACTCAGACTCAGTGGAAAC

3.1.3. Cell lines and cell culture

SuDHL4 was chosen as a representative model for GCB-DLBCL, whereas RI-1 and U2932 were utilized as models for nGCB-DLBCL. Additionally, BL-2 was selected as a model for Burkitt's lymphoma, renowned for its robust CXCR4 expression and migratory response to CXCL12, and was employed for *in vitro* experiments [169]. SuDHL4, U2932, and RI-1 cell lines were cultured in suspension using Roswell Park Memorial Institute (RPMI) 1640 medium (#11875093, Gibco, Thermo Fisher Scientific, Waltham, MA, USA), supplemented with 10% heat-inactivated fetal bovine serum (FBS) (#10500064, Gibco, Thermo Fisher Scientific, Waltham, MA, USA), and 1% antibiotic-antimycotic (#15240062, Gibco, Thermo Fisher Scientific, Waltham, MA, USA). BL-2 cells were cultured in suspension using RPMI 1640 medium supplemented with 20% FBS and 1% antibiotic-antimycotic. Regular PCR testing for mycoplasma was conducted on the cells, and all results were negative. The DLBCL cell lines' identity was authenticated via variable number tandem repeat (VNTR) analysis utilizing the Power Plex 16 system (Promega, Madison, WI, USA) and subsequently validated using the online service provided by the DSMZ cell bank (https://www.dsmz.de/) (accessed on 23 September 2019). All cell lines were treated with the commercially available CXCR4 antagonists AMD3100 and AMD070 (#HY-10046 and #HY-50101, MedChemExpress, Sollentuna, Sweden) [170] and the novel niacin derivative of AMD070, WK1, which we generated, in the range of 1µM to 90µM. These experiments were performed in triplicate and were repeated in at least two independent experiments.

3.1.4. Synthesis of WK1

40mg AMD070 (0.12 mmol, 1 equivalent) (#HY-50101, MedChemExpress, Sollentuna, Sweden) was dissolved in 800 µL of MeOH. Following this, nicotinyl chloride hydrochloride, weighing 20.4 mg (0.12 mmol, 1 equivalent), and Et3N, measuring 32 µL (0.23 mmol, 2 equivalents), were added successively. The reaction mixture was then stirred at room temperature for 24 hours. Once the starting material was fully consumed (confirmed via TLC using $CHCl_3$/MeOH/concentrated NH_4OH = 6/1/0.01, v/v/v), the reaction mixture underwent concentration under reduced pressure. Subsequently, purification was carried out through silica gel chromatography (using $CHCl_3$/MeOH/concentrated NH_4OH = 20/1/0.01, v/v/v). This process resulted in the isolation of WK1 (20 mg) as a colorless solid, yielding 36%.

3.1.5. RNA-Extraction and RQ-PCR

Total RNA was isolated from fresh frozen DLBCL patient tissues, non-neoplastic germinal center B cells and lymphoma cell lines, and cDNA synthesis was performed as previously described by our research group [129,130]. In short, total RNA was isolated using the RNeasy Mini Kit (#74104, Qiagen, Hilden, Germany) according to the manufacturer's protocol. RevertAid RT Reverse Transcription Kit was used to transcribe total RNA into cDNA (#K1691, Thermo Fisher Scientific, Waltham, MA, USA) according to the manufacturer's instructions. Semi-quantitative real-time PCR (RQ-PCR) was conducted for a panel of genes including *ADARB, BAX, BAD, BCL-2, BCL2A1, BCL-XL, BID, BIK, BIM isoform 9, BUB1, BAK, BMF, BMF, CCL12, CCL22, CCL3, CCL4, CCR7, CFLAR, CD44, COL1A, CXCR4, CXCR7, cFOS, cJUN, DUSP1, EGR3, ETV5, FN1, GAPDH, HPRT, IL10, JUNB, KFL10, MCL-1, MMP2, MXD1, NOXA, OAS3, PPIA, PUMA, RGS1, TNF*. Assays and primers were obtained from Eurofins Genomic, Ebersberg, Germany and Qiagen, Hilden, Germany, as listed in Table S 1, following previous experimental descriptions [129,130]. GAPDH, HPRT1, and PPIA, recognized for their minimal variability among lymphoid malignancies, were employed as housekeeping genes [171]. RQ-PCR was conducted using a Bio-Rad CFX384 Touch™ Real-Time PCR Detection System (Bio-Rad, Hercules, CA, USA). The cycling protocol commenced with an initial activation step at 95°C, followed by denaturation at 95°C for 5 seconds and annealing/extension at 60°C for 10 seconds. This cycle was repeated for 34 cycles. Melt curve analysis was employed to distinguish various reaction products, including nonspecific ones. Differences in gene expression were calculated using the 2-ΔΔCt method, as previously described by our group [129,130].

3.1.6. Immunohistochemistry

The formalin-fixed, paraffin-embedded tissue was subjected to pretreatment using Target Retrieval Solution (#S236784-2, 1:10, Dako, Glostrup, Denmark) in a water bath for 40

minutes. Anti-CXCR4 antibodies (1:200, # ab1640) were procured from Abcam (Cambridge, UK), while anti-CXCL12 antibodies (1:50, # MAB350) were obtained from R&D Systems (Minneapolis, MN, USA). Staining procedures were carried out utilizing the Dako K5001 kit (Dako, Glostrup, Denmark) and the intelliPATH FLX® automated stainer (Biocare Medical, Pacheco, CA, USA), following the manufacturer's guidelines. Positive controls, represented by reactive tonsils containing the antigens, were included in the analysis. To ensure specificity, negative controls were implemented by substituting the primary antibody with normal serum, consistently yielding negative results. DLBCL specimens underwent examination to assess staining intensities and the proportions of positively stained DLBCL cells, following a standardized procedure. To evaluate the expression of CXCR4 and CXCL12, the entire section was screened to ensure an even distribution of positively labeled cells. The percentage was determined by calculating the average proportion of CXCR4 and CXCL12-positive cells across a minimum of ten high-power fields, each measuring 0.242 mm² with a field diameter of 555.1 µm. The resulting percentages were rounded to the nearest 10%.

3.1.7. CXCL12 Binding Assay

To evaluate the interaction of CXCL12 to CXCR4 and CXCR7 expressing cells, we used $CXCL12^{AF647}$ (BD Biosciences, San Jose, CA). Initially, cells were treated with CXCR4 antagonists AMD3100, AMD070, or WK1 at final concentrations ranging from 0.01 to 20 µM. Alternatively, blocking antibodies specific to CXCR4 (clone: 9C4, MBL, Woburn, MA, USA), CXCR7 (clone: 11G8, ChemoCentryx Inc., Mountain View, CA, USA), or isotype controls were added at a concentration of 10 µg/mL. Following treatment, the cells were incubated for 45 minutes at 37°C. Subsequently, the treated cells were exposed to fluorescence-labeled $CXCL12A^{F647}$ (10 ng/mL) for 3 hours at 37°C. Measurements were performed using the LSRII flow cytometer (Becton Dickinson, Franklin Lakes, NJ, USA) and analyzed using the CellQuest analysis software (Becton Dickinson, Franklin Lakes, NJ, USA).

3.1.8. Assessment of cell growth

Lymphoma cells were seeded at a concentration of $1x10^4$ per milliliter in a 96-well plate and exposed to varying concentrations (1 µM to 90 µM) of CXCR4 antagonists, including AMD3100, AMD070 and WK1. Control groups included DMSO-treated cells and wells containing only pure medium, serving as blanks.

Following treatment, the cells were incubated at 37°C with 5% CO2 for a period of 72 hours. Cell proliferation and cytotoxicity were assessed by adding 20 µL of EZ4U reagent (#BI-5000, Biomedica Immunoassays, Vienna, Austria) to each well, followed by incubation for 4 hours at 37°C. Results were obtained by absorbance measurements at 492 nm with an additional reference measurement at 620 nm using the SpectroStar photometer (BMG

LABTECH, Ortenberg, Germany). Each experiment was conducted in triplicate and repeated at least two times.

3.1.9. Apoptosis assay

For Annexin V/7-AAD staining, cells underwent staining using the Annexin V/7-AAD kit (#640930, Biolegend, San Diego, CA, USA) through a standardized procedure. Initially, a 200µL aliquot of the cell suspension was centrifuged, and the supernatant was then discarded. The resulting pellet was resuspended in 100µL of Annexin V binding buffer (#422201, Biolegend, San Diego, CA, USA). Subsequently, 2.5µL each of Annexin V-APC and 7-AAD were added and incubated for 15 minutes at room temperature, shielded from light. Analysis was conducted using the LSRII flow cytometer (Becton Dickinson, Franklin Lakes, NJ, USA) and CellQuest analysis software (Becton Dickinson, Franklin Lakes, NJ, USA.

To assess caspase-3 cleavage, cells underwent a series of steps. Initially, they were washed and resuspended in 200µL of 4% paraformaldehyde, followed by a 15-minute incubation at room temperature in darkness. Subsequently, permeabilization was achieved by treating the cells with methanol, keeping them on ice for 30 minutes. For immunostaining, cells were exposed to a Cleaved Caspase-3 rabbit monoclonal antibody conjugated with AF647 (#9602, Cell Signaling, Cambridge, UK) for 1 hour. Analysis was performed using the LSRII flow cytometer (Becton Dickinson, Franklin Lakes, NJ, USA) and interpreted with CellQuest analysis software (Becton Dickinson, Franklin Lakes, NJ, USA).

3.1.10. Migration assay

For the migration assay, Transwell® inserts (Costar, 6.5mm diameter, 5µM pore polycarbonate membrane) were employed. Initially, 3×10^5 cells were suspended in 100µL of RPMI 1640 medium supplemented with 5% serum. These cells underwent pretreatment with either vehicle or 1µM of the CXCR4 antagonists AMD70 and WK1 at 37°C for 2 hours. Subsequently, the cells were transferred to Transwell® inserts and positioned in 24-well plates. The lower chamber was filled with 600µL of RPMI 1640 medium containing 5% serum and 100 ng/mL CXCL12 agonists (AMD070 and WK1) or vehicle. Migration was allowed to proceed for 18 hours at 37°C in a humidified atmosphere with 5% CO2. Flow cytometry was employed to quantify the number of cells migrating to the lower compartment. The results are presented as the mean ± standard error of the mean (SEM) from 3 to 4 independent experiments. The data is expressed as a percentage of the control.

3.1.11. Microarray analysis

The dataset E-GEOD-10846, generated from the Affymetrix GeneChip Human Genome U133 Plus 2.0 platform [106], was obtained from ArrayExpress and processed using

R version 3.5.1 [172]. Preprocessing was conducted using the 'oligo' [173] package in R, employing the robust multi-array average (rma) method. Only samples from 200 patients who received R-CHOP treatment or were diagnosed with a specific subtype were retained for subsequent analysis. Expression values corresponding to the set of probes annotated as CXCR4 were then extracted for further examination.

3.1.12. Statistical analysis

Statistical analysis was conducted using IBM SPSS Statistics version 23.0 (IBM Corp., New York, USA). A significance level of $p<0.05$ was considered statistically significant. Normality of distribution was assessed using the Shapiro-Wilk test. Differences in mRNA expression were evaluated using either a t-test or its non-parametric equivalent, the Mann-Whitney U-test, depending on the distribution of the data. Two-tailed p-values were reported.

Survival analysis was performed in R version 3.5.1, utilizing the 'survival' [174] and 'survminer' [175] packages. Patients were categorized into low and high expression groups based on the third quartile of CXCR4, CXCL12, and CXCR7 expression. Survival time of 5-years, defined as the period in months from the date of diagnosis to the date of death from any cause, was estimated using the Kaplan-Meier method. Group comparisons were conducted using the log-rank test.

3.2. Understanding the role of *Nr4a1* in aggressive lymphomas and the tumor microenvironment

3.2.1. Animal studies and tumor models

C57BL/6, *EμMyc* (#002728) and *Nr4a1-/-* (#006187) mice used for survival and tumorigenesis analyses were obtained from The Jackson Laboratory (Bar Harbor, ME, USA). The mice were bred and maintained in a controlled environment under specific pathogen-free (SPF) conditions. To explore the impact of Nr4a1 on oncogene-driven B cell lymphoma development, mice deficient in Nr4a1 were crossbred with *EμMyc* transgenic mice, alongside C57BL/6 (wild-type) controls. The mice underwent regular monitoring every other day for indications such as a hunched posture, ruffled fur, enlarged lymph nodes, and other manifestations of overt disease. When tumors were observed to develop, mice were humanely euthanized via cervical dislocation while under deep isoflurane anesthesia (#B506, AbbVie Ltd, Berkshire, UK). All animal procedures were performed in accordance with the guidelines and approved by the Austrian Ministry of Science, Research and Economy.

Murine lymphoma cells with and without *Nr4a1* loss were transplanted into female and male C57BL/6 mice aged six to eight weeks. Mice received an intravenous injection of $1x10^6$ murine lymphoma cells resuspended in 200μl sterile phosphate buffered saline (PBS,

#10010056, Gibco, Thermo Fisher Scientific, Waltham, MA, USA). Mice were monitored daily until the onset of overt signs of disease and humanely euthanized as previously described. Chicken ovalbumin $(OVA)_{257-264}$ specific TCR transgenic *OT-1* mice (#003831) were also obtained from Jackson Laboratory. *OT-1* mice carry a transgenic TCR designed to recognize the 8-unit SIINFEKL peptide from positions 257-264 of ovalbumin. These transgenic animals were identified by staining of splenocytes or peripheral blood with specific antibodies targeting CD8 (#100762, Biolegend, San Diego, CA, USA), Vα2 (#127812, Biolegend, San Diego, CA, USA) and Vβ5.1, 5.2 (#139504, Biolegend, San Diego, CA, USA) chains of the transgenic TCR (Table S 2) [176]. The transgenic T cell receptor was verified by the TCR Vβ5.1, 5.2, and TCR Vα2 expressing together. Experiments were conducted using mice that were matched for both sex and age, ranging from 5 to 7 weeks old. Spleens from *Ctla4-/- OT-1* mice were kindly provided by Dr Aditya Arra and Prof Weinzierl-Brunner from the Otto von Guericke University, Magdeburg, Germany. The mice were bred under specific pathogen-free conditions in the central animal facility of the Medical Faculty of the University of Magdeburg, Germany. *OT-1* mice were genotyped and phenotyped for TCRtg expression by flow cytometry as described above [176].

3.2.2. Generation of murine lymphoma cell lines

Single cell suspensions of *EμMyc Nr4a1-/-* and *EμMyc Nr4a+/+* lymphomas were prepared using a 70μm-pore cell strainer and cultured in 12-well plates in Dulbecco's Modification of Eagle's Medium (DMEM, #1243005, Gibco, Thermo Fisher Scientific, Waltham, MA, USA) supplemented with Iscove's Modified Dulbecco's Medium (IMDM, #12440053, Gibco, Thermo Fisher Scientific, Waltham, MA, USA) in a 1:1 ratio supplemented with 10% FBS, 1% antibiotic-antimycotic (100x) (#15240062, Gibco, Thermo Fisher Scientific, Waltham, MA, USA) and 0.1% 2-mercaptoethanol (#21985023, Gibco, Thermo Fisher Scientific, Waltham, MA, USA) in a humidified 5% CO2 incubator at 37°C. Viability and cell numbers were determined 3 times per week and cells were maintained at a density of 2-2.5x10^5/ml. Once lines were established *in vitro*, they were genotyped and their phenotype determined by flow cytometry.

3.2.3. Preparation of single-cell suspensions

The spleens were processed for flow cytometry to assess immune cell composition. Initially, the spleens were minced and filtered through a 70μm-pore cell strainer using a syringe plunger. After processing, the resulting suspension was centrifuged at 4°C for 5 minutes at 500 g, following which the supernatant was carefully discarded. Next, the pellet was then treated with 3mL of 1x BD Pharm Lyse solution (#555899, BD Biosciences, San Jose, CA USA) and incubated at 4°C for 5 minutes. To stop the lysis process, four volumes of PBS were

added, followed by another centrifugation at 4°C for 5 minutes at 500 g. The single cell suspensions were then washed twice with PBS, resuspended in PBS, counted using a CASY® Cell Counter and Analyzer (OLS OMNI Life Sciences), and prepared for surface antigen staining.

3.2.4. Flow cytometry for immune checkpoint molecules, MHC molecules and small immune cell population panel

Spleen single-cell suspensions (100µl) containing 1x10^6 cells were blocked for 10 minutes at 4°C with 1µg of TruStain FcXTM antibody (#101320, Biolegend, San Diego, CA, USA). Subsequently, cells were stained for 30 minutes at 4°C (protected from light) with the pre-mixed panel of antibodies as listed in Table S 2. The cells and antibodies were mixed together by vortexing. Afterward, the cells were washed once with 100µl of PBS, then centrifuged at 500 g for 5 minutes at RT. Following centrifugation, the supernatant was carefully removed, and the pellet was resuspended in 200µl of PBS. Subsequently, 3µl of 7-AAD (#559925, BD Biosciences, San Jose, CA) was added to each sample before measurement. The acquisition was carried out on Cytoflex SI (Beckman Coulter Life Sciences, Brea, CA, USA), and the raw data was analyzed using FlowJoTM (Version 10.10.0, BD Biosciences, San Jose, CA, USA).

3.2.5. Flow cytometry for immune cell populations

To eliminate dead cells, single-cell suspensions of spleens were initially treated with the fixable viability dye eFluor780 (1:2000, #65-0865, Thermo Fisher Scientific, Waltham, MA, USA) for 20 minutes at 4°C in the dark. Prior to staining with surface and intracellular antibodies, single-cell suspensions were incubated with 1µg of TruStain FcXTM (#101320, Biolegend, San Diego, CA, USA) for 10 minutes at 4°C. The immune cells were stained with a pre-mixed panel of antibodies for 30 minutes at 4°C, while being protected from light. The list of antibodies used is shown in Table S 2. The cells were washed and fixed in eBioscience™ IC Fixation Buffer (#00-8222-49, Thermo Fisher Scientific, Waltham, MA, USA) for 10 minutes at 4°C. To identify intracellular FoxP3 nuclear antigen, surface-stained cells were permeabilized and fixed in TF buffer set (#562574, BD Biosciences, San Jose, CA, USA) and then stained with FoxP3 antibody (Table S 2). Following fixation, the cells were washed, resuspended in 200µL SB (PBS+2% FBS), and stored at 4°C until further use in the assay. Subsequently, the cells were acquired using either a BD LSR FortessaTM or a BD CantoTM flow cytometer with FACSDiva software (BD Biosciences, San Jose, CA, USA). Data analysis and compensation were conducted using FlowJo™ (Version 10.10.0, BD Biosciences, San Jose, CA, USA). Fluorescence minus-one (FMO) controls were employed to establish gating strategies.

3.2.6. Isolation and activation of the *OT-1* CD8+ cells

OT-1 CD8+ T cells were isolated and purified, achieving a purity of over 85%, utilizing a CD8a (Ly-2) MicroBead isolation kit (#130-104-075, Miltenyi Biotec, Bergisch Gladbach, Germany), following the manufacturer's instructions. APCs were obtained from the spleens of C57BL/6 mice and subsequently isolated using a CD90.2 depletion kit (#130-049-101, Miltenyi Biotec, Bergisch Gladbach, Germany), following the instructions provided by Miltenyi Biotec. The separation process involved utilizing LS and LD Columns (#130-042-401 and #130-042-901, Miltenyi Biotec, Bergisch Gladbach, Germany) on the QuadroMACS™ Separator (#130-090-976, Miltenyi Biotec, Bergisch Gladbach, Germany). The *OT-1* CD8+ T cells' purity and the depletion of CD90.2 cells (APCs) were measured, making use of flow cytometry. To activate the T cells, *OT-1* CD8+ T cells were cultured immediately after isolation in presence of APCs in the ratio of 1:4: (APC to T cell) for 48 hours at a density of $2x10^6$ cells/ml, respectively. DMEM mixed with IMDM medium in a 1:1 ratio supplemented with 10% FBS, 1% antibiotic-antimycotic (100x), and 0,1% 2-mercaptoethanol, 1 µg/ml of LPS-free SIINFEKL peptide ($OVA_{257-264}$, #138831-86-4, Invivogen, San Diego, CA, USA), 3 ng/ml recombinant IL-2 (#130-120-662, Miltenyi Biotec, Bergisch Gladbach, Germany) and 3 ng/ml recombinant IL-12 (#577002, Biolegend, San Diego, CA, USA) was used for the activation.

3.2.7. Flow cytometry for *in vitro* cytotoxicity assay

T cells were assessed for differentiation and activation by flow cytometric staining after 48 hours. Cells were incubated with following antibodies: CD8-PE/Dazzle594 (#100762, Biolegend, San Diego, CA, USA), CD44-APC (#103012, Biolegend, San Diego, CA, USA), CD62L-BV605 (#104437, Biolegend, San Diego, CA, USA), CD279-FITC (#135214, Biolegend, San Diego, CA, USA), CD69-PE (#104507, Biolegend, San Diego, CA, USA) and CD25-BV421 (#102033, Biolegend, San Diego, CA, USA) at 4°C for 30 minutes (Table S 2). Cells were then washed and measured with Cytoflex SI (Beckman Coulter Life Sciences, Brea, CA, USA). Data were analyzed using FlowJo™ (Version 10.10.0, BD Biosciences, San Jose, CA, USA). The subpopulations of naive T cells, TCM and TEM were distinguished by analyzing their CD44 and CD62L expression patterns.

3.2.8. *In vitro* cytotoxicity assay

For the cytotoxicity assay, murine lymphoma cells with and without *Nr4a1* loss generated in our lab as described in section 3.2.2 were used. These cells serve as target in the co-culture with *OT-1* CD8+ T cells. Therefore, murine lymphoma cells were labelled with CFSE (#65-0850-84, eBioscience, Thermo Fisher Scientific, Waltham, MA, USA) in a concentration of either 7,5µM ($CSFE_{high}$) or 0,5µM ($CSFE_{low}$) at 37°C for 15 minutes in medium with 2% FBS. The labeling process was terminated by adding a solution consisting of five

volumes of medium with 10% FBS, followed by a 5-minute incubation period on ice . $CFSE^{high}$ stained lymphoma cells were then pulsed with 5nM SIINFEKL peptide ($OVA_{257-264}$, #138831-86-4, Invivogen, San Diego, CA, USA) for 1 hour at 37°C. After washing steps, $CFSE^{high}$ and $CFSE^{low}$ stained lymphoma cells were mixed in a ratio of 1:1. Successful staining is then controlled by flow cytometry. Finally, activated *OT-1* CD8+ T cells (effector cells, E) and $CSFE_{high}$ stained lymphoma cells (target cell, T) were co-cultured in different E:T and measured by flow cytometry after 4, 8, 16 and 24 hours of co-incubation with Cytoflex SI (Beckman Coulter Life Sciences, Brea, CA, USA). As control for calculation serves 1:1 $CFSE^{high}$ and $CFSE^{low}$ stained lymphoma cells. The percent specific lysis was determined by using the following formula:

$$Specific\ lysis = \left(1 - \frac{\frac{CFSE_{highT}}{CFSE_{lowT}}}{\frac{CFSE_{highC}}{CFSE_{lowC}}}\right) \times 100$$

3.2.9. Proteome profiler analysis of murine cell lines with and without *Nr4a1* loss

Two different types of commercially available phospho-protein arrays were employed to examine the relative phosphorylation levels of specific target molecules implicated in signal transduction pathways in murine lymphoma cells or murine lymphoma tissue. Proteome Profiler Human Phospho-Kinase Array Kit (ARY003B, R&D Systems, MN, USA) was used to analyze the relative phosphorylation levels of 43 kinases and 2 related proteins in murine lymphoma cell lines with and without *Nr4a1* loss (n=2 each group), whereas for lymphomas derived from *EμMyc* mice with and without *Nr4a1* loss (n=4 each group) the Proteome Profiler Human Phospho-Kinase Array Kit (ARY003C, R&D Systems, MN, USA) was used to screen 37 kinases and 2 related proteins according to the manufacturer's protocol. Signals were detected on a ChemiDoc Imaging System (Bio-Rad, Hercules, CA, USA) according to the manufacturer's instructions. ImageLab software (Bio-Rad, Hercules, CA, USA) was used to quantify the levels of phosphorylation and normalized to the positive control spots.

3.2.10. Statistical analysis

Statistical analyses of experiments were conducted using GraphPad Prism 10.2.1 (GraphPad Software, Boston, MA, USA). A significance level of $p<0.05$ was considered statistically significant. Differences in the expression of flow cytometric measurements were evaluated using either a t-test or its non-parametric equivalent, the Mann-Whitney U-test, with two-tailed p-values, depending on the result of the test.

4. Results

4.1. Investigation of the interplay between CXCR4 and CXCL12 in DLBCL

4.1.1. High *CXCR4* levels are linked to poor clinical outcome in DLBCL patients

RQ-PCR was used to determine the mRNA expression levels of *CXCR4*, *CXCR7* and their ligand *CXCL12* in nGCB- and GCB-DLCBLs, encompassing primary and transformed follicular lymphomas (n=71), with GC B cells (GC B, n=5) utilized as non-neoplastic controls. Compared to non-neoplastic GC B cells, a remarkable increase of CXCR4 expression was observed in DLBCL and all examined DLBCL subgroups such as nGCB- and GCB-DLBCL as well as in primary (pGCB-DLBCL) and transformed DLBCL (tGCB-DLBCL) originating from FL (140-fold, p<0.001). No significant differences were detected for the expression of *CXCR7* and *CXCL12* (Figure 13).

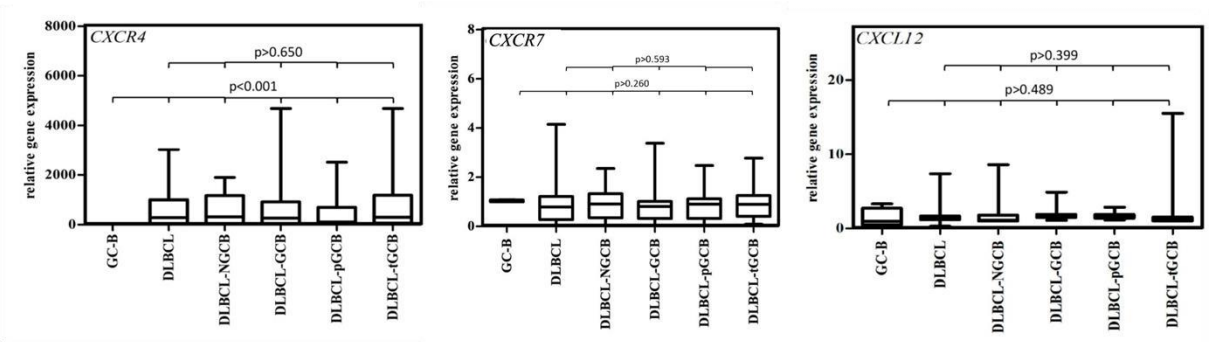

Figure 13: Gene expression levels of *CXCR4*, *CXCR7* and *CXCL12* in DLBCL. Gene expression analysis of CXCR4, CXCR7, and their ligand CXCL12 was conducted in non-neoplastic GC B cells and DLBCL, including nGCB-DLBCL and GCB-DLCBL, using RQ-PCR. The GCB-DLBCL was subsequently classified into primary (pGCB-DLBCL) and transformed DLBCL (tGCB-DLBCL) derived from follicular lymphoma. The mRNA expression levels were computed as relative expressions in comparison to the GC B cells. Each bar in the graph represents the mean expression value with standard error of the mean (SEM). Statistical comparisons of expression levels were conducted using either the Mann-Whitney U-test or Student's t-test.

In addition, in comparison to DLBCL patients diagnosed with clinical stage 1, we noted a 4.7-fold increase in the expression of *CXCR4* in advanced stage lymphoma (stage 2-4) (p=0.028). *CXCR4* expression was 3.1-fold higher in bone marrow (BM)-infiltrating DLBCL (p=0.023). Notably, a positive correlation was identified between the expression of *CXCR4* and BM infiltration (Spearman rho=0.550 and p<0.001, Figure 14a). *CXCL12* and *CXCR7* were not associated with BM infiltration (Figure 14b and c).

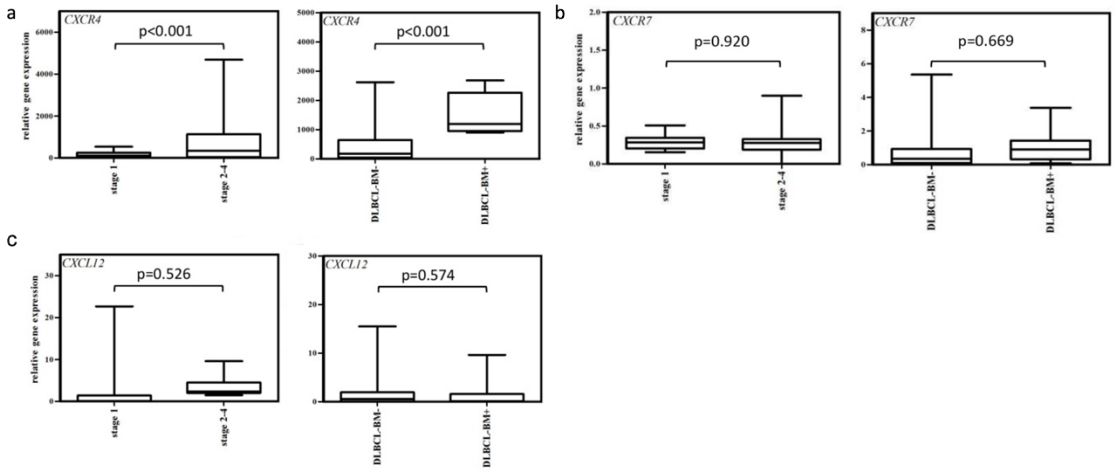

Figure 14: Gene expression levels of *CXCR4*, *CXCR7* and *CXCL12* in DLBCL samples at different stages of progression and DLBCL samples with or without BM-infiltration. The left graph shows results for expression in DLBCL samples, while the right graphs present results for BM-infiltrated DLBCL samples. This study presents the gene expression of *CXCR4* (a), *CXCR7* (b), and *CXCL12* (c) in early-stage (stage 1) and advanced-stage (stage 2-4) in samples of DLBCL patients, as well as samples of DLBCL patients with and without BM infiltration, using RQ-PCR. The mRNA expression levels were determined by calculating the relative mRNA expression compared to GC B cells. Each bar in the graph represents the mean expression value with standard error of the mean (SEM). Statistical comparisons of expression levels were conducted using either the Mann-Whitney U-test or Student's t-test.

When categorizing patients into two groups according to the third quartile of CXCR4 mRNA expression, we noticed a high correlation of high *CXCR4* expression and a low 5-year survival rate among our cohort (p=0.066, log-rank test, Figure 15a). Upon focusing specifically on *de novo* DLBCL cases, similar outcomes were observed (p=0.051, log-rank test, Figure 15b). This trend was further validated using a publicly available DLBCL dataset [106] (p=0.00018, log-rank test, Figure 15c).

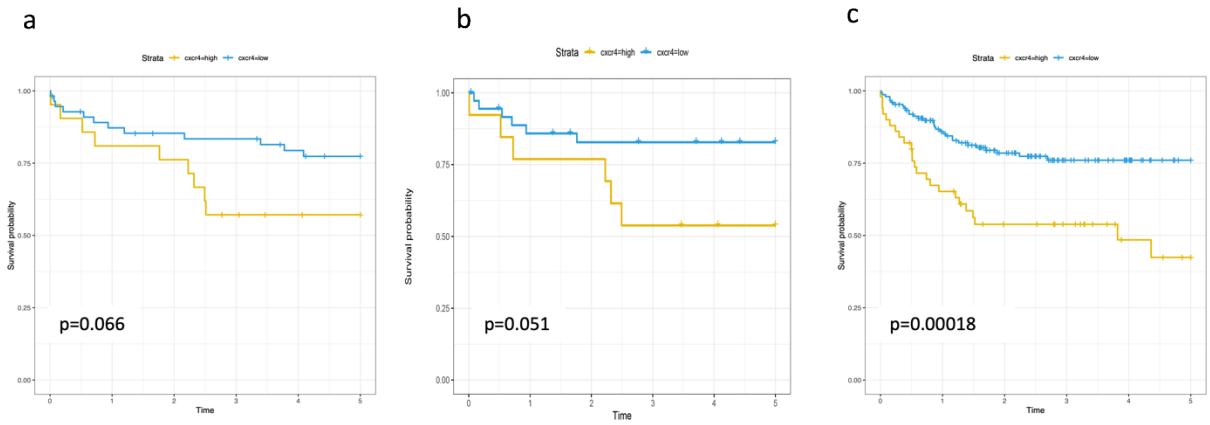

Figure 15: 5-year survival probability of DLBCL patients according to CXCR4 expression. 5-year survival based on the third quartile of CXCR4 expression (*CXCR4* high expression = yellow, *CXCR4* low expression = blue) in (a) our DLBCL cohort, (b) *de novo* DLBCL patients and the (c) cohort of Lenz *et al*. [106].

There was no discernible correlation detected between *CXCL12* (Figure 16a and b) and *CXCR7* (Figure 16c and d) mRNA expression levels within both the overall lymphoma cohort and the *de novo* group.

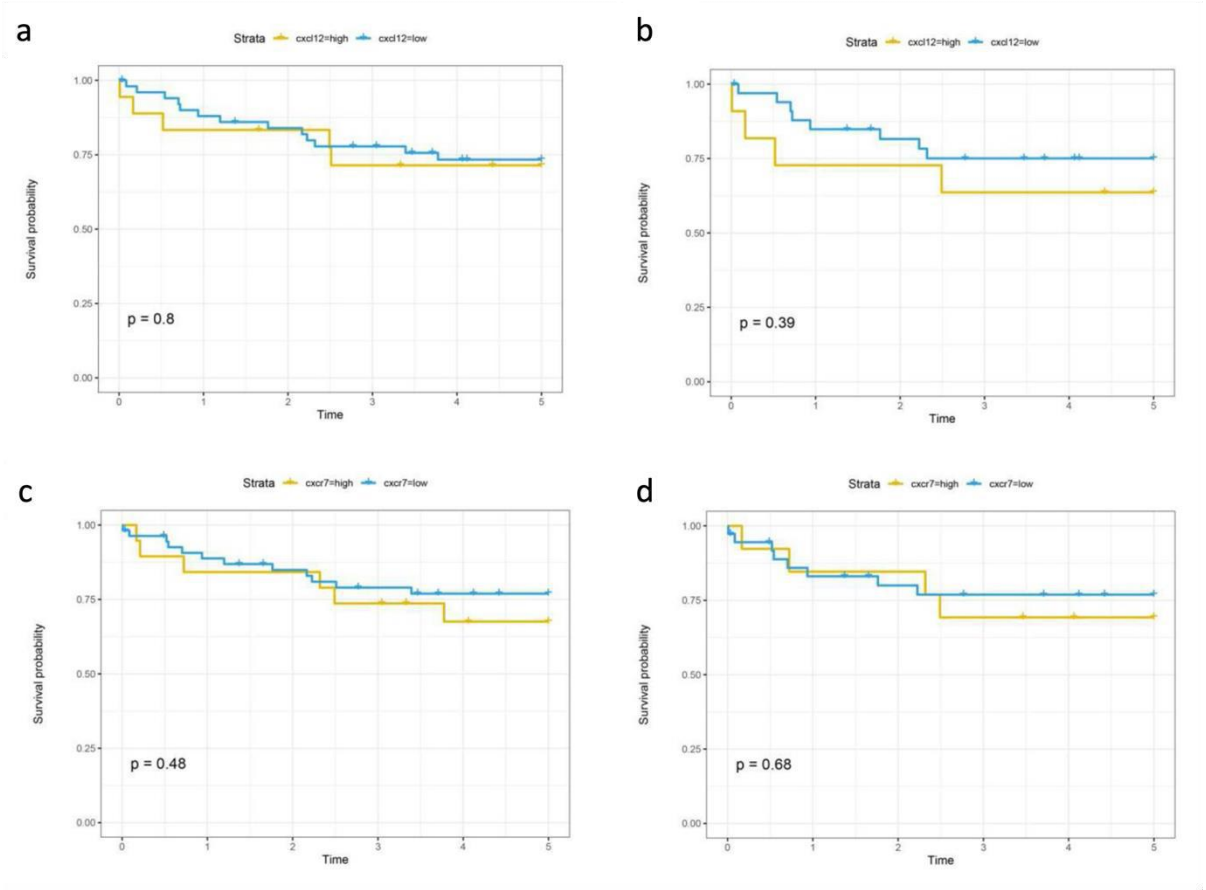

Figure 16: 5-year survival probability of DLBCL patients according to *CXCL12 and CXCR7* expression. 5-year survival probability in all (a) and *de novo* (b) DLBCL patients based on *CXCL12* (*CXCL12* high expression = yellow, *CXCL12* low expression = blue) expression. 5-year survival probability in all (c) and *de novo* (d) DLBCL patients based on *CXCR7* (*CXCR7* high expression = yellow, *CXCR7* low expression = blue) expression.

In order to determine whether the increased mRNA levels of *CXCR4* and *CXCL12* corresponded to increased protein expression, immunohistochemical analysis was carried out on samples obtained from DLBCL patients (n=40) with sufficient material remaining for this analysis. CXCR7 was omitted from subsequent analysis owing to its expression pattern. Notably, a significant positive correlation was observed between *CXCR4* and *CXCL12* (Spearman rho = 0.714 for CXCR4 and Spearman rho = 0.694 for CXCL12, $p < 0.01$). Furthermore, our observations showed that CXCR4 was exclusively present on lymphoma cells, representing on average 64.5% of lymphoma cells. In contrast, CXCL12, which was found in approximately 30.3% of lymphoma cells, was primarily expressed by lymphoma cells but was also detected in the microenvironment, including reactive immune cells and endothelial cells (Figure 17).

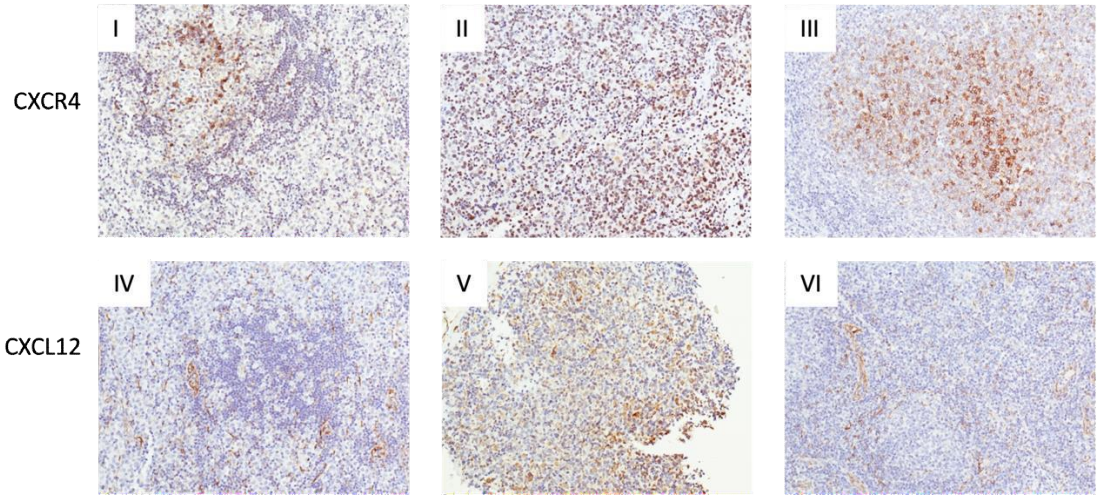

Figure 17: Representative immunohistochemical staining of CXCR4 (I-III) and CXCL12 (IV-VI) on DLBCL samples. Representative tissue sections (20x magnification) from DLBCL specimens subjected to immunohistochemical staining with the anti-CXCR4 antibody (I-III) and the anti-CXCL12 antibody (IV-VI). All images were taken using an Olympus BX51 microscope and an Olympus E-330 camera.

4.1.2. CXCR4 is not altered by somatic mutations in DLBCL

As mutations in the coding sequence of CXCR4 are known to be frequent in B-cell lymphomas [177,178], we performed direct sequence analysis on lymphoma samples (n=25) and lymphoma cell lines (n=4). Our analysis revealed the presence of a single nucleotide polymorphism (rs2228014) previously documented in publicly available databases [179]. This polymorphism is located in exon 2. Moreover, it was identified in three of 25 DLBCL patient samples and in one of four cell lines (U2932). Aside from rs2228014, no further changes of single nucleotide polymorphism were observed (Table 3).

Table 3: A single nucleotide polymorphism found within the coding sequence (CDS) of CXCR4 was identified in our DLBCL cohort (n=25) as well as in human lymphoma cell lines (n=4). WT indicates that it is unmutated.

Sample ID	Type		CXCR4 Exon1	CXCR4 Exon2
AI1	nGCB		WT	WT
AI2	GCB	transformed	WT	WT
AI3	GCB	transformed	WT	rs2228014
AI4	GCB	transformed	WT	WT
AI5	nGCB		WT	WT
AI6	GCB		WT	WT
AI8	GCB	transformed	WT	WT
AI9	GCB		WT	WT
AI10	nGCB		WT	WT
AI11	nGCB		WT	rs2228014

Sample ID	Type		CXCR4 Exon1	CXCR4 Exon2
AI12	nGCB		WT	WT
AI13	nGCB		WT	WT
AI14	GCB	transformed	WT	WT
AI16	GCB	transformed	WT	WT
AI17	GCB	transformed	WT	WT
AI18	GCB		WT	WT
AI19	GCB	transformed	WT	WT
AI20	GCB	transformed	WT	WT
AI21	nGCB		WT	WT
AI22	GCB		WT	rs2228014
AI26	GCB	transformed	WT	WT
AI28	GCB	transformed	WT	WT
AI33	nGCB		WT	WT
AI34	GCB	transformed	WT	WT
AI71	nGCB		WT	WT
BL2	cell line	Burkitt like	WT	WT
SuDHl4	cell line	GCB like	WT	WT
RI1	cell line	nGCB like	WT	WT
U2932	cell line	nGCB like	WT	rs2228014

4.1.3. The association between bone marrow infiltration in DLBCL and the CXCR4/CXCL12 axis demonstrates a significant correlation

To delve deeper into the influence of the CXCR4/CXCL12 axis on bone marrow infiltration by DLBCL, we conducted RQ-PCR analysis on matching bone marrow biopsies from our DLBCL cohort. A total of 63 bone marrow samples were analyzed, comprising 52 samples collected at time of diagnosis, and from 12 patient with DLBCL with initial bone marrow infiltration. In addition, 11 patients underwent multiple biopsies throughout the progression of their disease. Of these, seven patients achieved remission and four experienced a relapse.
Upon analyzing the mRNA expression levels of *CXCR4* and *CXCL12* in bone marrow samples with and without lymphoma infiltration at the time of diagnosis, we detected a 1.6-fold increase in *CXCR4* expression in bone marrow samples with infiltration of lymphoma (p=0.008, Figure 18a). Conversely, we did not observe any statistically significant difference for *CXCL12* levels (p=0.663, Figure 18a). Nevertheless, we found a strong positive correlation between *CXCL12* expression levels and the rate of infiltration in bone marrow biopsies (Spearman rho=0.764, p=0.001). In addition, we performed an analysis of the expression levels of *CXCR4* and

CXCL12 in seven paired bone marrow samples from individuals whose bone marrow was previously infiltrated but later showed remission after chemotherapy (bone marrow in remission). Loss of bone marrow infiltration resulted in a 3.2-fold decrease in the expression level of *CXCR4* (p=0.032, Figure 18b), while no difference was observed for the expression of *CXCL12* (p=0.382, Figure 18b).

Results from immunohistochemical analysis of CXCR4 and CXCL12 in a subset of BM samples (n=19) verified the mRNA expression data. There was a noticeable moderate positive correlation between the bone marrow infiltration and the protein levels of CXCR4 and CXCL12 (Spearman rho=0.595, p=0.031 for CXCR4 and Spearman rho=0.775, p=0.005 for CXCL12, Figure 18). Interestingly, within the infiltrated bone marrow samples, approximately 80% of the lymphoma cells expressed CXCR4 on average, while about 35% showed CXCL12 expression. Conversely, in the adjacent tissue (stroma) and in bone marrow samples without infiltration, fewer than 30% of stromal cells displayed CXCR4 and CXCL12 expression (Figure 18c I-IV).

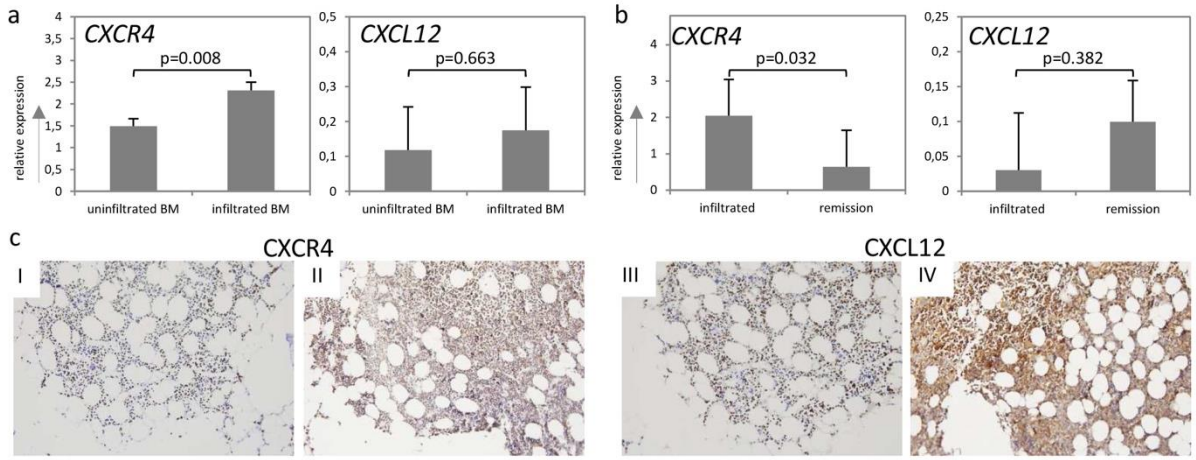

Figure 18: Expression of CXCR4 and CXCL12 in relation to bone marrow infiltration. (a) Examination of mRNA expression of CXCR4 and CXCL12 in bone marrow samples, comparing uninfiltrated and infiltrated samples at the time of diagnosis. (b) Evaluation of the mRNA expression of CXCR4 and CXCL12 with infiltration into bone marrow biopsies and matched samples from patients in remission (c) Examples of immunohistochemical staining for CXCR4 (I-II) and CXCL12 (III-IV) on selected bone marrow samples from patients with DLBCL (magnification 20x). (I) and (III) show the staining of CXCR4 and CXCL12 in uninfiltrated bone marrow samples, while (II) and (IV) show the matched staining in infiltrated bone marrow samples. mRNA expression levels were determined relative to uninfiltrated bone marrow samples. Each bar in the graph represents the mean expression value with standard error of the mean (SEM). Expression levels were assessed using either the Mann-Whitney U test or Students t-test. All images were taken using an Olympus BX51 microscope and an Olympus E-330 camera.

4.1.4. Lymphoma cell lines induced apoptosis when treated with CXCR4 antagonists

In our *in vitro* study of the effects of CXCR4 antagonists, we used the following cell lines: SuDHL4 (representing a GCB-DLBCL model), Rajii (representing an Burkitt's lymphoma model), RI-1 and U2932 (representing an nGCB-DLBCL model). In addition, we included the BL-2 lymphoma cell line, characterized by its notable CXCR4 expression and its propensity to migrate towards CXCL12 in transwell migration assays [169].

Initially, we assessed the surface expression of CXCR4 in all cell lines under examination using flow cytometry. Next, we conducted the $CXCL12^{AF647}$ binding assay, in

which we used antibodies for against CXCR4 and CXCR7. In all investigated cell lines CXCR4 expression was detected (Figure 19a). Furthermore, we observed that CXCL12^{AF647} bound specifically through CXCR4 in all investigated lymphoma cells, while it also bound through CXCR7 in RI-1 and Raji lymphoma cell lines. This observation suggests that Raji and RI-1 additionally express CXCR7 on their cell surface (Figure 19b).

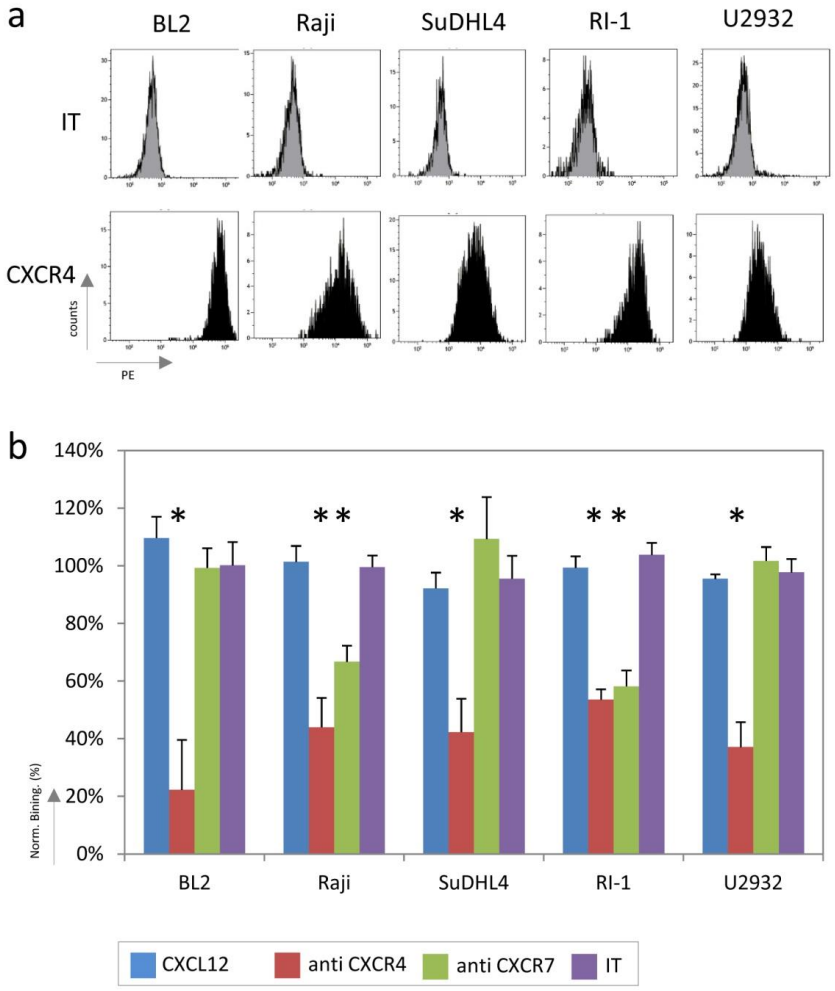

Figure 19: CXCR4 expression and CXCL12^{AF647} binding assay. (a) Surface expression of CXCR4 analyzed by flow cytometry in SuDHL4, RI-1, U2932, BL-2 and Raji cell lines. (b) Percentage of CXCL12^{AF647} binding in the presence and absence of blocking antibodies against CXCR4 and CXCR7, determined by flow cytometry. CXCL12 is bound by CXCR4 in all cell lines examined, with additional binding via CXCR7 observed in Raji and RI-1 cells. * indicates a significant reduction in CXCL12^{AF647} binding in the presence of antibodies against CXCR4 or CXCR7 compared to binding isotype controls ($p < 0.01$).

Subsequently, we conducted *in vitro* experiments to evaluate the impact of three CXCR4 antagonists: AMD3100 (FDA-approved drug), AMD070 (FDA-approved drug), and WK1, a niacin derivative of AMD070 synthesized in-house (Figure 20).

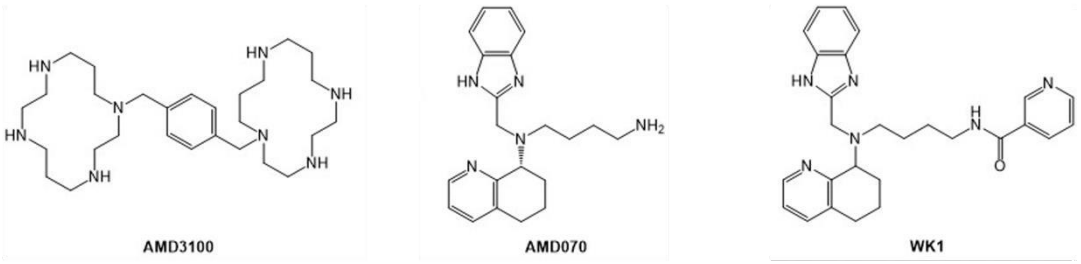

Figure 20: The molecular structure of the CXCR4 antagonists AMD3100, AMD070 and WK1.

All three antagonists showed the ability to prevent $CXCL12^{AF647}$ binding in a dose-dependent manner, as evidenced by the BL-2 cell binding assay (Figure 21a). Besides, AMD070 showed inhibition of transwell migration in BL-2 and U2932 lymphoma cells, whereas WK1 exhibited an inhibitory effect solely on U2932 cells (Figure 21b). It's worth noting that the effects of WK1 were significantly less pronounced in both assays compared to the other two inhibitors (as shown in Figure 21).

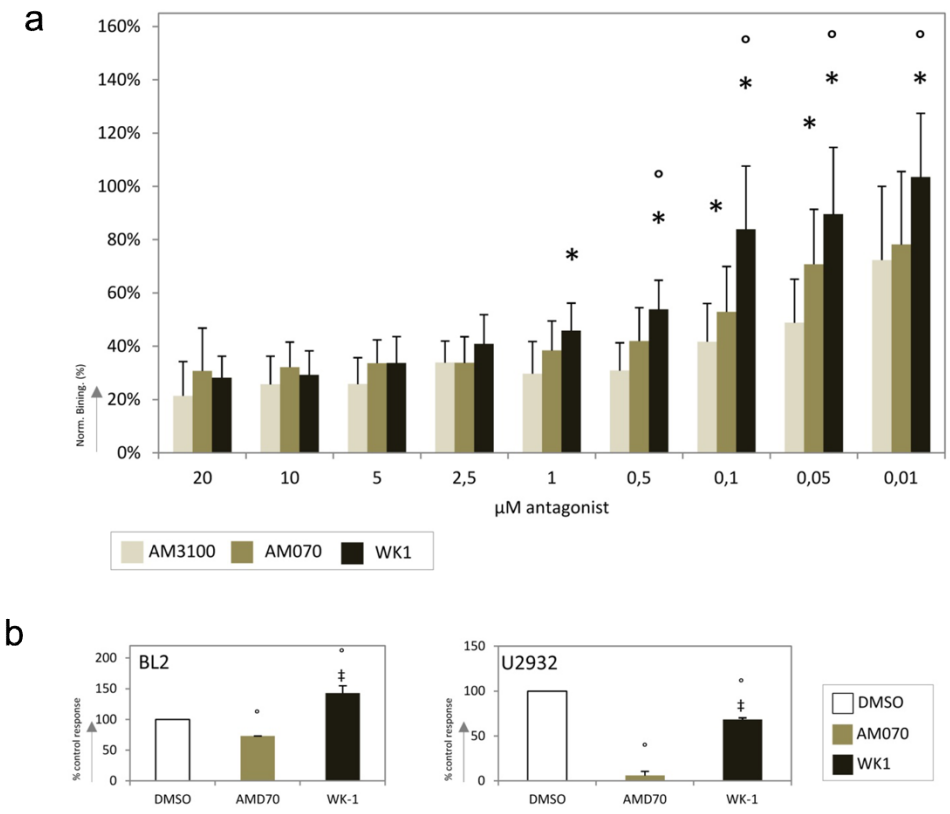

Figure 21: CXCR4 antagonists and CXCL12^{AF647} binding and CXCR4 antagonists and transmigration. (a) Percentage of CXCL12^{AF647} binding in the presence of AMD3100, AMD070 and its niacin derivative WK1 on BL-2 cells. All three antagonists tested effectively inhibit the binding of CXCL12^{AF647} to CXCR4. * indicates significant differences in CXCL12^{AF647} binding between AMD070 and WK1 compared to AMD3100 ($p < 0.01$). ° indicates significant differences in CXCL12^{AF647} binding between WK1 and AMD070. (b) Percentage of transmigration for BL2 (left graph) and U2932 (right graph) cells in the presence of AMD070 and its niacin derivative, WK1, compared to transmigration with DMSO as control. The use of AMD070 resulted in effective inhibition of transmigration in both cell lines, whereas the inhibitory effect of WK1 was less pronounced. ° indicates a significant inhibition of transmigration compared to the DMSO control ($p < 0.01$). ‡ indicates a significantly lower level of inhibition with WK1 compared to AMD070.

In particular, we observed a decrease in growth rates for WK1 and AMD070 in SuDHL4 and BL-2 lymphoma cells. In contrast, the growth rates of all other examined cell lines remained unaffected (Figure 22). Importantly, AMD3100 and niacin, when used individually, had no detectible effect (Figure 22).

WK1 displayed lower IC_{50} values than AMD070, at 15.4µM in BL-2 lymphoma cells and 26.76µM in SuDHL4 lymphoma cells. In contrast, AMD070 exhibited IC_{50} values of 31.18µM in BL-2 lymphoma cells and 26.76µM in SuDHL4 lymphoma cells (as shown in Figure 22).

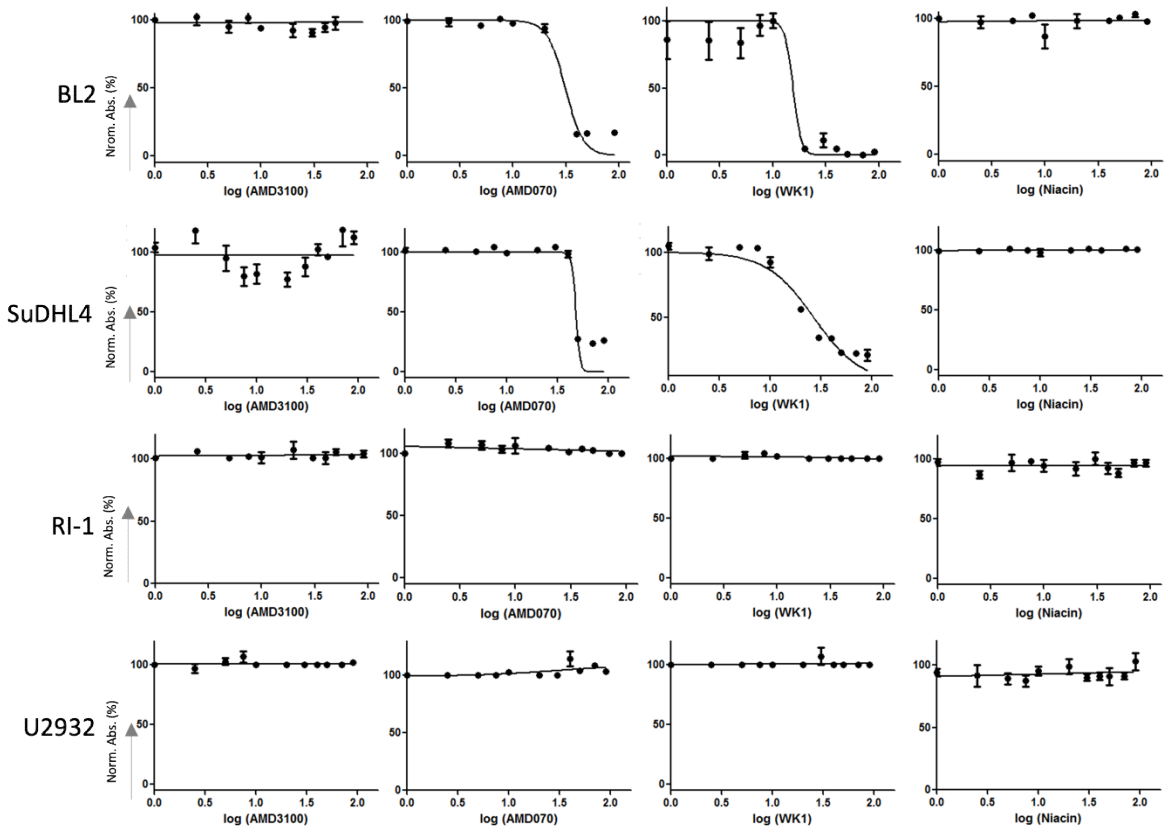

Figure 22: Growth inhibition of B cell lymphoma cell lines treated with CXCR4 antagonists. Cell growth of SuDHL4 (representing the GCB-DLBCL model), RI-1 and U2932 (representing the nGCB-DLBCL model) and BL-2 (representing the Burkitts model) cell lines was assessed under the influence of escalating concentrations (ranging from 1 to 90 μM) of CXCR4 antagonists, namely AMD3100, AMD070, its niacin derivative WK1 and niacin. This assessment utilized the EZ4U proliferation assay, with outcomes presented as a percentage of normal absorption.

To validate these findings, we exposed each of the four lymphoma cell lines to the three CXCR4 antagonists at varying concentrations, specifically ranging from 1μM to 40μM. Remarkably, after 48 hours of treatment, we observed a notable rise in the proportion of Annexin V+ cells in BL-2 and SuDHL4 with AMD070 and WK1 at 40μM compared to AMD3100 and DMSO ($p<0.005$, Figure 24a), indicating a pro-apoptotic effect of both CXCR4 antagonists.

Moreover, the proportion of viable lymphoma cells (Annexin V-/7AAD-) declined notably in BL-2 and SuDHL4 upon treatment with WK1 at concentrations of 10μM, 20μM, and 40μM, in contrast to treatment with DMSO and AMD3100 ($p<0.05$, Figure 23a and b). Conversely, U2932 and RI-1 displayed no significant response to any of the three CXCR4 antagonists used in the study (Figure 23c and d).

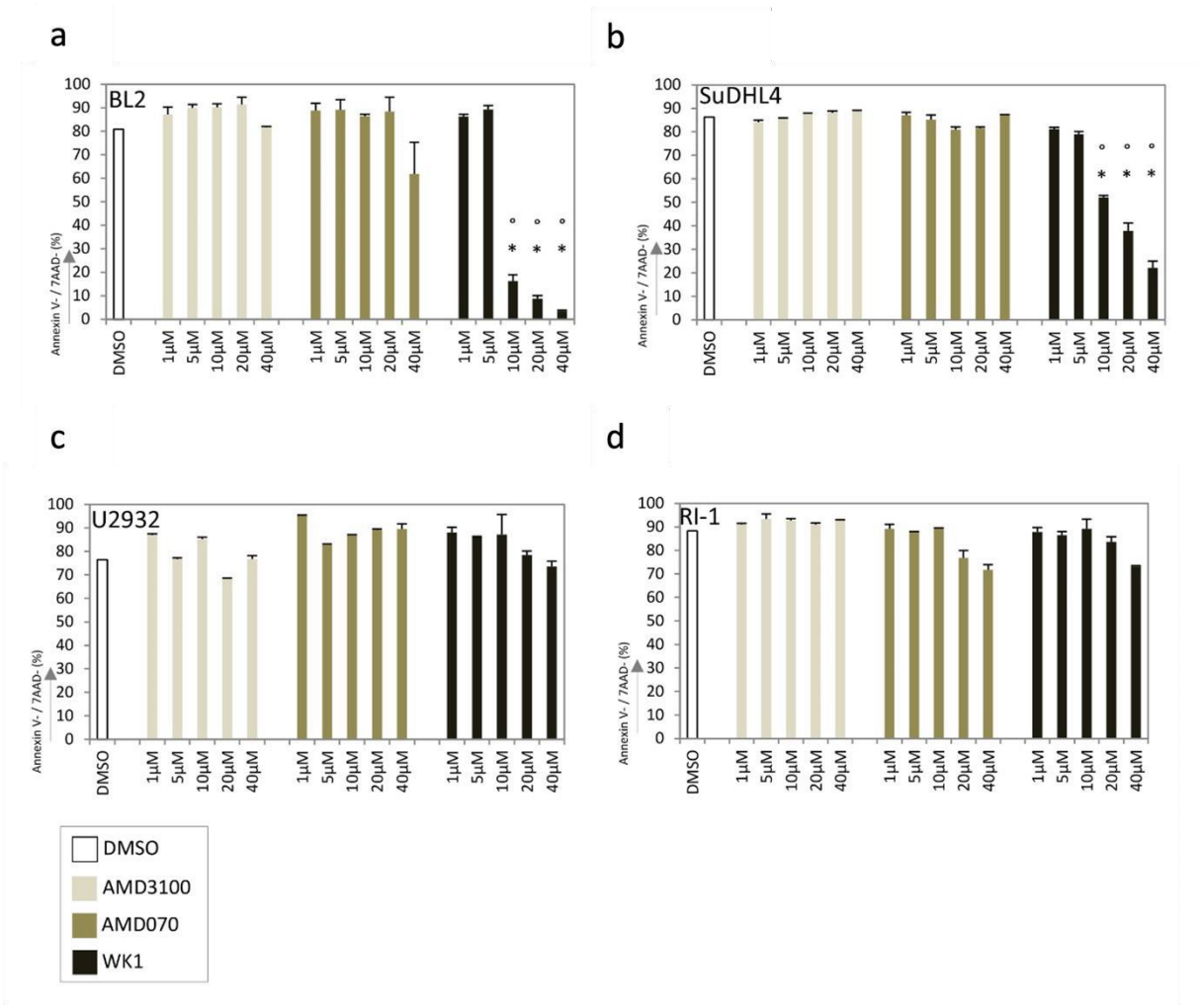

Figure 23: CXCR4 antagonists and their effect on cell viability. Cell viability was assessed by flow cytometry to determine the percentage of Annexin V/7AAD+ cells in the BL-2, SuDHL4, U2932 and RI-1 cell lines. Increasing concentrations of AMD3100, AMD070 and the niacin derivative WK1 were used and the results were compared with control cells treated with DMSO. Only BL-2 and SuDHL4 cells showed a decrease in viable (Annexin V/7AAD -) cells when treated with 10µM, 20µM and 40µM WK1 (a and b), while no such effect was observed in the other cell lines or with other antagonists. * indicates a significant reduction in viability when compared to AMD3100 ($p<0.05$). ° indicates a significant reduction in viability when compared to AMD070 ($p<0.05$).

Considering that all investigated lymphoma cell lines showed BCL-2 overexpression [180–183], it seems that the apoptotic impacts of AMD070 and WK1 are not contingent on the levels of BCL-2 expression. Finally, to validate the apoptotic effects of AMD070 and WK1, we assessed the proportion of cells exhibiting cleaved caspase 3 following DMSO, AMD070, or WK1 treatment in BL-2 and SuDHL4 cell lines. In both cell lines, two treatments with AMD070 and WK1 led to a notably increased proportion of lymphoma cells showing positivity for cleaved caspase 3 staining ($p<0.01$, Figure 24b). It's worth noting that the percentage of cleaved caspase 3 was notably greater with WK1 treatment, even when using lower concentrations, in contrast to AMD070. ($p<0.005$, Figure 24b). Taken together, these findings indicate that the newly introduced CXCR4-WK1 antagonism exerts potent pro-apoptotic effects on particular lymphoma cell lines.

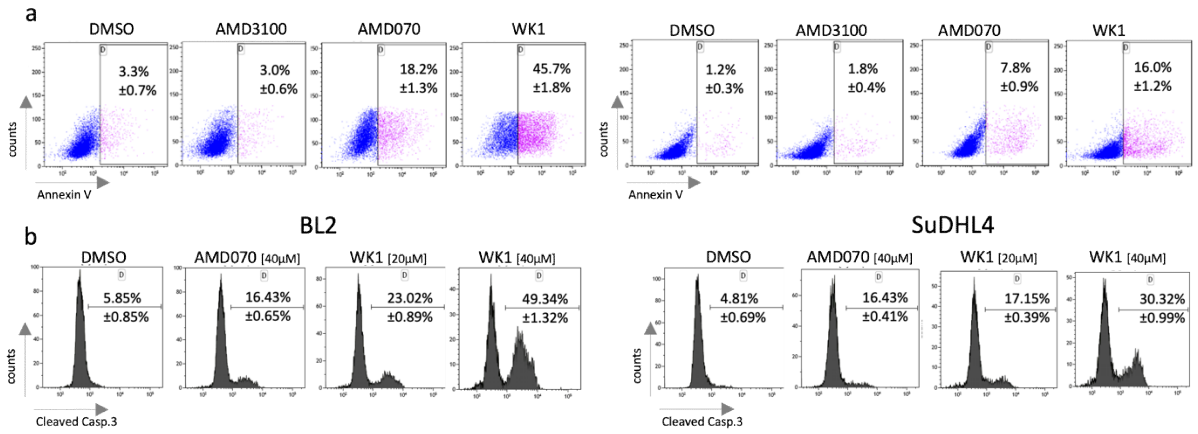

Figure 24: Apoptosis assays of B cell lymphoma cell lines treated with CXCR4 antagonists. (a) Annexin V positivity in BL-2 (representing the Burkitt's model) and SuDHL4 (representing the GCB-DLBCL model) cells treated with AMD3100, AMD070 and its niacin derivative WK1 (at a concentration of 40μM for 48 hours) as determined by flow cytometry and compared to control cells treated with DMSO. Treatments and Annexin V staining were performed in triplicate and results are presented as medians with standard deviations. (b) The percentage of cleaved caspase-3-positive BL-2 (Burkitt's model) and SuDHL4 (GCB-DLBCL model) cells treated with 40μM AMD070 or 20 μM and 40 μM of its niacin derivative WK1 for 24 hours as determined by flow cytometry and compared to control cells treated with DMSO. Treatments and cleaved caspase staining were performed in triplicate and results are presented as medians with standard deviations.

4.1.5. WK1 and AMD070 upregulated pro-apoptotic BCL-2 family members

To further investigate the pro-apoptotic impacts of the three CXCR4 antagonists, we performed treatments on BL-2 lymphoma cells, where apoptosis was triggered by AMD070 and WK1. In contrast, U2932 cell line showed no response to the treatment. We then evaluated the gene expression levels of both pro- and anti-apoptotic members of the BCL-2 family.

In BL-2 cells, treatment with AMD070 resulted in increased mRNA expression levels for two of the eight pro-apoptotic genes tested compared to DMSO (as shown in Figure 25a I) compared to DMSO. The genes exhibiting increased expression levels were *BAK*, showing a 2.4-fold increase after one hour (p=0.025), and *NOXA*, with a 3.3-fold increase after six hours (p=0.03). Two of the three anti-apoptotic genes also examined (as shown in Figure 25a II), specifically *BCL-XL* (with a 4.8-fold increase after three hours, p=0.039) and MCL-1 (with a 3.4-fold increase after six hours and a 3.7-fold increase at twelve hours, p<0.031) showed overexpression in comparison to DMSO treatment. In addition, AMD070 treatment resulted in a decrease in the expression levels of three pro-apoptotic genes (as shown in Figure 25a I). These genes comprised *BID*, demonstrating a 5.2-fold decrease after six hours (p = 0.032), *PUMA*, exhibiting a 2.3-fold decrease after six hours (p=0.042), and *BIM isoform 9*, showcasing a 3.1-fold decrease after twelve hours (p=0.049). In contrast, when U2932 cells were treated with AMD070, the expression of five out of the eight pro-apoptotic BCL-2 family members investigated was induced, with at least a 2-fold increase (as shown in Figure 25b I). Among these genes were *BAX*, showing a 2.7-fold increase after one hour (p=0.014), *NOXA*, indicating a 5.3-fold increase after six hours (p=0.043), *BID*, exhibiting a 2-fold increase at twelve hours (p = 0.048), *BIK*, demonstrating a 6-fold increase after six hours (p=0.015), and

BIM isoform 9, with a 2.2-fold increase after twelve hours (p=0.046). Moreover, one of the three anti-apoptotic members within the BCL-2 family, *BCL-XL*, exhibited overexpression, showing a 3.7-fold increase after one hour (p=0.044, shown in Figure 25b II). Furthermore, a decrease in expression was noted for three pro-apoptotic members (shown in Figure 25b I), comprising *BAK*, which displayed a 3.7-fold decrease after one hour (p=0.018), *BMF*, demonstrating a 3-fold decrease after one hour (p=0.043), and *PUMA*, showing a 2.21-fold decrease after one hour (p=0.035).

In BL-2 cells, WK1 treatment induced the expression of seven out of eight pro-apoptotic genes by at least 2-fold in comparison to DMSO control ($p<0.05$, as shown in Figure 25a I). These genes encompassed *BAK*, displaying a 3.4-fold increase after one hour (p=0.006), *BIM isoform 9*, indicating a 2.4-fold increase after one hour (p=0.011), *BIK*, exhibiting a 3.4-fold increase after three hours (p=0.041), *BMF*, showing an 11.2-fold increase after three hours and a 3.6-fold increase after six hours ($p<0.041$), *NOXA*, demonstrating a 4.2-fold increase after three hours and a 3.9-fold increase after twelve hours ($p<0.0041$), *BAX*, with a 33.1-fold increase after 12 hours (p=0.029), *PUMA*, displaying a 2.4-fold increase (p=0.023), and *BCL-XL*, with a 4.1-fold increase after twelve hours ($p<0.0001$, Figure 25a II). In contrast to the response in BL-2 cells, treatment with WK1 in U2932 cells (as shown in Figure 25b I and II) led to a minimum 2-fold increase in the expression of the pro-apoptotic genes *BID*, indicating a 2.1-fold increase after twelve hours (p=0.042), and *BIK*, showing a 7.8-fold increase after six hours (p=0.04). Additionally, there was a 2-fold decrease in the expression of *MCL-1*, with a 3-fold decrease after six hours (p=0.04), and *BCL-XL*, displaying a 4.1-fold decrease after twelve hours (p=0.041), as anti-apoptotic genes. Moreover, there was lower expression of *BAK*, indicating a 3.5-fold decrease after one hour (p=0.02), as a pro-apoptotic member of the BCL2 family.

Comparing WK1-treated BL-2 cells with AMD070, WK1 showed higher expression of five of the eight pro-apoptotic genes (as shown in Figure 25a I, $p<0.043$). These genes comprised *BIK*, displaying a 2.1-fold increase after three hours and a 4-fold increase after six hours ($p<0.043$), BMF, exhibiting a 2.4-fold increase after three hours (p=0.027), *BAX*, showing a 33.9-fold increase after twelve hours (p=0.028), the *BIM isoform 9*, indicating a 3.4-fold increase after 12 hours (p=0.011), *NOXA*, demonstrating a 3.8-fold increase after twelve hours (p=0.034), *PUMA*, with a 3.8-fold increase after twelve hours (p=0.025), and *BCL-2*, showcasing a 2.4-fold increase after six hours (p=0.044, Figure 25a II). Conversely, U2932 cell treated with WK1 showed at a minimum 2-fold decrease in the expression of four of the eight apoptotic genes examined (as shown in Figure 25b I and II). Among these genes, *BMF* showed a 2.4-fold decrease after six hours (p=0.045), *NOXA* exhibited a 3.4-fold decrease after six hours (p=0.043), *BCL-XL* displayed a 2.4-fold decrease after 12 hours ($p<0.001$), and *MCL-1* demonstrated a 2.4-fold decrease after six hours (p=0.044).

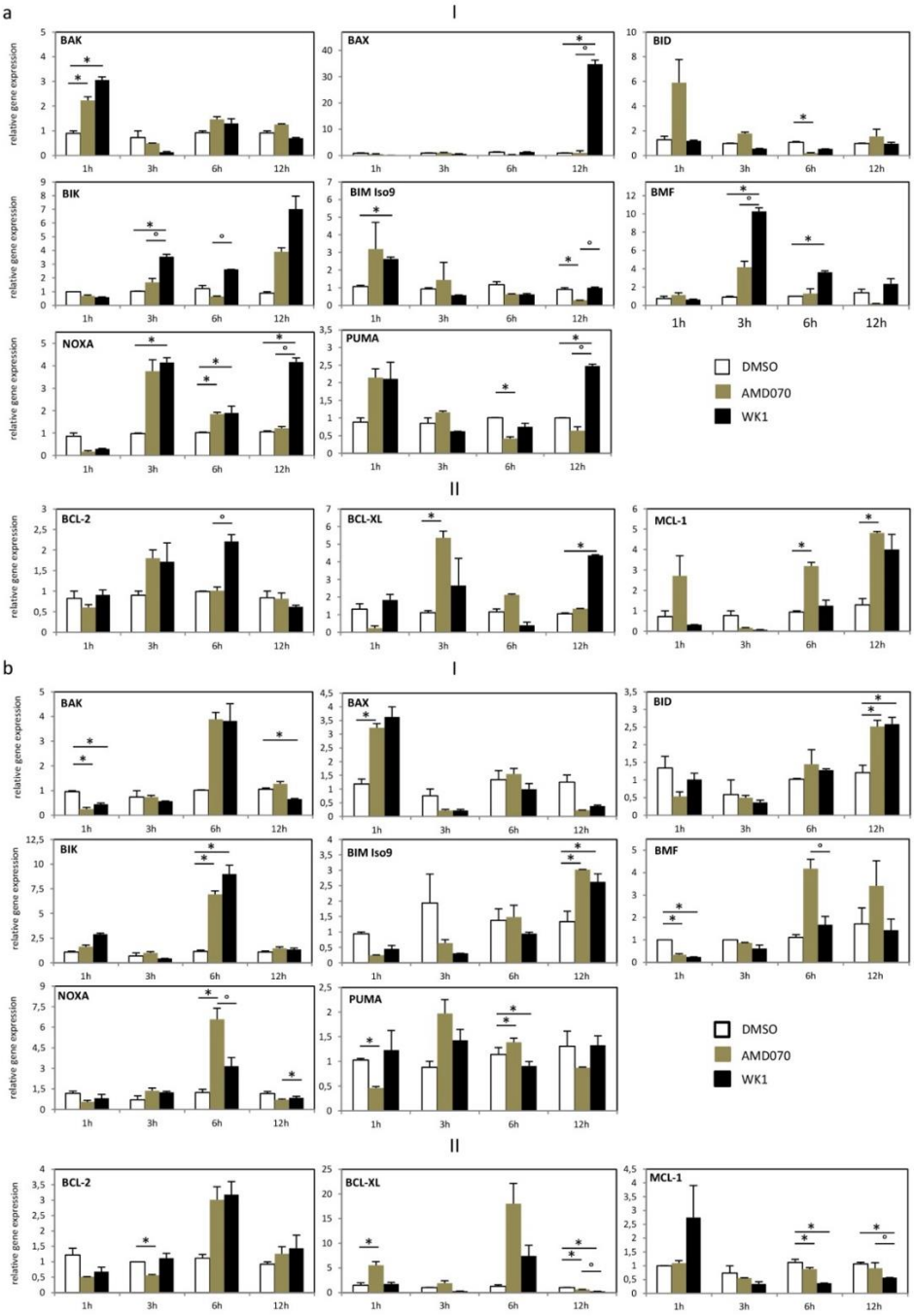

Figure 25: Gene expression levels of pro- and anti-apoptotic BCL-2 family members after treatment with AMD070 and WK1. (a) BL2 (as Burkitt's model) and (b) U2932 (as nGCB-DLBCL model) were exposed to 40µM AMD070 or its niacin derivative WK1 and gene expression levels of (I) pro-apoptotic and (II) anti-apoptotic BCL-2 family members were assessed at one, three, six and twelve hours compared to DMSO-treated control cells using RQ PCR. mRNA expression levels were calculated as relative expression by comparison to DMSO controls. Each bar represents the mean of the expression levels ± standard error of the mean (SEM). Comparison of expression levels was performed using Mann-Whitney U test or Student's t-test. * indicates a significant difference in expression when comparing to DMSO ($p \leq 0.05$). ° indicates a significant difference in expression when comparing treatment with AMD070 and WK1 ($p \leq 0.05$).

Treatment of BL-2 cells with AMD3100 (Figure 26a II) resulted in a minimum 2-fold upregulation in the expression of the anti-apoptotic *MCL-1* gene, exhibiting a 6.4-fold increase after one hour ($p=0.009$). Additionally, it resulted in decreased expression of two pro-apoptotic

members of the BCL-2 family (Figure 26a I), namely *BID*, showing a 2.4-fold decrease after six hours ($p=0.032$), and *PUMA*, with a 2.1-fold decrease after six hours and a 3.3-fold decrease after 12 hours ($p=0.031$).

In U2932 cells, treatment with AM3100 resulted in a minimum 2-fold decrease in the expression of three of the eight pro-apoptotic genes ($p<0.031$, Figure 26b I). Among these genes were *BAK*, exhibiting a 2-fold decrease after one hour ($p=0.031$), *BIM isoform 9*, showing a 2.2-fold decrease after one hour ($p=0.0286$), and *BMF*, demonstrating a 4.8-fold decrease after one hour ($p=0.001$). Additionally, it induced upregulation of the anti-apoptotic gene *BCL-XL*, with a 3.2-fold increase after twelve hours ($p=0.008$, Figure 26b II).

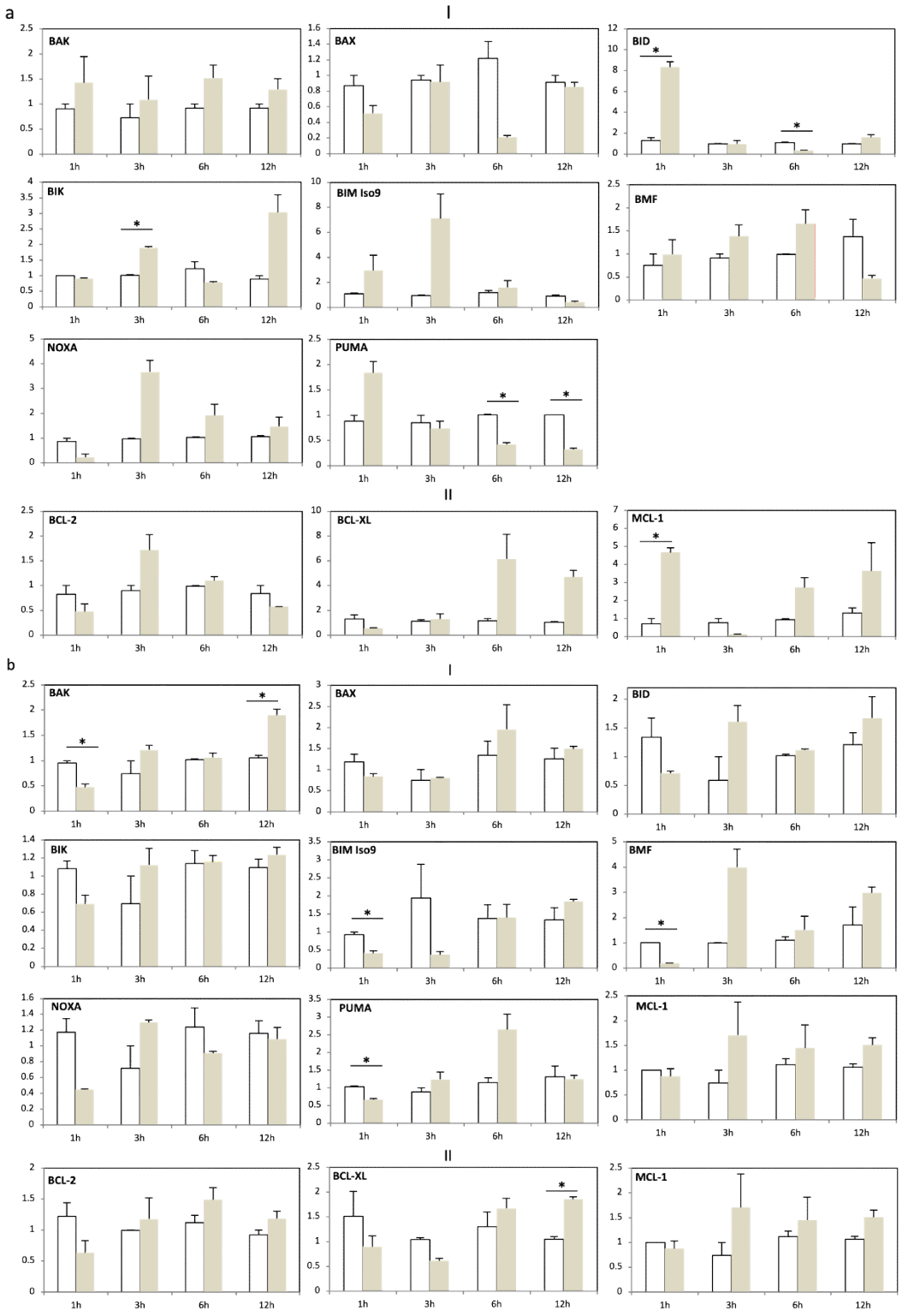

Figure 26: Gene expression levels of pro- and anti-apoptotic BCL-2 family members after treatment with AMD3100. (a) BL-2 and (b) U2932 cells were treated with 40µM AMD3100 and gene expression levels of (I) pro-apoptotic and (II) anti-apoptotic BCL-2 members were assessed after one, three, six and twelve hours of treatment. Relative expression levels were calculated in by comparison with DMSO-treated controls. Experiments were performed in duplicate and each bar in the graphs represents the mean expression values with standard error of the mean (SEM). Statistical comparisons of expression levels were made using the Mann-Whitney U test or Student's t-test. * indicates a significant difference in expression when comparing to DMSO ($p \leq 0.05$).

4.1.6. Treatment with WK1 results in the downregulation of JNK, ERK1/2, and NF-κB/BCR-targets

To investigate whether the treatment with CXCR4 antagonists influences NF-κB/BCR, JNK and ERK1/2, three critical pathways associated with lymphomagenesis [184–188], we administered AMD070 and WK1 to BL-2 cells, which exhibited induced apoptosis, and to the unaffected U2932 cell line. At 24 hours of treatment, we then measured the gene expression levels of target genes associated with the JNK pathway (including *ADARB, CFLAR, CCL22, CCR7*, *FN1* and *IL-10*, as determined by the Ingenuity Pathway Analysis tool), the ERK1/2 pathway (including *DUSP1, MXD1, cJUN, cFOS*, *JUNB*, *ETV5,* and *BUB1* [189]) and the NF-κB/BCR pathway (including *CCL4, BCL2A1, KLF10, OAS1, RGS1*, and *TNF* [190]).

In BL-2 cells, AMD070 treatment resulted in a reduction in the expression of *BUB1*, an ERK1/2 target, by 2-fold (p=0.0115). Additionally, it decreased the expression of *EGR3*, a NF-κB/BCR target, by 1.6-fold (p=0.0164). In contrast, it elevated the expression of MXD1, an ERK1/2 target, by 1.6-fold (p = 0.0343), and RGS1, a NF-κB/BCR target, by 1.6-fold (p=0.0343, Figure 27a). Treatment with WK1 resulted in the absence or diminished expression of three out of the six JNK targets analyzed (Figure 27a): *IL-10* was absent (p=0.021), while *CFLAR* exhibited reduced expression by 4.8-fold (p=0.0226), and *ADARB* showed a decrease of 9.9-fold (p=0.0001). It also led to reduced expression of four of the seven ERK1/2 targets analyzed (Figure 27a): *BUB1* decreased by 95.3-fold (p=0.0045), *MXD1* by 12.6-fold (p=0.0355), *JUNB* by 4.8-fold (p=0.0079), and *DUSP1* by 13.7-fold (p=0.0275). Additionally, it led to either decreased or increased expression of five out of seven NF-κB/BCR targets (Figure 27a): *EGR3* was downregulated by 27.9-fold (p=0.0215), and *BCL2A1*, *OAS1*, and *CCL4* were downregulated by 5.3-fold (p=0.044), 16.3-fold (p=0.029), and 4.3-fold (p=0.0034), respectively, while *TNF* was upregulated by 6.4-fold (p=0.042). In contrast, AMD3100 treatment did not induce any changes in the expression levels of the examined genes.

When comparing WK1-treated BL-2 cells with those treated with AMD070, three ERK1/2 targets—*BUB1*, *MXD1*, and *DUSP1*—were downregulated by 46.5-fold (p=0.001), 20.8-fold (p=0.028), and 22.8-fold (p=0.038). Upon WK1 treatment, four NF-κB/BCR targets—*CCL4*, *EGR3*, *BCL2A1*, and *RGS1*—were downregulated by 6-fold (p=0.003), 18.3-fold (p=0.035), 8.4-fold (p=0.014), and 9.8-fold (p=0.026), respectively (Figure 27a).

In U2932 cells, treatment with AMD070 led to the downregulation of two ERK1/2 targets (Figure 27b): *BUB1* exhibited a 1.7-fold decrease (p=0.048), and *DUSP1* showed a 2.5-fold decrease (p=0.019). Additionally, *RGS1*, a NF-κB/BCR target, displayed a 1.3-fold decrease (p=0.042). Moreover, AMD070 treatment resulted in the upregulation of *MXD1,* an ERK1/2 target, by 1.7-fold (p=0.049). Treatment with WK1 (Figure 27b) led to increased expression levels of FN1 by 4.4-fold (p=0.0097), ADARB by 3-fold (p=0.008), and MXD1 by 1.7-fold

(p=0.0135). Additionally, it upregulated RGS1 by 1.3-fold (p=0.045), EGR3 by 17-fold (p=0.0452), and TNF by 13.7-fold (p=0.044), all of which are NF-κB/BCR targets.

When comparing U2932 cells treated with WK1 to those treated with AMD070 (Figure 27b), WK1 treatment showed upregulated expression of IL-10 by 1.4-fold (p=0.0132) and *FN1* by 3.7-fold (p=0.0217). Moreover, in WK1-treated cells, three JNK targets - *MXD1* (1.4-fold increase, p=0.0095), *cJUN* (2.1-fold increase, p=0.025), and *cFOS* (1.6-fold increase, p=0.05) - exhibited elevated expression levels. Additionally, three ERK1/2 targets - *RGS1* (1.7-fold increase, p=0.0349), *EGR2* (2.1-fold increase, p=0.025), and *TNF* (3.2-fold increase, p=0.0278) - were also detected.

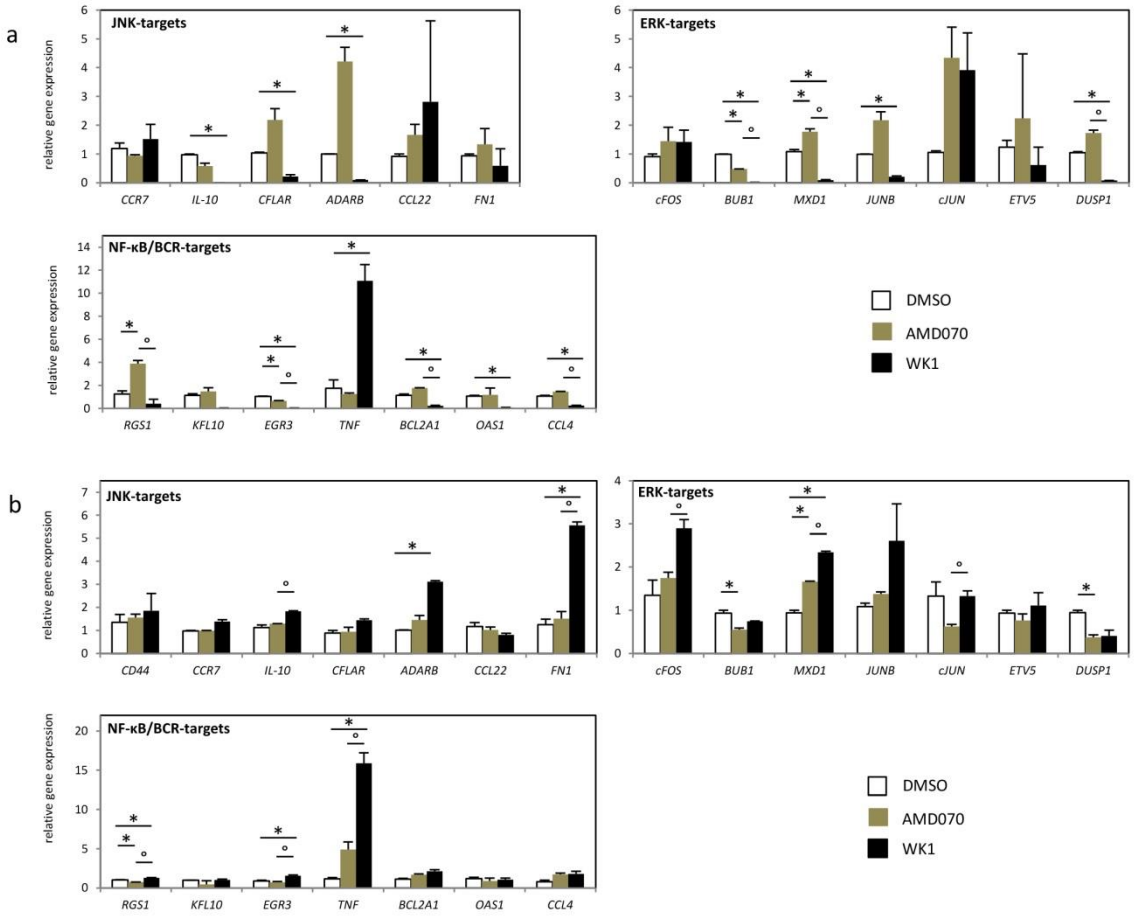

Figure 27: Expression of genes related to ERK1/2, NF-κB/BCR and JNK targets after treatment with AMD070 and WK1. (a) BL-2 cells, representing the Burkitt's model, and (b) U2932 cells, representing the nGCB-DLBCL model, were exposed to 40μM AMD070 or its niacin derivative WK1, and after 24 hours, the gene expression levels of ERK1/2 targets (BUB1, cFOS, cJUN, DUSP1, ETV5, JUNB, MXD1), JNK targets (ADARB, CCL22, CCR7, CFLAR, FN1, IL-10), and NF-κB/BCR targets (BCL2A1, CCL4, KLF10, OAS1, RGS1, TNF) were assessed by RQ-PCR and compared to the expression in DMSO-treated control cells. The mRNA expression levels were calculated as relative expression compared to DMSO controls. Each bar represents the mean of the expression levels ± standard error of the mean (SEM). Co Comparison of expression levels was conducted using Mann-Whitney U-test or Student's t-test. * indicates significant difference in expression compared to the DMSO control (p≤0.05). ° indicates a significant difference in expression between AMD070 and WK1 treatments (p≤0.05).

4.2. Understanding the role of *Nr4a1* in aggressive lymphomas and the tumor microenvironment

4.2.1. *Nr4a1* loss shapes TME in lymphoma mouse model

We intravenously transplanted murine lymphoma cells with and without *Nr4a1* loss into C57BL/6 wild-type mice (n=9 per genotype) as a model exhibiting a functional immune system and TME to characterize the relationship between TME and lymphoma cells with and without *Nr4a1* loss. On day 18, mice were euthanized and spleens were excised. We then prepared single-cell suspensions of splenocytes, which were stained with antibodies and subjected to multicolor flow cytometry to analyze immune cell infiltration (Figure 28a).

Six out of nine mice in each group developed a characteristic infiltration of lymphoma cells that manifested as paralysis and splenomegaly, and we also found a higher ratio of spleen weight to body surface area (BSA) in mice injected with *Nr4a1*-deficient lymphoma cells (p=0.0592) (Figure 28b). Furthermore, we detected a higher frequency of CD45+ B220+ IgM- B cells, which was the phenotype of the transplanted lymphoma cells, in the spleen by flow cytometry in the *Nr4a1 -/-* setting (p=0.0087) (Figure 28c), indicating a greater occurrence of lymphoma mass. The gating strategy to detect transplanted lymphoma cells is shown in Figure S 1.

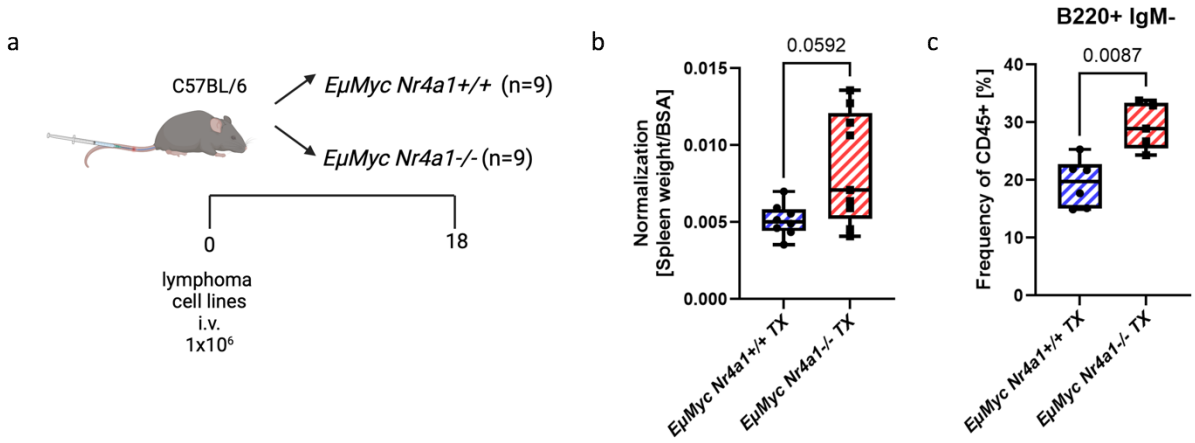

Figure 28: *Nr4a1* shapes TME in lymphoma. (a) Schematic representation of the experimental procedure that was carried out on the *in vivo* syngeneic mouse model. C57BL/6J wild-type mice were injected intravenously (i.v.) with murine lymphoma cells with and without *Nr4a1* loss**.** After 18 days, mice were euthanized and spleens were harvested. (b) Body surface area (BSA) was calculated. (c) The figure displays box plot of the frequency of CD45+ B220+ IgM- B cells transplanted murine lymphoma cells with and without *Nr4a1* loss. Statistical differences were evaluated using the Mann-Whitney U test.

4.2.2. Transplantation of *Nr4a1*-deficient murine lymphoma cells into wt mice results in altered lymphoid cell subsets in the TME, but in no changes in myeloid cell subsets

Flow cytometric analysis to study the major lymphoid cell subsets in immunocompetent mice transplanted with murine lymphoma cells with and without *Nr4a1* loss (gating strategies shown in Figure S 2) revealed a lower CD3+ T cell content (p=0.0101), including their subtypes of CD4+ (p=0.0051) and CD8+ T cells (0.0164), in the *Nr4a1*-deficient setting. Interestingly,

there was no difference in the γδ T cell content (p=0.7917). Also, a lower NKT cell content was observed (p=0.0164), while NK cells were detectable in a slightly lower frequency in the *Nr4a1-/-* setting (p=0.2020) (Figure 29a).

Next, we analyzed the myeloid cell populations in the TME. The gating strategy used for this analysis is shown in Figure S 3. We analyzed myeloid cell populations in the TME and found no differences in the frequency of myeloid cells, including macrophages, DCs, neutrophils, eosinophils, monocytes, and macrophages, between the two conditions (p>0.1375, Figure 29b). In a further subanalysis focusing on inflammatory M1 macrophages and anti-inflammatory macrophages M2, we observed a higher content of M2 macrophages in the engrafted lymphomas *Nr4a1* loss (p=0.021) (Figure 29b). In contrast, no differences for DC subsets such as monocyte-derived DCs (mDCs), plasmacytoid DCs as well as conventional DC type 1 cells (cDCs1) were detected (p>0.432) (Figure 29b).

Collectively, these findings suggest that *Nr4a1* likely influences the composition of lymphoid cells within the TME, notably CD3+ T cells encompassing CD4+ and CD8+ T cells, as well as NKT cells and NK cells. Moreover, the *Nr4a1* loss appears to lead to an immune-cell-depleted and anti-inflammatory TME, characterized by diminished lymphoid cell populations and an increased prevalence of M2 macrophages.

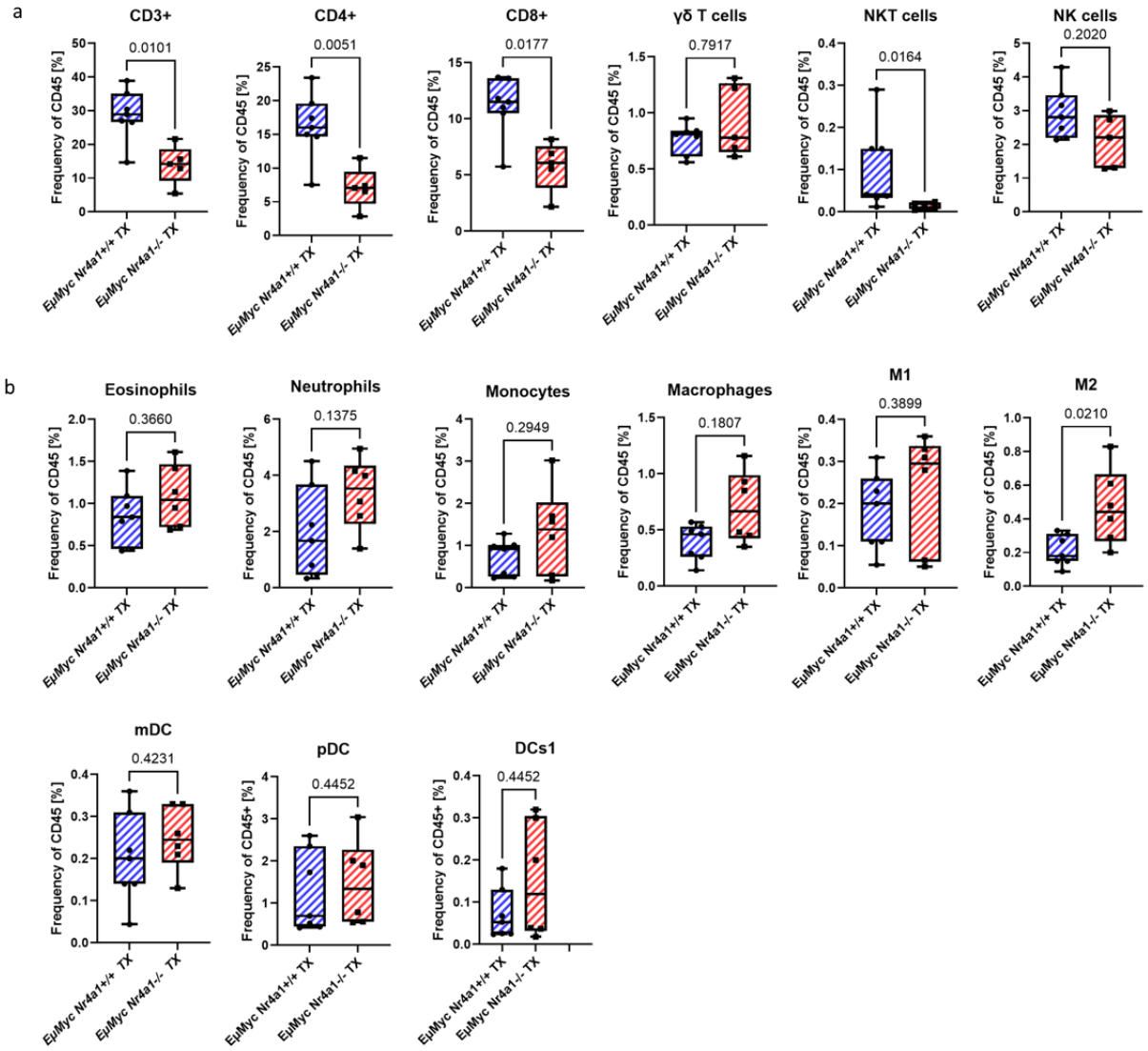

Figure 29: Lymphoid immune microenvironment of immunocompetent mice transplanted with murine lymphoma cells with and without *Nr4a1* loss. Flow cytometric analysis was performed on single-cell suspensions of spleens to determine the percentage of infiltrating CD45+ lymphoid cells. (a) The figures display box plots of the frequency of CD45+ lymphoid cells in transplanted murine lymphoma cells with and without *Nr4a1* loss. (b) The figures display box plots of the frequency of CD45+ myeloid cells in transplanted murine lymphoma cells with and without *Nr4a1* loss. Statistical differences were evaluated using the Mann-Whitney U test.

4.2.3. Mice transplanted with *Nr4a1*-deficient murine lymphoma cells showed differences in CD4+ and CD8+ T cells

Regarding the activation status of CD4+ and CD8+ T populations in engrafted lymphomas with or without *Nr4a1* loss, we observed a lower content of naïve CD4+ (p=0.0303) and CD8+ T cells (p=0.0480) in the *Nr4a1*-deficient setting, whereas the prevalence of effector CD4+ (p=0.048) and CD8+ T cells (p=0.0101) (characterized by CD44+ CD62L-) was higher. For memory CD4+ and CD8+ T cells, on the other hand, no differences were detected (p>0.03433, Figure 30a and b). Interestingly, we found a higher CD4+ Tregs content in engrafted *Nr4a1* -/- lymphomas (p=0.0025) (Figure 30c). Gating strategies for the analyses for

the *Nr4a1+/+* and *Nr4a1-/-* lymphomas derived from the immune-competent transplantation model are shown in Figure S 2.

The results suggest that the T cells potentially encounter continuous tumor-specific antigens and drive the activation and differentiation into an effector T cell state in the *Nr4a1* deficient setting. Moreover, the higher CD4+ Tregs content indicates immunosuppressive conditions within the TME, as given that Tregs are recognized for their ability to dampen the activity of effector T cells [191].

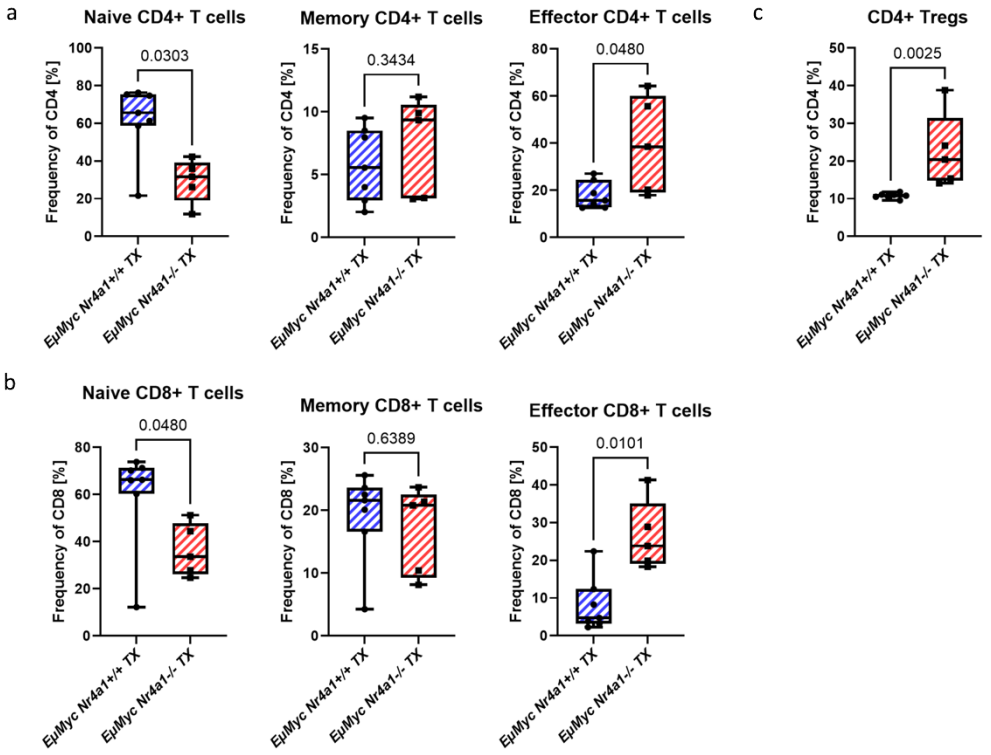

Figure 30: The activation status of CD4+ and CD8+ T cells and the frequency of CD4+ Tregs were analyzed in immunocompetent mice transplanted with murine lymphoma cells with and without *Nr4a1* loss. Flow cytometric analysis was performed on single-cell suspensions of spleens to determine the percentage of infiltrating CD45+ lymphoid cells. (a) The figures show box plots of the frequency of CD45+ of naive, memory and effector CD4+ T cells in transplanted murine lymphoma cells with and without *Nr4a1* loss. (b) The figures show box plots of the frequency of CD45+ of naive, memory and effector CD8+ T cells in transplanted murine lymphoma cells with and without *Nr4a1* loss. (c) The figure shows a box plot of the frequency of CD45+ of CD4+ Tregs in transplanted murine lymphoma cells with and without *Nr4a1* loss. Statistical differences were evaluated using the Mann-Whitney U test.

4.2.4. Increased levels of immune checkpoints on CD3+ T cells and their corresponding ligands on malignant B cells in mice transplanted with *Nr4a1*-deficient murine lymphoma cells

Our preliminary data generated by our mouse models and human samples (Figure 10-8) indicate that *Nr4a1* is potentially involved in the modulation of immune checkpoint components, leading to a TME characterized by immune cell exhaustion. To further dissect this function of *Nr4a1*, we measured the surface expression of various immune checkpoint proteins and their corresponding ligands (Figure 31). Gating strategies for the analyses for the

Nr4a1+/+ and *Nr4a1-/-* lymphomas derived from the immune-competent transplantation model are shown in Figure S 4-9.

In *Nr4a1*-deficient lymphomas, we observed a notable increase in the proportion of CD3+ T cells expressed PD1 (p=0.0401), CTLA-4 (p=0.0426), TIGIT (p=0.0541), TIM-3 (p=0.0530), and CD160 (p=0.0089) in *Nr4a1*-deficient lymphomas (Figure 32 a-f). In contrast, no differences were detected for LAG3 (p=0.126) and VISTA (p=0.1136) between the two genotypes (Figure 29 e).

Analyzing the corresponding ligands on malignant B220+ B cells, we only observed a higher frequency of malignant cells expressing CD155 (0.0263), which is involved in the TIGIT axis, and CD86, which is implicated in the CTLA-4 axis (p=0.020) (Figure 28b and c). There was no evidence for different expressions on the surface of B cells for any other ligands, but most of the ligands showed a trend towards higher expression on B cells, especially PDL1, PDL2, and CD80 (Figure 31a and c, p>0.4634).

These findings suggest a potential association between *Nr4a1* loss and immune exhaustion in aggressive lymphoma. This is characterized by the upregulation of diverse immune checkpoints on T cells, along with their corresponding ligands on the malignant B cells.

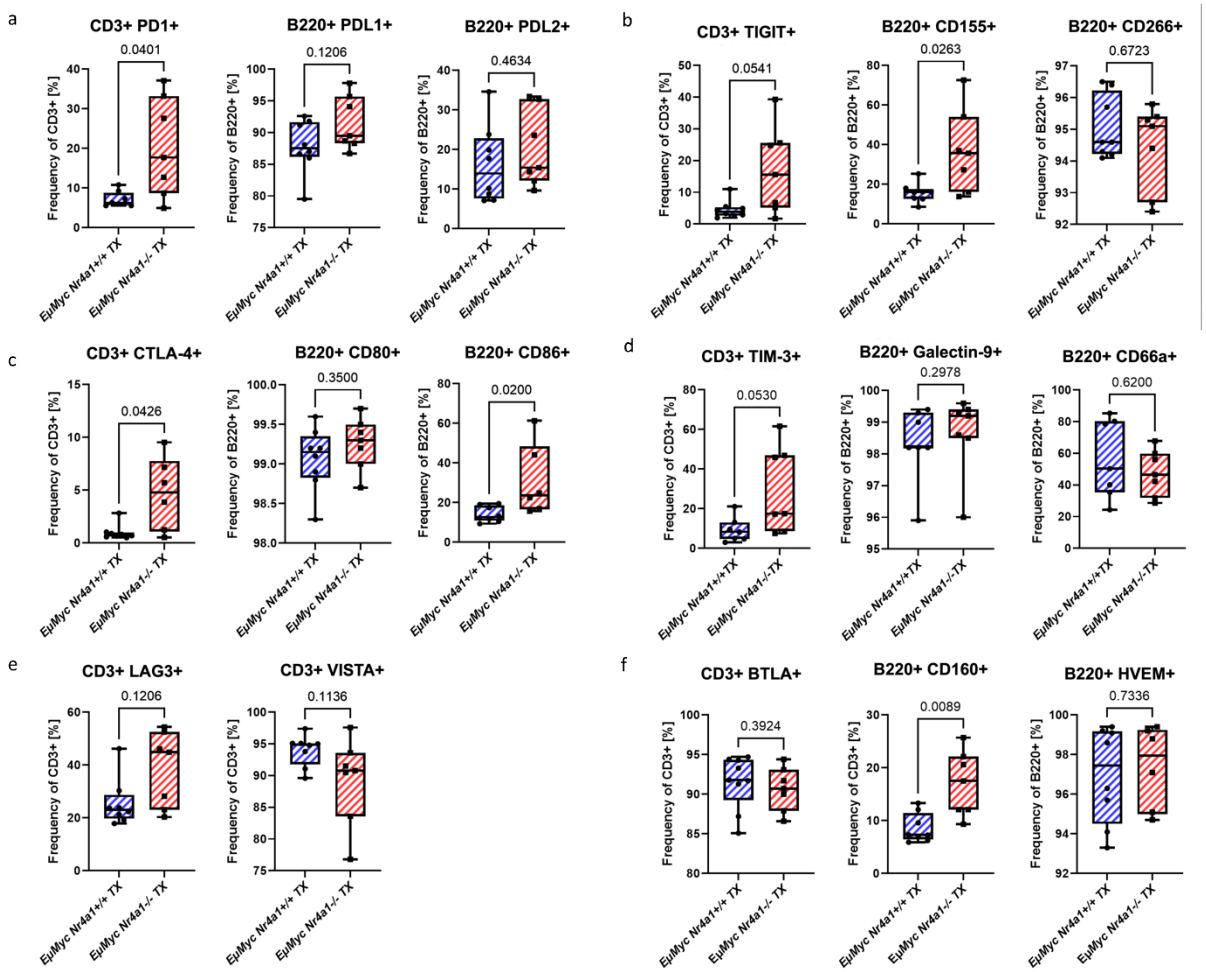

Figure 31: Expression of immune checkpoints proteins on CD3+ T cells and their corresponding ligands on B220+ B cells in mice transplanted with murine lymphoma cells with and without *Nr4a1* loss. Flow cytometric analysis was conducted on single-cell suspensions of spleens. Box plots show percentage of CD3+ T cells expressing (a) PD1, (b) TIGIT, (c) CTLA-4, (d) TIM-3, (e) LAG3, VISTA, and (f) BTLA, as well as their corresponding ligands on B220+ B cells. Statistical differences were assessed using the Mann-Whitney U test.

4.2.5. Elevated expression of immune checkpoints on CD3+ T Cells and multiple immune checkpoints on CD3+ PD1+ T cells suggest an exhausted phenotype

To strengthen the evidence supporting the occurrence of T cell exhaustion to a greater extent in *Nr4a1*-deficient lymphomas, we examined the co-expression of multiple immune checkpoints on CD3+ T cells. Such co-expression serves as a hallmark of this immune suppressive mechanism [191]. Gating strategies for the analyses for the *Nr4a1+/+* and *Nr4a1-/-* lymphomas derived from the immune-competent transplantation model are shown in Figure S 10.

In these analyses, a higher proportion of CD3+ T cells expressed PD1, CTLA-4, LAG3, TIM-3 and TIGIT ($p<0.0402$, Figure 32a) in the *Nr4a1*-deficient setting, whereas no differences for Vista was detected ($p=0.1206$, Figure 32a). Remarkably, a higher proportion of CD3+ PD1+ T cells co- expressed CTLA-4, LAG3, TIM-3, TIGIT, and VISTA ($p<0.093$, Figure 32b). Our data, along with increased lymphoid cell populations and higher expression of immune

checkpoints on T cells, indicate an immune-depleted-exhausted TME in murine lymphoma cells with *Nr4a1* loss.

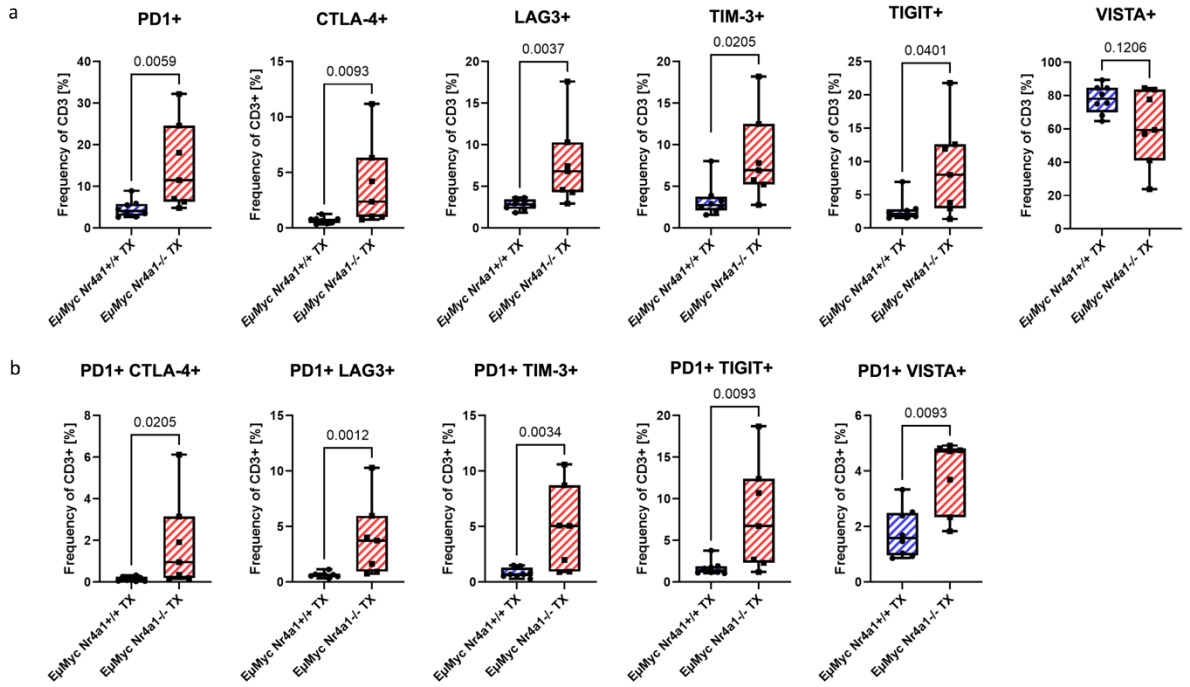

Figure 32: The expression of immune checkpoint proteins on CD3+ T cells and the co-expression of multiple immune checkpoints on CD3+ PD1+ T cells in mice transplanted with murine lymphoma cells with and without *Nr4a1* loss. (a) Flow cytometric analysis was performed on single-cell suspensions of spleens. Box plots show the percentage of CD3+ T cells expressing PD1, TIGIT, CTLA-4, BTLA, TIM-3, LAG3, and VISTA. (b) Co-expression of CTLA-4, LAG3, TIM-3, TIGIT, and VISTA on CD3+ PD1+ T cells was also analyzed. Statistical differences were assessed using the Mann-Whitney U test.

4.2.6. Mice transplanted with *Nr4a1*-deficient lymphoma cells showed no change in MHC I expression, but a trend towards to higher expression of MHC II

To further study the effect of Nr4a1 on the antigen presentation, we investigated the surface expression via flow cytometry of MHC I and II on B220+ B cells in the engrafted lymphoma with and without *Nr4a1* loss. The gating strategies for the analyses for the *Nr4a1+/+* and *Nr4a1-/-* lymphomas derived from the immune-competent transplantation model are in Figure S 11.

All B220+ B cells express MHC I (Figure 33a). In contrast, a higher percentage of B220+ B cells expressed MHC II molecules in the *Nr4a1*-deficient setting (p=0.0649, Figure 33b). These findings indicate a potential mechanism by which *Nr4a1* loss may a more affect CD4+ T cell activation and response to lymphoma cells.

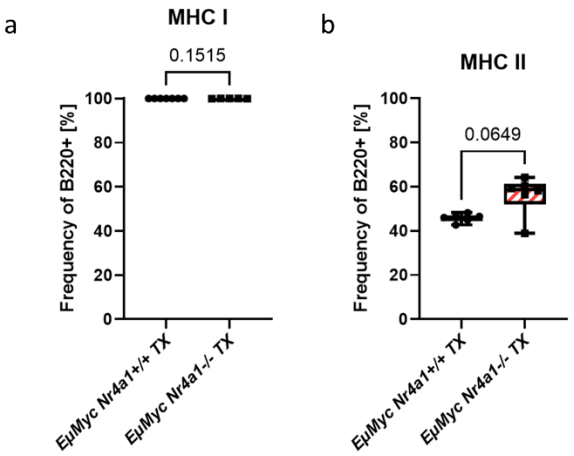

Figure 33: The surface expression of MHC I and MHC II molecules on B220+ B cells in mice transplanted with murine lymphoma cells with and without *Nr4a1* loss. Flow cytometric analysis was performed on single-cell suspensions of spleens. (a) Box plot shows surface expression of MHC I molecules. (b) Box plot shows surface expression of MHC II molecules. Statistical differences were assessed using the Mann-Whitney U test.

4.2.7. Loss of *Nr4a1* leads to reduced lymphoma cell lysis *in vitro*

Our preliminary results indicate that the absence of *Nr4a1* results in increased expression of various immune checkpoints, which in turn accelerates lymphoma progression in an immunocompetent environment. Therefore, we conducted experiments to investigate whether the presence of *Nr4a1* positively influences T cell functionality.

Therefore, we conducted co-culture cytotoxicity assays to determine the influence of *Nr4a1* on T cell-mediated lysis of aggressive lymphomas. For this experiment, *OT-1* transgenic mice were used as a model system. These mice possess CD8+ T cells expressing a transgenic T cell receptor (TCR) specific for ovalbumin ($OVA_{257-264}$) [176,192–195]. Pre-activated *OT-1* CD8+ T cells were co-cultured with *EμMyc Nr4a1+/+* and *EμMyc Nr4a1-/-* cells. Before co-culturing, the lymphoma cells were stained with low and high levels of the cell tracer dye CFSE as $CFSE_{low}$ and $CFSE_{high}$ cells, respectively. Additionally, $CFSE_{high}$ lymphoma cells were pulsed with the $OVA_{257-264}$ peptide, which serves as a target for *OT-1* CD8+ T cells, while the unpulsed $CFSE_{low}$ lymphoma cells served as a control, which should not be lysed by *OT-1* CD8+ T cells. The staining pattern of $CFSE_{low}$ and $CFSE_{high}$ lymphoma cells with and without *Nr4a1* loss (in a ratio of 1:1) is shown in Figure S 13b. This figure presents a representative histogram of the co-culture experiment with *OT-1* CD8+ T cells co-cultured with CFSE-stained lymphoma cells with or without *Nr4a1* loss. Co-culture experiments were conducted using two different ratios of effector cells (*OT-1* T cells, E) to target cells (lymphoma cells, T), namely 3:1 and 5:1. The cells were co-incubated for 4, 8, 16, and 24 hours, and then analyzed using flow

cytometry to determine the ratios of $CFSE_{low}$ and $CFSE_{high}$ lymphoma cells for calculation of the specific lysis.

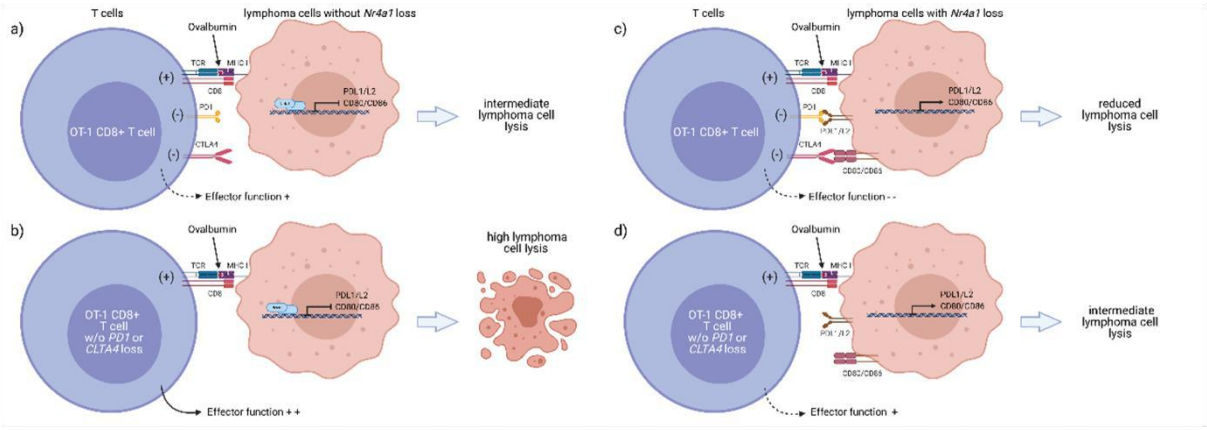

Figure 34: Schematic illustration of the interaction between *Ctla-4+/+* and *Ctla-4-/- OT-1* CD8+ T cells and lymphoma cells with or without *Nr4a1* loss. (a) Interaction between *OT-1* CD8+ T cells and lymphoma cells without *Nr4a1* loss leads to intermediate lymphoma cell lysis. In general, the major histocompatibility complex (MHC) complex on lymphoma cells presents OVA antigen to OVA-specific T cell receptor (TCR) on *OT-1* T cells to induce activation. (b) Loss of *Nr4a1* and the loss of *Ctla-4* on *OT-1 CD8+* T cells could lead to a high lymphoma cell lysis. (c) The interaction of immune checkpoints specially *Ctla4* on T cells with its ligands on lymphoma cells with *Nr4a1* loss leads to a reduced lymphoma cell lysis caused by reduced effector function of the T cells. (d) *Ctla4-/- OT1* CD8+ T cells might lead to an intermediate lymphoma cell lysis. Created with BioRender.com

The co-culture experiments with E:T ratios of 3:1 and 5:1 showed that *OT-1* CD8+ T cell-mediated lymphoma cell lysis is reduced in *Nr4a1*-deficient lymphoma cells compared to lymphoma cells without *Nr4a1* loss at 8h, 16h and 24h (percentage of specific lysis is shown in Figure 35a and b). In the co-culture experiment using an E:T ratio of 3:1, lower percentage of tumor cell lysis was observed in the experiment using lymphoma cells with *Nr4a1* loss (36.1% at 16h and 55.7% at 24h in the *Nr4a+/+* setting and 13.2% at 16h and 22.9% at 24h in the *Nr4a1-/-* setting; $p<0.084$, Figure 3c). As expected, the level of T cell-mediated lymphoma cell lysis was increased by increasing the number of effector cells, but also a lower percentage of tumor cell lysis was observed in the Nr4a1 deficient setting (44.8% at 16h and 72% at 24h in the *Nr4a1+/+* setting and 22.3% at 16h and 36% at 24h in *the Nr4a1-/-* setting, $p<0.025$, Figure 35d).

Collectively, these findings support the data generated in our murine model on the immunoregulatory function of *Nr4a1* in aggressive lymphomas and suggest that *Nr4a1* has the ability to modulate T cell-mediated lysis by the modulation of immune checkpoint molecules.

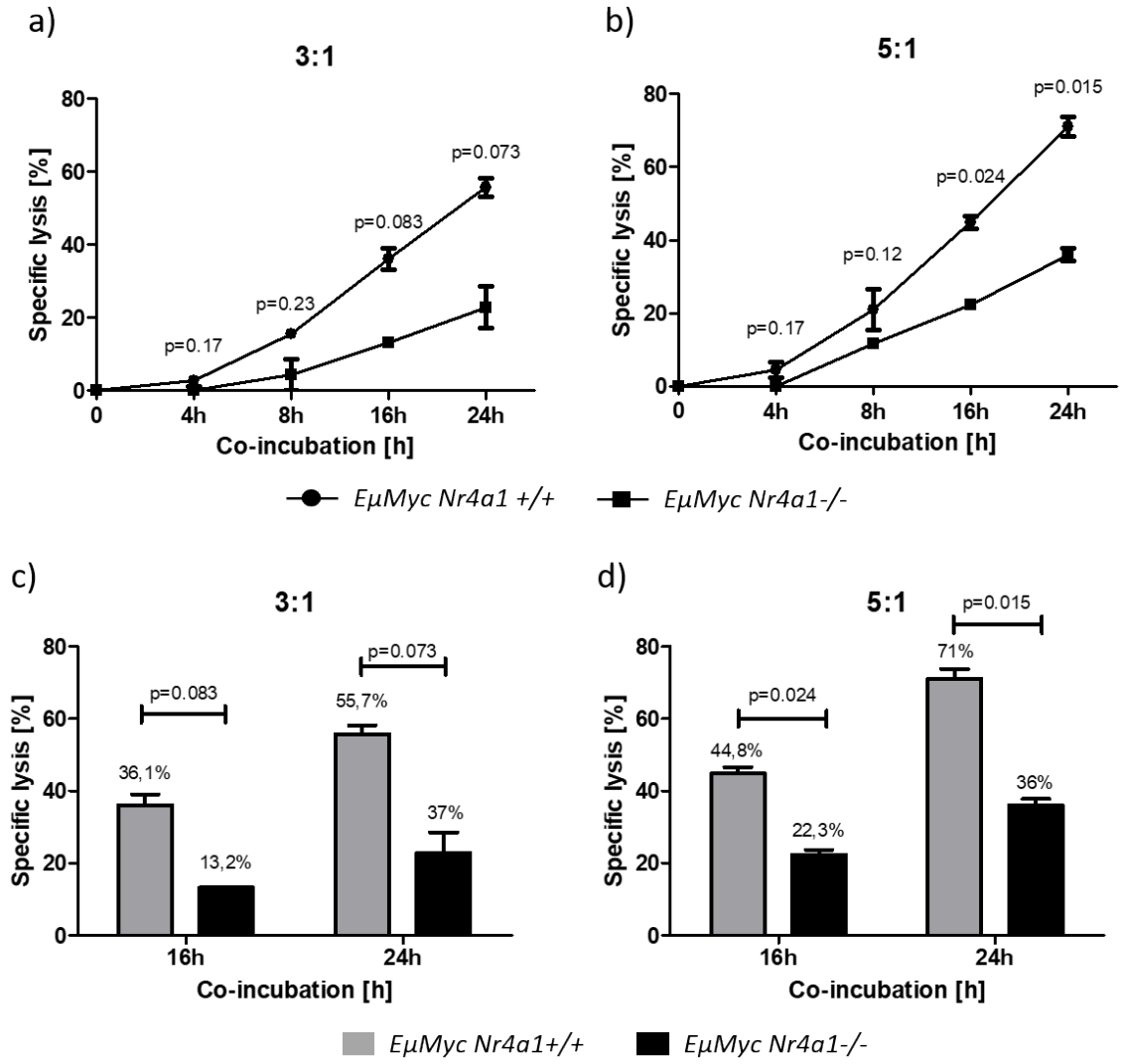

Figure 35: OVA-specific lysis of murine lymphoma cells with or without *Nr4a1* loss in co-culture with *Ctla4+/+ OT-1* CD8+ T cells. E:T ratios of a) 3:1 and b) 5:1 were analyzed via flow cytometry and specific lysis was determined at different time points. c) and d) Bar chart of specific lysis of co-culture experiments with *Ctla4+/+ OT-1* CD8+ in co-culture with lymphoma cells with or without *Nr4a1* loss after 16h and 24h. Each bar represents the mean and error bars represent standard deviation (SD). The p-values calculated using Students t-test are as shown in the figure.

To investigate whether the diminished lymphoma cell lysis in the *N4a1*-deficient setting is influenced by the CTLA-4-CD80-CD86 axis, we performed the co-culture cytotoxicity assay. Therefore, we used *Ctla4-/- OT-1* CD8+ T cells instead of *Ctla4+/+ OT-1* CD8+ T cells. After 16h of co-culture, we detected a slightly reduced lymphoma cells lysis in the E:T ratio of 3:1 (39.5% in the *Nr4a1+/+* setting vs. 34.4% in the *Nr4a1-/-* setting, p=0.2262, Figure 33) and a reduced lysis rate in a higher extend in the E:T ratio of 5:1 (39.8% in the *Nr4a1+/+* setting vs. 30.2% in the *Nr4a1-/-* setting, p=0.036, Figure 36). Comparing the results of co-cultures using *Ctla4-/- OT-1* CD8+ T cells to the ones using *Ctla4+/+ OT-1* CD8+ T cells, we noticed higher lysis of lymphoma cells in the co-cultures using *Ctla4-/- OT-1* CD8+ T cells in the *Nr4a1*-deficient setting (in the E:T ratio of 3:1: 13.2% in *Ctla4+/+* condition vs. 34.4% in *Ctla4-/-* condition, in the E:T ratio of 5:1: 22.3% in *Ctla4+/+* condition vs. 30.2% in *Ctla4-/-* condition,

p<0.027, Figure 36). Conversely, no difference in the lymphoma cell lysis was for both E:T ratios found between the *Ctla4+/+* and *Ctla4-/-* conditions (p>0.12,Figure 36). This data suggests that the reduced CD8+ T cell-mediated lysis of *Nr4a1*-deficient lymphoma cells may be attributed to the *Ctla4-Cd80-Cd86* axis.

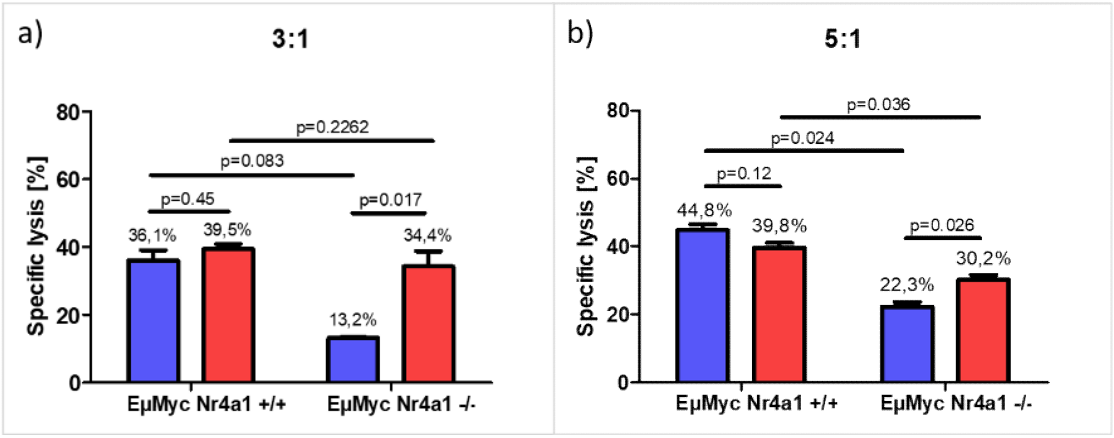

Figure 36: Comparison of OVA-specific lysis of murine lymphoma cells with or without *Nr4a1* loss in co-culture with *Ctla4+/+ OT-1* CD8+ T cells and *Ctla4-/- OT-1* CD8+ T cells. Co-Culture using *Ctla4+/+ and Ctla4-/- OT-1* T cells displayed reduced specific lysis in co-culture experiments using lymphoma cells with *Nr4a1* loss in ratios a) and b) 3:1 and 5:1 after 16h. Each bar represents the mean and error bars represent standard deviation (SD). The p-values calculated using Student's t-test are as shown in the figure.

4.2.8. Loss of *Nr4a1* results in increased site-specific phosphorylation of kinases in murine lymphoma cells

To identify the pathways regulated by *Nr4a1*, we used a phospho-kinase array to detect the phosphorylation levels of 43 kinases in murine lymphoma cells with and without *Nr4a1* loss (n=2 per group) (Figure 37).

Phosphorylation levels were quantified using Biorad's ImageLab software and normalized to the positive control spots (integrated pixel density [x1000]) (Figure 37a).

The heat map showed a general increase in phosphorylation levels in murine lymphoma cell lines with *Nr4a1* loss compared to lymphoma cell lines without *Nr4a1* loss. As expected, the heat map revealed two distinct clusters between the lymphoma cell lines based on their genotype. The hierarchical cluster tree shows three distinct clusters. In cluster one, one out of two samples of murine lymphoma cell lines with *Nr4a1* loss showed higher phosphorylation levels compared to lymphoma cell lines without *Nr4a1* loss. Most of the kinases in this group are involved in signal transduction such as JAK/STAT pathway, PI3K/AKT pathway, calcium signaling, cell growth and apoptosis or are transcription factors such as CREB and c-Jun. Interestingly, in cluster two, both murine lymphoma cell lines exhibited a higher phosphorylation pattern. Kinases are implicated in metabolic regulation or various signaling pathways for expample PI3K/AKT, mTor, MAPK/ERK pathway, regulate cell growth

and apoptosis, or belong to non-receptor tyrosine kinases. In cluster three, the phosphorylation levels appear to be enhanced in both murine lymphoma cell lines with *Nr4a1* loss. Additionally, one sample of murine lymphoma cell lines without *Nr4a1* loss shows a moderate increase in phosphorylation levels. This cluster includes non-receptor tyrosine kinases, receptor tyrosine kinases, and kinases implicated in the JAK-STAT pathway (Figure 37b).

Volcano blot analysis revealed higher site-specific phosphorylation of all kinases in murine lymphoma cell lines lacking *Nr4a1* compared to lymphoma cell lines without *Nr4a1* loss. In particular, we found seven kinases that were significantly higher phosphorylated ($p<0.05$) (Figure 37c and d). The bar graph displays the absolute values of the integrated pixel density of the various kinases that were considered significant from the volcano blot (Figure 37d). MAPKs showed high phosphorylation levels. Specifically, the phosphorylation of p38α at residue Thr^{180}/Tyr^{182} ($p=0.0116$) and extracellular signal-related kinase 1 (ERK1) at residue Thr^{202}/ Tyr^{204} and Thr^{185}/Tyr^{187} ($p=0.0176$), which are downstream of MAPK, increased significantly. The non-receptor tyrosine kinases Hck Tyr^{411} ($p=0.0269$), FAK Tyr^{397} ($p=0.0135$) and Src Tyr^{419} ($p=0.0475$) of the Src family exhibited a significant increase in site-specific phosphorylation. Proline-rich Akt substrate of 40 kDa (PRAS40), serving as a substrate for Akt and a constituent of the mammalian target of rapamycin complex 1 (mTORC1), also shows higher phosphorylation level on residue Thr^{246} ($p=0.033$). The phosphorylation of the transcription factor p53 at Ser^{392} was enhanced ($p=0.0158$) (Figure 37 d). Murine lymphoma cell lines with *Nr4a1* did not demonstrate a noteworthy rise in the phosphorylation levels of any kinases within the first and third cluster (Figure S 14 a and c).

In summary, these findings suggest that loss of *Nr4a1* leads to increased site-specific phosphorylation of kinases in murine lymphoma cells.

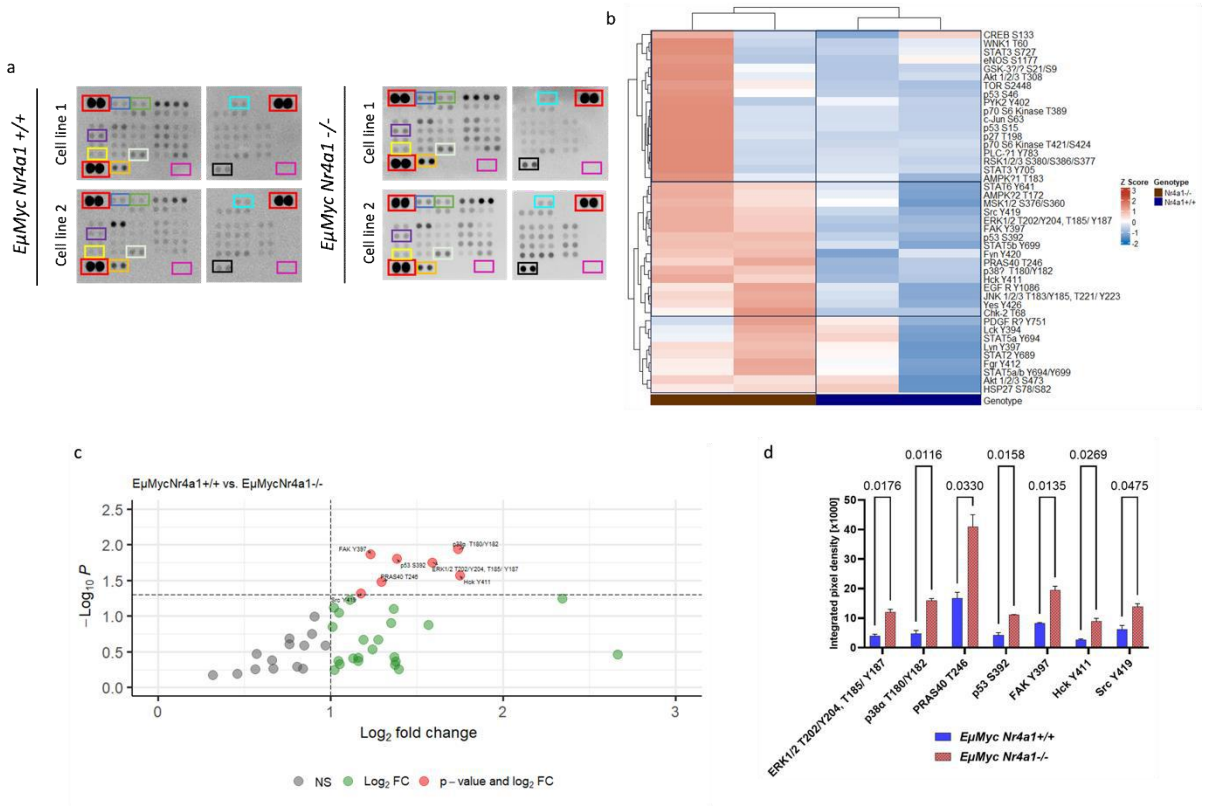

Figure 37: Phospho-kinase array, heat map, volcano blot and bar charts of phosphorylation levels of murine lymphoma cell lines with and without *Nr4a1* loss. (a) Array images show relative signal intensities of kinases. Positive reference spots are marked with red rectangles; the area of negative control spots is marked in pink. The colors used to mark the kinases are as follows: p38α (blue), ERK1/2 (green), Src (purple), Hck (yellow), FAK (mint), PRAS40 (orange), and p53 (turquoise). (b) Heat map and hierarchical clustering of phosphorylation levels of murine lymphoma cell lines with and without *Nr4a1* loss. Each column represents a murine lymphoma cell line and each row represents a kinase. Changes in signal intensities are shown using a color scale, with red and resenting the highest level of phosphorylation and blue representing the lowest level of phosphorylation. (c) Volcano blot showing the different phosphorylation levels of murine lymphoma cell lines with and without *Nr4a1* loss. Log2 fold changes and their corresponding p-values were used to construct the volcano blot. All detected phosphorylation levels are increased in murine lymphoma cell lines with *Nr4a1* loss. P values of $p<0.05$ and a fold change of ≥1.3 were considered significant (red dots). (d) The bar graphs display the absolute values of the integrated pixel density of the different kinases that were considered significant from the volcano blot. Each bar represents the mean of the expression levels ± standard error of the mean (SEM). Comparison of phosphorylation levels was performed using Students t-test.

4.2.9. Differential phosphorylation patterns in murine lymphomas derived from *EμMyc* mice with and without *Nr4a1* loss

Next, we performed a phospho-kinase array analysis on murine lymphomas derived from *EμMyc* mice with and without *Nr4a1* loss (n=2 per group) to compare the phosphorylation pattern for 37 kinases with cell lines and check for similarities.

Heat map revealed two distinct clusters between lymphomas derived from *EμMyc* mice with and without *Nr4a1* loss. The hierarchical cluster tree shows four distinct clusters (Figure 38b). In cluster one, both lymphomas derived from *EμMyc* mice with *Nr4a1* loss exhibit a higher phosphorylation pattern compared to lymphomas derived from *EμMyc* mice without *Nr4a1* loss. This cluster includes STAT1, STAT3, and STAT6 of the JAK-STAT pathway, as well as kinases of the PI3K/AKT, MAPK/ERK pathway, calcium signaling pathway or kinases that are

involved in cell growth and apoptosis (Figure 38b). Notably, this cluster has a similar phosphorylation pattern to the second cluster of the cell lines and contains similar kinases (Figure 37b and Figure 38b). Cluster two shows a more diverse phosphorylation pattern. Both clusters contain one sample per genotype with a higher phosphorylation level. In this cluster, kinases involved in the mTor, MAPK/ERK and JAK-STAT pathways and transcription factors such as CREB and c-Jun are found (Figure 38b). In cluster three, lymphomas derived from *EμMyc* mice with *Nr4a1* loss exhibit a higher level of phosphorylation. One lymphoma derived from *EμMyc* mice with *Nr4a1* loss exhibits slightly higher phosphorylation levels. For instance, the phosphorylated kinases in this cluster are involved in the MAPK/ERK and NF-κB signaling pathways or in metabolism (Figure 38b). In contrast, this phosphorylation pattern was not observed in murine lymphoma cell lines (Figure 37b and Figure 38b). Cluster four has a higher phosphorylation level in lymphomas derived from *EμMyc* mice without *Nr4a1* loss. This pattern of phosphorylation has not been observed in murine lymphoma cell lines and contains several non-receptor tyrosine kinases and signal transduction kinases involved in the JAK-STAT, PI3K/AKT, and MAPK/ERK pathways or in transmembrane signaling. Interestingly, ERK1/2, which was higher phosphorylated in murine lymphoma cell lines with *Nr4a1* loss, appears to be lower phosphorylated in lymphomas derived from *EμMyc* mice with *Nr4a1* loss (Figure 37b and Figure 38b).

The volcano blot analysis revealed that the transmembrane protein epidermal growth factor receptor (EGFR) at residue Thy^{1017} was lower phosphorylated (p=0.043) and STAT3 at residue TYR^{705} is higher phosphorylated (p=0.0298) in lymphomas derived from *EμMyc* mice with *Nr4a1* loss (Figure 38c). The bar graph shows the absolute values of the integrated pixel density of the various kinases that were found to be significant from the volcano blot (Figure 38d). In the first cluster, there is a significant increase in phosphorylation of AKT1/2/3 on residue Ser^{473} in lymphomas derived from *EμMyc* mice with *Nr4a1* loss (p=0.0472). AKT1/2/3 plays a crucial role in regulating cellular survival and metabolism by binding and regulating downstream effectors. The phosphorylation of the transcription factor p53 at Ser^{46} was increased (p=0.0115) (Figure 38c and Figure S 15a). Contrarily, the heat map's third cluster shows that in *Eumyc* mice lymphomas with *Nr4a1* loss, Lyn at residue Thy^{397} is significantly less phosphorylated (p=0.036) (Figure 38c and Figure S 15c). In contrast to the phosphorylation level of Scr in murine lymphoma cell lines, Src on residue Thy^{419} appears to be significant lower phosphorylated in lymphomas derived from *Eμmyc* mice with *Nr4a1* loss (p=0.0108) (Figure 38c and Figure S 15d).

These data suggest that the phosphorylation pattern is more diverse in lymphoma tissue than in our established murine lymphoma cell lines. Compared to murine lymphoma cell lines, interactions with other cell types, the ECM, or paracrine signaling occur in lymphoma tissue, leading to a more complex interplay of protein kinase-regulated signaling pathways.

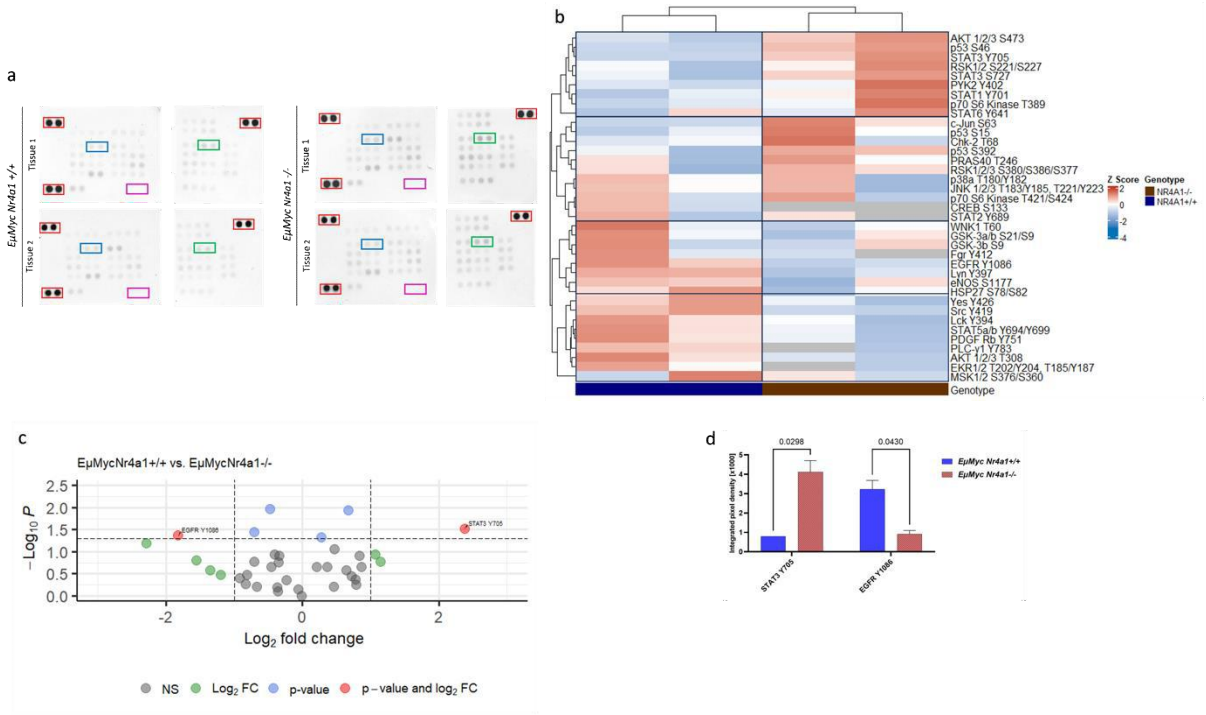

Figure 38: Phospho-kinase array, heat map, volcano blot and bar charts of phosphorylation levels of murine lymphoma tissue with and without *Nr4a1* loss. (a) Array images show relative signal intensities of kinases. Positive reference spots are marked with red rectangles; the area of negative control spots is marked in pink. The colors used to mark the kinases are as follows: EGFR (blue) and STAT3 (green). (b) Heat map and hierarchical clustering of phosphorylation levels of murine lymphoma tissue with and without *Nr4a1* loss. Each column represents a murine lymphoma tissue and each row represents a kinase. Changes in signal intensities are shown using a color scale, with red and resenting the highest level of phosphorylation and blue representing the lowest level of phosphorylation. (c) Volcano blot showing the different phosphorylation levels of murine lymphoma tissues with and without *Nr4a1* loss. Log2 fold changes and their corresponding p-values were used to construct the volcano blot. P values of $p < 0.05$ and a fold change of ≥1.3 were considered significant (red dots). (d) The bar graphs display the absolute values of the integrated pixel density of the different kinases that were considered significant from the volcano blot. Each bar represents the mean of the expression levels ± standard error of the mean (SEM). Comparison of phosphorylation levels was performed using Students t-test.

5. Discussion

In this work, we focused on the pathogenesis of aggressive lymphomas, a group of B-cell malignancies encompassing various subtypes such as Burkitt lymphoma, DLBCL, and FLIII [196]. The diverse molecular and genetic characteristics found within different types of lymphoma contribute to differences in how the disease presents clinically and how patients respond to treatment. Additionally, there has been a noticeable increase in the occurrence of aggressive lymphomas in recent years [197]. These findings underscore the urgency for comprehensive research endeavors aimed at enhancing our understanding of these lymphoid malignancies, thereby paving the way for novel therapeutic strategies.

Therefore, we conducted two distinct projects, supported by preliminary data from my research group that underscores their scientific significance.

5.1. Investigation of the interplay between CXCR4 and CXCL12 in DLBCL

In the first part of the thesis, we focused on two pivotal chemokine receptors, CXCR4 and CXCR7, along with their common ligand, CXCL12, [198–200] in the context of DLBCL.These three genes have been implicated in cancer surveillance in over 20 different types of solid tumors [201–203]. Their role has also been explored in DLBCL [104,105,107,204–207]. However, the results of these studies are inconsistent and somewhat constrained.

In our prior research, we found a correlation between CXCR4 expression and bone marrow infiltration in nodal DLBCL, prompting a deeper examination into the functional intricacies of CXCR4 within this specific lymphoma subtype [105]. Thus, we decided to further dissect the function of CXCR4 in the bone marrow infiltration process of this lymphoma entity, we determined the mRNA expression levels of *CXCR4*, *CXCR7*, and *CXCL12* in primary nodal DLBCL samples (n=71) as well as GC-B cells serving as non-malignant controls (n=5). mRNA transcripts for *CXCR4* were detected in all of the investigated lymphoma and control samples. When we compared *de novo* DLBCL with transformed DLBCL, we found no detectible difference, suggesting a comparable role of *CXCR4* in both categories. We observed elevated levels of *CXCR4* expression in DLBCL compared to non-malignant controls. We also observed increased expression of *CXCR4* in DLBCL cases with more advanced disease. Our results align with prior studies indicating decreased CXCR4 expression in certain subsets of germinal center B cells and enhanced expression in DLBCL, especially among patients with advanced stages of the disease [104,205,207,208]. Moreover, we detected no difference in the *CXCR4* mRNA levels between nGCB- and GCB-DLBCL, a finding consistent with Moreno *et al.* [107], but in contrast to previously reported data [207]. This discrepancy may be due to differences

in the algorithms used by us and others to classify nGCB- and GCB-DLBCL, as well as differences in the DLBCL patient cohorts. A considerable portion of the GCB-DLBCL cases examined in our study had undergone transformation from follicular lymphoma. The unique genetic and epigenetic alterations associated with this type of disease [209] may, at least in part, account for the differences observed. In our analysis, no distinctions were observed between DLBCL and control groups, as well as among different lymphoma subgroups, regarding *CXCR7* and *CXCL12* mRNA levels. Our findings regarding CXCR7 align with those of Moreno et al. [210], who similarly observed comparable CXCR7 levels between nGBC- and GCB-DLBCL. The exploration of CXCL12 expression levels in DLBCL has been primarily conducted through analyses of TGCA, Oncomine, GEPIA, and cBioportal datasets [211]. However, these analyses did not incorporate additional clinical variables, making them incomparable to our observations. Moreover, we set the expression levels of *CXCR4*, *CXCR7*, *CXCL12* in relation to clinical data. We found an association of elevated CXCR4 levels with BM infiltration in our DLBCL cohort, consistent with previous studies [104,105]. This association is further discussed together in the section, in which the CXCR4 and CXCL12 expression analysis of the bone marrow samples is discussed. Remarkably, our survival analyses, conducted on our lymphoma cohort along with the publicly available dataset of Lenz *et al*. [106], revealed that high *CXCR4* expression was associated with poor 5-year survival. This finding consistent with results reported by two other research teams [106,206].

Considering that *CXCR4-CXCL12* signaling activates molecular pathways, such as JAK/STAT, PI3K, MAPK, and NF-κB [99,212,213], we propose that the interplay of CXCR4 and CXCL12 may significantly contribute to lymphoma cell growth and proliferation. Furthermore, it was shown that the lymphoma cell growth mediated by Rituximab, a monoclonal antibody commonly used as standard therapy for DLCBL treatment [214], inversely correlated with CXCR4 expression and was enhanced by an FDA-approved CXCR4 antagonist [206]. This finding supports our hypothesis that CXCR4 exerts a negatively influences the chemosensitivity of lymphoma cells and thereby impacts on worse clinical outcome in DLBCL. Finally, our immunohistochemical staining of CXCR4 and CXCL12 revealed that CXCR4 was exclusively expressed on lymphoma cells, whereas CXCL12 was expressed on cells of the tumor microenvironment and on lymphoma cells. To our knowledge, there has been no comprehensive investigation of CXCL12 expression in DLBCL. Given our discovery that both CXCR4 and CXCL12 are co-expressed on lymphoma cells, one could speculate on the existence of an autocrine stimulatory loop in aggressive lymphomas. In our cohort, we were not able to detect any association between CXCR7 expression and survival. This observation is in stark contrast to the findings of Moreno *et al.* [210], who identified CXCR7 as a prognostic factor associated with improved clinical outcomes, particularly in CXCR4+

DLBCLs, we did not find a statistically significant association with survival in our study cohort. This discrepancy may again be due to differences in the composition of the two lymphoma cohorts, as our analysis included a significant number of transformed follicular lymphomas. Based on our findings regarding CXCR7, we opted not to pursue further investigations into this chemokine receptor.

Furthermore, we directly sequenced DLBCL (n=25) and lymphoma cell line (n=4) samples to investigate whether our cohort is somatically mutated in the CXCR4 locus, as it has been described to be frequently mutated in other lymphoma entities [215]. We detected rs2228014, previously documented in publicly available databases [200], in exon 2 in three DLBCL samples and one lymphoma cell line. Rs2228014 is a synonymous polymorphism [200], reported to be linked with an elevated risk of cancer development when present at the germline level [216–219]. However, we did not include germline DNA in our analysis and therefore cannot provide evidence that rs2228014 is of somatic or germline origin. However, we plan to use our whole-exome sequencing dataset, which we will generate in another project next year, containing genomic data from more than 100 newly diagnosed DLBCL samples.

To further investigate the CXCR4 and CXCL12 axis in the process of bone marrow infiltration in DLBCL, we used BM biopsies (n=12) from our lymphoma cohort. To our knowledge, such an analysis has never been performed before. We found a strong association between CXCR4 expression and lymphoma infiltration in the BM. Our immunohistochemical analysis of CXCR4 and CXCL12 revealed that around 35% of lymphoma cells contained CXCR4 and CXCL12, whereas around 50% of lymphoma cells exclusively expressed CXCR4. Furthermore, less than 30% of stromal cells expressed CXCR4 and CXCL12 in BM samples without infiltration. This observation further suggests the presence of an autocrine loop governing the interplay between CXCR4 and CXCL12 in aggressive lymphomas. CXCR4 has been shown to be upregulated in lymphoma under hypoxic conditions [220] as well as in several other cell lines [221–223] in *in vitro* experiments. Given the known associations between the *CXCR4/CXCL12* axis, hypoxic conditions and bone marrow metastasis in solid tumors [224–226], and evidence from xenograft experiments suggesting a role for CXCR4 in BM infiltration in DLBCL [207], it is plausible that CXCR4 and CXCL12 plays a key role in lymphoma progression and dissemination, especially in the bone marrow.

To provide evidence that the CXCR4 might serve as therapeutic target for DLBCL, we treated lymphoma cells originated from Burkitt lymphoma, nGCB- or GCB expressing CXCR4 and/or CXCR7 with AMD3100 (an FDA-approved drug) [109,227], AMD070 [111,228], and a niacin derivative of AMD070 called WK1 (synthesized in-house). All three antagonists showed the ability to inhibit CXCL12 binding in a dose-dependent manner. Furthermore, AMD070

inhibited transwell migration of lymphoma cells expressing exclusive CXCR4 or expressing CXCR4 and CXCR7, whereas WK1 only showed inhibitory effects on lymphoma cells expressing both chemokine receptors, indicating that modification of the antagonist might change the properties of the antagonist. In addition, we found that AMD070 and WK1 exhibited pro-apoptotic effects in CXCR4+ Burkitt lymphoma and a CXCR4+ GCB-DLBCL cell line, as confirmed by functional assays and gene expression analysis. In contrast, all cell lines, including both nGCB- and GCB-DLBCL, which were unresponsive to these two treatments, were positive for both CXCR4 and CXCR7. Moreover, an nGCB-DLBCL cell line that was unresponsive to both treatments expressed only CXCR4. Notably, WK1 showed even more notable apoptotic effects compared to AMD070, as demonstrated by the induction of a greater number of pro-apoptotic genes and a higher proportion of apoptotic cells. In contrast, AMD3100 and niacin alone did not induce any cytotoxic effects on the lymphoma cell lines. These results are consistent with previously published data that only reported inhibition of cell migration for AMD3100 and growth inhibition for AMD070 in both malignant and non-malignant cell types [110,111]. Nevertheless, our results suggest that the cytotoxic and/or apoptotic effects of AMD070 are enhanced when combined with niacin and that these effects are dependent on the expression patterns of CXCR4 and CXCR7 but also on the molecular subtype of lymphoma. In particular, gene expression analysis revealed that WK1 led to a more notable induction of pro-apoptotic genes. This suggests that the specific type and/or subtype of lymphoma cells, particularly GCB-DLBCL, may play a role in influencing the activation of pro-apoptotic genes and the corresponding response rates. However, considering that AMD070 and WK1 (the two CXCR4 antagonists with apoptotic properties) did not induce up- or downregulation of the same genes, it appears that the molecular mechanism responsible for the induction of cell death is not mediated by the pro-apoptotic BCL-2 family members. To the best of our understanding, BKT140 is the only CXCR4 antagonist known to have significant cytotoxic and apoptotic effects in a number of solid tumor, lymphoma and leukemia cell lines [169,229,230]. Thus, WK1 serves as a second agent with similar effects to BKT140 and could therefore serve as a basis for the development of new agents with anti-lymphoma properties for the treatment of DLBCLs, especially those with BM infiltration. However, further *ex vivo* and *in vivo* studies using primary patient material as well as mouse experiments are required.

In gene expression analysis related to ERK1/2, JNK, and NF-κB/BCR targets, we found that in WK1-treated cells, three out of five JNK targets, four out of seven ERK1/2 target genes and five out of seven NF-κB/BCR targets were downregulated. In contrast, the effects of AMD070 were reduced and those of AMD3100 were not detectable. Given the critical role of the ERK1/2, JNK, and NF-κB/BCR signaling pathways in DLBCL development [184–186], it is

likely that the growth inhibitory effects of WK1 may be related to the inhibition of these pathways.

Conclusion

In conclusion of the first part, our findings suggest an important role for the CXCR4/CXCL12 axis in the development of aggressive lymphomas. The mechanisms by which this axis affects prognosis may involve lymphoma cell proliferation and dissemination, particularly to the bone marrow. Given the observed anti-lymphoma effects of the novel CXCR4 antagonist WK1, which specifically targets CXCR4, the CXCR4/CXCL12 axis emerges as an interesting therapeutic target for CXCR4+ GCB-DLCBL, especially in advanced disease stages and cases with potential bone marrow infiltration.

Outlook

As mentioned above, we will continue our work on WK1. We will use the Graz Lymphoma Biobank, where we have already cryopreserved viable patient-derived lymphoma single cell suspensions. These samples will be used to test the apoptotic effects of WK1 and AMD070 on primary samples. Protocols are currently being optimized for this purpose. In addition, we are planning xenograft experiments with human lymphoma cells as well as with murine lymphoma cell lines in our transplantable mouse model, which is known to have a high rate of lymphoma cell infiltration into the bone marrow. However, murine cell lines are being tested for sensitivity to AMD070 and WK1. Based on our preliminary data to date, we expect that these two antagonists will also induce apoptosis in the murine cell lines. In the *in vivo* studies using both models, we will determine the *in vivo* response rate in terms of lymphoma cell growth and side effects. Using these two approaches, we will decipher whether WK1 represents a compound for the development of novel anti-lymphoma therapies. Moreover, our future plan demonstrates a comprehensive and systematic approach to evaluating the therapeutic potential of WK1, integrating both *in vitro* and *in vivo* studies. This approach is essential to understanding the efficacy and safety profile of WK1 as a potential anti-lymphoma therapy and lays the foundation for future clinical translation.

5.2. Understanding the role of *Nr4a1* in aggressive lymphomas and the tumor microenvironment

In the second part of this work, we focus on the role of *Nr4a1* in lymphomagenesis. In our previously published study, we documented decreased NR4A1 expression in DLBCL patients, a finding correlated with poorer cancer-specific survival. The ectopic expression of

NR4A1 triggers apoptosis *in vitro* and suppresses lymphoma growth in xenograft models, indicating the tumor-suppressive potential of NR4A1 [129–131]. Using the *EμMyc* lymphoma mouse model, we observed that loss of *Nr4a1* leads to accelerated lymphomagenesis accompanied by elevated expression of immune checkpoint components *in vivo*. Furthermore, the transplantation experiment demonstrated an accelerated lymphomagenesis and upregulation of immune checkpoint components in immunocompetent but not immunodeficient mice transplanted with *Nr4a1*-deficient lymphoma cells as in the primary model. In our human DLBCL cohort, low NR4A1 expression correlated with increased expression of immune checkpoint molecules, broadly similar to our mouse data. These results suggest that loss of *Nr4a1* accelerates lymphomagenesis in a *Myc*-driven system and has implications for the regulation of immune evasion in *Myc*-driven lymphomagenesis.

Thus, the aim of the second part of my thesis was to comprehensively investigate the extent to which lymphoma-specific *Nr4a1*-deficiency shapes the composition and activation of immune cells in the TME and regulates tumor-immune cell interactions during the process of lymphomagenesis. Furthermore, we wanted to investigate which pathways are regulated by *Nr4a1* in aggressive lymphoma cells. Therefore, we mainly used our *Nr4a1* proficient and deficient murine lymphoma cells generated in our laboratory and derived from our primary *EμMyc* lymphoma model with and without *Nr4a1* loss. We also generated transplantation protocols to transfer *Nr4a1*-proficient and -deficient lymphoma cells into immunocompetent mice to study tumor immunological processes in the TME, which was mainly done in the initial experiments.

In the first experiments, we intravenously transplanted murine lymphoma cells with and without *Nr4a1* loss into C57BL/6 wild-type mice as an immunocompetent model to characterize the relationship between immune cells of the TME and *Nr4a1*-deficient or -proficient lymphomas. On day 18, mice were sacrificed and single cell suspensions of splenocytes were analyzed by multicolor flow cytometry using antibody panels to characterize the most common immune cell populations and immune checkpoint axes, as well as malignant B cells.

In mice transplanted with *Nr4a1*-deficient lymphoma cells, we found a higher content of B220+ IgM- B cells, representing the phenotype of the transplanted malignant cells, on day 18. This finding suggests a higher tumor mass in the spleen of mice transplanted with *Nr4a1*-deficient lymphoma cells and confirms the accelerated lymphomagenesis in immunocompetent mice as reported in our previous experiments.

Furthermore, we observed reduced content of several lymphoid immune cell populations in the *Nr4a1*-deficient setting, while myeloid cell content was not affected. CD3+

T cells as well as the CD4+ and CD8+ T cell subsets and NKT cells were present at lower frequencies. All of them are critical for effective anti-tumor immune responses [231]. Based on our previous findings of accelerated lymphomagenesis exclusively in immuno-competent models, it is plausible to propose that *Nr4a1* contributes significantly to the depletion of lymphoid cells within the tumor microenvironment (TME). This depletion likely compromises the anti-tumor immune response, thereby precipitating the accelerated onset of disease.

Moreover, we also detected an increased content of M2 macrophages and that a higher percentage of CD4+ T cells in the Treg state in the *Nr4a1*-deficient settings. M2 macrophages contribute to increased angiogenic sprouting and poor prognosis in B-NHL [232–234] and induce immunosuppressive conditions in the TME [235]. Tregs can also inhibit antitumor immune responses by directly interfering with the function of cytotoxic T cells [236]. Pro- and antitumorigenic effects for Tregs have been reported in B-NHL patients [237]. However, in *Nr4a1*-deficient lymphomas, a high content of Tregs was associated with a more aggressive subtype in our experiments, indicating their immune suppressive function. Considering both findings collectively, it appears that *Nr4a1* also governs immune-suppressive conditions within the TME.

In addition, we observed that CD4+ and CD8+ T cells exhibited a higher extent the effector cell state in the *Nr4a1*-deficient setting, in stark contrast to the *Nr4a1*-proficient setting. Furthermore, we also found that the majority of T cells exhibited a lower naïve cell state in the *Nr4a1*-deficient setting. A decrease in naive T cells and an increase in effector cells are hallmarks of cancer [238]. Changes in activation status may indicate immune responses induced by tumor antigen in the *Nr4a1*-deficient setting. However, we did not test the cytotoxic function of these effector T cells via IFN-γ and/or CD107a [239,240].

We also examined the expression of single immune checkpoints in CD3+ T cells and their corresponding ligands in malignant B220+ B cells and found that the *Nr4a1*-deficient setting shows a significant increase in the expression of immune checkpoint molecules on CD3+ T cells such as PD1, CTLA-4, BTLA, LAG3, TIM-3, TIGIT, and CD160, which may indicate a state of T cell exhaustion or an inhibitory signaling environment [241]. Furthermore, we also observed an increased expression of PDL1, PDL2, CD80, CD86 and CD155, consistent with our preliminary gene expression data from transplanted tumors. This suggests potential alterations in the PD1-PDL1-PDL2 axes, CTLA-4-CD80-CD86 axes, as well as TIGIT-CD155-CD112 axes, along with higher expression of PD1, CTLA-4 and TIGIT on T cells. These findings indicate that loss of *Nr4a1* in lymphoma cells leads to induction T cell exhaustion mediated by a complex of immune checkpoint expression and their corresponding inhibitory ligands, potentially contributing to lymphomagenesis. Taken together, these findings support

a regulatory role for *Nr4a1* in the expression of immune checkpoint molecules. The presence of multiple immune checkpoint axes suggests that multiple checkpoint molecules may influence these immune evasion processes and may also somehow explain that PD-1/PD-L1 blockade as monotherapy, which only shows moderate response rates in aggressive lymphomas [242] is not sufficient to restore antitumor immune responses [243]. Furthermore, we observed higher MHC II surface expression on malignant B cells in the *Nr4a1*-deficient setting, suggesting that CD4+ T cells may be activated in the TME.

To further decipher whether *Nr4a1*-deficient lymphoma cells possess the ability to suppress CD8+ lymphoma cell lysis, we performed co-culture cytotoxicity using Nr4a1-proficient and -deficient lymphoma cells and CD8+ T cells isolated from OT-1 mice, which possess a transgenic TCR targeting the OVA peptide to initiate an antigen-mediated immune response [197,213-216]. Pre-activated OT-1 CD8+ T cells were co-cultured with *Nr4a1*-proficient or -deficient lymphoma cells pulsed with the OVA peptide.

In these co-culture assays, we observed decreased CD8+ T cell-mediated lymphoma cell lysis in the *Nr4a1*-deficient setting. In addition, we observed that co-culture assays using *Ctla4-/-* CD8+ T cells resulted in increased lymphoma cell killing, particularly in the *Nr4a1-/-* setting. Therefore, Ctla-4 appears to play a role in mediating T cell-mediated lymphoma cell lysis. Collectively, these data indicate that *Nr4a1* is a crucial regulator of T cell-mediated immune responses in aggressive lymphomas, suggesting its potential as a therapeutic target for enhancing anti-tumor immunity. In addition, the findings highlight the importance of immune checkpoint molecules such as CTLA-4 in modulating T cell functionality and tumor cell lysis. However, in ongoing clinical trials with ICs and ipilimumab, a CTLA-4 mAB, rare but durable efficacy activity was observed in the phase 1 trial in some patients, including those with FL and DLBCL [244]. Due to the complex immunoregulatory networks in lymphoma, combination therapies targeting multiple immune checkpoints, such as CTLA-4, PD-1/PD-L1, TIM-3, or TIGIT, may be more effective in overcoming immune evasion mechanisms and enhancing anti-tumor immune responses.

In the final experiment, we aim to investigate the impact of *Nr4a1* on molecular pathways in a broad and unbiased manner. Therefore, we used a phospho-protein array, which is a helpful and innovative tool to study the activation of different signaling pathways, and protein cell lysates of our *Nr4a1*-proficient and -deficient murine lymphoma cells (n=2 per genotype) and lymphoma tissues (n=2 per genotype).

Our phospho-array of lymphoma cells revealed that seven phosphoproteins, including prominent participants in MAPK signaling (p38α and ERK1/2), non-receptor tyrosine kinases

(Hck, FAK, and Src), as well as the Akt substrate PRAS40, were found to be phosphorylated in a higher extend in the *Nr4a1*-deficient setting, indicating a higher activation of these pathways in *Nr4a1-/-* lymphoma cell lines in the used culturing conditions. The activation of non-receptor tyrosine kinases, MAPK, and ERK, which are known to be involved in BCR signaling, has been linked to lymphomagenesis and cell survival [245]. Consistent with our findings, MAPK family members such as p38α are upregulated in DLBCL cell lines [246]. In FL and various cancers, elevated levels of activated p38 MAPK (phosphorylated p38 MAPK) have been linked to cancer progression. A portion of DLBCL patients with tumors showing high levels of phosphorylated p38 MAPK displayed less favorable responses to treatment and experienced diminished overall survival rates [247]. The phosphorylation of PRAS40, which plays a role in controlling the PI3K/Akt and mTOR pathways, is commonly linked to the advancement of tumors in melanoma, prostate cancer, and breast cancer. Elevated levels of phosphorylated PRAS40 are often correlated with the progression of malignancy or unfavorable outcomes for patients [248].

Phospho-array data from lymphoma tissue analysis revealed different phosphorylation patterns compared to the cell lines. These differences might be caused by more diverse landscapes, potentially influenced by interactions with other cell types, ECM, and paracrine signaling, of lymphoma tissue. Cell lines fail to capture the complexity and heterogeneity of tissues, primarily because they only consist of a single cell type, which fails to interact with the TME, highlighting the importance of studying dynamics in a more physiological context. In the lymphoma tissue, we observed lower phosphorylation of ERK1/2 and higher phosphorylation levels of STAT3 in the *Nr4a1*-deficient setting. Phosphorylation of STAT3 is mainly caused by cytokine receptors including those for IL-6, IL-10, IL-21, IL-23, and IFNs [249]. The phosphorylation of this transcription factor in tissue samples suggests that cells within the TME may secrete factors responsible for STAT3 phosphorylation. Moreover, studies have indicated that activated STAT3 suppresses immune cell activation and prompts the secretion of anti-inflammatory molecules [250], indicating its involvement in the induction of immuno-suppressive conditions in *Nr4a1*-deficient lymphomas. In contrast to our findings, ERK1/2 has been reported to be constitutively activated in NHL, including DLBCL [251]. Given that the ERK1/2 pathway is primarily responsive to inflammatory cytokines [252], and considering our findings linking immunosuppression in the TME with *Nr4a1*-deficiency, it is reasonable to speculate that the phosphorylation of ERK1/2 may be caused by the presence of pro-inflammatory molecules within the TME and may finally contribute to the higher expression of the immune checkpoint components. Combining data from lymphoma cell lines and tissues, it appears that *Nr4a1*-deficiency activates a broader set of molecular pathways. This is consistent with the RNA-seq data from *Nr4a1*-deficient and -proficient tumors presented in the

preliminary data section, where we observed up-regulation of numerous genes, suggesting that *Nr4a1* plays a suppressive role in various cellular processes. However, to fully elucidate the molecular mechanism, further investigations are warranted. In particular, Western blot analyses using antibodies capable of detecting specific phosphorylated proteins are essential.

Conclusion

In conclusion, our findings strongly support the role of *Nr4a1* as a tumor suppressor in aggressive lymphomas, primarily by regulating immune evasion mechanisms through modulation of multiple immune checkpoints, leading to decreased immune cell-mediated lysis of lymphoma cells. Moreover, *Nr4a1*-deficiency appears to result in an immune cell-depleted TME characterized by decreased lymphoid cell presence and increased levels of Tregs and M2-like macrophages with immunosuppressive properties. In addition, our data suggest that loss of *Nr4a1* correlates with tumor antigen-induced immune responses. Our phosphor array analysis further demonstrates that *Nr4a1*-deficiency is associated with enhanced activation of several pathways typically stimulated by pro-inflammatory cytokines, thereby promoting the secretion of anti-inflammatory molecules and fostering immune evasion processes. These findings have significant clinical implications for the development of novel therapies aimed at restoring anti-lymphoma immune responses in *Nr4a1*-deficient lymphomas or in DLBCL cases with low NR4A1 expression in humans. In addition, our study underscores the complex nature of tumor-immune interactions and highlights the need for comprehensive approaches to understand and effectively target these interactions in lymphoma treatment strategies.

Outlook

The second part of my thesis will also be expanded, with new experiments planned to generate novel findings for high impact publications, as well as to raise new research questions for future research projects. Currently, we are planning a new *in vivo* experiment. This experiment will involve depletion of CD8+ T cells in C57BL/6 wild-type mice followed by transplantation of *Nr4a1*-deficient and deficient lymphoma cells compared to isotype controls. This will further investigate whether accelerated lymphomagenesis is dependent on the presence of CD8+ T cells. In addition, we intend to expand our bioinformatic analyses of our RNA-seq dataset of *EμMyc Nr4a1+/+* and *EμMyc Nr4a1-/-* lymphomas. This will include gene set enrichment analyses to identify potential pathways regulated by *Nr4a1*, as well as connectivity map analyses to discover agents to which *Nr4a1*-deficient lymphomas may be more responsive. In addition, we aim to identify direct functional targets of *Nr4a1* in aggressive lymphomas. To achieve this, we will perform chromatin immunoprecipitation followed by sequencing of *Nr4a1*-deficient and -proficient lymphomas to uncover genome-wide binding

patterns and direct targets of *Nr4a1*. *Nr4a1*-deficient tumors will serve as negative controls to validate the specificity of the antibodies used. Using this approach, we will identify how the immune checkpoint axes as well as the TME shaping function are regulated by *Nr4a1* in aggressive lymphomas. In addition, we plan to transplant *Nr4a1*-deficient and -proficient lymphoma cells into C57BL/6 wild-type mice and perform single-cell RNA sequencing to analyze the impact of *Nr4a1* on TME composition and the interactome. This experiment will provide novel insights into the pathways by which the observed immunosuppressive effects are mediated by *Nr4a1* loss in lymphoma cells and to which lymphoma cells and immune cells of the TME interact with immune cells of the TME. Thus, we are confident to identify interactions that can be targeted therapeutically. Using all of these approaches, we will identify targets that can be used to restore anti-lymphoma immune responses in our well-established murine *in vitro* and *in vivo* lymphoma models, with which we will generate novel therapeutic approaches. Finally, we aim to translate important findings into the human setting by utilizing the Graz Lymphoma Cohort, which includes tissue samples as well as viable cryopreserved lymphoma single cell suspensions. Lymphoma tissue samples will be used to validate direct targets of NR4A1. In addition, the human lymphoma single cell suspensions will be used for functional *ex vivo* validation of novel therapeutic approaches generated in our mouse models. Our experimental design appears to be rigorous and well thought out and has the potential to make significant contributions to the understanding and treatment of aggressive lymphomas.

6. References

[1] Marshall JS, Warrington R, Watson W, Kim HL. An introduction to immunology and immunopathology. Allergy, Asthma and Clinical Immunology 2018;14:1–10. https://doi.org/10.1186/S13223-018-0278-1/TABLES/4.

[2] Murphy K (Kenneth M), Weaver C, Berg L, Barton G (Professor of immunology and pathogenesis), Replacement of (work): Janeway Charles. Janeway's immunobiology n.d.:800.

[3] Lebien TW, Tedder TF. B lymphocytes: how they develop and function. Blood 2008;112:1570–80. https://doi.org/10.1182/BLOOD-2008-02-078071.

[4] B Cell Development, Activation and Effector Functions. Primer to the Immune Response 2014:111–42. https://doi.org/10.1016/B978-0-12-385245-8.00005-4.

[5] LeBien TW. B Cell Development. Fetal and Neonatal Physiology, 2-Volume Set 2017:1202–7. https://doi.org/10.1016/B978-0-323-35214-7.00124-4.

[6] Hardy RR, Hayakawa K. B Cell Development Pathways. Https://DoiOrg/101146/AnnurevImmunol191595 2003;19:595–621. https://doi.org/10.1146/ANNUREV.IMMUNOL.19.1.595.

[7] Honjo T, Kinoshita K, Muramatsu M. Molecular Mechanism of Class Switch Recombination: Linkage with Somatic Hypermutation. Https://DoiOrg/101146/AnnurevImmunol20090501112049 2003;20:165–96. https://doi.org/10.1146/ANNUREV.IMMUNOL.20.090501.112049.

[8] Han JH, Akira S, Calame K, Beutler B, Selsing E, Imanishi-Kari T. Class switch recombination and somatic hypermutation in early mouse B cells are mediated by B cell- and Toll-like receptors. Immunity 2007;27:64. https://doi.org/10.1016/J.IMMUNI.2007.05.018.

[9] Muramatsu M, Kinoshita K, Fagarasan S, Yamada S, Shinkai Y, Honjo T. Class switch recombination and hypermutation require activation-induced cytidine deaminase (AID), a potential RNA editing enzyme. Cell 2000;102:553–63. https://doi.org/10.1016/S0092-8674(00)00078-7.

[10] Di Noia JM, Neuberger MS. Molecular Mechanisms of Antibody Somatic Hypermutation. Https://DoiOrg/101146/AnnurevBiochem76061705090740 2007;76:1–22. https://doi.org/10.1146/ANNUREV.BIOCHEM.76.061705.090740.

[11] Mesin L, Ersching J, Victora GD. Germinal Center B Cell Dynamics. Immunity 2016;45:471–82. https://doi.org/10.1016/J.IMMUNI.2016.09.001.

[12] De Silva NS, Klein U. Dynamics of B cells in germinal centres. Nature Reviews Immunology 2015 15:3 2015;15:137–48. https://doi.org/10.1038/nri3804.

[13] Stebegg M, Kumar SD, Silva-Cayetano A, Fonseca VR, Linterman MA, Graca L. Regulation of the germinal center response. Front Immunol 2018;9:2469. https://doi.org/10.3389/FIMMU.2018.02469/XML/NLM.

[14] Hwang* JK, Alt* FW, Yeap L-S. Related Mechanisms of Antibody Somatic Hypermutation and Class Switch Recombination. Microbiol Spectr 2015;3. https://doi.org/10.1128/MICROBIOLSPEC.MDNA3-0037-2014.

[15] Maul RW, Gearhart PJ. AID AND SOMATIC HYPERMUTATION. Adv Immunol 2010;105:159. https://doi.org/10.1016/S0065-2776(10)05006-6.

[16] Stavnezer J, Schrader CE. Ig heavy chain class switch recombination: mechanism and regulation. J Immunol 2014;193:5370. https://doi.org/10.4049/JIMMUNOL.1401849.

[17] Young C, Brink R. The unique biology of germinal center B cells. Immunity 2021;54:1652–64. https://doi.org/10.1016/J.IMMUNI.2021.07.015.

[18] Meng X, Min Q, Wang JY. B Cell Lymphoma. Adv Exp Med Biol 2020;1254:161–81. https://doi.org/10.1007/978-981-15-3532-1_12/COVER.

[19] Armitage JO, Gascoyne RD, Lunning MA, Cavalli F. Non-Hodgkin lymphoma. The Lancet 2017;390:298–310. https://doi.org/10.1016/S0140-6736(16)32407-2.

[20] Alaggio R, Amador C, Anagnostopoulos I, Attygalle AD, Araujo IB de O, Berti E, et al. The 5th edition of the World Health Organization Classification of Haematolymphoid Tumours: Lymphoid Neoplasms. Leukemia 2022 36:7 2022;36:1720–48. https://doi.org/10.1038/s41375-022-01620-2.

[21] PDQ Adult Treatment Editorial Board. Adult Non-Hodgkin Lymphoma Treatment (PDQ®): Patient Version. PDQ Cancer Information Summaries 2002.

[22] Batlevi CL, Sha F, Alperovich A, Ni A, Smith K, Ying Z, et al. Follicular lymphoma in the modern era: survival, treatment outcomes, and identification of high-risk subgroups. Blood Cancer Journal 2020 10:7 2020;10:1–12. https://doi.org/10.1038/s41408-020-00340-z.

[23] Tarella C, Gueli A, Delaini F, Barbui AM, Bruna R, Caracciolo D, et al. Life Expectancy in Follicular Lymphoma Is Mainly Determined By Response to First LINE Treatment: A LONG-TERM Survey on 597 Patients. Blood 2015;126:3989–3989. https://doi.org/10.1182/BLOOD.V126.23.3989.3989.

[24] Gascoyne RD. Hematopathology approaches to diagnosis and prognosis of indolent B-cell lymphomas. Hematology Am Soc Hematol Educ Program 2005:299–306. https://doi.org/10.1182/ASHEDUCATION-2005.1.299.

[25] Küppers R. Mechanisms of B-cell lymphoma pathogenesis. Nature Reviews Cancer 2005 5:4 2005;5:251–62. https://doi.org/10.1038/nrc1589.

[26] Lenz G, Staudt LM. Aggressive Lymphomas. N Engl J Med 2010;362:1417. https://doi.org/10.1056/NEJMRA0807082.

[27] Dave S. Gene Expression Profiling and Outcome Prediction in Non-Hodgkin Lymphoma. Biology of Blood and Marrow Transplantation 2006;12:50–2. https://doi.org/10.1016/J.BBMT.2005.10.017.

[28] Monika H, Petra I. KREBSERKR ANKUNGEN IN ÖSTERREICH 2 0 2 2 2 0 2 2 1999.

[29] Stevenson FK, Sahota SS, Ottensmeier CH, Zhu D, Forconi F, Hamblin TJ. The occurrence and significance of V gene mutations in B cell—Derived human malignancy. Adv Cancer Res 2001;83:81–116. https://doi.org/10.1016/S0065-230X(01)83004-9.

[30] Küppers R, Klein U, Hansmann M-L, Rajewsky K. Cellular Origin of Human B-Cell Lymphomas. Https://DoiOrg/101056/NEJM199911113412007 1999;341:1520–9. https://doi.org/10.1056/NEJM199911113412007.

[31] Dave SS, Fu K, Wright GW, Lam LT, Kluin P, Boerma E-J, et al. Molecular Diagnosis of Burkitt's Lymphoma. New England Journal of Medicine 2006;354:2431–42. https://doi.org/10.1056/NEJMOA055759/SUPPL_FILE/NEJM_DAVE_2431SA1.PDF.

[32] Alizadeh AA, Elsen MB, Davis RE, Ma CL, Lossos IS, Rosenwald A, et al. Distinct types of diffuse large B-cell lymphoma identified by gene expression profiling. Nature 2000 403:6769 2000;403:503–11. https://doi.org/10.1038/35000501.

[33] Nicolae A, López C, Mozas P, López-Guillermo A, Beà S. Molecular Pathogenesis of Follicular Lymphoma: From Genetics to Clinical Practice. Hemato 2022, Vol 3, Pages 595-614 2022;3:595–614. https://doi.org/10.3390/HEMATO3040041.

[34] Wright G, Tan B, Rosenwald A, Hurt EH, Wiestner A, Staudt LM. A gene expression-based method to diagnose clinically distinct subgroups of diffuse large B cell lymphoma. Proc Natl Acad Sci U S A 2003;100:9991–6. https://doi.org/10.1073/PNAS.1732008100/ASSET/92AA9B02-6108-40B0-A0A5-63B879259633/ASSETS/GRAPHIC/PQ1732008004.JPEG.

[35] Basso K, Dalla-Favera R. Germinal centres and B cell lymphomagenesis. Nature Reviews Immunology 2015 15:3 2015;15:172–84. https://doi.org/10.1038/nri3814.

[36] Bilajac E, Mahmutović L, Lundstrom K, Glamočlija U, Šutković J, Sezer A, et al. Viral Agents as Potential Drivers of Diffuse Large B-Cell Lymphoma Tumorigenesis. Viruses 2022, Vol 14, Page 2105 2022;14:2105. https://doi.org/10.3390/V14102105.

[37] Thurner L, Hartmann S, Neumann F, Hoth M, Stilgenbauer S, Küppers R, et al. Role of Specific B-Cell Receptor Antigens in Lymphomagenesis. Front Oncol 2020;10:2685. https://doi.org/10.3389/FONC.2020.604685/XML/NLM.

[38] Niemann CU, Wiestner A. B-cell receptor signaling as a driver of lymphoma development and evolution. Semin Cancer Biol 2013;23:410–21. https://doi.org/10.1016/J.SEMCANCER.2013.09.001.

[39] Liu Y, Zhou X, Wang X. Targeting the tumor microenvironment in B-cell lymphoma: challenges and opportunities. Journal of Hematology & Oncology 2021 14:1 2021;14:1–17. https://doi.org/10.1186/S13045-021-01134-X.

[40] Sehn LH, Salles G. Diffuse Large B-Cell Lymphoma. Https://DoiOrg/101056/NEJMra2027612 2021;384:842–58. https://doi.org/10.1056/NEJMRA2027612.

[41] Montoto S, Fitzgibbon J. Transformation of indolent B-cell lymphomas. J Clin Oncol 2011;29:1827–34. https://doi.org/10.1200/JCO.2010.32.7577.

[42] Condoluci A, Rossi D. Richter Syndrome. Curr Oncol Rep 2021;23:1–10. https://doi.org/10.1007/S11912-020-01001-X/TABLES/1.

[43] Frontzek F, Karsten I, Schmitz N, Lenz G. Current options and future perspectives in the treatment of patients with relapsed/refractory diffuse large B-cell lymphoma. Ther Adv Hematol 2022;13. https://doi.org/10.1177/20406207221103321.

[44] Rosenwald A, Wright G, Chan WC, Connors JM, Campo E, Fisher RI, et al. The use of molecular profiling to predict survival after chemotherapy for diffuse large-B-cell lymphoma. N Engl J Med 2002;346:1937–47. https://doi.org/10.1056/NEJMOA012914.

[45] Lenz G, Wright GW, Emre NCT, Kohlhammer H, Dave SS, Davis RE, et al. Molecular subtypes of diffuse large B-cell lymphoma arise by distinct genetic pathways. Proc Natl Acad Sci U S A 2008;105:13520–5. https://doi.org/10.1073/PNAS.0804295105.

[46] Roschewski M, Staudt LM, Wilson WH. Diffuse large B-cell lymphoma—treatment approaches in the molecular era. Nature Reviews Clinical Oncology 2013 11:1 2013;11:12–23. https://doi.org/10.1038/nrclinonc.2013.197.

[47] Shaffer AL, Shapiro-Shelef M, Iwakoshi NN, Lee AH, Qian SB, Zhao H, et al. XBP1, Downstream of Blimp-1, Expands the Secretory Apparatus and Other Organelles, and Increases Protein Synthesis in Plasma Cell Differentiation. Immunity 2004;21:81–93. https://doi.org/10.1016/J.IMMUNI.2004.06.010.

[48] Eric Davis R, Brown KD, Siebenlist U, Staudt LM. Constitutive Nuclear Factor κB Activity Is Required for Survival of Activated B Cell–like Diffuse Large B Cell Lymphoma Cells. Journal of Experimental Medicine 2001;194:1861–74. https://doi.org/10.1084/JEM.194.12.1861.

[49] Maffei R, Fiorcari S, Atene CG, Martinelli S, Mesini N, Pilato F, et al. The dynamic functions of IRF4 in B cell malignancies. Clin Exp Med 2022:1–10. https://doi.org/10.1007/S10238-022-00968-0/FIGURES/3.

[50] Klein U, Casola S, Cattoretti G, Shen Q, Lia M, Mo T, et al. Transcription factor IRF4 controls plasma cell differentiation and class-switch recombination. Nature Immunology 2006 7:7 2006;7:773–82. https://doi.org/10.1038/ni1357.

[51] Pasqualucci L, Dominguez-Sola D, Chiarenza A, Fabbri G, Grunn A, Trifonov V, et al. Inactivating mutations of acetyltransferase genes in B-cell lymphoma. Nature 2011;471:189. https://doi.org/10.1038/NATURE09730.

[52] Yang H, Green MR. Epigenetic Programing of B-Cell Lymphoma by BCL6 and Its Genetic Deregulation. Front Cell Dev Biol 2019;7:272. https://doi.org/10.3389/FCELL.2019.00272/XML/NLM.

[53] Bakhshi TJ, Georgel PT. Genetic and epigenetic determinants of diffuse large B-cell lymphoma. Blood Cancer Journal 2020 10:12 2020;10:1–23. https://doi.org/10.1038/s41408-020-00389-w.

[54] Basso K, Dalla-Favera R. Roles of BCL6 in normal and transformed germinal center B cells. Immunol Rev 2012;247:172–83. https://doi.org/10.1111/J.1600-065X.2012.01112.X.

[55] Fangazio M, Ladewig E, Gomez K, Garcia-Ibanez L, Kumar R, Teruya-Feldstein J, et al. Genetic mechanisms of HLA-I loss and immune escape in diffuse large B cell lymphoma. Proc Natl Acad Sci U S A 2021;118. https://doi.org/10.1073/PNAS.2104504118/-/DCSUPPLEMENTAL.

[56] Yoshihama S, Roszik J, Downs I, Meissner TB, Vijayan S, Chapuy B, et al. NLRC5/MHC class I transactivator is a target for immune evasion in cancer. Proc Natl Acad Sci U S A 2016;113:5999–6004. https://doi.org/10.1073/PNAS.1602069113/SUPPL_FILE/PNAS.201602069SI.PDF.

[57] Roberts RA, Wright G, Rosenwald AR, Jaramillo MA, Grogan TM, Miller TP, et al. Loss of major histocompatibility class II gene and protein expression in primary mediastinal large B-cell lymphoma is highly coordinated and related to poor patient survival. Blood 2006;108:311–8. https://doi.org/10.1182/BLOOD-2005-11-4742.

[58] Ennishi D, Takata K, Béguelin W, Duns G, Mottok A, Farinha P, et al. Molecular and genetic characterization of MHC deficiency identifies ezh2 as therapeutic target for enhancing immune recognition. Cancer Discov 2019;9:546–63. https://doi.org/10.1158/2159-8290.CD-18-1090/42877/AM/MOLECULAR-AND-GENETIC-CHARACTERIZATION-OF-MHC.

[59] Challa-Malladi M, Lieu YK, Califano O, Holmes AB, Bhagat G, Murty V V., et al. Combined Genetic Inactivation of β2-Microglobulin and CD58 Reveals Frequent Escape from Immune Recognition in Diffuse Large B Cell Lymphoma. Cancer Cell 2011;20:728–40. https://doi.org/10.1016/J.CCR.2011.11.006.

[60] Georgiou K, Chen L, Berglund M, Ren W, De Miranda NFCC, Lisboa S, et al. Genetic basis of PD-L1 overexpression in diffuse large B-cell lymphomas. Blood 2016;127:3026–34. https://doi.org/10.1182/BLOOD-2015-12-686550.

[61] Chong LC, Twa DDW, Mottok A, Ben-Neriah S, Woolcock BW, Zhao Y, et al. Comprehensive characterization of programmed death ligand structural rearrangements in B-cell non-Hodgkin lymphomas. Blood 2016;128:1206–13. https://doi.org/10.1182/BLOOD-2015-11-683003.

[62] Asrini R, Ham MF, Asmarinah A, Harahap AS, Hardjolukito ESR. Expression of programmed cell death ligand-1 protein in germinal center B-cell-like and non-germinal center B-cell-like subtypes of diffuse large B-cell lymphoma. Mol Clin Oncol 2022;16:1–5. https://doi.org/10.3892/MCO.2021.2474/HTML.

[63] Godfrey J, Tumuluru S, Bao R, Leukam M, Venkataraman G, Phillip J, et al. PD-L1 gene alterations identify a subset of diffuse large B-cell lymphoma harboring a T-cell–inflamed phenotype. Blood 2019;133:2279–90. https://doi.org/10.1182/BLOOD-2018-10-879015.

[64] Li L, Sun R, Miao Y, Tran T, Adams L, Roscoe N, et al. PD-1/PD-L1 expression and interaction by automated quantitative immunofluorescent analysis show adverse prognostic impact in patients with diffuse large B-cell lymphoma having T-cell infiltration: a study from the International DLBCL Consortium Program. Modern Pathology 2019;32:741–54. https://doi.org/10.1038/s41379-018-0193-5.

[65] Pascual M, Mena-Varas M, Robles EF, Garcia-Barchino MJ, Panizo C, Hervas-Stubbs S, et al. PD-1/PD-L1 immune checkpoint and p53 loss facilitate tumor progression in activated B-cell diffuse large B-cell lymphomas. Blood 2019;133:2401–12. https://doi.org/10.1182/BLOOD.2018889931.

[66] Iqbal J, Sanger WG, Horsman DE, Rosenwald A, Pickering DL, Dave B, et al. BCL2 translocation defines a unique tumor subset within the germinal center B-cell-like diffuse large B-cell lymphoma. American Journal of Pathology 2004;165:159–66. https://doi.org/10.1016/S0002-9440(10)63284-1.

[67] Nguyen L, Papenhausen P, Shao H. The Role of c-MYC in B-Cell Lymphomas: Diagnostic and Molecular Aspects. Genes 2017, Vol 8, Page 116 2017;8:116. https://doi.org/10.3390/GENES8040116.

[68] Burotto M, Berkovits A, Dunleavy K. Double hit lymphoma: from biology to therapeutic implications. Http://DxDoiOrg/101080/1747408620161182858 2016;9:669–78. https://doi.org/10.1080/17474086.2016.1182858.

[69] Li B, Chng WJ. EZH2 abnormalities in lymphoid malignancies: underlying mechanisms and therapeutic implications. Journal of Hematology & Oncology 2019 12:1 2019;12:1–13. https://doi.org/10.1186/S13045-019-0814-6.

[70] Muppidi JR, Schmitz R, Green JA, Xiao W, Larsen AB, Braun SE, et al. Loss of signalling via Gα13 in germinal centre B-cell-derived lymphoma. Nature 2014 516:7530 2014;516:254–8. https://doi.org/10.1038/nature13765.

[71] Xia Z, Zhang X, Liu P, Zhang R, Huang Z, Li D, et al. GNA13 regulates BCL2 expression and the sensitivity of GCB-DLBCL cells to BCL2 inhibitors in a palmitoylation-dependent manner. Cell Death & Disease 2021 12:1 2021;12:1–11. https://doi.org/10.1038/s41419-020-03311-1.

[72] Healy JA, Nugent A, Rempel RE, Moffitt AB, Davis NS, Jiang X, et al. GNA13 loss in germinal center B cells leads to impaired apoptosis and promotes lymphoma in vivo. Blood 2016;127:2723. https://doi.org/10.1182/BLOOD-2015-07-659938.

[73] Boice M, Salloum D, Mourcin F, Sanghvi V, Amin R, Oricchio E, et al. Loss of the HVEM Tumor Suppressor in Lymphoma and Restoration by Modified CAR-T Cells. Cell 2016;167:405-418.e13. https://doi.org/10.1016/j.cell.2016.08.032.

[74] Schmitz R, Wright GW, Huang DW, Johnson CA, Phelan JD, Wang JQ, et al. Genetics and Pathogenesis of Diffuse Large B-Cell Lymphoma. New England Journal of Medicine 2018;378:1396–407. https://doi.org/10.1056/NEJMOA1801445/SUPPL_FILE/NEJMOA1801445_DISCLOSURES.PDF.

[75] Davis RE, Ngo VN, Lenz G, Tolar P, Young RM, Romesser PB, et al. Chronic Active B Cell Receptor Signaling in Diffuse Large B Cell Lymphoma. Nature 2010;463:88. https://doi.org/10.1038/NATURE08638.

[76] Minderman M, Lantermans H, van der Zwaan C, Hoogendijk AJ, van den Biggelaar M, Kersten MJ, et al. The oncogenic human B-cell lymphoma MYD88 L265P mutation genocopies activation by phosphorylation at the Toll/interleukin-1 receptor (TIR) domain. Blood Cancer Journal 2023 13:1 2023;13:1–10. https://doi.org/10.1038/s41408-023-00896-6.

[77] Zhang F, Yang L, Li Y. The role of A20 in the pathogenesis of lymphocytic malignancy. Cancer Cell Int 2012;12:1–7. https://doi.org/10.1186/1475-2867-12-44/TABLES/1.

[78] Honma K, Tsuzuki S, Nakagawa M, Tagawa H, Nakamura S, Morishima Y, et al. TNFAIP3/A20 functions as a novel tumor suppressor gene in several subtypes of non-Hodgkin lymphomas. Blood 2009;114:2467–75. https://doi.org/10.1182/BLOOD-2008-12-194852.

[79] Xia Y, Xu-Monette ZY, Tzankov A, Li X, Manyam GC, Murty V, et al. Loss of PRDM1/BLIMP-1 function contributes to poor prognosis of activated B-cell-like diffuse large B-cell lymphoma. Leukemia 2017;31:625–36. https://doi.org/10.1038/LEU.2016.243.

[80] Martin AR, Weisenburger DD, Chan WC, Ruby EI, Anderson JR, Vose JM, et al. Prognostic Value of Cellular Proliferation and Histologic Grade in Follicular Lymphoma. Blood 1995;85:3671–8. https://doi.org/10.1182/BLOOD.V85.12.3671.BLOODJOURNAL85123671.

[81] Horn H, Schmelter C, Leich E, Salaverria I, Katzenberger T, Ott MM, et al. Follicular lymphoma grade 3B is a distinct neoplasm according to cytogenetic and immunohistochemical profiles. Haematologica 2011;96:1327–34. https://doi.org/10.3324/HAEMATOL.2011.042531.

[82] Roulland S, Navarro JM, Grenot P, Milili M, Agopian J, Montpellier B, et al. Follicular lymphoma-like B cells in healthy individuals: a novel intermediate step in early lymphomagenesis. J Exp Med 2006;203:2425. https://doi.org/10.1084/JEM.20061292.

[83] Nath K, Tsang H, Gandhi MK. Tumor microenvironment of follicular lymphoma. Ann Lymphoma 2021;5:28–28. https://doi.org/10.21037/AOL-20-55.

[84] Amin R, Braza MS. The follicular lymphoma epigenome regulates its microenvironment. Journal of Experimental and Clinical Cancer Research 2022;41:1–7. https://doi.org/10.1186/S13046-021-02234-9/TABLES/2.

[85] Dave SS, Wright G, Tan B, Rosenwald A, Gascoyne RD, Chan WC, et al. Prediction of survival in follicular lymphoma based on molecular features of tumor-infiltrating immune cells. N Engl J Med 2004;351:2159–69. https://doi.org/10.1056/NEJMOA041869.

[86] Bödör C, Grossmann V, Popov N, Okosun J, O'Riain C, Tan K, et al. EZH2 mutations are frequent and represent an early event in follicular lymphoma. Blood 2013;122:3165–8. https://doi.org/10.1182/BLOOD-2013-04-496893.

[87] Grande BM, Gerhard DS, Jiang A, Griner NB, Abramson JS, Alexander TB, et al. Genome-wide discovery of somatic coding and noncoding mutations in pediatric endemic and sporadic Burkitt lymphoma. Blood 2019;133:1313–24. https://doi.org/10.1182/BLOOD-2018-09-871418.

[88] Havelange V, Pepermans X, Ameye G, Théate I, Callet-Bauchu E, Barin C, et al. Genetic differences between paediatric and adult Burkitt lymphomas. Br J Haematol 2016;173:137–44. https://doi.org/10.1111/BJH.13925.

[89] Magrath I. Epidemiology: clues to the pathogenesis of Burkitt lymphoma. Br J Haematol 2012;156:744–56. https://doi.org/10.1111/J.1365-2141.2011.09013.X.

[90] Zech L, Haglund U, Nilsson K, Klein G. Characteristic chromosomal abnormalities in biopsies and lymphoid-cell lines from patients with burkitt and non-burkitt lymphomas. Int J Cancer 1976;17:47–56. https://doi.org/10.1002/IJC.2910170108.

[91] Taub R, Kirsch I, Morton C, Lenoir G, Swan D, Tronick S, et al. Translocation of the c-myc gene into the immunoglobulin heavy chain locus in human Burkitt lymphoma and murine plasmacytoma cells. Proceedings of the National Academy of Sciences 1982;79:7837–41. https://doi.org/10.1073/PNAS.79.24.7837.

[92] Rohde M, Bonn BR, Zimmermann M, Lange J, Möricke A, Klapper W, et al. Relevance of ID3-TCF3-CCND3 pathway mutations in pediatric aggressive B-cell lymphoma

treated according to the non-Hodgkin Lymphoma Berlin-Frankfurt-Münster protocols. Haematologica 2017;102:1091–8. https://doi.org/10.3324/HAEMATOL.2016.156885.

[93] Pranzatelli MR. Advances in biomarker-guided therapy for pediatric- and adult-onset neuroinflammatory disorders: Targeting chemokines/cytokines. Front Immunol 2018;9:1. https://doi.org/10.3389/FIMMU.2018.00557/FULL.

[94] Miller MC, Mayo KH. Chemokines from a Structural Perspective. International Journal of Molecular Sciences 2017, Vol 18, Page 2088 2017;18:2088. https://doi.org/10.3390/IJMS18102088.

[95] Hughes CE, Nibbs RJB. A guide to chemokines and their receptors. FEBS J 2018;285:2944. https://doi.org/10.1111/FEBS.14466.

[96] Shi Y, Riese DJ, Shen J. The Role of the CXCL12/CXCR4/CXCR7 Chemokine Axis in Cancer. Front Pharmacol 2020;11:1969. https://doi.org/10.3389/FPHAR.2020.574667/BIBTEX.

[97] Moll NM, Ransohoff RM. CXCL12 and CXCR4 in bone marrow physiology. Expert Rev Hematol 2010;3:315–22. https://doi.org/10.1586/EHM.10.16.

[98] Karpova D, Bonig H. Concise Review: CXCR4/CXCL12 Signaling in Immature Hematopoiesis--Lessons From Pharmacological and Genetic Models. Stem Cells 2015;33:2391–9. https://doi.org/10.1002/STEM.2054.

[99] Zhou W, Guo S, Liu M, Burow ME, Wang G. Targeting CXCL12/CXCR4 Axis in Tumor Immunotherapy. Curr Med Chem 2019;26:3026. https://doi.org/10.2174/0929867324666170830111531.

[100] Mezzapelle R, Leo M, Caprioglio F, Colley LS, Lamarca A, Sabatino L, et al. CXCR4/CXCL12 Activities in the Tumor Microenvironment and Implications for Tumor Immunotherapy. Cancers (Basel) 2022;14. https://doi.org/10.3390/CANCERS14092314.

[101] Voermans C, van Heese WPM, de Jong I, Gerritsen WR, van der Schoot CE. Migratory behavior of leukemic cells from acute myeloid leukemia patients. Leukemia 2002 16:4 2002;16:650–7. https://doi.org/10.1038/sj.leu.2402431.

[102] Ahn JY, Seo K, Weinberg OK, Arber DA. The prognostic value of CXCR4 in acute myeloid leukemia. Applied Immunohistochemistry and Molecular Morphology 2013;21:79–84. https://doi.org/10.1097/PAI.0B013E3182606F4D.

[103] Jahnke K, Coupland SE, Na IK, Loddenkemper C, Keilholz U, Korfel A, et al. Expression of the chemokine receptors CXCR4, CXCR5, and CCR7 in primary central nervous system lymphoma. Blood 2005;106:384–5. https://doi.org/10.1182/BLOOD-2005-01-0324.

[104] Du H, Zhang L, Li G, Liu W, Tang W, Zhang H, et al. CXCR4 and CCR7 Expression in Primary Nodal Diffuse Large B-Cell Lymphoma—A Clinical and Immunohistochemical Study. Am J Med Sci 2019;357:302–10. https://doi.org/10.1016/J.AMJMS.2019.01.008.

[105] Deutsch AJA, Steinbauer E, Hofmann NA, Strunk D, Gerlza T, Beham-Schmid C, et al. Chemokine receptors in gastric MALT lymphoma: Loss of CXCR4 and upregulation of CXCR7 is associated with progression to diffuse large B-cell lymphoma. Modern Pathology 2013;26:182–94. https://doi.org/10.1038/MODPATHOL.2012.134/ATTACHMENT/F26B2320-A8B2-4708-8FA5-106C0E5F029B/MMC1.DOC.

[106] Lenz G, Wright G, Dave SS, Xiao W, Powell J, Zhao H, et al. Stromal Gene Signatures in Large-B-Cell Lymphomas. New England Journal of Medicine 2008;359:2313–23. https://doi.org/10.1056/NEJMOA0802885/SUPPL_FILE/NEJM_LENZ_2313SA1.PDF.

[107] Moreno MJ, Bosch R, Dieguez-Gonzalez R, Novelli S, Mozos A, Gallardo A, et al. CXCR4 expression enhances diffuse large B cell lymphoma dissemination and decreases patient survival. J Pathol 2015;235:445–55. https://doi.org/10.1002/PATH.4446.

[108] Schroeder MA, DiPersio JF. Mobilization of hematopoietic stem and leukemia cells. J Leukoc Biol 2012;91:47–57. https://doi.org/10.1189/JLB.0210085.

[109] Wang J, Tannous BA, Poznansky MC, Chen H. CXCR4 antagonist AMD3100 (plerixafor): From an impurity to a therapeutic agent. Pharmacol Res 2020;159:105010. https://doi.org/10.1016/J.PHRS.2020.105010.

[110] De Clercq E. AMD3100/CXCR4 Inhibitor. Front Immunol 2015;6. https://doi.org/10.3389/FIMMU.2015.00276.

[111] Uchida D, Kuribayashi N, Kinouchi M, Sawatani Y, Shimura M, Mori T, et al. Effect of a novel orally bioavailable CXCR4 inhibitor, AMD070, on the metastasis of oral cancer cells. Oncol Rep 2018;40:303–8. https://doi.org/10.3892/OR.2018.6400/HTML.

[112] Andtbacka RHI, Wang Y, Pierce RH, Campbell JS, Yushak M, Milhem M, et al. Mavorixafor, an Orally Bioavailable CXCR4 Antagonist, Increases Immune Cell Infiltration and Inflammatory Status of Tumor Microenvironment in Patients with Melanoma. Cancer Research Communications 2022;2:904–13. https://doi.org/10.1158/2767-9764.CRC-22-0090.

[113] Wang S, Wang X, Liu S, Zhang S, Wei X, Song Y, et al. The CXCR4 Antagonist, AMD3100, Reverses Mesenchymal Stem Cell-Mediated Drug Resistance in Relapsed/Refractory Acute Lymphoblastic Leukemia. Onco Targets Ther 2020;13:6583. https://doi.org/10.2147/OTT.S249425.

[114] Safe S, Karki K. The paradoxical roles of orphan nuclear receptor 4A (NR4A) in cancer. Molecular Cancer Research 2021;19:180–91. https://doi.org/10.1158/1541-7786.MCR-

20-0707/81367/AM/THE-PARADOXICAL-ROLES-OF-ORPHAN-NUCLEAR-RECEPTOR.

[115] Weikum ER, Liu X, Ortlund EA. The nuclear receptor superfamily: A structural perspective. Protein Sci 2018;27:1876. https://doi.org/10.1002/PRO.3496.

[116] Kurakula K, Koenis DS, van Tiel CM, de Vries CJM. NR4A nuclear receptors are orphans but not lonesome. Biochimica et Biophysica Acta (BBA) - Molecular Cell Research 2014;1843:2543–55. https://doi.org/10.1016/J.BBAMCR.2014.06.010.

[117] Maira M, Martens C, Batsché É, Gauthier Y, Drouin J. Dimer-Specific Potentiation of NGFI-B (Nur77) Transcriptional Activity by the Protein Kinase A Pathway and AF-1-Dependent Coactivator Recruitment. Mol Cell Biol 2003;23:763. https://doi.org/10.1128/MCB.23.3.763-776.2003.

[118] Safe S, Shrestha R, Mohankumar K. Orphan nuclear receptor 4A1 (NR4A1) and novel ligands. Essays Biochem 2021;65:877–86. https://doi.org/10.1042/EBC20200164.

[119] Chintharlapalli S, Burghardt R, Papineni S, Ramaiah S, Yoon K, Safe S. Activation of Nur77 by selected 1,1-bis(3′-indolyl)-1-(p-substituted phenyl)methanes induces apoptosis through nuclear pathways. Journal of Biological Chemistry 2005;280:24903–14. https://doi.org/10.1074/jbc.M500107200.

[120] Zhan Y, Du X, Chen H, Liu J, Zhao B, Huang D, et al. Cytosporone B is an agonist for nuclear orphan receptor Nur77. Nature Chemical Biology 2008 4:9 2008;4:548–56. https://doi.org/10.1038/nchembio.106.

[121] Pearen MA, Muscat GEO. Minireview: Nuclear Hormone Receptor 4A Signaling: Implications for Metabolic Disease. Molecular Endocrinology 2010;24:1891–903. https://doi.org/10.1210/ME.2010-0015.

[122] Moran AE, Holzapfel KL, Xing Y, Cunningham NR, Maltzman JS, Punt J, et al. T cell receptor signal strength in Treg and iNKT cell development demonstrated by a novel fluorescent reporter mouse. Journal of Experimental Medicine 2011;208:1279–89. https://doi.org/10.1084/JEM.20110308.

[123] Beard JA, Tenga A, Chen T. The interplay of NR4A receptors and the oncogene–tumor suppressor networks in cancer. Cell Signal 2015;27:257–66. https://doi.org/10.1016/J.CELLSIG.2014.11.009.

[124] Pawlak A, Strzadala L, Kalas W. Non-genomic effects of the NR4A1/Nur77/TR3/NGFIB orphan nuclear receptor. Steroids 2015;95:1–6. https://doi.org/10.1016/J.STEROIDS.2014.12.020.

[125] Li H, Kolluri SK, Gu J, Dawson MI, Cao X, Hobbs PD, et al. Cytochrome c release and apoptosis induced by mitochondrial targeting of nuclear orphan receptor TR3. Science (1979) 2000;289:1159–64.

https://doi.org/10.1126/SCIENCE.289.5482.1159/SUPPL_FILE/1053201S1_THUMB.GIF.

[126] Chen L, Fan F, Wu L, Zhao Y. The nuclear receptor 4A family members: mediators in human disease and autophagy. Cell Mol Biol Lett 2020;25:1–15. https://doi.org/10.1186/S11658-020-00241-W/FIGURES/2.

[127] Mullican SE, Zhang S, Konopleva M, Ruvolo V, Andreeff M, Milbrandt J, et al. Abrogation of nuclear receptors Nr4a3 and Nr4a1 leads to development of acute myeloid leukemia. Nat Med 2007;13:730–5. https://doi.org/10.1038/nm1579.

[128] Ramirez-Herrick AM, Mullican SE, Sheehan AM, Conneely OM. Reduced NR4A gene dosage leads to mixed myelodysplastic/myeloproliferative neoplasms in mice. Blood 2011;117:2681–90. https://doi.org/10.1182/BLOOD-2010-02-267906.

[129] Deutsch AJA, Rinner B, Wenzl K, Pichler M, Troppan K, Steinbauer E, et al. NR4A1-mediated apoptosis suppresses lymphomagenesis and is associated with a favorable cancer-specific survival in patients with aggressive B-cell lymphomas. Blood 2014;123:2367–77. https://doi.org/10.1182/blood-2013-08-518878.

[130] Deutsch AJA, Rinner B, Pichler M, Prochazka K, Pansy K, Bischof M, et al. NR4A3 suppresses lymphomagenesis through induction of proapoptotic genes. Cancer Res 2017;77:2375–86. https://doi.org/10.1158/0008-5472.CAN-16-2320.

[131] Fechter K, Feichtinger J, Prochazka K, Unterluggauer JJ, Pansy K, Steinbauer E, et al. Cytoplasmic location of NR4A1 in aggressive lymphomas is associated with a favourable cancer specific survival. Scientific Reports 2018 8:1 2018;8:1–11. https://doi.org/10.1038/s41598-018-32972-4.

[132] Harris AW, Pinkert CA, Crawford M, Langdon WY, Brinster RL, Adams JM. The E mu-myc transgenic mouse. A model for high-incidence spontaneous lymphoma and leukemia of early B cells. J Exp Med 1988;167:353–71. https://doi.org/10.1084/JEM.167.2.353.

[133] Adams JM, Harris AW, Pinkert CA, Corcoran LM, Alexander WS, Cory S, et al. The c-myc oncogene driven by immunoglobulin enhancers induces lymphoid malignancy in transgenic mice. Nature 1985;318:533–8. https://doi.org/10.1038/318533A0.

[134] Sidman CL, Denial TM, Marshall JD, Roths JB. Multiple mechanisms of tumorigenesis in E mu-myc transgenic mice. Cancer Res 1993;53:1665–9.

[135] Eischen CM, Weber JD, Roussel MF, Sherr CJ, Cleveland JL. Disruption of the ARF–Mdm2–p53 tumor suppressor pathway in Myc-induced lymphomagenesis. Genes Dev 1999;13:2658. https://doi.org/10.1101/GAD.13.20.2658.

[136] Valente LJ, Grabow S, Vandenberg CJ, Strasser A, Janic A. Combined loss of PUMA and p21 accelerates c-MYC-driven lymphoma development considerably less than loss

of one allele of p53. Oncogene 2016 35:29 2015;35:3866–71. https://doi.org/10.1038/onc.2015.457.

[137] Strasser A, Harris AW, Bath ML, Cory S. Novel primitive lymphoid tumours induced in transgenic mice by cooperation between myc and bcl-2. Nature 1990 348:6299 1990;348:331–3. https://doi.org/10.1038/348331a0.

[138] Eischen CM, Woo D, Roussel MF, Cleveland JL. Apoptosis Triggered by Myc-Induced Suppression of Bcl-XL or Bcl-2 Is Bypassed during Lymphomagenesis. Mol Cell Biol 2001;21:5063. https://doi.org/10.1128/MCB.21.15.5063-5070.2001.

[139] Pansy K, Uhl B, Krstic J, Szmyra M, Fechter K, Santiso A, et al. Immune Regulatory Processes of the Tumor Microenvironment under Malignant Conditions. Int J Mol Sci 2021;22. https://doi.org/10.3390/IJMS222413311.

[140] Ciavarella S, Vegliante MC, Fabbri M, De Summa S, Melle F, Motta G, et al. Dissection of DLBCL microenvironment provides a gene expression-based predictor of survival applicable to formalin-fixed paraffin-embedded tissue. Annals of Oncology 2018;29:2363–70. https://doi.org/10.1093/annonc/mdy450.

[141] Kotlov N, Bagaev A, Revuelta M V., Phillip JM, Cacciapuoti MT, Antysheva Z, et al. Clinical and biological subtypes of b-cell lymphoma revealed by microenvironmental signatures. Cancer Discov 2021;11:1468–89. https://doi.org/10.1158/2159-8290.CD-20-0839/333553/AM/CLINICAL-AND-BIOLOGICAL-SUBTYPES-OF-B-CELL.

[142] Nicholas NS, Apollonio B, Ramsay AG. Tumor microenvironment (TME)-driven immune suppression in B cell malignancy. Biochimica et Biophysica Acta (BBA) - Molecular Cell Research 2016;1863:471–82. https://doi.org/10.1016/J.BBAMCR.2015.11.003.

[143] Bauer V, Ahmetlić F, Hömberg N, Geishauser A, Röcken M, Mocikat R. Immune checkpoint blockade impairs immunosuppressive mechanisms of regulatory T cells in B-cell lymphoma. Transl Oncol 2021;14:101170. https://doi.org/10.1016/J.TRANON.2021.101170.

[144] Chen BJ, Zhao JW, Zhang DH, Zheng AH, Wu GQ. Immunotherapy of Cancer by Targeting Regulatory T cells. Int Immunopharmacol 2022;104:108469. https://doi.org/10.1016/J.INTIMP.2021.108469.

[145] Liu S, Sun Q, Ren X. Novel strategies for cancer immunotherapy: counter-immunoediting therapy. Journal of Hematology & Oncology 2023 16:1 2023;16:1–37. https://doi.org/10.1186/S13045-023-01430-8.

[146] Marin-Acevedo JA, Kimbrough EMO, Lou Y. Next generation of immune checkpoint inhibitors and beyond. Journal of Hematology & Oncology 2021 14:1 2021;14:1–29. https://doi.org/10.1186/S13045-021-01056-8.

[147] Cai L, Li Y, Tan J, Xu L, Li Y. Targeting LAG-3, TIM-3, and TIGIT for cancer immunotherapy. Journal of Hematology & Oncology 2023 16:1 2023;16:1–34. https://doi.org/10.1186/S13045-023-01499-1.

[148] Zhao B, Zhao H, Zhao J. Efficacy of PD-1/PD-L1 blockade monotherapy in clinical trials. Ther Adv Med Oncol 2020;12. https://doi.org/10.1177/1758835920937612.

[149] Jia Q, Wang A, Yuan Y, Zhu B, Long H. Heterogeneity of the tumor immune microenvironment and its clinical relevance. Experimental Hematology & Oncology 2022 11:1 2022;11:1–14. https://doi.org/10.1186/S40164-022-00277-Y.

[150] Li X, Song W, Shao C, Shi Y, Han W. Emerging predictors of the response to the blockade of immune checkpoints in cancer therapy. Cellular & Molecular Immunology 2018 16:1 2018;16:28–39. https://doi.org/10.1038/s41423-018-0086-z.

[151] Hassanian H, Asadzadeh Z, Baghbanzadeh A, Derakhshani A, Dufour A, Rostami Khosroshahi N, et al. The expression pattern of Immune checkpoints after chemo/radiotherapy in the tumor microenvironment. Front Immunol 2022;13:938063. https://doi.org/10.3389/FIMMU.2022.938063/BIBTEX.

[152] Hatic H, Sampat D, Goyal^ G, Goyal G. Immune checkpoint inhibitors in lymphoma: challenges and opportunities. Ann Transl Med 2021;9:1037–1037. https://doi.org/10.21037/ATM-20-6833.

[153] Armengol M, Santos JC, Fernández-serrano M, Profitós-pelejà N, Ribeiro ML, Roué G. Immune-Checkpoint Inhibitors in B-Cell Lymphoma. Cancers (Basel) 2021;13:1–41. https://doi.org/10.3390/CANCERS13020214.

[154] Green MR, Monti S, Rodig SJ, Juszczynski P, Currie T, O'Donnell E, et al. Integrative analysis reveals selective 9p24.1 amplification, increased PD-1 ligand expression, and further induction via JAK2 in nodular sclerosing Hodgkin lymphoma and primary mediastinal large B-cell lymphoma. Blood 2010;116:3268–77. https://doi.org/10.1182/BLOOD-2010-05-282780.

[155] Green MR, Rodig S, Juszczynski P, Ouyang J, Sinha P, O'Donnell E, et al. Constitutive AP-1 activity and EBV infection induce PD-L1 in Hodgkin lymphomas and posttransplant lymphoproliferative disorders: implications for targeted therapy. Clin Cancer Res 2012;18:1611–8. https://doi.org/10.1158/1078-0432.CCR-11-1942.

[156] Twa DDW, Chan FC, Ben-Neriah S, Woolcock BW, Mottok A, Tan KL, et al. Genomic rearrangements involving programmed death ligands are recurrent in primary mediastinal large B-cell lymphoma. Blood 2014;123:2062–5. https://doi.org/10.1182/BLOOD-2013-10-535443.

[157] Crump M, Neelapu SS, Farooq U, Van Den Neste E, Kuruvilla J, Westin J, et al. Outcomes in refractory diffuse large B-cell lymphoma: results from the international

SCHOLAR-1 study. Blood 2017;130:1800–8. https://doi.org/10.1182/BLOOD-2017-03-769620.

[158] Pardoll DM. The blockade of immune checkpoints in cancer immunotherapy. Nat Rev Cancer 2012;12:252–64. https://doi.org/10.1038/nrc3239.

[159] Vick E, Mahadevan D. Programming the immune checkpoint to treat hematologic malignancies. Expert Opin Investig Drugs 2016;25:755–70. https://doi.org/10.1080/13543784.2016.1175433.

[160] Höfer T, Nathansen H, Löhning M, Radbruch A, Heinrich R. GATA-3 transcriptional imprinting in Th2 lymphocytes: A mathematical model. Proc Natl Acad Sci U S A 2002;99:9364–8. https://doi.org/10.1073/PNAS.142284699/SUPPL_FILE/2846SUPPINFOTEXT.PDF.

[161] Cogdill AP, Andrews MC, Wargo JA. Hallmarks of response to immune checkpoint blockade. Br J Cancer 2017;117:1–7. https://doi.org/10.1038/bjc.2017.136.

[162] Ghanekar SA, Nomura LE, Suni MA, Picker LJ, Maecker HT, Maino VC. Gamma Interferon Expression in CD8+ T Cells Is a Marker for Circulating Cytotoxic T Lymphocytes That Recognize an HLA A2-Restricted Epitope of Human Cytomegalovirus Phosphoprotein pp65. Clinical and Vaccine Immunology 2001;8:628–31. https://doi.org/10.1128/CDLI.8.3.628-631.2001.

[163] Schroder K, Hertzog PJ, Ravasi T, Hume DA. Interferon-γ: an overview of signals, mechanisms and functions. J Leukoc Biol 2004;75:163–89. https://doi.org/10.1189/jlb.0603252.

[164] Swerdlow SH, Campo E, Harris NL, Jaffe ES, Pileri SA, Stein H. Weltgesundheitsorganisation. WHO classification of tumours of haematopoietic and lymphoid tissues. vol. 4th. 2017.

[165] Hans CP, Weisenburger DD, Greiner TC, Gascoyne RD, Delabie J, Ott G, et al. Confirmation of the molecular classification of diffuse large B-cell lymphoma by immunohistochemistry using a tissue microarray. Blood 2004;103:275–82. https://doi.org/10.1182/BLOOD-2003-05-1545.

[166] Davies AJ, Rosenwald A, Wright G, Lee A, Last KW, Weisenburger DD, et al. Transformation of follicular lymphoma to diffuse large B-cell lymphoma proceeds by distinct oncogenic mechanisms. Br J Haematol 2007;136:286–93. https://doi.org/10.1111/J.1365-2141.2006.06439.X.

[167] Deutsch AJA, Aigelsreiter A, Staber PB, Beham A, Linkesch W, Guelly C, et al. MALT lymphoma and extranodal diffuse large B-cell lymphoma are targeted by aberrant somatic hypermutation. Blood 2007;109:3500–4. https://doi.org/10.1182/blood-2006-06-030494.

[168] Bahler DW, Swerdlow SH. Clonal Salivary Gland Infiltrates Associated With Myoepithelial Sialadenitis (Sjögren's Syndrome) Begin as Nonmalignant Antigen-Selected Expansions. Blood 1998;91:1864–72. https://doi.org/10.1182/BLOOD.V91.6.1864.

[169] Beider K, Ribakovsky E, Abraham M, Wald H, Weiss L, Rosenberg E, et al. Targeting the CD20 and CXCR4 pathways in non-hodgkin lymphoma with rituximab and high-affinity CXCR4 antagonist BKT140. Clinical Cancer Research 2013;19:3495–507. https://doi.org/10.1158/1078-0432.CCR-12-3015/85919/AM/TARGETING-THE-CD20-AND-CXCR4-PATHWAYS-IN-NON.

[170] Debnath B, Xu S, Grande F, Garofalo A, Neamati N. Small molecule inhibitors of CXCR4. Theranostics 2013;3:47–75. https://doi.org/10.7150/THNO.5376.

[171] Lossos IS, Levy R. Diffuse large B-cell lymphoma: insights gained from gene expression profiling. Int J Hematol 2003;77:321–9. https://doi.org/10.1007/BF02982638.

[172] R: The R Project for Statistical Computing n.d. https://www.r-project.org/ (accessed October 19, 2023).

[173] Carvalho BS, Irizarry RA. A framework for oligonucleotide microarray preprocessing. Bioinformatics 2010;26:2363–7. https://doi.org/10.1093/BIOINFORMATICS/BTQ431.

[174] Therneau TM, Grambsch PM. The Cox Model 2000:39–77. https://doi.org/10.1007/978-1-4757-3294-8_3.

[175] Package "survminer" Type Package Title Drawing Survival Curves using "ggplot2" 2022.

[176] Hogquist KA, Jameson SC, Heath WR, Howard JL, Bevan MJ, Carbone FR. T cell receptor antagonist peptides induce positive selection. Cell 1994;76:17–27. https://doi.org/10.1016/0092-8674(94)90169-4.

[177] Treon SP, Cao Y, Xu L, Yang G, Liu X, Hunter ZR. Somatic mutations in MYD88 and CXCR4 are determinants of clinical presentation and overall survival in Waldenström macroglobulinemia. Blood 2014;123:2791–6. https://doi.org/10.1182/BLOOD-2014-01-550905.

[178] Hunter ZR, Xu L, Yang G, Zhou Y, Liu X, Cao Y, et al. The genomic landscape of Waldenström macroglobulinemia is characterized by highly recurring MYD88 and WHIM-like CXCR4 mutations, and small somatic deletions associated with B-cell lymphomagenesis. Blood 2014;123:1637–46. https://doi.org/10.1182/BLOOD-2013-09-525808.

[179] Home - SNP - NCBI n.d. https://www.ncbi.nlm.nih.gov/snp/ (accessed October 19, 2023).

[180] Finke J, Fritzen R, Ternes P, Trivedi P, Bross KJ, Lange W, et al. Expression of bcl-2 in Burkitt's Lymphoma Cell Lines: Induction by Latent Epstein-Barr Virus Genes. Blood 1992;80:459–69. https://doi.org/10.1182/BLOOD.V80.2.459.459.

[181] Masir N, Campbell LJ, Jones M, Mason DY. Pseudonegative BCL2 protein expression in a t(14;18) translocation positive lymphoma cell line: a need for an alternative BCL2 antibody. Pathology 2010;42:212–6. https://doi.org/10.3109/00313021003631296.

[182] Klanova M, Andera L, Brazina J, Svadlenka J, Benesova S, Soukup J, et al. Targeting of BCL2 Family Proteins with ABT-199 and Homoharringtonine Reveals BCL2- and MCL1-Dependent Subgroups of Diffuse Large B-Cell Lymphoma. Clin Cancer Res 2016;22:1138–49. https://doi.org/10.1158/1078-0432.CCR-15-1191.

[183] Amini RM, Berglund M, Rosenquist R, Von Heideman A, Lagercrantz S, Thunberg U, et al. A novel B-cell line (U-2932) established from a patient with diffuse large B-cell lymphoma following Hodgkin lymphoma. Leuk Lymphoma 2002;43:2179–89. https://doi.org/10.1080/1042819021000032917.

[184] Young RM, Shaffer AL, Phelan JD, Staudt LM. B-Cell Receptor Signaling in Diffuse Large B-Cell lymphoma. Semin Hematol 2015;52:77–85. https://doi.org/10.1053/J.SEMINHEMATOL.2015.01.008.

[185] Dai B, Zhao XF, Mazan-Mamczarz K, Hagner P, Corl S, Bahassi EM, et al. Functional and molecular interactions between ERK and CHK2 in diffuse large B-cell lymphoma. Nature Communications 2011 2:1 2011;2:1–9. https://doi.org/10.1038/ncomms1404.

[186] Tian X, Pelton A, Shahsafaei A, Dorfman DM. Differential expression of enhancer of zeste homolog 2 (EZH2) protein in small cell and aggressive B-cell non-Hodgkin lymphomas and differential regulation of EZH2 expression by p-ERK1/2 and MYC in aggressive B-cell lymphomas. Modern Pathology 2016;29:1050–7. https://doi.org/10.1038/modpathol.2016.114.

[187] Schmid CA, Robinson MD, Scheifinger NA, Müller S, Cogliatti S, Tzankov A, et al. DUSP4 deficiency caused by promoter hypermethylation drives JNK signaling and tumor cell survival in diffuse large B cell lymphoma. J Exp Med 2015;212:775–92. https://doi.org/10.1084/JEM.20141957.

[188] Nguyen TK, Jordan N, Friedberg J, Fisher RI, Dent P, Grant S. Inhibition of MEK/ERK1/2 sensitizes lymphoma cells to sorafenib-induced apoptosis. Leuk Res 2010;34:379–86. https://doi.org/10.1016/J.LEUKRES.2009.07.013.

[189] Grill C, Gheyas F, Dayananth P, Jin W, Ding W, Qiu P, et al. Analysis of the ERK1,2 transcriptome in mammary epithelial cells. Biochem J 2004;381:635–44. https://doi.org/10.1042/BJ20031688.

[190] Herman SEM, Mustafa RZ, Gyamfi JA, Pittaluga S, Chang S, Chang B, et al. Ibrutinib inhibits BCR and NF-κB signaling and reduces tumor proliferation in tissue-resident cells of patients with CLL. Blood 2014;123:3286–95. https://doi.org/10.1182/BLOOD-2014-02-548610.

[191] Wherry EJ, Kurachi M. Molecular and cellular insights into T cell exhaustion. Nature Reviews Immunology 2015 15:8 2015;15:486–99. https://doi.org/10.1038/nri3862.

[192] Carbone FR, Bevan MJ. Induction of ovalbumin-specific cytotoxic T cells by in vivo peptide immunization. J Exp Med 1989;169:603–12. https://doi.org/10.1084/jem.169.3.603.

[193] Lipford GB, Hoffman M, Wagner H, Heeg K. Primary in vivo responses to ovalbumin. Probing the predictive value of the Kb binding motif. J Immunol 1993;150:1212–22.

[194] McFarland BJ, Sant AJ, Lybrand TP, Beeson C. Ovalbumin(323-339) peptide binds to the major histocompatibility complex class II I-A(d) protein using two functionally distinct registers. Biochemistry 1999;38:16663–70. https://doi.org/10.1021/bi991393l.

[195] Clarke SR, Barnden M, Kurts C, Carbone FR, Miller JF, Heath WR. Characterization of the ovalbumin-specific TCR transgenic line OT-I: MHC elements for positive and negative selection. Immunol Cell Biol 2000;78:110–7. https://doi.org/10.1046/j.1440-1711.2000.00889.x.

[196] Swerdlow SH, Campo E, Pileri SA, Lee Harris N, Stein H, Siebert R, et al. The 2016 revision of the World Health Organization classification of lymphoid neoplasms. Blood 2016;127:2375–90. https://doi.org/10.1182/blood-2016-01-643569.

[197] de Jong D, Balagué Ponz O. The molecular background of aggressive B cell lymphomas as a basis for targeted therapy. J Pathol 2011;223:274–82. https://doi.org/10.1002/path.2807.

[198] Okada T, Ngo VN, Ekland EH, Förster R, Lipp M, Littman DR, et al. Chemokine requirements for B cell entry to lymph nodes and Peyer's patches. J Exp Med 2002;196:65–75. https://doi.org/10.1084/JEM.20020201.

[199] Balabanian K, Lagane B, Infantino S, Chow KYC, Harriague J, Moepps B, et al. The chemokine SDF-1/CXCL12 binds to and signals through the orphan receptor RDC1 in T lymphocytes. J Biol Chem 2005;280:35760–6. https://doi.org/10.1074/JBC.M508234200.

[200] Stein J V., Nombela-Arrieta C. Chemokine control of lymphocyte trafficking: a general overview. Immunology 2005;116:1–12. https://doi.org/10.1111/J.1365-2567.2005.02183.X.

[201] Gangadhar T, Nandi S, Salgia R. The role of chemokine receptor CXCR4 in lung cancer. Cancer Biol Ther 2010;9:409–16. https://doi.org/10.4161/CBT.9.6.11233.

[202] Sun X, Cheng G, Hao M, Zheng J, Zhou X, Zhang J, et al. CXCL12 / CXCR4 / CXCR7 chemokine axis and cancer progression. Cancer Metastasis Rev 2010;29:709–22. https://doi.org/10.1007/S10555-010-9256-X.

[203] Cojoc M, Peitzsch C, Trautmann F, Polishchuk L, Telegeev GD, Dubrovska A. Emerging targets in cancer management: Role of the CXCL12/CXCR4 axis. Onco Targets Ther 2013;6:1347–61. https://doi.org/10.2147/OTT.S36109.

[204] Xu ZZ, Shen JK, Zhao SQ, Li JM. Clinical significance of chemokine receptor CXCR4 and mammalian target of rapamycin (mTOR) expression in patients with diffuse large B-cell lymphoma. Leuk Lymphoma 2018;59:1451–60. https://doi.org/10.1080/10428194.2017.1379077.

[205] Shin HC, Seo J, Kang BW, Moon JH, Chae YS, Lee SJ, et al. Clinical significance of nuclear factor κB and chemokine receptor CXCR4 expression in patients with diffuse large B-cell lymphoma who received rituximab-based therapy. Korean J Intern Med 2014;29:785–92. https://doi.org/10.3904/KJIM.2014.29.6.785.

[206] Laursen MB, Reinholdt L, Schönherz AA, Due H, Jespersen DS, Grubach L, et al. High CXCR4 expression impairs rituximab response and the prognosis of R-CHOP-treated diffuse large B-cell lymphoma patients. Oncotarget 2019;10:717. https://doi.org/10.18632/ONCOTARGET.26588.

[207] Chen J, Xu-Monette ZY, Deng L, Shen Q, Manyam GC, Martinez-Lopez A, et al. Dysregulated CXCR4 expression promotes lymphoma cell survival and independently predicts disease progression in germinal center B-cell-like diffuse large B-cell lymphoma. Oncotarget 2015;6:5597–614. https://doi.org/10.18632/ONCOTARGET.3343.

[208] Weber TS. Cell Cycle-Associated CXCR4 Expression in Germinal Center B Cells and Its Implications on Affinity Maturation. Front Immunol 2018;9. https://doi.org/10.3389/FIMMU.2018.01313.

[209] Casulo C, Burack WR, Friedberg JW. Transformed follicular non-Hodgkin lymphoma. Blood 2015;125:40–7. https://doi.org/10.1182/BLOOD-2014-04-516815.

[210] Moreno MJ, Gallardo A, Novelli S, Mozos A, Arago M, Pavón MÁ, et al. CXCR7 expression in diffuse large B-cell lymphoma identifies a subgroup of CXCR4+ patients with good prognosis. PLoS One 2018;13. https://doi.org/10.1371/JOURNAL.PONE.0198789.

[211] Zhou X, Guo S, Shi Y. Comprehensive analysis of the expression and significance of CXCLs in human diffuse large B-cell lymphoma. Scientific Reports 2022 12:1 2022;12:1–12. https://doi.org/10.1038/s41598-022-06877-2.

[212] Du H, Gao L, Luan J, Zhang H, Xiao T. C-X-C Chemokine Receptor 4 in Diffuse Large B Cell Lymphoma: Achievements and Challenges. Acta Haematol 2019;142:64–70. https://doi.org/10.1159/000497430.

[213] Döring Y, Pawig L, Weber C, Noels H. The CXCL12/CXCR4 chemokine ligand/receptor axis in cardiovascular disease. Front Physiol 2014;5. https://doi.org/10.3389/FPHYS.2014.00212.

[214] Sehn LH, Donaldson J, Chhanabhai M, Fitzgerald C, Gill K, Klasa R, et al. Introduction of combined CHOP plus rituximab therapy dramatically improved outcome of diffuse large B-cell lymphoma in British Columbia. J Clin Oncol 2005;23:5027–33. https://doi.org/10.1200/JCO.2005.09.137.

[215] Schmidt J, Federmann B, Schindler N, Steinhilber J, Bonzheim I, Fend F, et al. MYD88 L265P and CXCR4 mutations in lymphoplasmacytic lymphoma identify cases with high disease activity. Br J Haematol 2015;169:795–803. https://doi.org/10.1111/BJH.13361.

[216] Wu Y, Zhang C, Xu W, Zhang J, Zheng Y, Lu Z, et al. CXC motif chemokine receptor 4 gene polymorphism and cancer risk. Medicine 2016;95:e5317. https://doi.org/10.1097/MD.0000000000005317.

[217] Chang CC, Chen SC, Hsieh YH, Chen YC, Chen TY, Chu YH, et al. Stromal cell-derived factor-1 but not its receptor, CXCR4, gene variants increase susceptibility and pathological development of hepatocellular carcinoma. Clin Chem Lab Med 2009;47:412–8. https://doi.org/10.1515/CCLM.2009.092.

[218] Lee YL, Kuo WH, Lin CW, Chen W, Cheng WE, Chen SC, et al. Association of genetic polymorphisms of CXCL12/SDF1 gene and its receptor, CXCR4, to the susceptibility and prognosis of non-small cell lung cancer. Lung Cancer 2011;73:147–52. https://doi.org/10.1016/J.LUNGCAN.2010.12.011.

[219] Cai C, Wang LH, Dong Q, Wu ZJ, Li MY, Sun YH. Association of CXCL12 and CXCR4 gene polymorphisms with the susceptibility and prognosis of renal cell carcinoma. Tissue Antigens 2013;82:165–70. https://doi.org/10.1111/TAN.12170.

[220] Piovan E, Tosello V, Indraccolo S, Masiero M, Persano L, Esposito G, et al. Differential regulation of hypoxia-induced CXCR4 triggering during B-cell development and lymphomagenesis. Cancer Res 2007;67:8605–14. https://doi.org/10.1158/0008-5472.CAN-06-4722.

[221] Schioppa T, Uranchimeg B, Saccani A, Biswas SK, Doni A, Rapisarda A, et al. Regulation of the chemokine receptor CXCR4 by hypoxia. J Exp Med 2003;198:1391–402. https://doi.org/10.1084/JEM.20030267.

[222] Guo M, Cai C, Zhao G, Qiu X, Zhao H, Ma Q, et al. Hypoxia Promotes Migration and Induces CXCR4 Expression via HIF-1α Activation in Human Osteosarcoma. PLoS One 2014;9. https://doi.org/10.1371/JOURNAL.PONE.0090518.

[223] Oh YS, Kim HY, Song IC, Yun HJ, Jo DY, Kim S, et al. Hypoxia induces CXCR4 expression and biological activity in gastric cancer cells through activation of hypoxia-

inducible factor-1α. Oncol Rep 2012;28:2239–46. https://doi.org/10.3892/OR.2012.2063.

[224] Shi J, Wei Y, Xia J, Wang S, Wu J, Chen F, et al. CXCL12-CXCR4 contributes to the implication of bone marrow in cancer metastasis. Future Oncol 2014;10:749–59. https://doi.org/10.2217/FON.13.193.

[225] Hiraga T. Hypoxic Microenvironment and Metastatic Bone Disease. Int J Mol Sci 2018;19. https://doi.org/10.3390/IJMS19113523.

[226] Chatterjee S, Behnam Azad B, Nimmagadda S. The Intricate Role of CXCR4 in Cancer. Adv Cancer Res 2014;124:31. https://doi.org/10.1016/B978-0-12-411638-2.00002-1.

[227] De Clercq E. Potential Clinical Applications of the CXCR4 Antagonist Bicyclam AMD3100. Mini-Reviews in Medicinal Chemistry 2005;5:805–24. https://doi.org/10.2174/1389557054867075.

[228] Kinouchi M, Uchida D, Kuribayashi N, Wakui T, Kuribayashi K, Okubo M, et al. Abstract 4117: AMD070, a novel orally bioavailable CXCR4 inhibitor, inhibits the metastases of oral cancer via SDF-1/CXCR4 system. Cancer Res 2016;76:4117–4117. https://doi.org/10.1158/1538-7445.AM2016-4117.

[229] Fahham D, Weiss ID, Abraham M, Beider K, Hanna W, Shlomai Z, et al. In vitro and in vivo therapeutic efficacy of CXCR4 antagonist BKT140 against human non-small cell lung cancer. J Thorac Cardiovasc Surg 2012;144:1167-1175.e1. https://doi.org/10.1016/J.JTCVS.2012.07.031.

[230] Beider K, Darash-Yahana M, Blaier O, Koren-Michowitz M, Abraham M, Wald H, et al. Combination of imatinib with CXCR4 antagonist BKT140 overcomes the protective effect of stroma and targets CML in vitro and in vivo. Mol Cancer Ther 2014;13:1155–69. https://doi.org/10.1158/1535-7163.MCT-13-0410.

[231] Brummel K, Eerkens AL, de Bruyn M, Nijman HW. Tumour-infiltrating lymphocytes: from prognosis to treatment selection. Br J Cancer 2023;128:451. https://doi.org/10.1038/S41416-022-02119-4.

[232] Shen L, Li H, Shi Y, Wang D, Gong J, Xun J, et al. M2 tumour-associated macrophages contribute to tumour progression via legumain remodelling the extracellular matrix in diffuse large B cell lymphoma. Sci Rep 2016;6. https://doi.org/10.1038/SREP30347.

[233] Nam SJ, Go H, Paik JH, Kim TM, Heo DS, Kim CW, et al. An increase of M2 macrophages predicts poor prognosis in patients with diffuse large B-cell lymphoma treated with rituximab, cyclophosphamide, doxorubicin, vincristine and prednisone. Leuk Lymphoma 2014;55:2466–76. https://doi.org/10.3109/10428194.2013.879713/SUPPL_FILE/DISCLOSURE.ZIP.

[234] Clear AJ, Lee AM, Calaminici M, Ramsay AG, Morris KJ, Hallam S, et al. Increased angiogenic sprouting in poor prognosis FL is associated with elevated numbers of

CD163+ macrophages within the immediate sprouting microenvironment. Blood 2010;115:5053–6. https://doi.org/10.1182/BLOOD-2009-11-253260.

[235] Boutilier AJ, Elsawa SF. Macrophage Polarization States in the Tumor Microenvironment. Int J Mol Sci 2021;22. https://doi.org/10.3390/IJMS22136995.

[236] Toker A, Ohashi PS. Expression of costimulatory and inhibitory receptors in FoxP3+ regulatory T cells within the tumor microenvironment: Implications for combination immunotherapy approaches. Adv Cancer Res 2019;144:193–261. https://doi.org/10.1016/BS.ACR.2019.05.001.

[237] Wang J, Ke XY. The Four types of Tregs in malignant lymphomas. J Hematol Oncol 2011;4:1–10. https://doi.org/10.1186/1756-8722-4-50/FIGURES/1.

[238] van der Leun AM, Thommen DS, Schumacher TN. CD8+ T cell states in human cancer: insights from single-cell analysis. Nat Rev Cancer 2020;20:218. https://doi.org/10.1038/S41568-019-0235-4.

[239] Tau GZ, Cowan SN, Weisburg J, Braunstein NS, Rothman PB. Regulation of IFN-gamma signaling is essential for the cytotoxic activity of CD8(+) T cells. J Immunol 2001;167:5574–82. https://doi.org/10.4049/JIMMUNOL.167.10.5574.

[240] Betts MR, Brenchley JM, Price DA, De Rosa SC, Douek DC, Roederer M, et al. Sensitive and viable identification of antigen-specific CD8+ T cells by a flow cytometric assay for degranulation. J Immunol Methods 2003;281:65–78. https://doi.org/10.1016/S0022-1759(03)00265-5.

[241] Joshi M, Ansell SM. Activating the Antitumor Immune Response in Non-Hodgkin Lymphoma Using Immune Checkpoint Inhibitors. J Immunol Res 2020;2020. https://doi.org/10.1155/2020/8820377.

[242] Davoodi-Moghaddam Z, Jafari-Raddani F, Noori M, Bashash D. A systematic review and meta-analysis of immune checkpoint therapy in relapsed or refractory non-Hodgkin lymphoma; a friend or foe? Transl Oncol 2023;30:101636. https://doi.org/10.1016/J.TRANON.2023.101636.

[243] Xu-Monette ZY, Zhou J, Young KH. PD-1 expression and clinical PD-1 blockade in B-cell lymphomas. Blood 2018;131:68–83. https://doi.org/10.1182/BLOOD-2017-07-740993.

[244] Ansell SM, Hurvitz SA, Koenig PA, LaPlant BR, Kabat BF, Fernando D, et al. Phase I study of ipilimumab, an anti-CTLA-4 monoclonal antibody, in patients with relapsed and refractory B-cell non-Hodgkin lymphoma. Clin Cancer Res 2009;15:6446–53. https://doi.org/10.1158/1078-0432.CCR-09-1339.

[245] Ke J, Chelvarajan RL, Sindhava V, Robertson DA, Lekakis L, Jennings CD, et al. Anomalous constitutive Src kinase activity promotes B lymphoma survival and growth. Mol Cancer 2009;8:132. https://doi.org/10.1186/1476-4598-8-132.

[246] Matthews JM, Bhatt S, Patricelli MP, Nomanbhoy TK, Jiang X, Natkunam Y, et al. Pathophysiological significance and therapeutic targeting of germinal center kinase in diffuse large B-cell lymphoma. Blood 2016;128:239. https://doi.org/10.1182/BLOOD-2016-02-696856.

[247] Wagner EF, Nebreda ÁR. Signal integration by JNK and p38 MAPK pathways in cancer development. Nature Reviews Cancer 2009 9:8 2009;9:537–49. https://doi.org/10.1038/nrc2694.

[248] Lv D, Guo L, Zhang T, Huang L. PRAS40 signaling in tumor. Oncotarget 2017;8:69076. https://doi.org/10.18632/ONCOTARGET.17299.

[249] Deenick EK, Pelham SJ, Kane A, Ma CS. Signal transducer and activator of transcription 3 control of human T and B cell responses. Front Immunol 2018;9:338231. https://doi.org/10.3389/FIMMU.2018.00168/BIBTEX.

[250] Rébé C, Végran F, Berger H, Ghiringhelli F. STAT3 activation: A key factor in tumor immunoescape. JAKSTAT 2013;2:e23010. https://doi.org/10.4161/JKST.23010.

[251] Asslan M, Martel G, Rousseau S. Inhibition of the TPL2-MKK1/2-ERK1/2 pathway has cytostatic effect on B-Cell Lymphoma. BioRxiv 2022:2022.06.13.495940. https://doi.org/10.1101/2022.06.13.495940.

[252] Kitanaka N, Nakano R, Sugiura K, Kitanaka T, Namba S, Konno T, et al. Interleukin-1β promotes interleulin-6 expression via ERK1/2 signaling pathway in canine dermal fibroblasts. PLoS One 2019;14. https://doi.org/10.1371/JOURNAL.PONE.0220262.

7. Supplements

Table S 1: Oligonucleotide sequences of used primers for RQ-PCR.

GAPDH3428-f	AAG GTC GGA GTC AAC GGA TTT
GAPDH3428-r	ACC AGA GTT AAA AGC AGC CCT G
HPRT1-f	ATG GGA GGC CAT CAC ATT
HPRT1-r	ATG TAA TCC AGC AGG TCA GCA A
PPIA-f	CTC CTT TGA GCT GTT TGC AG
PPIA-r	CAC CAC ATG CTT GCC ATC C
CCL22	Qiagen #QT00089817
CCR7	Qiagen #QT01666686
CD44	Qiagen #QT00073549
IL10	Qiagen #QT00041685
MMP2	Qiagen #QT00088396
FN1	Qiagen #QT00038024
COL1A1	Qiagen #QT00037793
CFLAR	Qiagen #QT00064554
ADARB	Qiagen #QT00081655
EGR3	Qiagen #QT00246498
cFOS	Qiagen #QT00007070
BUB1	Qiagen #QT00082929
MXD1	Qiagen #QT00082915
JUNB	Qiagen #QT00201341
cJUN	Qiagen #QT00242956
ETV5	Qiagen #QT00009485
DUSP1	Qiagen #QT00036638
CCL3-f	CTC CAA GCC CGG TGT CAT CT
CCL3-r	TTC TGG ACC CAC TCC TCA CT GG
CCL4-f	TAT GAG ACC AGC AGC CTC TG
CCL4-r	GCT TCT TTT GGT TTG GAA TAC C
KLF10-f	ATG CTC AAC TTC GGT GCC T
KLF10-r	TTC CAT TCT TTC CTC CGC
OAS3-f	CTG GTG TCC ACA GCC CTG AA
OAS3-r	TGC CAG AAC TGA GCT GCC C
RGS1-f	AAC TTC TTG CCA ACC AAA CTG
RGS1-r	CAA GCC AGC CAG AAC TCA
TNF-f	AAG CCT GTA GCC CAT GTT GTA G
TNF-r	AGA TGA GGT ACA GGC CCT CTG A
BCL2A1-f	CAC AGG AGA ATG GAT AAG GCA A
BCL2A1-r	TGA TTG TGC CAT TTC CCC C
BAD-f	GGT AGG AGC TGT GGC GAC T
BAD-r	CAA GCA TCA TCG CCA GG
PUMA-f	CGG AGA CAA GAG GAG CA
PUMA-r	ATG ATG AGA TTG TAC AGG ACC
BAX-f	CCT TTT CTA CTT TGC CAG CAA AC

BAX-r	GAG GCC GTC CCA ACC AC
BCL-XL-f	CAG TGA CCT GAC ATC CCA GC
BCL-XL-r	CCC ATA GAG TTC CAC AAA AGT ATC C
BCL-2-f	GGA GGA TTG TGG CCT TCT TTG
BCL-2-r	GCC GGT TCA GGT ACT CAG TCA T
MCL-1-f	CCA AGG ACA CAA AGC CAA TG
MCL-1-r	AAG AAC TCC ACA AAC CCA TCC
BIK-f	CTT GAT GGA GAC CCT CCT GTA TG
BIK-r	AGG GTC CAG GTC CTC TTC AGA
BAK-f	ATGGTCACCTTACCTCTGCAA
BAK-r	TCATAGCGTCGGTTGATGTCG
BIM Isoform 9-f	AAC CAC TAT CTC AGT GCA ATG G
BIM Isoform 9-r	TTG ACT ATG GTG GTG GCC A
BID-f	GGA ACC GTT GTT GAC CTC AC
BID-r	GAG GAG CAC AGT GCG GAT
BMF-f	TTC AAA GCA AGG TTG TGC AG
BMF-r	TTG TGG GGT GAC TGA GGA AC
NOXA-f	AGC TGG AAG TCG AGT GTG CT
NOXA-r	TCC TGA GCA GAA GAG TTT GGA
CXCR4	Qiagen #QT00223188
CXCR7	Qiagen #QT00069650
CXCL12	Qiagen #QT01008133
CXCR4-ex1 seq fw	CAGCAGGTAGCAAAGTGAC
CXCR4-ex1 seq rev	TCAAGAAAACTCCTTTCGGTG
CXCR4-ex2 seq fw	ATGGGAAAAGATGGGGAGG
CXCR4-ex2 seq rev	AGACTCAGACTCAGTGGAAAC

Table S 2: List of antibodies that are used in flow cytometry.

Antibody	Fluorophore	Clone	Company	Catalogue #	µL/Test
7AAD			BD Biosciences	559925	3
CD3	BV605	17A2	Biolegend	100237	1.5
CD45R (B220)	APC-Cy7	RA3-6B2	BD Biosciences	552094	1
CD279 (PD-1)	FITC	29F.1A12	Biolegend	135214	1
CD274 (PD-L1)	PE-Cy7	MIH5	eBioscience	25-5982-80	0.1
CD273 (PD-L2)	PE	122	eBioscience	12-9972-81	2
CD45	AF700	30-F11	Biolegend	103128	0.25
CD152 (CTLA-4)	PE-Cy7	UC10-4B9	Biolegend	106314	1
CD86	FITC	GL-1	Biolegend	105006	0.1
CD80	APC	16-10A1	Biolegend	104714	0.5
CD366 (TIM3)	PE-Cy7	RMT3-23	eBioscience	25-5870-80	1.25
CD66a (CEACAM1a)	APC	MAb-CC1	Biolegend	134510	0.1
Galectin-9	PE	108A2	Biolegend	137903	0.1
CD226 (DNAM-1)	APC	10E5	eBioscience	17-2261-80	0.1
CD155	BV421	TX56	Biolegend	131517	0.1
TIGIT	PE	4D4/mTIGIT	Biolegend	156104	0.5
CD272 (BTLA)	PerCP-eFluor™ 710	6F7	eBioscience	46-5950-82	0.5
CD270 (HVEM)	PE	HMHV-1B18	Biolegend	136304	0.1
CD160	APC	7H1	Biolegend	143012	2.5
VISTA	PerCP-eFluor™ 710	MIH64	eBioscience	46-1083-82	1
LAG-3	APC	C9B7W	Biolegend	125210	0.1
TIM-3	BV421	5D12/TIM-3	BD Biosciences	747626	1
CD279 (PD-1)	APC	J43	eBioscience	17-9985-80	1.25
LAG-3	BV650	C9B7W	Biolegend	125227	1
H-2Kb/H-2Db (MHCI)	APC	28-8-6	Biolegend	114613	0.5
I-A/I-E (MHCII)	FITC	M5/114.15.2	Biolegend	107605	0.01
IgM	eF450	II/41	eBioscience	48-5790-80	0.25
CD19	BV510	1D3	BD Biosciences	562956	0.3
GR1(Ly-6C)	PE	AL-21	BD Biosciences	560592	0.0333
CD45R (B220)	APC	RA3-6B2	Biolegend	103212	0.3
TCR	FITC	H57-597	eBioscience	11-5961-85	0.2
Fixable Viability Dye	eFluor™ 780		eBioscience	65-0865-18	0.05
CD45	BV785	30-F11	Biolegend	103149	0.313
CD11b	BUV737	M1/70	BD Biosciences	612801	0.625
Ly6C	APC	HK1.4	Biolegend	128015	0.63
Ly6G	PE/Dazzle594	1A8	Biolegend	127648	0.3
CD11c	BV605	N418	Biolegend	117334	2.5
F4/80	BUV395	T45-2342	BD Biosciences	565614	1.25
PDL1	PE-Cy7	10F.9G2	Biolegend	124313	0.63
SiglecF	PE	E50-2440	BD Biosciences	562068	1.25
CD206-FITC	FITC	C068C2	Biolegend	141704	0.31

MHCII	PerCP-Cy5.5	M5/114.15.2	Biolegend	107625	0.31
CD107a	BV421	1D4B	Biolegend	121618	0.5
CD103	BV510	2E7	Biolegend	121423	1.25
CD3	BUV395	145-2C11	BD Biosciences	563565	1.25
CD4	BUV496	GK1.5	BD Biosciences	564667	0.625
CD8	PerCPCy5.5	53-6.7	Biolegend	100734	0.625
gdTCR	PECF594	GL3	BD Biosciences	563532	1.25
NKp46	BV510	29A1.4	Biolegend	137623	2.5
CD19	FITC	6D5	Biolegend	115506	0.31
CD44	BUV737	IM7	BD Biosciences	612799	0.31
CD62L	BV605	MEL-14	Biolegend	104438	1
PD1-APC	APC	29F.1A12	Biolegend	135210	1.25
FoxP3	PE	FJK-16s	eBioscience	12-5773-82	1.25
CD8	PE/Dazzle594	53-6.7	Biolegend	100762	0.1
TCR Vα2	AF647	B20.1	Biolegend	127812	0.75
TCR Vβ5.1, 5.2	PE	MR9-4 PE	Biolegend	139504	0.1
CD44	APC	IM7	Biolegend	103012	0.1
CD62L	BV605	MEL-14	Biolegend	104437	0.75
CD69	PE	H1.2F3	Biolegend	104508	0.25
CD25	BV421	PC61	Biolegend	102033	0.75

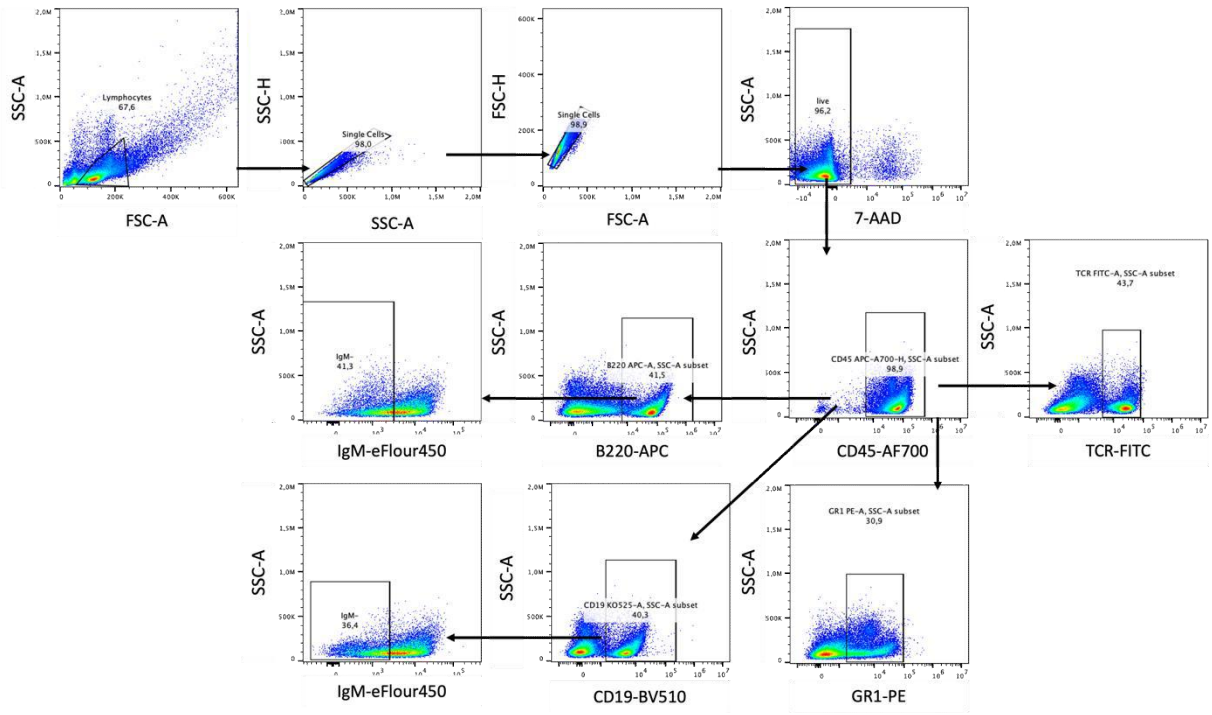

Figure S 1: The gating strategy to evaluate the myeloid cells (GR1+), T cells (TCR+), and B cells (CD19+ or B220+) with their IgM status. Flow cytometric analysis was performed on single cell suspensions of mouse spleens. All lymphocytes were gated by forward scatter/side scatter (SSC/FSC). Dead cells were excluded by using 7-AAD. IgM- B220+ B cells were identified as CD45+/B220+/IgM-; IgM- CD19+ B cells were CD45+/B220+ B cells/IgM-. T cells were characterized as CD45+/TCR+ and myeloid cell as CD45+/Gr-1+.

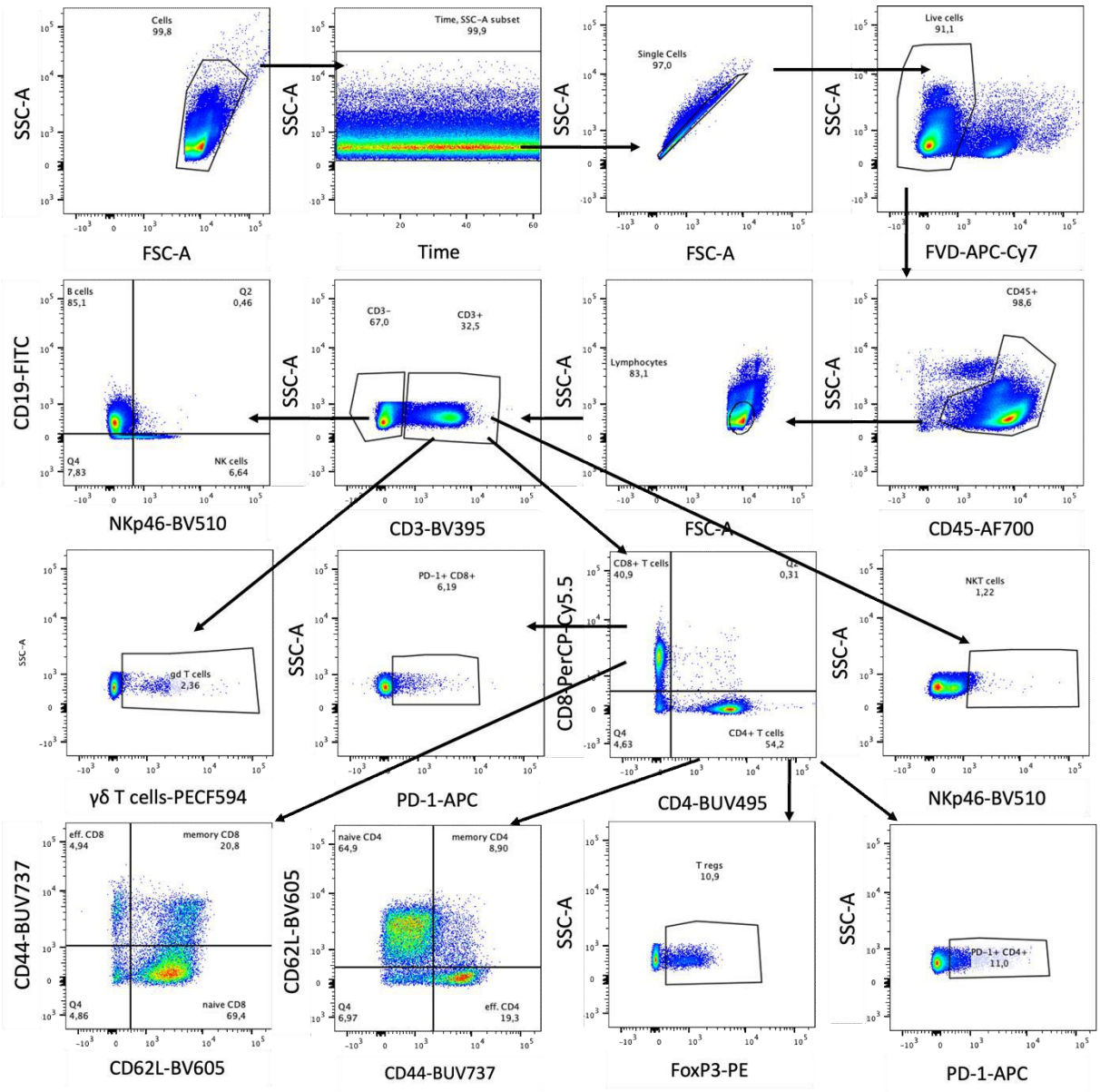

Figure S 2: Gating strategy of lymphoid cells. Flow cytometric analysis was performed on single cell suspensions of mouse spleens. Tumor infiltrating leucocytes (CD45+) were pregated for time and singlets. Dead cells were excluded by the use of fixable viability dye (FVD). To pre-gate the lymphoid populations, a lymphoid size gate was used. The T cells were identified as CD45+/CD3+, the NK cells as CD45+/CD3-/NKp46+, the B cells as CD45+/CD3-/CD19+, the CD8+ T cells as CD45+/CD3+/CD8+, the CD4+ T cells as CD45+/CD3+/CD4, the Tregs as CD45+/CD3+/CD4+/FoxP3+, the γδ T cells as CD45+/CD3+/gdTCR+, and the NKT cells as CD45+/CD3+/NKp46+. To characterize different T cell subpopulations, we further gated CD44+CD62L- (effector T cells), CD44+/CD62L+ (memory T cells), and CD44-/CD62L+ (naïve T cells).

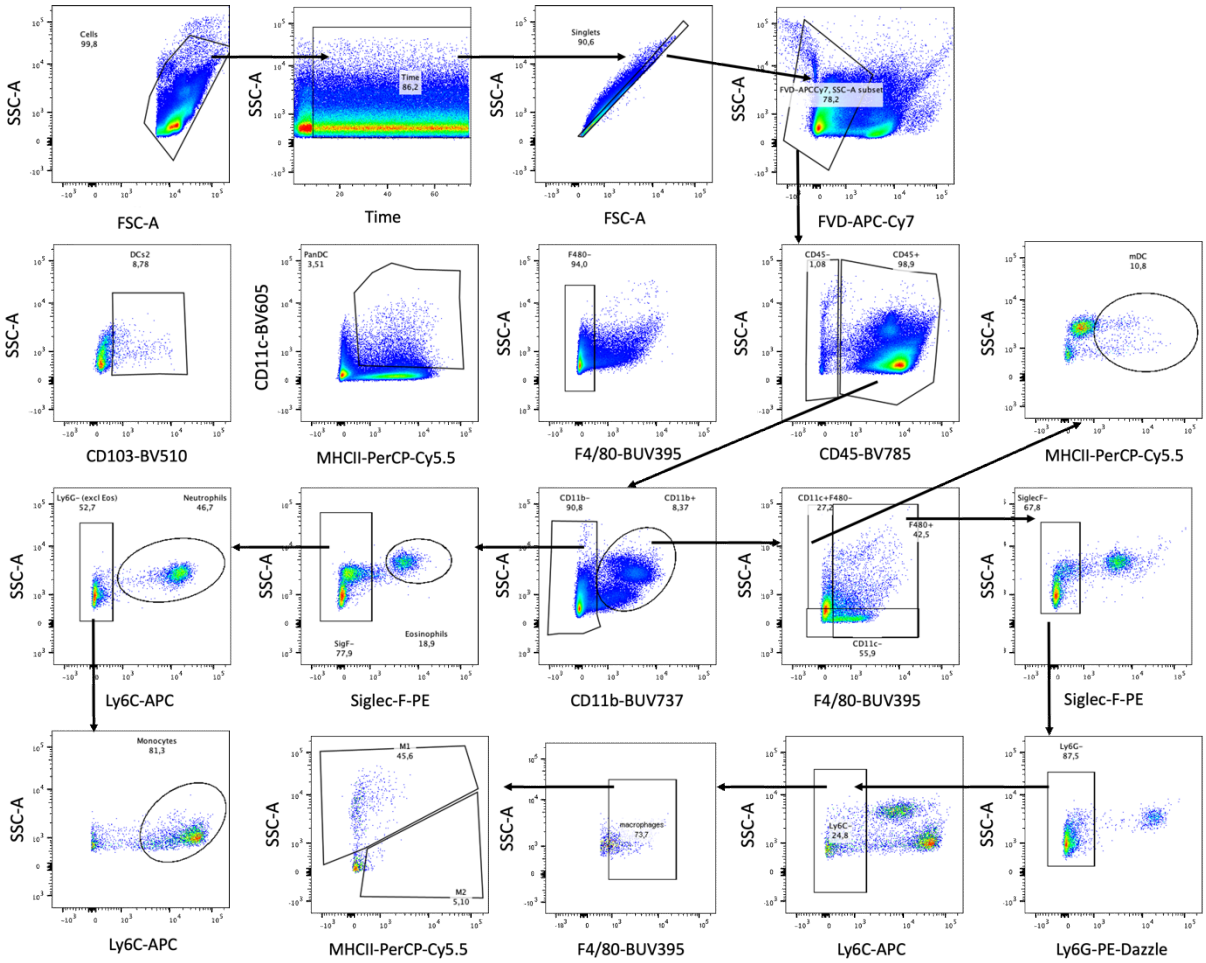

Figure S 3: Gating strategy of myeloid cells. Flow cytometric analysis was performed on single cell suspensions of mouse spleens. Tumor infiltrating leucocytes (CD45+) were pregated for time and singlets. Dead cells were excluded by the use of fixable viability dye (FVD). Eosinophils were identified as CD45+/CD11b+/CD11c-/F4_80/Siglec-F+. Neutrophils were identified as CD45+/CD11b+/CD11c-/Siglec-F-/Ly6G-/Ly6C+. Macrophages were identified as CD45+/CD11b+/CD11c+/-/SiglecF-F-/Ly6G-/Ly6C-/F4_80. The subsets of macrophages were characterized by MHC-II+/CD206^{int} (M1) and MHC-II$^{int/}$CD206+ (M2) in this study. Subsets of DC were gated as: m(DC) as CD45+/CD11b+/CD11c+/F4_80-/MHC-II+, pDC as CD45+/CD11b-/CD11c+/MHC-II+, and cDCs1 as CD45+/CD11b-/CD11c+/MHC-II+/CD103.

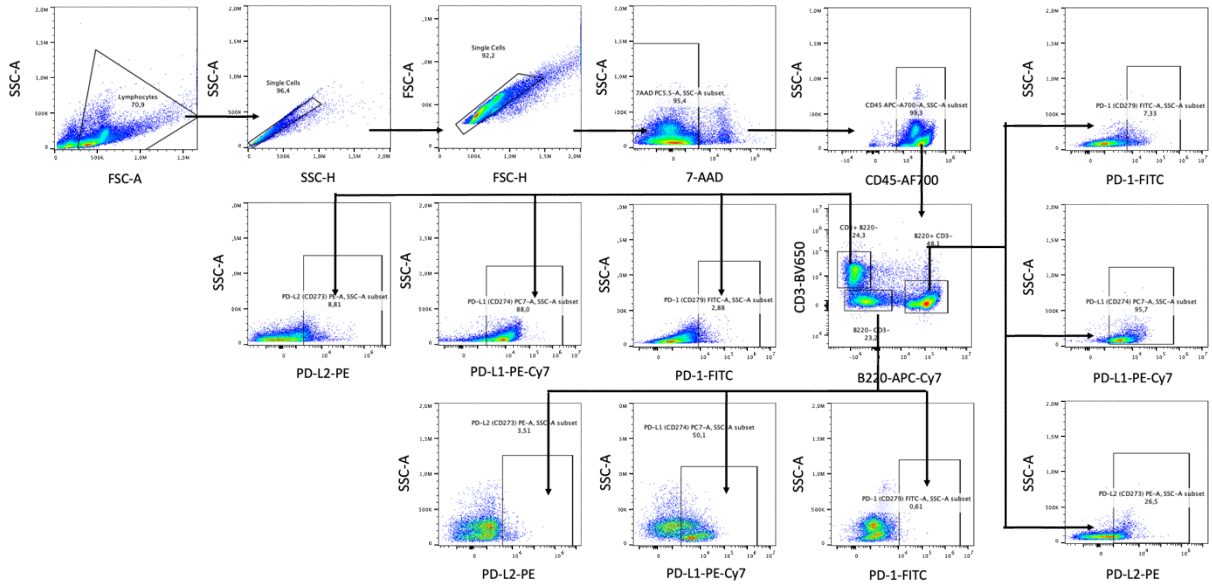

Figure S 4: The gating strategy to evaluate the expression of PD1-PDL1-PDL2 axes on T and B cells and CD45+ B220- CD3- population. Flow cytometric analysis was performed on single cell suspensions of mouse spleens. All lymphocytes were gated by forward scatter/side scatter (SSC/FSC). Dead cells were excluded by using 7-AAD. CD3+ T cells and B220+ B cells were identified as CD45+/CD3+ and CD45+/B220+, respectively. Expression of the immune checkpoint PD1 and their corresponding ligands PDL1 and PDL2 were analyzed in these populations.

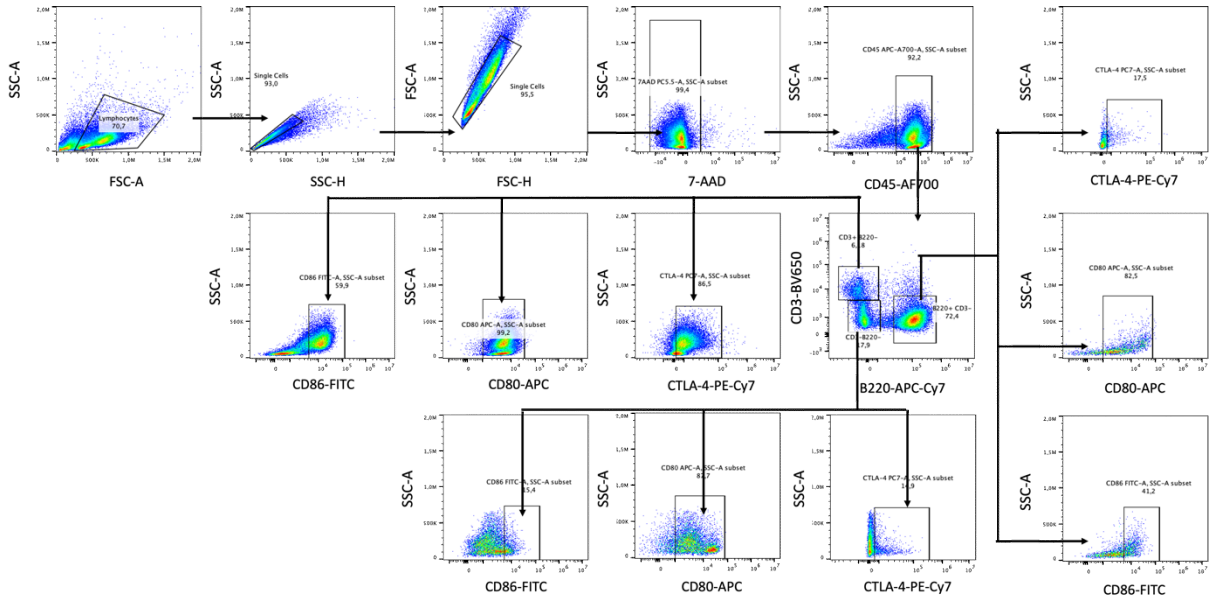

Figure S 5: The gating strategy to evaluate the expression of CTLA-4-CD80-CD86 axes on T and B cells and CD45+ B220- CD3- population. Flow cytometric analysis was performed on single cell suspensions of mouse spleens. All lymphocytes were gated by forward scatter/side scatter (SSC/FSC). Dead cells were excluded by using 7-AAD. CD3+ T cells and B220+ B cells were identified as CD45+/CD3+ and CD45+/B220+, respectively. Expression of the immune checkpoint CTLA-4 and their corresponding ligands CD80 and CD86 were analyzed in these populations.

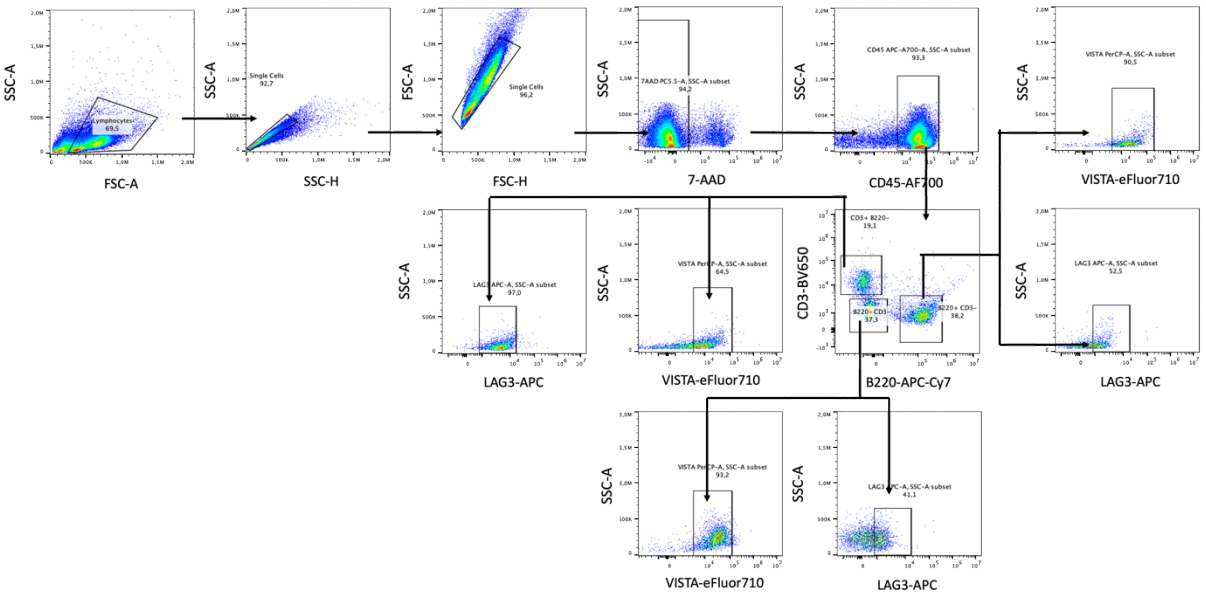

Figure S 6: The gating strategy to evaluate the expression of VISTA and LAG3 on T and B cells and CD45+ B220- CD3- population. Flow cytometric analysis was performed on single cell suspensions of mouse spleens. All lymphocytes were gated by forward scatter/side scatter (SSC/FSC). Dead cells were excluded by using 7-AAD. CD3+ T cells and B220+ B cells were identified as CD45+/CD3+ and CD45+/B220+, respectively. Expression of the immune checkpoints VISTA and LAG3 in these populations.

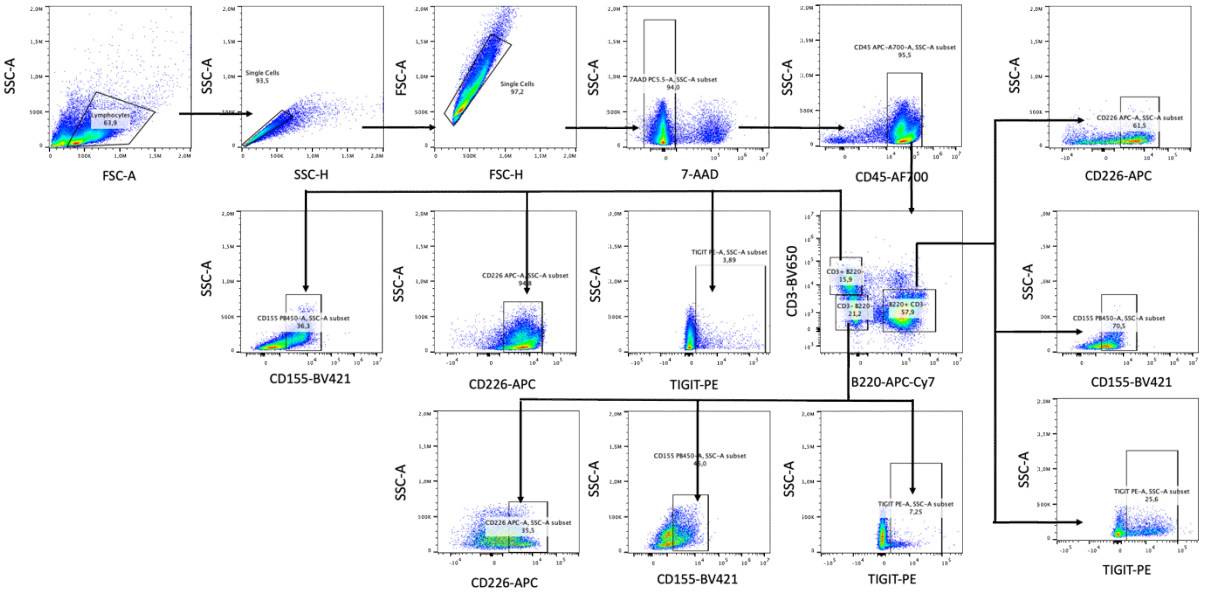

Figure S 7: The gating strategy to evaluate the expression of TIGIT, CD226 and CD155 on T and B cells and CD45+ B220- CD3- population. Flow cytometric analysis was performed on single cell suspensions of mouse spleens. All lymphocytes were gated by forward scatter/side scatter (SSC/FSC). Dead cells were excluded by using 7-AAD. CD3+ T cells and B220+ B cells were identified as CD45+/CD3+ and CD45+/B220+, respectively. Expression of the immune checkpoints Tigit and their corresponding ligands Cd226 and Cd155 in these populations.

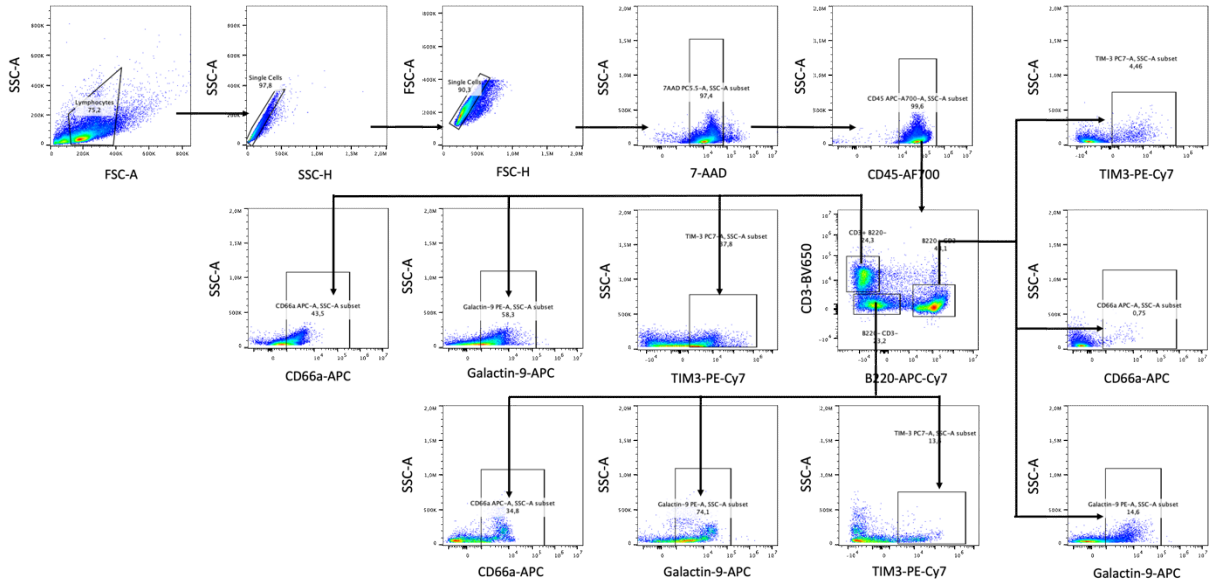

Figure S 8: The gating strategy to evaluate the expression of TIM-3, Galectin-9 and CD66a on T and B cells and CD45+ B220- CD3- population. Flow cytometric analysis was performed on single cell suspensions of mouse spleens. All lymphocytes were gated by forward scatter/side scatter (SSC/FSC). Dead cells were excluded by using 7-AAD. CD3+ T cells and B220+ B cells were identified as CD45+/CD3+ and CD45+/B220+, respectively. Expression of the immune checkpoints TIM-3 and their corresponding ligands Galectin-9 and CD66a in these populations.

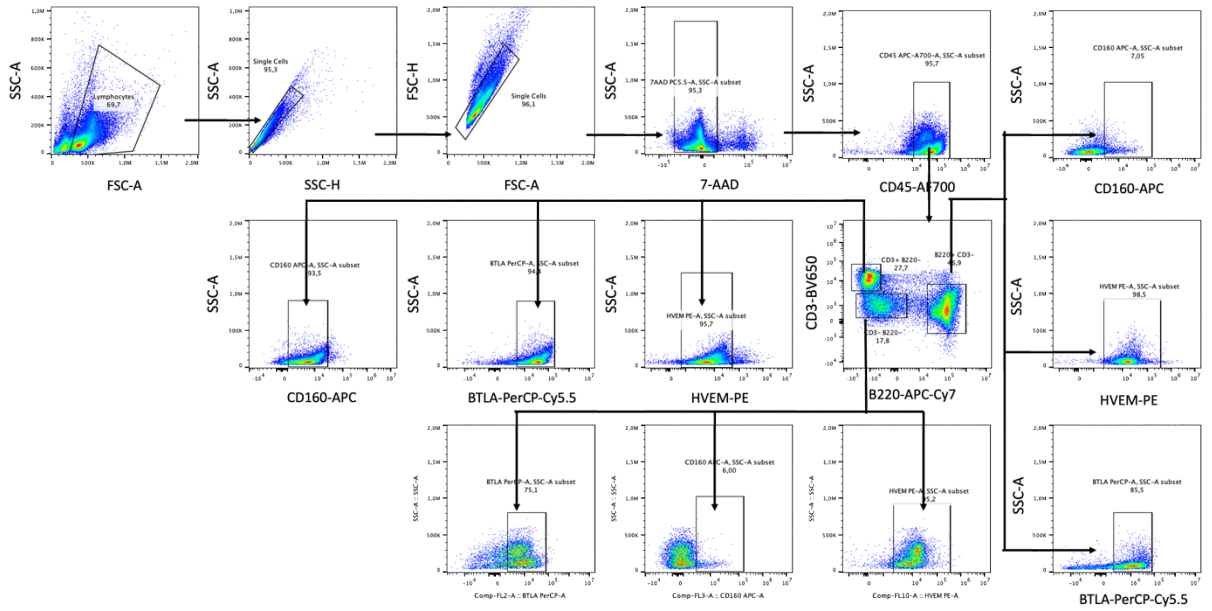

Figure S 9: The gating strategy to evaluate the expression of BTLA, HVEM and CD160 on T and B cells and CD45+ B220- CD3- population. Flow cytometric analysis was performed on single cell suspensions of mouse spleens. All lymphocytes were gated by forward scatter/side scatter (SSC/FSC). Dead cells were excluded by using 7-AAD. CD3+ T cells and B220+ B cells were identified as CD45+/CD3+ and CD45+/B220+, respectively. Expression of the immune checkpoints BTLA and their corresponding ligands HVEM and CD160 in these populations.

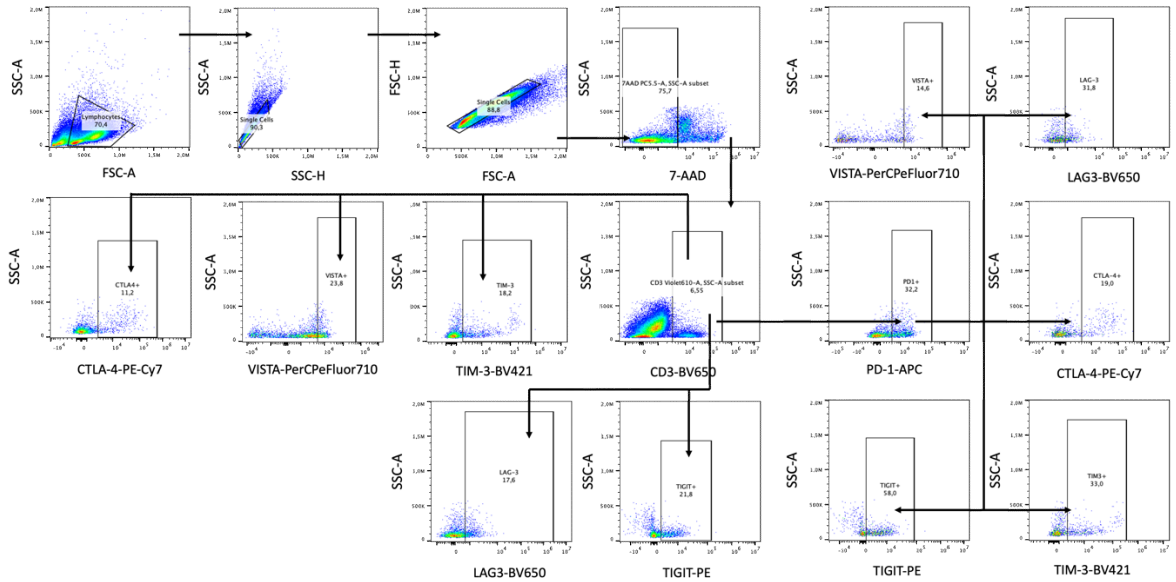

Figure S 10: The gating strategy for the evaluation of immune checkpoint expression on T cells and co-expression of immune checkpoints on PD1+ T cells. Flow cytometric analysis was performed on single cell suspensions of mouse spleens. All lymphocytes were gated by forward scatter/side scatter (SSC/FSC). Dead cells were excluded by using 7-AAD. CD3+ T cells were gated to evaluate the expression of various immune checkpoints. Additionally, CD3+ PD1+ T cells were analyzed for co-expression of other immune checkpoints.

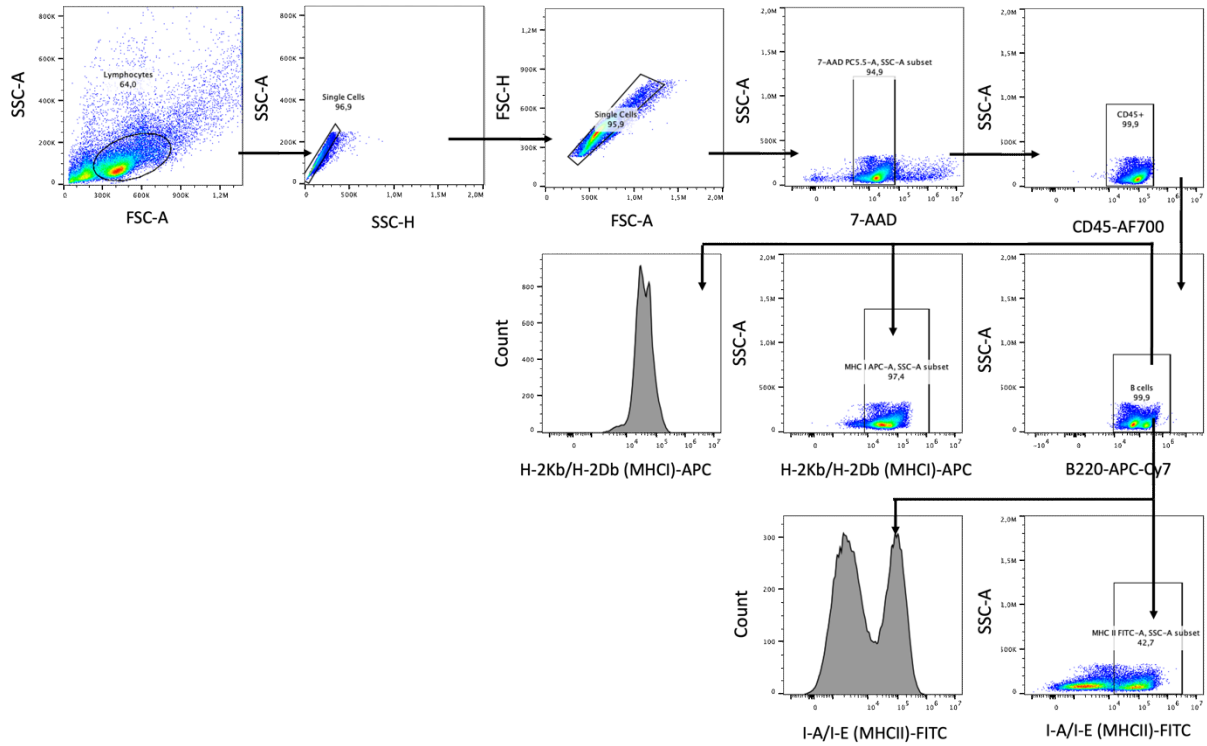

Figure S 11: The gating strategy for the evaluation of MHC I and MHC II expression of B220+ B cells. Flow cytometric analysis was performed on single cell suspensions of mouse spleens. All lymphocytes were gated by forward scatter/side scatter (SSC/FSC). Dead cells were excluded by using 7-AAD. B220+ B cells were gated for MHC I and MHC II expression.

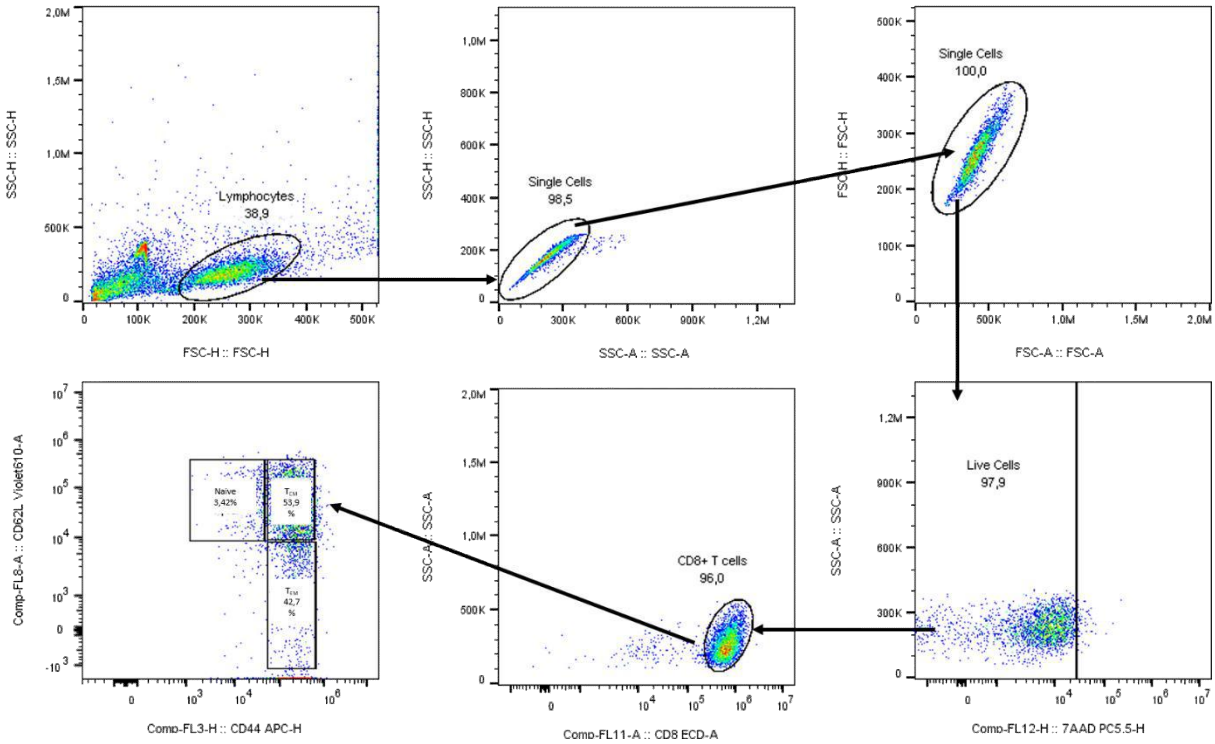

Figure S 12: Phenotyping of T cells subsets after activation. The gating strategy to evaluate the T cell subset distribution of CD8+ T cells. T cells were classified into three populations according to the expression of CD62L-BV610 and CD44-APC to identify subpopulations of naïve T cells (CD44-CD62+), T_{CM} (CD44+CD62+), and T_{EM} (CD44+CD62L-).

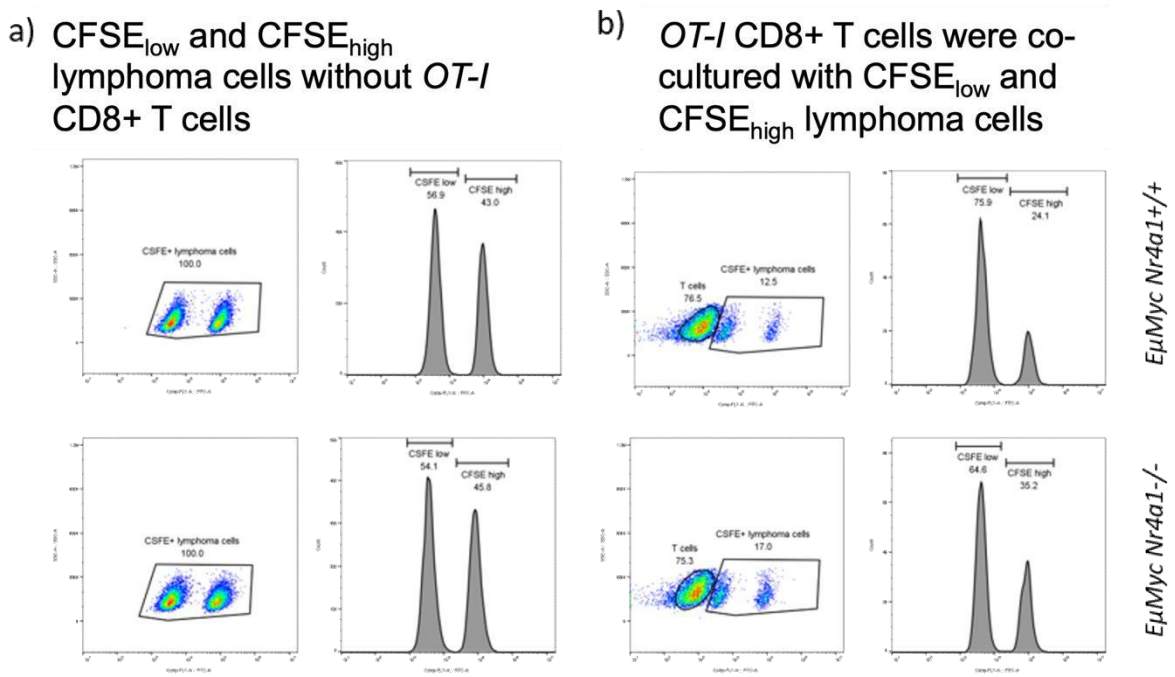

Figure S 13: Representative dot plots and histograms showing the gating strategy for the cytotoxicity assay. (a) Percentage of CFSE$_{low}$ and CFSE$_{high}$ lymphoma cells with or without *Nr4a1* loss mixed in a ratio of 1:1 without the presence of *OT-1* CD8+ T cells after 24h served as control (b) Histogram illustrating CSFE$_{high}$ stained lymphoma cells, which represent target cells pulsed with OVA peptide, while CFSE$_{low}$ populations represent target cells not pulsed with any peptide. Percentage of CFSE$_{low}$ and CFSE$_{high}$ lymphoma cells with or without *Nr4a1* loss in presence of *OT-1* CD8+ T cells after 24h of co-incubation.

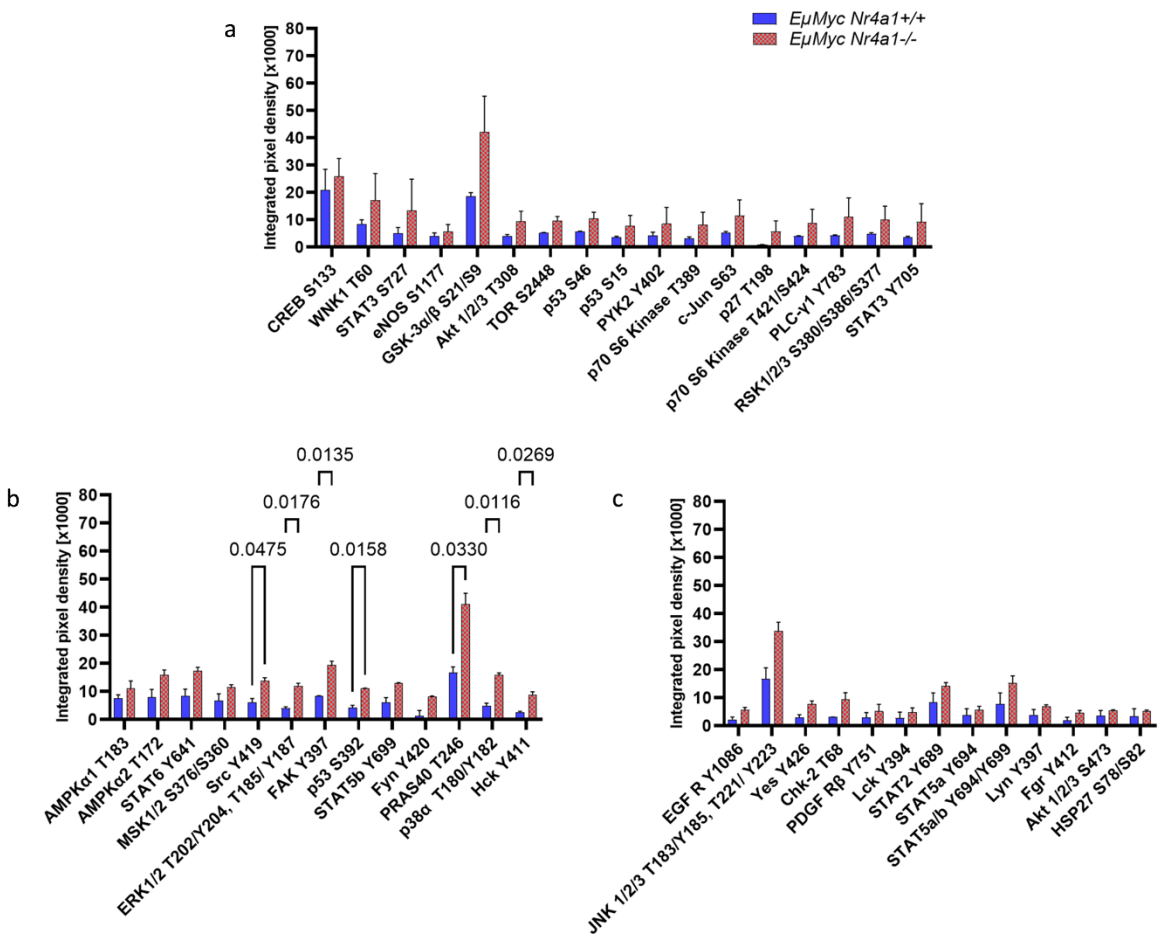

Figure S 14: Bar charts of phosphorylation levels of murine lymphoma cell lines with and without *Nr4a1* loss. The absolute values of the integrated pixel density of cluster one (a), two (b) and three (c) of the different kinases are displayed in three bar graphs, which are obtained from the heat map analysis. Each bar represents the mean of the expression levels ± standard error of the mean (SEM). Comparison of phosphorylation levels was performed using Students t-test.

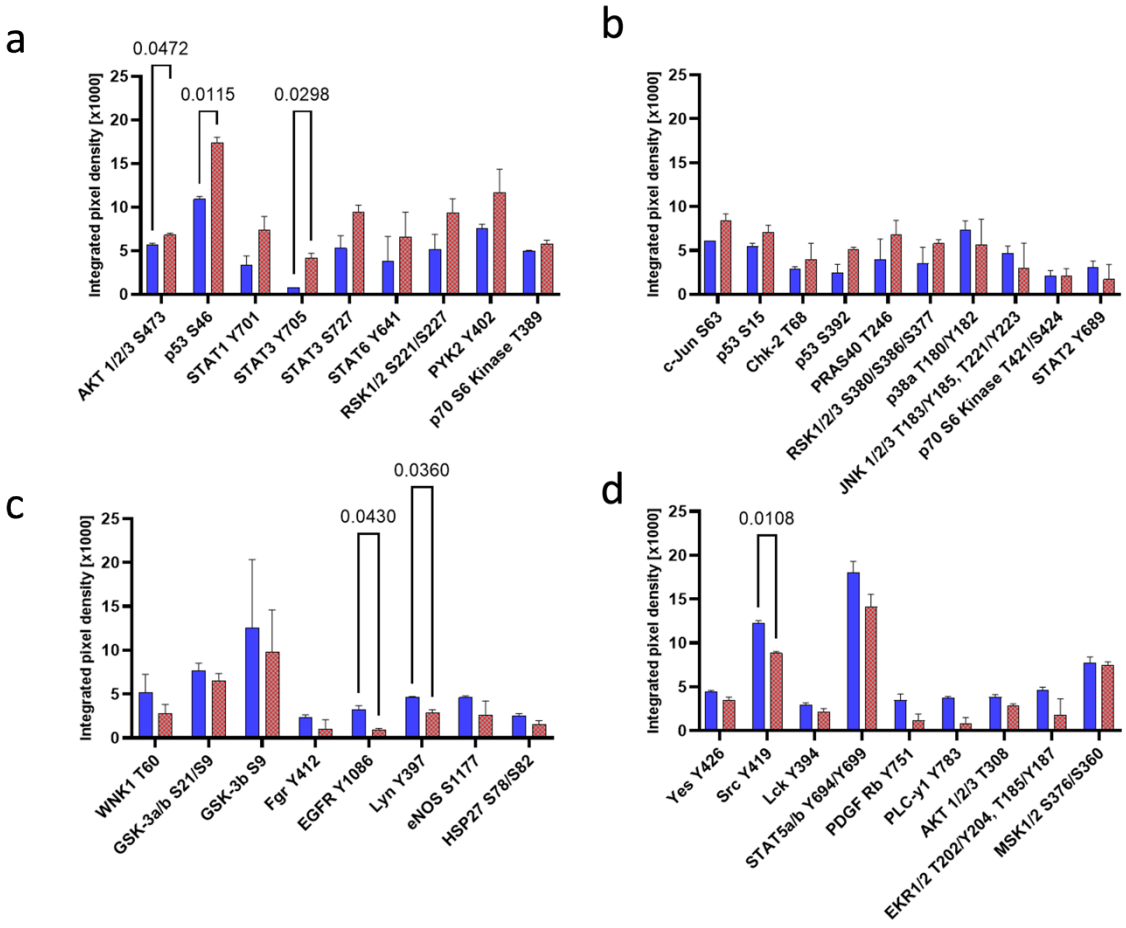

Figure S 15: Bar charts of phosphorylation levels of lymphomas derived *EμMyc* with and without *Nr4a1* loss. The absolute values of the integrated pixel density of cluster one (a), two (b), three (c) and four (d) of the different kinases are displayed in three bar graphs, which are obtained from the heat map analysis. Each bar represents the mean of the expression levels ± standard error of the mean (SEM). Comparison of phosphorylation levels was performed using Students t-test.